

**FRAMEWORK FOR ACCURACY CONTROL AND CONTACTLESS
INSPECTION OF PARTS WITH FREE-FORM SURFACES AND GD&T
FEATURES USING REVERSE ENGINEERING APPROACH**

Submitted in

fulfillment of the requirements for the degree of

Doctor of Philosophy

by

Vimal Kumar Pathak

ID: 2013RME9053

Under the Supervision of

Dr. Amit Kumar Singh



**DEPARTMENT OF MECHANICAL ENGINEERING
MALAVIYA NATIONAL INSTITUTE OF TECHNOLOGY JAIPUR, INDIA
MARCH 2018**

**FRAMEWORK FOR ACCURACY CONTROL AND CONTACTLESS
INSPECTION OF PARTS WITH FREE-FORM SURFACES AND GD&T
FEATURES USING REVERSE ENGINEERING APPROACH**

Ph.D. Thesis

VIMAL KUMAR PATHAK

(ID. No. 2013RME9053)



**DEPARTMENT OF MECHANICAL ENGINEERING
MALAVIYA NATIONAL INSTITUTE OF TECHNOLOGY JAIPUR, INDIA**

MARCH 2018

Certificate

This is to certify that the thesis entitled “**Framework for accuracy control and contactless inspection of parts with free-form surfaces and GD&T features using reverse engineering approach**” being submitted by **Mr. Vimal Kumar Pathak (2013RME9053)** is a bonafide research work carried out under my supervision and guidance in fulfilment of the requirement for the award of the degree of **Doctor of Philosophy** in the Department of Mechanical Engineering, Malaviya National Institute of Technology, Jaipur, India. The matter embodied in this thesis is original and has not been submitted to any other University or Institute for the award of any Degree or Diploma.

Place: Jaipur

Date:

Dr. Amit Kumar Singh

Assistant Professor

Mechanical Engineering Department

Malaviya National Institute of Technology Jaipur

Jaipur-302017, India

Declaration

I, Vimal Kumar Pathak declare that this thesis titled, “**Framework for accuracy control and contactless inspection of parts with free-form surfaces and GD&T features using reverse engineering approach**” and the work presented in it, are my own. I confirm that:

- This work was done wholly or mainly while in candidature for a research degree at this University.
- Where any part of this thesis has previously been submitted for a degree or any other qualification at this university or any other institution, this has been clearly stated.
- Where I have consulted the published work of others, this is always clearly attributed.
- Where I have quoted from the work of others, the source is always given. With the exception of such quotations, this thesis is entirely my own work.
- I have acknowledged all main sources of help.
- Where the thesis is based on work done by myself, jointly with others, I have made clear exactly what was done by others and what I have contributed myself.

Date:

Vimal Kumar Pathak
(2013RME9053)

Acknowledgements

I would like to express my deep and sincere gratitude to my thesis supervisor, Dr. Amit Kumar Singh, for his invaluable guidance and support. He is an excellent teacher and his knowledge and logical way of thinking has been of great value for me. This research is impossible without his inspiring guidance, experience, and subject knowledge.

I also take this opportunity to express my heartfelt thanks to the members of Departmental Research Evaluation Committee (DREC), Dr. Himanshu Chaudhary, Dr. T. C. Gupta and Dr. Dinesh Kumar, who spared their valuable time and experiences to evaluate my research plan and the synopsis. I would also like to thank Prof. G. S. Dangayach, Head of the Mechanical Engineering Department, and his office team for helping in all administrative works regarding the thesis.

I also like to convey my heartfelt gratitude to seniors Dr. Swati Gangwar, Dr. Sumit Gupta, Dr. Kailash Chaudhary, Dr. Chitresh Nayak and Manoj Gupta for sharing their valuable knowledge. I also like to thank my friends Ramanpreet Singh, Sagar Kumar, NRNV Gowripathi Rao and Prashant Athanker for their support and help which was extremely needed to complete my work successfully. Finally, but not the least I am very thankful to my parents, my brother Dr. Sitla Prasad Pathak, sister-in-law Dr. Priyanka Pathak and wife Riya who have surrendered their priority and time for me.

Vimal Kumar Pathak
Department of Mechanical Engineering
Malaviya National Institute of Technology Jaipur

ABSTRACT

The research presented in this thesis proposed a two stage inspection framework for parts with free-form surfaces, dimensional and geometrical features using contactless scanning system. The overall objective of this thesis is to provide an iterative framework for accuracy control and contactless inspection of parts with free-form surfaces and GD&T features using reverse engineering approach. The first stage deals with the digitization of the part surface using a commercial 3D scanner and accurate surface reconstruction using software application. The test components in this thesis were manufactured using advanced manufacturing process like additive manufacturing (AM). To get improved quality products, the challenges and issues associated with the AM process are studied first by printing several parts. Afterwards, corrective actions were suggested to minimize these issues.

The scanning parameters affects the final output of acquired point cloud data. Prior to its digitization, important scanning parameters were identified based on the object surface morphology i.e. scanning distance and scanning incidence angle. Further, a full factorial experimental design is considered for different combination of scanning distance and scanning angle. A mathematical prediction model for estimating the standard deviation of the final surface is developed in terms of the above scanning parameters using response surface methodology (RSM). The mathematical model is further optimized using a modified particle swarm optimization (MPSO) algorithm. After improved quality point data acquisition, an accurate path of surface reconstruction from unorganized raw point cloud data is presented. For this purpose, two commercially available software CATIA and Solidworks are employed. The accuracy obtained for the reconstructed surface model in this study is in accordance with published literature results. This completes the first stage of the proposed framework.

The second stage begins with illustrating the importance of correct selection of points during alignment for effective and accurate inspection. This study assesses the influence of 3-2-1 method for aligning of the point clouds in the same Cartesian reference frame prior to inspection. Several dissimilar points were selected on each aligning feature for each repetition with the purpose of examining the effect of point selection with respect to inspection results. Further, for exact evaluation of GD&T error

mathematical model was formulated as an unconstrained optimization problem. Numerical examples have been illustrated to verify form errors from coordinate data effectively. Compared to conventional or existing heuristics optimization methods, the proposed MPSO algorithm not only has the advantage of a simple realization in computers and good flexibility, but it was shown to have improved the form error evaluation accuracy.

Based on the results, an iterative framework was proposed that would be a handy tool to the end users and quality personnel as it provides the systematic guideline to be followed in an automated dimensional inspection system using contactless scanning systems. Finally, a standard benchmark part was proposed with typical features conforming to different families of geometrical dimensioning and tolerancing (GD&T) for verification of proposed framework. The benchmark part designed consists of various canonical features widely used in an engineering and industrial applications. Further, the adopted approach includes the proposal of different scanning orientation methods. Surface reconstruction of the benchmark model performed using different reverse engineering software used in chapter 5 (COMET PLUS, CATIA v5 and Solidworks Scan-to-3D), and results are analyzed to study the correlation between various critical parameters. Considering the contact based measurement as a reference, different models developed were analyzed and compared in terms of geometrical and dimensional tolerance. The proposal of standard benchmark part and methodology for GD&T verification will provide a simple way of performance evaluation for various contactless laser-scanning systems.

CONTENTS

Certificate.....	i
Declaration.....	ii
Acknowledgements.....	iii
ABSTRACT.....	iv
CONTENTS.....	vi
List of Figures	ix
List of Tables	xii
1.1 Additive manufacturing (AM) principles.....	4
1.2 Reverse engineering (RE) principles.....	5
1.3.1 Straightness.....	7
1.3.2 Flatness	8
1.3.3 Circularity.....	8
1.3.4 Cylindricity	9
1.4 Motivation of Research.....	10
1.5 Thesis Statement.....	11
1.6 Thesis Organization.....	11
1.7 Chapter Summary	13
2.1 Additive manufacturing challenges - geometrical issues and process parameter optimization	14
2.1.1 Overview of AM process	14
2.1.1.1 Material Jetting process.....	17
2.1.1.2 Directed Energy Deposition	17
2.1.1.3 Powder Bed Fusion	19
2.1.1.4 Binder Jetting	19
2.1.1.5 Vat photopolymerization	20
2.1.1.6 Sheet Lamination	20
2.1.1.7 Material Extrusion.....	21
2.1.2 Challenges and issues in FDM based parts	22
2.1.3 Process parameter optimization in FDM process.....	27
2.2 Advances in 3D scanning systems and optimal parameter selection.....	31
2.3 Surface reconstruction from point cloud data to accurate surface model	37
2.4 GD&T error evaluation and optimization	43

2.5 Inspection planning, procedures and development of benchmark part for scanner characterization	51
2.6 The Knowledge Gap in Earlier Investigations.....	60
2.7 Research objectives	61
2.8 Chapter summary	62
3.1 Entry Level Additive Manufacturing (ELAM): Basics	64
3.2 Objectives of the experiment	65
3.3 Fabrication of CAD models and Observed issues.....	68
3.3 Summary of Issues found and Actions performed	79
3.4 GD&T error minimization.....	79
3.4.1 Material and Methods	81
3.4.2 Development of mathematical model.....	83
3.4.3 Checking the model accuracy	83
3.5 Multi-objective optimization	85
3.6 Case study	87
3.7 Chapter Summary	89
4.1 Adopted methodology for optimal scanning parameter evaluation.....	91
4.2 Experimental tests and results.....	93
4.3 ANOVA analysis and mathematical model development.....	94
4.4 Modified particle swarm optimization (MPSO) and optimization problem formulation ..	97
4.4.1 Definition of different terms used	99
4.4.2 Standard particle swarm optimization algorithm.....	100
4.4.3 Modified particle swarm optimization (MPSO) algorithm.....	103
4.4.4 Numerical Examples.....	106
4.5 Case Study Validation	114
4.6 Chapter summary	117
5.1 Introduction	118
5.2 Study Model.....	119
5.3 Point clouds digitization.....	119
5.4 RE tools application.....	120
5.4.1 CATIA Methodology	121
5.4.1.1 Filtering technique effect.....	123
5.4.1.2 Mesh smoothing process analysis	124
5.4.1.3 Decimation and optimization mesh process	124

5.4.1.4 Surface generation.....	126
5.4.2. Solidworks study	128
5.5 Results and discussion	131
5.6 Summary	133
6.1 Minimum zone straightness formulation	134
6.2 Minimum zone flatness formulation	135
6.3 Minimum zone circularity formulation	136
6.4 Minimum zone cylindricity formulation	136
6.5 Experimental implementation	138
6.6 Summary	146
7.1 Introduction	148
7.2 Development of Framework for accuracy control and contactless inspection	149
7.3 Case study validation	152
7.3.1 Benchmark Part Design.....	153
7.3.2 Common reference system definition (Contact and non-contact).....	155
7.3.3 Non-Contact digitization strategy	157
7.3.4 Surface reconstruction using different software.....	158
7.4 Importance of correct alignment technique.....	159
7.5 Comparison of developed surface models	169
7.6 GD&T comparison of reconstructed surface models.....	171
7.7 Summary	177
References	184
PAPER PUBLISHED BASED ON THIS WORK.....	212
BRIEF BIO-DATA OF THE AUTHOR.....	214

List of Figures

Figure 1.1	(a) Ducati engine made by AM technology (b) 3D printed prosthetic socket (c) 3D printed optimized Airbus A380 bracket	2
Figure 1.2	Additive manufacturing specific applications areas (Wohlers, 2015)	2
Figure 1.4	Tolerance with their geometric entities and symbols	6
Figure 1.5	Straightness Tolerance description	7
Figure 1.6	Flatness Tolerance description	8
Figure 1.7	Circularity tolerance description	8
Figure 1.8	Cylindricity tolerance description	9
Figure 2.1	Layer variation in AM process (Gibson et al., 2014)	10
Figure 2.2	Schematic of Directed energy deposition (DED) process (Shin et al., 2003)	15
Figure 2.3	Schematic of Vat photopolymerization process (Chartrain et al., 2016)	18
Figure 2.4	Schematic diagram of FDM based AM process	20
Figure 2.5	Conversion of CAD model (left) into STL model (right) for FDM fabrication (Gibson et al., 2010)	22
Figure 2.6	Part warpage drifting (a) towards the edges (b) towards a side	23
Figure 2.7	Fishbone diagram of FDM process parameters (Mohammed et al., 2015)	24
Figure 2.8	Laser triangulation principle (Curles, 1997), (α_s is incident scanning angle)	29
Figure 2.9	Point acquisition of (a) turbine blade (b) point of view 1 (c) point of view	32
Figure 2.10	Hubcap master model and its point data after filtering (Soni et al., 2009)	40
Figure 2.11	Convex hull around data points (Kim et al., 2000)	41
Figure 2.12	Straightness error evaluation (Cui et al., 2013)	45
Figure 2.13	Flatness error evaluation (Cui et al., 2013)	46
Figure 2.14	The inspection path planning for CMM (Zhang et al. 2000)	47
Figure 2.15	Integrated inspection planning strategy (Cho et al., 2005)	52
Figure 2.16	The Computer aided inspection planning system (Elmarghy and Gu, 1987)	53
Figure 2.17	Inspection framework using CMM and laser scanner (Zhao et al., 2012)	54
Figure 3.1	Schematic of R3D2 entry-level AM Printer	55
Figure 3.2	(a) 30x30x30 mm cube (b) Measurement direction for cube along x, y and z direction	65
Figure 3.3	(a) Circularity Tolerance (b) CMM Measurement	69
Figure 3.4	Variation of linear dimension, diameter and circularity for six standard cubes	70
Figure 3.5	(a) Stepped blocks with globbing (b) Stepped blocks with clean surface	71
Figure 3.6	(a) Multiple cubes (b) Zoom view showing strings at the edges (c) Cubes with clean edges and surface	72
Figure 3.7	Assembled Knuckle Joint	73
		74

Figure 3.8	Sculpture model of Visvesvaraya	74
Figure 3.9	(a) 80mm/s speed (b) 100 mm/s speed with little distortion (c) Part with 120 mm/s speed with maximum warpage	75
Figure 3.10	Open cubes printed with raft having no warpage	76
Figure 3.11	Calibration plate showing oozing defect	76
Figure 3.12	(a) Circularity deviation of ten holes (b) 3D printed grinding	77
Figure 3.13	Position of measure angles in ramp plate for angular deviation	78
Figure 3.14	Angular tolerance of parts printed with different angles	78
Figure 3.15	Bevel gear model with small surface blemishes	79
Figure 3.16	Test sample for GD&T error analysis. (All dimensions in mm)	82
Figure 3.17	Normal plot residuals for Circularity C_1	85
Figure 3.18	Normal plot residuals for Flatness F_1	85
Figure 3.19	Normal plot residuals for Flatness F_2	86
Figure 3.20	(a) Case study (b) Cubes printed with AM machine	89
Figure 4.1	Laser triangulation principle (α_s is incident scanning angle)	92
Figure 4.2	Adopted methodology for optimum scanning parameters determination	93
Figure 4.3	Standard deviation of various measurements at different incidence angles	94
Figure 4.4	(a) Contour plot of angle-distance (b) Surface plot of angle-distance relation	97
Figure 4.5	Measured and predicted standard deviation of randomly chosen distance-angle values	97
Figure 4.6	Flowchart of classical particle swarm optimization (PSO)	103
Figure 4.7	Flowchart of modified particle swarm optimization (MPSO) algorithm	107
Figure 4.8	Visualization of (a) sphere (b) Rosenbrock parabolic valley benchmark function	108
Figure 4.9	Visualization of Rastrgin benchmark function	109
Figure 4.10	Visualization of Goldstein-Price benchmark function	110
Figure 4.11	Convergence for benchmark function using PSO and MPSO	112
Figure 4.12	Convergence of MPSO for optimization of scanning process	115
Figure 4.13	(a) Case study (b) Optimized parameters result using developed analytical model	116
Figure 4.14	(a) Case study 2 (b) Optimized parameters result using developed analytical model	117
Figure 5.1	The Plaster of Paris socket model (left), 3D scanning arrangement (right)	121
Figure 5.2	Flowchart of CATIA study	124
Figure 5.3	Methodology applied for surface generation	129
Figure 5.4	Plot between mean deviation and number of faces	130
Figure 5.5	Plot between mean deviation, surface detail and number of surfaces	130
Figure 5.6	Proposed methodology for Solidworks study	132
Figure 5.7	Plot for smoothing factor effect	133
Figure 5.8	Developed model using (a) CATIA V5 (b) Solidworks software	134
Figure 6.1	Straightness error by minimum zone method	138
Figure 6.2	Schematic for determining circularity error using MZC	139
Figure 6.3	Schematic for determining cylindricity error using MZC	140

Figure 6.4	Convergence of PSO and MPSO algorithm for straightness error evaluation	143
Figure 6.5	Average Straightness error versus dataset size ($0 < \text{dataset} < 500$) using bootstrap methodology for example 1	143
Figure 6.6	Convergence of PSO and MPSO algorithm for Flatness error evaluation	145
Figure 6.7	Average Flatness error versus dataset size ($0 < \text{dataset} < 500$) using bootstrap methodology	145
Figure 6.8	Convergence of PSO and MPSO algorithm for Circularity error evaluation	147
Figure 6.9	Average Circularity error versus dataset size ($0 < \text{dataset} < 500$) using bootstrap methodology	147
Figure 6.10	Convergence of PSO and MPSO algorithm for Cylindricity error evaluation	148
Figure 6.11	Average Cylindricity error versus dataset size ($0 < \text{dataset} < 500$) using bootstrap methodology	149
Figure 7.1	Proposed framework for GD&T features and free-form surface verification in contactless scanning system	153
Figure 7.2	Proposed benchmark part with nomenclature	157
Figure 7.3	Benchmark part with three similar spheres for establishing common reference system	159
Figure 7.4	Sphere matching for part alignment	160
Figure 7.5	Sphere radius variation for part alignment	160
Figure 7.6	Path for accurate surface reconstruction (a) CATIA v5 (b) Solidworks	162
Figure 7.7	Surface (a) CATIA v5 (b) COMET PLUS (c) Scan-to-3D	162
Figure 7.8	Proposed flowchart of the experimental procedure	165
Figure 7.9	(a) Stepped bar (AM part) selected as case study (b) Definition of part reference frame	166
Figure 7.10	Deviation chart of COMET data 1st alignment vs. the theoretical STL model	167
Figure 7.11	Average distance distribution for second replication in 2nd alignment of COMET data	170
Figure 7.12	Average distance distribution for second replication in 3rd alignment of COMET data	171
Figure 7.13	Average distance distribution for second replication in 4th alignment of COMET data	171
Figure 7.14	Average deviation comparison using contact and non-contact (CATIA v5) scanning	173
Figure 7.15	Average deviation comparison using contact and non-contact (COMET PLUS) scanning	173
Figure 7.16	Average deviation comparison using contact and non-contact (Solidworks) scanning	174
Figure 7.17	(a) Distance comparison of benchmark part for (b) vertical (c) horizontal planes (d) angular planes	175
Figure 7.18	GD&T results for (a) CATIA and (b) COMET PLUS developed surface	178
Figure 7.19	GD&T results2 for (a) CATIA and (b) COMET PLUS developed surface	179
Figure 7.20	Circularity comparison of the reconstructed surface	179

List of Tables

Table 2.1	AM process terminology and definitions (ASTM, 2012)	16
Table 2.2	Summary of process parameter optimization in FDM	29
Table 2.3	Summary of published work on scanning parameters investigation	34
Table 2.4	Summary of methods used for geometric error evaluation	48
Table 2.5	Summary of literatures on inspection process planning	56
Table 3.1	Technical Specifications of ELAM systems	64
Table 3.2	CAD part fabrication using R3D2 printer	66
Table 3.3	Linear Dimension, diameter and circularity measurement of standard size cube	69
Table 3.4	Problem, cause and corrective action	80
Table 3.5	Factors and their levels	82
Table 3.6	Experimental run using L_9 orthogonal array	82
Table 3.7	ANOVA for the Circularity (C_1) model	84
Table 3.8	ANOVA for the Flatness (F_1) model	84
Table 3.9	ANOVA for the Flatness (F_2) model	84
Table 3.10	PSO parameters	87
Table 3.11	Optimal process parameters with different weighting factors	88
Table 3.12	Experimental validation of the developed model	89
Table 4.1	ANOVA results for chosen cubic model	96
Table 4.2	Comparison of simulation results for benchmark functions	111
Table 4.3	Comparison of std. dev. prediction using Analytical, PSO and MPSO results	114
Table 4.4	Case study results for three RE models of case study 1	116
Table 4.5	Case study results for three RE models of case study 2	117
Table 5.1	Filtering results for point data using homogeneous filter and adaptive filter	125
Table 5.2	Results obtained after smoothing effect	127
Table 5.3	Filtering process output for point cloud data	132
Table 5.4	Comparison of the reconstructed models	135
Table 6.1	Parameters used for PSO and MPSO	142
Table 6.2	Results of straightness Evaluation (inch)	142
Table 6.3	Results of Flatness Evaluation (mm)	144
Table 6.4	Results of Circularity Evaluation	146
Table 6.5	Results of Cylindricity Evaluation	148
Table 7.1	COMET L3D scanner parameters (Pathak et al., 2016)	156
Table 7.2	Differently aligned point data comparison of COMET (in mm)	167
Table 7.3	Comparison of differently aligned point data (in mm)	168
Table 7.4	CMM inspection results with 3-2-1 alignment of COMET data (mm)	169
Table 7.5	Results of GD&T comparison	177

CHAPTER 1

BACKGROUND & MOTIVATION

Introduction

In recent times, growing global competition compels industries to explore new methods and tools for providing competitive products with better quality and reliability. The most important and challenging tasks encountered by manufacturing industry is shortening of product development cycle time. The conventional manufacturing processes are facing enormous difficulties to cope with the continuous changing competitive environment. Lately, the industrial focus has shifted from traditional manufacturing methods to advanced manufacturing technologies. With the evolution of advanced technologies like rapid tooling (RT), rapid manufacturing (RM) and additive manufacturing (AM), it has now become possible to design and produce products with complex profile and geometry. The use of AM technology have increased substantially in different industrial applications i.e. aerospace, automobile and biomedical engineering (Annex Business media, 2016; Gausemeier et al., 2011; Nayak et al., 2016) (see Figure 1.1).

AM fabrication follows layer-by-layer material deposition allowing the fabrication of intricate and freeform shapes with ease and simplicity. AM technology occupies a prime position in the rapid product development cycle thanks to significant time compression in part fabrication. In different industrial applications, AM fabricates products with high degree of geometric complexity without any additional expenditure as compared to conventional manufacturing processes like milling, injection casting, plastic and metal forming. According to Wohler's report, the market share for AM product and services has grown up to \$3.8 billion in 2015 from \$2.2 billion in 2012 (Wohlers, 2014). Figure 1.2 shows the specific application areas of AM with percentage distribution. However, large number of parts produced using AM are either scrapped or altered due to their lack in true reproducibility (Bandyopadhyay and Bose, 2015; Lindemann et al., 2012). In high value products such as turbine blades, it is mandatory to produce accurate dimensions and geometry with better quality for longer sustainability and energy efficiency. Therefore, it is desirable to improve dimensional

and geometric accuracy of parts manufactured for expanding the applicability of AM processes in industrial applications.

The above discussion forces a clamour within the industries to minimize various challenges and issues faced by AM technologies. Thus product inspection becomes important, to assess the quality of the part fabricated, in terms of geometric and dimensional tolerances (GD&T). In general, inspection is very time-consuming process which takes a lot of manufacturing lead time (Lee and Park, 2000; Son et al., 2002).

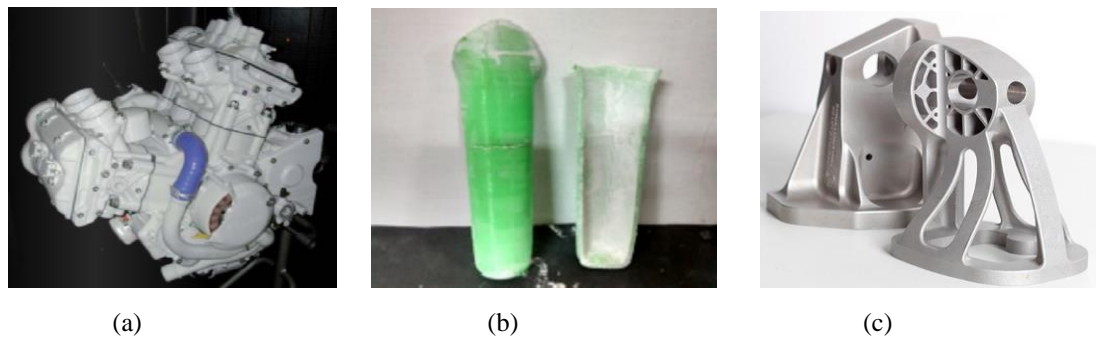


Figure 1.1 (a) Ducati engine made by AM technology (b) 3D printed prosthetic socket (c) 3D printed optimized Airbus A380 bracket

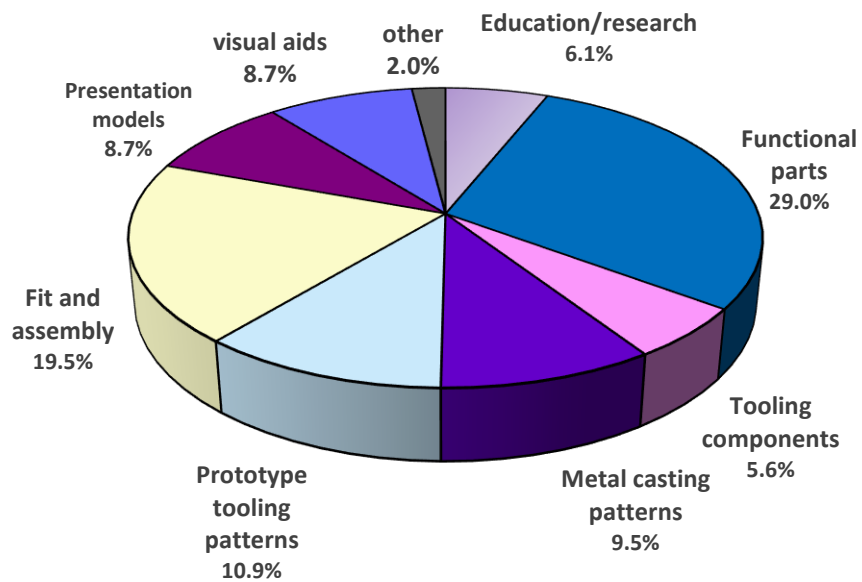


Figure 1.2. Additive manufacturing specific applications areas (Wohlers, 2015)

For effective inspection and evaluation of each part, its features need to be broken down in most primitive features. Further, a method or tool is required to measure these primitive features. Geometric Dimensioning and Tolerancing (GD&T) is a means

of defining part features by specifying the size, shape, form, position and location. The GD&T inspection process helps in examining the conformance of part features with actual design specifications defined in part drawings (Lee et al., 1997). GD&T was introduced to assure proper assembly among mating parts and to reduce cost incurred due to damage of improperly assembled parts. A reliable and effective inspection framework with iterative procedures will be highly useful for improving manufacturing flexibility, reducing the product manufacturing-to-market time and will enhance the product sustainability in market.

In industries, product inspection is usually a contact based operation performed using conventional gauges, templates and coordinate measuring machine (CMM). Generally, CMMs used are computer controlled and have high measuring accuracy. However, to achieve automatic measurement and improving inspection efficiency, numerous significant issues need to be tackled. The CMM inspection is inherently a time-consuming process as they have to make contact with part surface for each and every point that is sampled (Morini et al., 1998). Furthermore, inspection using CMM is a complex task that demands skilled operators as in most cases they do not possess easily identifiable reference features, demanding the use of special purpose inspection jigs. CMM inspection is not suitable for soft material parts as the touch probe can deform the part surface. For complete part inspection, it is required to obtain large amount of point data at fast speed. The potential of non-contact three dimensional laser scanners in obtaining thousands of points in seconds can provide a possible alternative to this problem. The accuracy of non-contact scanners is relatively lower as compared to contact type CMM measurement. Nevertheless, with the development of high resolution contactless scanner (such as Steinbichler COMET L3D), a measuring accuracy of 18 μm can be achieved (Steinbichler, 2016).

Besides the advancement in optical control of 3D laser scanners, there are many factors that affects the quality and overall accuracy of scanned data. It is important to determine these parameters which depends on morphology of part surface and find their optimum value. The optimum values can help in improving the accuracy of surface model developed using reverse engineering (RE). Thus, the inspection process can become more reliable and effective if the point data acquired are more accurate. Further, conversion of point data into accurate surface model is very critical step in RE process. For surface reconstruction, raw point data are processed through a number of steps such

as filtering, segmentation, mesh smoothing, surface fitting and generation. These steps can strongly influence the final accuracy of the developed three dimensional surface model. Thus, it is imperative to find an optimum balance between the best obtainable accuracy and maximum allowable deviation to lesser computer handling and processing time. After successful model reconstruction, inspection of the scanned part is important for conforming the geometrical and dimensional tolerances specifications provided at the design stage. Traditionally, the least squares method (LSM) is the most common used technique for form error evaluation in industry because of its simplicity in computation and uniqueness in solution. However, LSM does not adhere to the standards and does not guarantee the minimum zone solution, which may lead to overestimation of tolerances. Therefore, potentially functional parts can be rejected, resulting in an economic loss. So, there is need of an algorithm which can accurately determine these form errors and saving the time and cost involved during manufacturing process. The below sections deals with introducing the different areas of importance.

1.1 Additive manufacturing (AM) principles

Additive manufacturing (AM) technology follows a sequential layer-by-layer process of material deposition from a virtual CAD model, to develop a three-dimensional (3D) physical object. The technical committee formed within American Society for Testing and Materials (ASTM) (ASTM, 2012) and National Institute of Standards and Technology (NIST) coined the term additive manufacturing and succeeding processes terminology. AM process builds product by adding material, instead of removing material as opposed to conventional manufacturing processes like machining. It is therefore, inherently prevents the wastage of material as compared to traditional manufacturing methods. Additionally, AM can add multiple materials like Acrylonitrile Butadiene Styrene (ABS), Poly lactic acid (PLA), polycarbonate etc. in a single part and produce fully practical assembled mechanisms. Most of the materials mentioned above are difficult to process through traditional manufacturing techniques.

Although AM technology is gaining popularity among different industrial applications and have above mentioned advantages, but it has certain limitations in the area of dimensional and geometrical control. The parts manufactured should conform to the required geometric and dimensional tolerances specified in design stage.

Therefore there is a need to study various issues and process parameters affecting the quality of the parts manufactured by AM.

1.2 Reverse engineering (RE) principles

While a traditional engineering process begins with a design step, reverse engineering (RE) starts with digital capturing of the physical entities of the real part. In recent times, RE has reformed from skilled manual process into a significant industrial tool using sophisticated software and modern instruments. Currently, its application area has been changed from maintenance into the areas of designing, production and inspection of parts. The reverse engineering procedure is depicted in Figure 1.3, showing various stages from point cloud data to CAD model. RE is useful in situations when no part drawings are available and copy of that part is required. It will be helpful in cases when some design and modifications are required for improving the performance of the product. One of the important step in RE process is acquiring the actual shape data and maintaining the accuracy of reconstructed virtual model of physical part. The final quality of the reconstructed surface model highly depends on the type and accuracy of measured point data, as well as the type of measuring device.

Presently, there are different methods available for acquiring data shape (Varady et al., 1997). Essentially, each of the methods works on some specific principle and mechanism for collecting profile data of the object. Nowadays, two important methods used are contact based coordinate measuring machine (CMM) and non-contact 3D laser scanner. CMM uses a touch probe for acquiring point data by touching the part surface, such that it is suitable for primitive features measurement where small point data is required for defining the shape of the object. CMM touch probe is a very accurate method, however it is time consuming. As compared to laser scanners, CMM acquire point data with slow speed and it cannot be used for measuring parts made of soft material. In contrast, 3D laser scanners capture point cloud data at fast speed with precision. Some of the drawbacks of these systems are missing point data due to the occlusion. Occlusion defined as the blocking of laser beam due to obstruction and shadowing (Bradely and Currie, 2005). Also, inaccurate surface reconstruction due to the potential diffraction resulting from shiny or transparent surface. However, this problem can be eliminated by pre-processing the part surface with a white spray prior to 3D scanning.

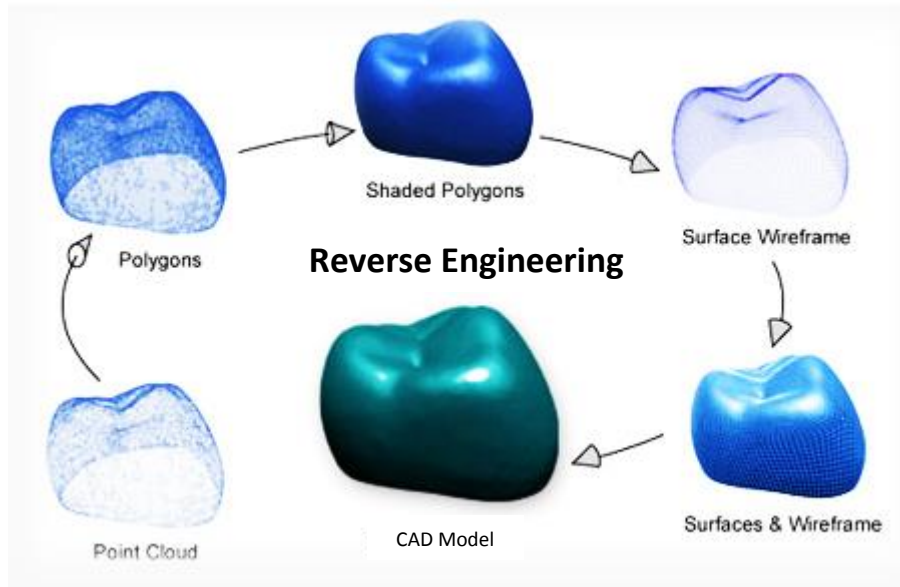


Figure 1.3. Reverse engineering process (Ke et al., 2001)

1.3 Geometric dimensioning and tolerancing (GD&T) inspection in industry

For AM process to be accepted as mainstream manufacturing process, parts fabricated must conform to the critical geometrical and dimensional tolerances specifications for different features of the part. For this reason, the AM process parameters selection becomes an important task which results in the development of GD&T errors in the parts manufactured. For most of the design and manufacturing industries, geometric dimensioning and tolerancing (GD&T) is quite a new domain. GD&T came into existence in 1966, when United States of America Standards Institute (USASI) documents were based on earlier standards and industry practices. Afterwards, some revisions occurred in the standards and the latest was ASME Y14.5M-2009 that specifies the proper application of GD&T (ASME, 2009).

In comparison to conventional tolerancing methods, GD&T used for proper locating and orienting part features. According to this standard, there are four parameters that geometry can control: form, size, angle and location. There are fourteen geometric characteristic symbols as shown in Figure 1.4, divided into five categories. The theoretical features that are used as reference and assumed to be exact is known as datum. Among all the geometric entities depicted in Figure 1.4, datum are used for all except for the form tolerances. Since the form tolerances are used for single features or

elements of single features. This work deals with only the form tolerance evaluation and its optimization. These form tolerances are defined as follows (Cogorno, 2006):

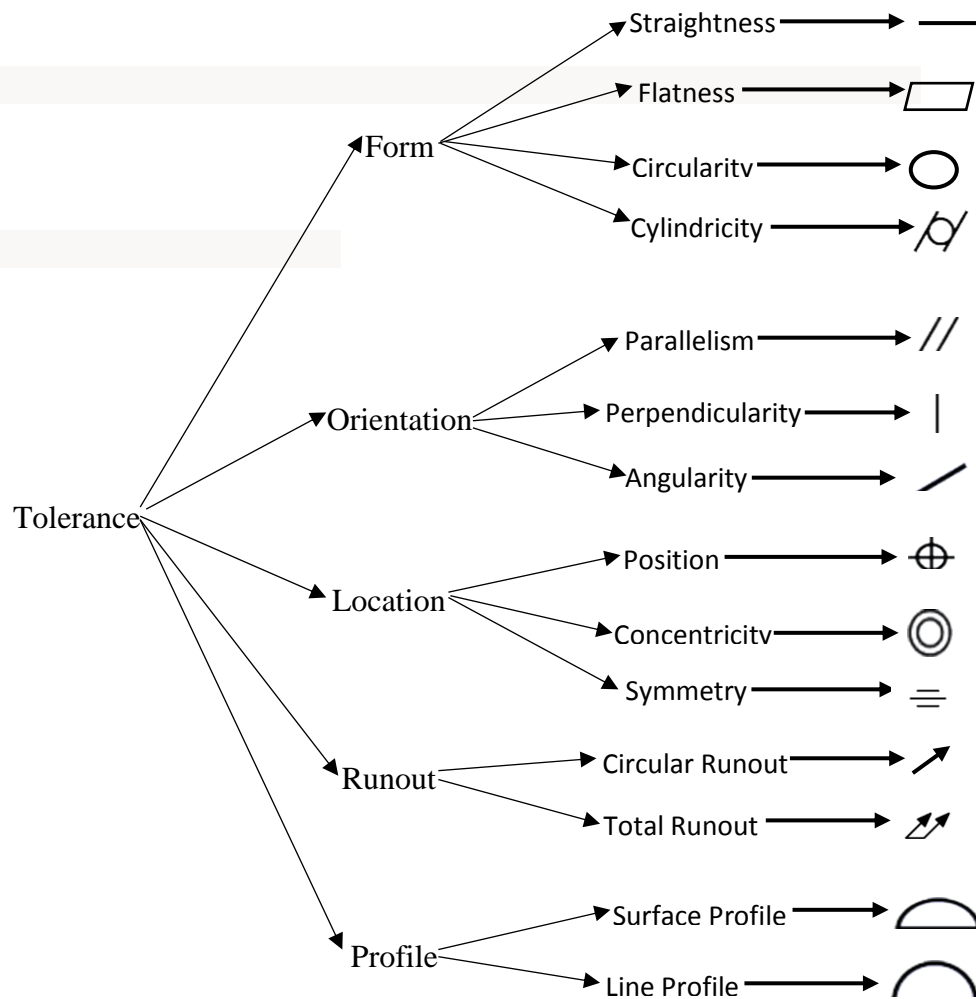


Figure 1.4. Tolerance with their geometric entities and symbols

1.3.1 Straightness

Straightness is a condition where a line element of a surface, or an axis, is a straight line. A straightness tolerance specifies a tolerance zone define by two parallel lines within which the considered line element must lie. Figure 1.5 shows an example of how the straightness tolerance is specified on drawing and what actually it means:

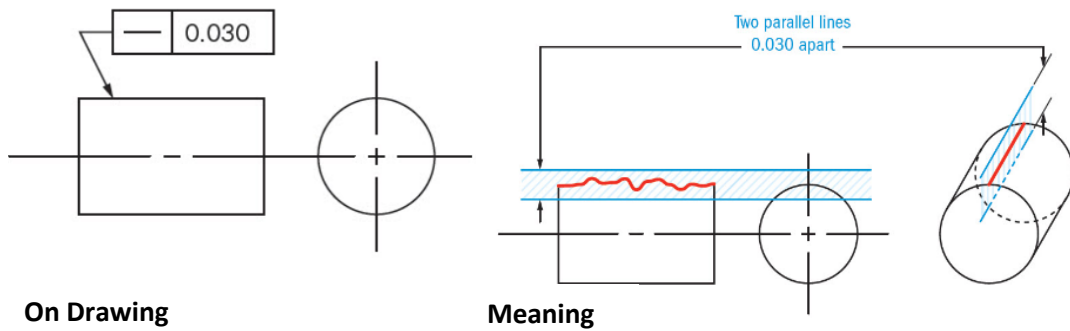


Figure 1.5. Straightness Tolerance description

1.3.2 Flatness

Flatness is a condition of the surface having all elements in one plane. A flatness tolerance is specified by two parallel planes within which the surface must lie. An illustration of flatness tolerance is shown in Figure 1.6 on how the flatness tolerance is specified on drawing and what actually it means:

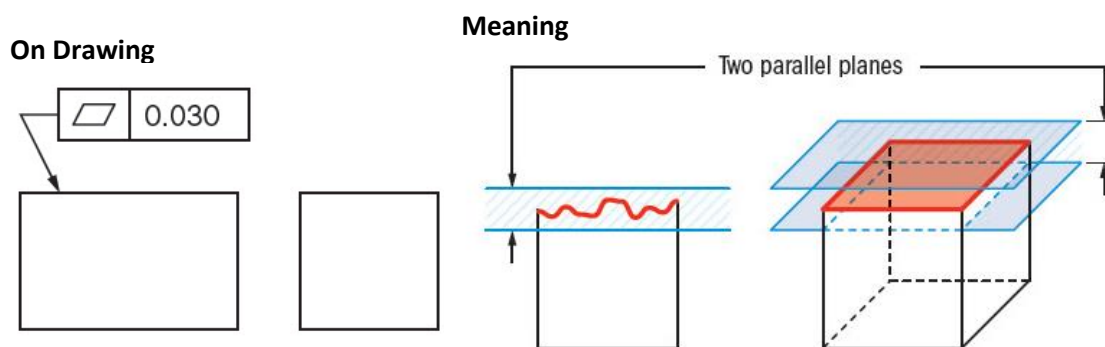


Figure 1.6. Flatness Tolerance description

1.3.3 Circularity

Circularity is the condition of the surface where:

- (1) For sphere, all points of the surface intersected by any plane passing through a common center are equidistant from that center.
- (2) For non-spherical features, all points of a surface intersected by any plane perpendicular to any axis are equidistant from that axis.

Circularity tolerance is defined as the area between two concentric circles within which all the point of surface must lie. The illustration of circularity tolerance is shown in Figure 1.7.

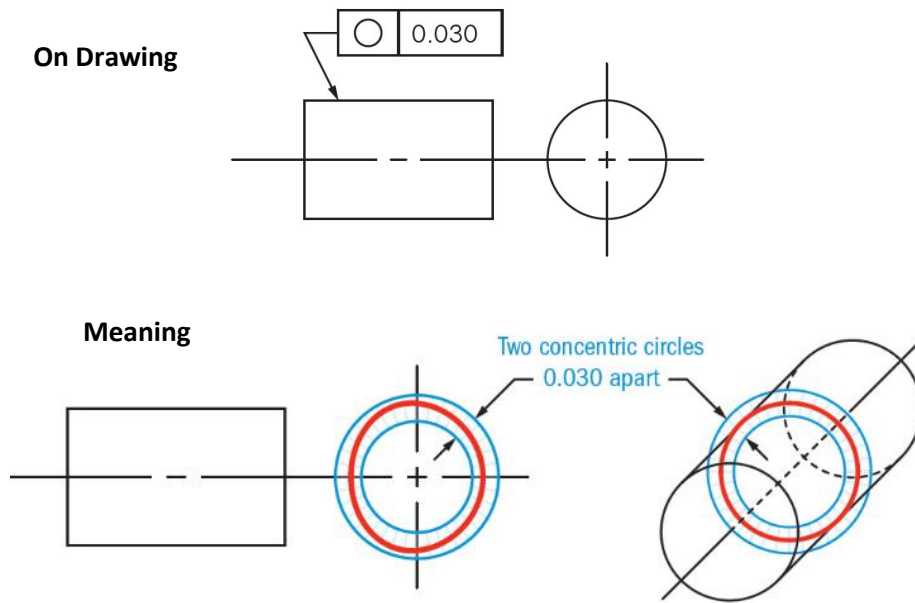


Figure 1.7. Circularity tolerance description

1.3.4 Cylindricity

Cylindricity is defined as the condition in which all the points of the surface are equidistant from a common axis. Cylindricity tolerance specifies a tolerance zone bound by two concentric cylinders within which the surface must lie. The illustration of cylindricity tolerance zone is depicted in Figure 1.8.

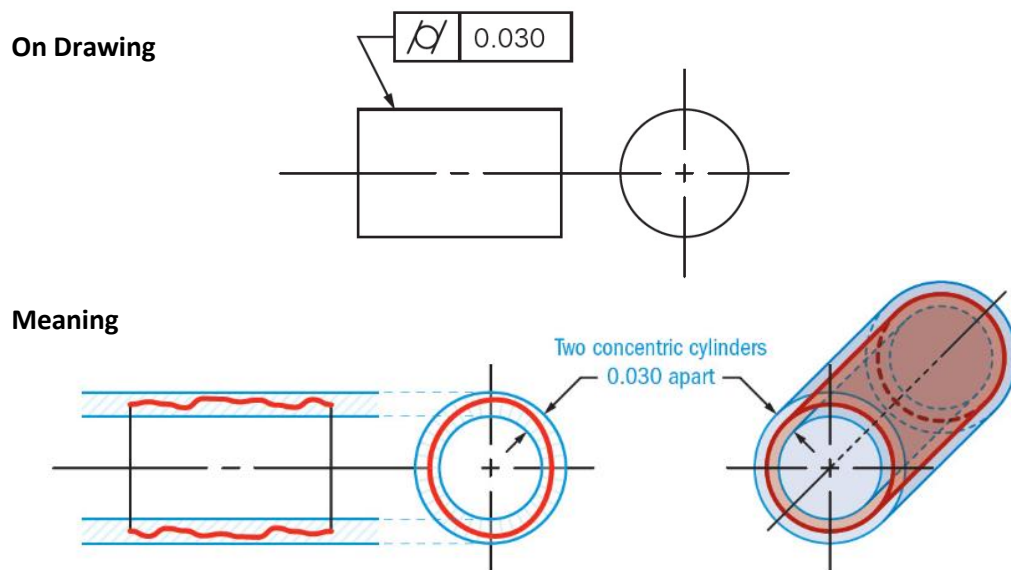


Figure 1.8. Cylindricity tolerance description

1.4 Motivation of Research

In general, products are consist of several key components, manufactured individually and then assembled. Tolerances are provided at the design stage to each individual components dimensions for manufacturing variability and also it allows interchangeability in assembly. In case of additive manufacturing (AM), the product specification is achieved by producing near net shape 3D parts with complex features and inclined structures, difficult to manufactured using conventional machining and casting methods. Near net shape parts fabricated using AM can allow for achieving critical tolerances, making it of particular interest for aerospace and biomedical applications. The optimal selection of process parameters and minimizing various issues can help in fabrication of accurate parts for industrial applications. Recently, with the advent of new manufacturing technologies, AM parts are gaining importance due to its complexity and market demand. Since the solid to layer (STL) file required for AM fabrication is tessellated and approximated version of the CAD model. It produces the approximate geometry of the part with some errors. Therefore, AM parts need to be inspected in order to examine their quality in terms of geometrical and dimensional tolerances. Evaluation of established GD&T errors in manufactured components is indispensable for determining the conformance to tolerance specifications. Most of the methods used for determining the GD&T error are based on Least Square Method (LSM). However, the LSM algorithm results in overestimation of the tolerance forcing the bad parts to be accepted. Thus, there is a need of efficient algorithm for evaluating more precise tolerances. Optimization of mathematical equations can be the answer for evaluating exact tolerances.

However, complex parts produced by AM is restricting the use of conventional touch probe measuring instruments. Even though the CMM used for inspection is highly accurate in comparison to non-contact 3D scanners. The parts fabricated by AM does not require tight tolerances, so contactless 3D scanners are useful for inspection as they have high acquisition speed. Furthermore, the surface texture of AM parts can restrict the use of touch probe as the probe can slip from one stair to other due to inherent staircase effect in AM parts. Subsequently, the contact based measurements and inspection could be inaccurate for AM parts. In contrast, the contactless optical scanner can easily measure and inspect the parts without requiring any jigs and fixtures for part holding.

Moreover, the optical scanner parameters can play significant role in improving the final accuracy of acquired data. Among other factors, the final quality of acquired data not only affected by the scanner accuracy, but it also depends on the critical steps and their parameters used during point cloud data to CAD model reconstruction. Therefore, all the above steps becomes highly important for the successful measurement and inspection of AM parts. The main requirement of an inspection plan is the capability to provide the desired precision and accuracy in the measurement with low cost and time. Thus keeping in mind above discussions, there is a definite clamour among the industries to develop a detailed, iterative and systematic inspection plan framework. The research presented in this thesis aims a step closer towards the development of framework for AM parts using reverse engineering.

1.5 Thesis Statement

This thesis presents a GD&T based inspection planning framework for parts with GD&T features using non-contact laser scanners system. The main aim of the research is to improve the accuracy at each and every step of inspection framework, beginning with manufacturing to the final model developed. At last, a benchmark part is proposed for characterizing the accuracy commercial scanner accuracy. Unlike previous works, this thesis begins with improving the accuracy issues in additive manufactured parts. The next step is improving the accuracy during scanning of part surface by optimizing the morphological process parameters. Furthermore, for accurate surface reconstruction from unorganized point clouds, an optimum path is determined. After successful model reconstruction, the GD&T error in the part is evaluated using different nature inspired algorithms, particularly particle swarm optimization and its improved variant. Finally, a benchmark part with different geometric features is proposed for performing and testing the developed procedure and framework for effective and reliable inspection.

1.6 Thesis Organization

This thesis contains seven chapters arranged as follows:

Chapter 1: Introduction

The background, motivation, and significance of the research work to develop an inspection framework for effective and accurate inspection in industries are presented in this chapter. It also highlights the outlines the organization of the thesis.

Chapter 2: Literature Survey

This chapter includes a literature review on various challenges and issues related to AM. Followed by advances in 3D scanning systems and optimal parameter selection for data capturing. Further, discussion over accuracy control during conversion of raw point cloud data to three dimensional (3D) surface model is presented. The discussion is followed by GD&T error evaluation and optimization methods for effective inspection of AM parts.

Chapter 3: Minimization of Additive manufacturing challenges and issues

This chapter discusses various issues related to AM machines and the corrective actions to eliminate these issues for producing improved quality products. From the models printed as part of current evaluation it was observed that only one out of ten revealed warping symptoms. Additionally, this chapter deals with the optimal AM part production with minimum GD&T error so that part build by AM can be functional and used in industrial applications.

Chapter 4: Data acquisition using optimum scanning parameter

This chapter identified and explained that morphology of scanned surface is an important factor to be considered for high quality output in 3D scanning processes. Based on surface morphology, two critical parameters were identified and their influence on final accuracy of scanned model was studied. The drawbacks of classical PSO was determined and an improved variant of particle swarm optimization i.e. MPSO is proposed for improved results.

Chapter 5: Methodology for accurate surface reconstruction

For accurate surface reconstruction two unified solutions using different CAD methodologies for modelling and analysing a freeform surface from a raw unorganized point cloud is proposed.

Chapter 6: GD&T error evaluation using PSO and MPSO

This chapter deals with the determination of different GD&T error that incurred during manufacturing of the part. A simple objective function for form tolerance evaluation was formulated as an unconstrained optimization problem. Compared to conventional

or existing heuristics optimization methods, the proposed MPSO algorithm not only has the advantage of a simple realization in computers and good flexibility, but it was shown to have improved the form error evaluation accuracy.

Chapter 7: Development of framework for contactless inspection and GD&T verification

This chapter proposes a novel and iterative framework for accuracy control and effective inspection using contactless scanning. To validate the proposed framework, a benchmark part consisting of canonical features for the GD&T verification of contactless laser scanning was proposed.

Chapter 8: Conclusions and Future Scope

The results obtained in this research work are summarized in this chapter. It also addresses the contribution and future scope of the research work.

1.7 Chapter Summary

This chapter begins with a background followed by a brief introduction of additive manufacturing, its applications and advantages. Further reverse engineering principles with its importance in industrial applications is discussed. The significance of geometric dimensioning and tolerancing for inspection in industries is presented. The motivation behind developing an iterative and detailed inspection plan is presented here. At last, brief information about various chapters is discussed.

CHAPTER 2

LITERATURE SURVEY

This chapter presents an extensive literature survey which provides background information on the research topics of the present investigation. Since, the present work emphasis is on the metrology of industrial parts produced by advanced manufacturing processes, this chapter summarizes overview of different advanced manufacturing technologies like additive manufacturing (AM), various challenges and issues related to AM, followed by advances in 3D scanning systems for quality inspection and need for optimal parameter selection in data capturing. Further, discussion over accuracy control during conversion of raw point cloud data to three dimensional (3D) surface model is presented. The discussion is followed by GD&T error evaluation and optimization methods for effective inspection of industrial parts. At last, inspection planning procedures for quality inspection in industries are discussed. The topics briefly reviewed all the relevant literature and still needs further research to minimize the above covered challenges and issues for industrial applications.

The literature was classified on the following basis:

2.1 Additive manufacturing challenges – geometrical issues and process parameter optimization

2.2 Optimum Parameter selection in 3D scanning process

2.3 Surface reconstruction from point cloud data to accurate surface model

2.4 GD&T error evaluation and optimization

2.5 Inspection planning, procedures and development of benchmark part for scanner characterization

At the end of the chapter a summary of the literature survey and the knowledge gap in the earlier investigations are presented.

2.1 Additive manufacturing challenges - geometrical issues and process parameter optimization

2.1.1 Overview of AM process

With the inception of advanced manufacturing technologies, and with increasing customer demands for customized parts and services, there is a significant rise in manufacturing scaling and distribution (Huang et al., 2013; Lipson, 2012). AM term is coined by ASTM F42 technical committee, responsible for development of AM technology and standards. Additive manufacturing (AM) is an advanced manufacturing process used for joining materials to make objects from 3D model data, usually layer by layer (ASTM, 2012). The AM parts are fabricated by succeeding cross-sectional layers through bottom to top. The cross-sectional layers thickness can vary from object to object (see Figure 2.1). The AM process initiates with the 3D virtual model, either scanned or modelled as a CAD or STL file and then sliced into number of layers along the direction of fabrication (Gibson et al., 2010). The slicing process is performed, depending upon the resolution, using a suitable preparation software like Cura, slic3r etc. The processed file is fed to the machine to form a printed primitive layer by layer. After a part has been printed, necessary post processing methods (Yoon et al., 2014) can be used in order to bring the accuracy of part closer to the actual model.



Figure 2.1 Layer variation in AM process (Gibson et al., 2014)

Table 2.1 AM process terminology and definitions (ASTM, 2012)

S. No.	AM terminology	Technology	Definitions
1	Material jetting	Polyjet/inkjet printing	Process in which droplets of build material are selectively deposited.
2	Directed energy deposition	Laser Engineering Net Shape (LENS), Direct Metal Deposition (DMD)	Process focused on thermal energy is used to fuse materials by melting as they are being deposited.
3	Powder bed fusion	Selective Laser Sintering (SLS)	Process in which thermal energy selectively fuses regions of a powder bed.
4	Binder jetting	Indirect inkjet Printing	Process in which liquid bond agent selectively deposited to join powder materials.
5	Vat photopolymerization	Stereolithography (SLA)	Process in which liquid photopolymer in a vat is selectively cured by light-activated polymerization.
6	Sheet lamination	Laminated Object Manufacturing (LOM)	Process in which sheets of material are bonded to form an object.
7	Material Extrusion	Fused Deposition Modelling (FDM)	Process in which material is dispensed through nozzle or orifice.

AM technology has been in use since the early 1980s. In 1991, various additive manufacturing processes were classified as powder-based, liquid-based and solid-based systems (Kruth, 1991) based on the different types of materials for part fabrication. Further, various AM processes and systems using a functional classification scheme has also been presented (William, 2014). Most recently, ASTM has provided seven categories for AM process with their terminology and definition as shown in Table 2.1.

2.1.1.1 Material Jetting process

Material jetting is similar to the inkjet printing in which droplets of wax or photopolymer material are selectively deposited through an orifice to build a 3D artefact (Calvert, 2001; Gans et al., 2004; Stucker, 2012). In material jetting process, material droplets are created using two different modes: (1) Continuous inkjet (CIJ) and (2) Drop on demand (DoD). Generally, CIJ systems are used at places where high printing speed is required. In contrast, DoD is used where higher accuracy along with small droplets are required (Vaezi et al., 2013). A lot of research have been done in the field of direct ink jetting, which suggests that different parameters and factors are responsible for improving the quality of ink jetting process.

The material jetting process can successfully print with multi-materials as well as functionally graded materials (FGM). Several researchers have applied inkjet printers for printing structures using different FGM materials. In the late 90s, one dimensional FGM based structure was printed using a thin zirconia-alumina (Mott and Evans, 1999; Wang and Shaw 2006). Some of the studies reported modifies the design and fabrication of commercial inkjet printers for printing multi-materials (Ibrahim et al., 2006; Xie et al., 2010). Researchers have used this process successfully for different applications such as wearable products (Yap and Yeong, 2014), functional lightweight honeycombs (Yap and Yeong, 2015) and scaffolds (Naing et al., 2005). Besides, the advantages discussed above, the material jetting process growth is clogged by the limited choice of materials such as wax and photopolymer are only commercially available materials. The other drawback is the part accuracy which is not as good as material extrusion process.

2.1.1.2 Directed Energy Deposition

Directed energy deposition (DED) process uses a focused thermal energy (laser beam) for creating a molten pool and subsequently fusing the material as it is being deposited (Kakinuma et al., 2016). The multi-axis table is rastered to develop the cross-section of each layer. The laser head is incremented upwards until all the desired cross-sectional slices of the part are created and 3D model is developed (see Figure 2.2). There are different types of DED technology available, which includes Direct Light Fabrication (DLF), Laser Engineered Net Shaping (LENS), Direct Metal Deposition (DMD) (Lewis et al., 1994; Keicher and Miller, 1998). The DED process include wire as well as powder feeding mechanisms for material delivery. A wide choice of materials and alloys are used for fabrication of parts using DED process. The printed materials accommodate metals like stainless and tool steel, nickel base-super alloys, titanium and chromium based alloys and composites (Schwendner et al. 2001; Banerjee et al., 2003; Krishna et al. 2008).

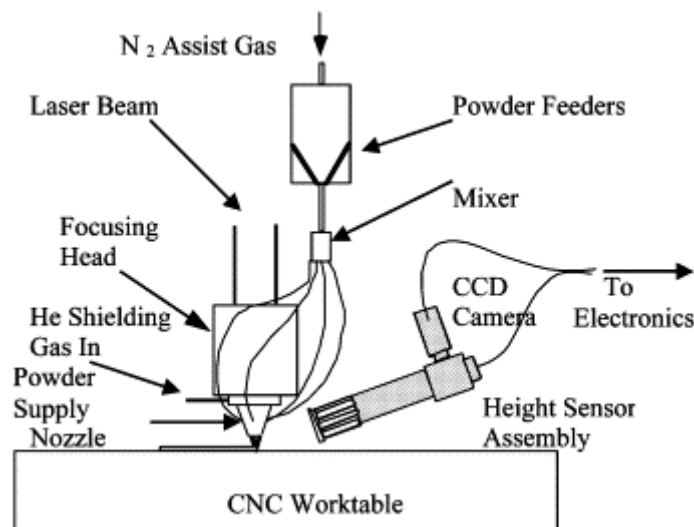


Figure 2.2. Schematic of Directed energy deposition (DED) process (Shin et al., 2003)

The process parameters responsible for improving the quality of DED process includes powder flow rate, laser diameter, scanning rate, laser power (Laeng et al., 2000). Recent research shows that powder material characteristics is also a key factor in improving the quality of printed part (Kakinuma et al., 2016). The prime advantage of this process is its controlling ability in the microstructure of build parts. Another advantage of this process is in improving the tribological properties of printed parts by allowing coating to the surfaces (Wilson et al., 2013). One of the important application

of DED is the repair and feature addition of parts like turbine blades (Wilson et al., 2014). Besides these advantages, the main limitations of DED processes include poor surface finish and resolution. The surface roughness of 25 μm and lesser is difficult to achieve by using all DED processes (Gibson et al., 2014). Furthermore, the build speed of the print is very slow as the material deposition rates are very low (Cooper, 2001; Gibson et al., 2010).

2.1.1.3 Powder Bed Fusion

Powder bed fusion process is one of the first commercialized AM processes. This process used a thermal source to melt and fuse the powder particles of metal, ceramics and polymers into the desired patterns (Stucker, 2012). Some of the most popular powder bed fusion systems known are Selective Laser Sintering (SLS), Selective Laser Melting (SLM) and Electron Beam Melting (EBM). The SLS and SLM system employs laser source while EBM uses a scanned electron beam (Kruth et al., 2005; Buchbinder et al., 2011; Murr et al., 2012). Several studies have been reported for determining the process parameters (over 50) characterizing the bed fusion processes. The process parameter can be categorized into mainly four groups namely, laser related, scan related, temperature related and powder related parameters.

2.1.1.4 Binder Jetting

In the early 1990s, binder jetting methods based on ink jet technology was introduced in Massachusetts Institute of Technology (MIT) and commercialized by Z Corp. and Ex one. The process deals with printing a binder in to powder bed to build a structure. The binder droplet helps in sticking the powder material together providing desire shape to the part. Once this step is complete, it is followed by lowering the powder bed and new layer is deposited and again the above process is repeated (Sachs et al., 1992). A wide choice of materials are processed through binder jetting process such as metals (Williams et al., 2010), foundry sand (Snelling et al., 2013), ceramics (Yoo et al., 1993), and polymers (Lam et al., 2002; Leong et al., 2003; Lee et al., 2005; Tay et al., 2007). Distinguished researchers have worked on binder jetting process involving different applications. One of the main applications include scaffold development (Sherwood et al., 2002), The prime significance of this process is fast build time of parts as very less amount of material is dispensed through orifice. Additionally, the combination of metal powder and additive in binder enables material composition not easily achieved by

other AM processes (Gibson et al., 2010). However, the parts printed employing the binder jetting process have inferior accuracy and poor surface finish as compared to parts of material jetting process.

2.1.1.5 Vat photopolymerization

In the early 80s, C. Hull introduced first AM system commercially based on SLA process. SLA is the main photopolymer method in which ultraviolet laser is used to polymerize the UV curable resin selectively, layer by layer (Cooper, 2001; Noorani, 2006) as shown in Figure 2.3. Most of the research found for this process involves the processing of ceramics (Chartier et al., 2008; Bian et al., 2012; Chopra et al., 2012). The process of vat photopolymerization is widely used in different applications like dental fillings, ear hearing aids and scaffolds (Bartolo, 2011; Serrine et al., 2015).

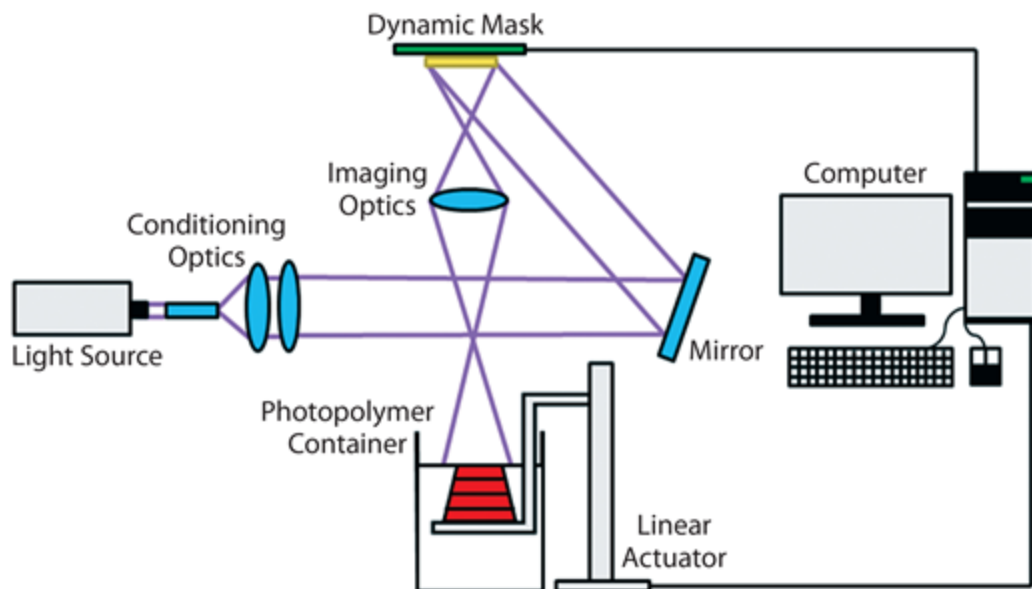


Figure 2.3 Schematic of Vat photopolymerization process (Chartrain et al., 2016)

The prime advantage of this process is its high resolution and ability to fabricate complex objects. However, main limitation of this process is its inherency to use only photopolymers. Further, some of the more problems reported by different studies includes errors due to overcuring, scanned line shape, trapped volumes and shadowing obstruction of earlier build layers (Kim et al., 2011; Wong and Hernandez, 2012; Choi et al., 2011).

2.1.1.6 Sheet Lamination

The sheet lamination additive manufacturing is the process in which sheets of material are bonded to form an object. There are two systems that has been commercialized yet are Laminated Object Manufacturing (LOM) and Ultrasonic Consolidation (UC) (Mueller and Kochan, 1999; Ram et al; 2007). Usually, the sheet lamination AM processes was used to fabricate metal parts stacking, cutting, and gluing outlined metallic laminates. In the late 1990, few studies reported the first laminated tooling sheets for sheet metal fabrication (Himmer et al., 1999). Several researchers have tried to enhance the laminated bonding (Wimpenny et al., 2003; Janaki Ram et al., 2006) with reduced stair step effects (Walczyk and Yoo, 2009).

2.1.1.7 Material Extrusion

AM machines based on material extrusion deposit material through nozzle by pressure created using tractor-feed system in continuous layer form to fabricate objects. Fused deposition modeling (FDM) is among the most widely used AM process (Wohlers, 2011). The FDM based printer was developed by Stratasys in 1988 that produced sliced layers by extruding molten thermoplastic material (Bernard and Fischer, 2002; Noorani, 2006; Kai et al., 2010). FDM process used amorphous thermoplastics for part manufacturing having acrylonitrile butadiene styrene (ABS) being the most common. The other materials available in market for FDM process are poly lactic acid (PLA), polyimide, and polyphenylsulfone.

The gradual expiring of a few valuable patents in 2009 offers a level playing field for the technology innovators to incubate, alter or harness the FDM process (Gridlogics, 2014). FDM based AM process schematic is shown in Figure 2.4. In FDM process, material is melted and flow through liquefier head and passed through the nozzle. Further, the material is deposited layer by layer as shown in below Figure. The FDM process is clean, safe, and highly automatic and also produces minimum waste. Other FDM advantages includes easiness of support removal, short cycle time, easy integration with CAD software. These features make it appropriate for variety of applications (Chua et al., 2010; Ingole et al., 2009; Elliot et al., 2013). Lately, a new trend in FDM has emerged, which can be referred to as entry level additive manufacturing (ELAM) that is comparatively inexpensive, desktop sized and usually have an open chamber (Lotz et al., 2012).

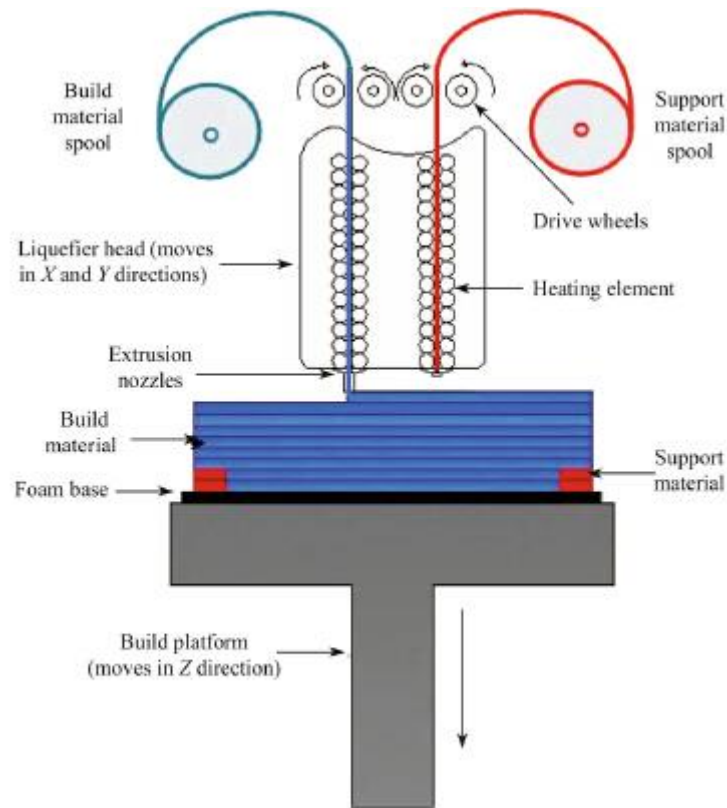


Figure 2.4 Schematic diagram of FDM based AM process

These devices are gaining importance among higher education institutions and product developers unable to afford a professional system. The entry level (EL) systems can be developed using existing tools and expertise as compared to the development of full-fledged AM system (Malone and Lipson, 2007). One of the key characteristics of the ELAM is that lots of tutorials and blogs are available on the internet for sharing and exchanging ideas among users and developers to account for betterment of the machine. Despite the increasing importance of ELAM machines in different fields, very little research has been undertaken to study various quality issues or limitations in use of these machines. Due to these aspects, this thesis concerns FDM based study in particular, as it has caught hold in the hobbyist and do-it-yourself communities with the availability of low-cost machines that are approaching the part quality capabilities of commercial machines.

2.1.2 Challenges and issues in FDM based parts

Due to the recent expiry of patents on FDM based printers, very little research have been performed till date (Crump, 1992). Further, the main sources of error developed during material deposition in FDM systems are tessellation related, process related and

materials related (Yan and Gu, 1996; Bochman et al., 2015). The tessellation errors arises due to approximation of part surfaces in the standard file input. Prior to fabrication, the part is pre-processed which includes the instructions for extruder path generation and part building. Usually, the standard file format used for part fabrication for most of the printing process is Stereolithography (STL) (Navangul et al., 2013). The STL file format is the approximated representation of nominal surface model in form of triangles, depending upon its positioning and geometry as shown in Figure 14. Thus, the part build using the approximated STL file results in inaccuracy, especially in curved surfaces (Ahn et al., 2009; Moroni et al., 2014). Additionally, the missing triangles or redundant faces can also result in errors (Tong, 2003).



Figure 2.5 Conversion of CAD model (left) into STL model (right) for FDM fabrication (Gibson et al., 2010)

The process related errors were influenced by two linear movements of extruder. First motion along x-y plane affect the form of the layer due to translation motion of the extruder head and second motion along the z-axis due to the subsequent bonding of different layers (Song et al., 2014). Different studies have been reported in FDM for material related errors such as shrinkage, warpage etc that affect the geometric accuracy. The shrinkage is referred to as a by-product result of solidification after cooling down of the material with FDM processes. Shrinkage contributed to a weak interlayer bonding, high porosity and hence reduces load bearing area (Es-said et al., 2000). It is important to add possible dimensional shrinkage that can be compensated by scaling the CAD model. Few studies have suggested that the shrinkage level can vary from bottom to top throughout the part (Es-said et al., 2000; Sun et al., 2005). Consequently, shrinkage is maximum in bottom most layer and it decrease as the model is built (Pandey et al., 2004). The main reason is that the bottom layer is free to contract

and as a result it is free to contract. But as the part built, the upper layer contraction is restricted by the earlier printed layer, enabling less contraction (Islam et al., 2013; Islam et al., 2016). Further, Guralla and Regalla (2014) investigated shrinkage and concluded that, for lower shrinkage value material deposition should be lower in the horizontal direction and optimal setting for the vertical direction.

Due to shrinkage, internal stresses are developed due to contraction in deposited layers during its fabrication, results in part deformation or warpage. Warpage has an antagonistic effect on the geometric accuracy of the fabricated parts and which increases with increase in part stacking length (Zhang and Chou, 2008). It may be in the forms as shown in Figure 15(a-b), either in curling towards the edges or towards one of the edges. Most of the errors in FDM parts are developed as a result of shrinkage during cooling and warping because of irregular heat distribution which creates internal stresses within a part (Peng 2012; Anhua and Xingming 2012).

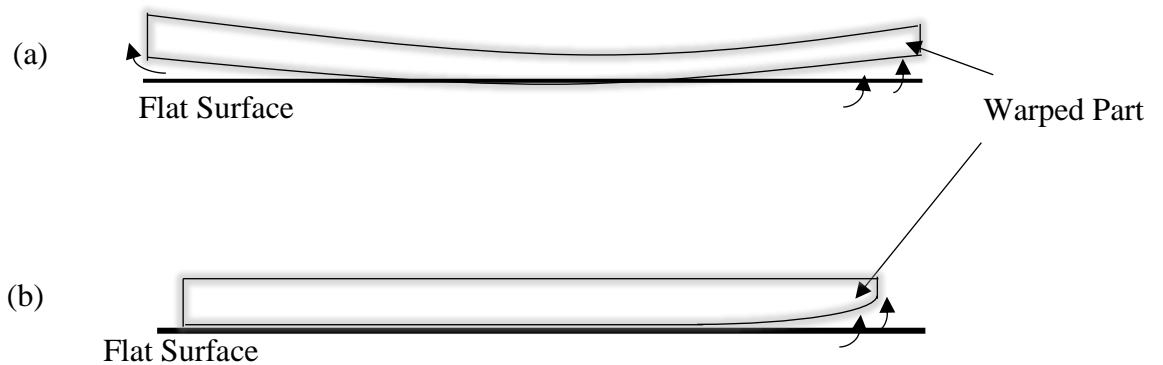


Figure 2.6 Part warpage drifting (a) towards the edges (b) towards a side

At times, stresses produced as a result of thermal gradient can cause cracking in parts (Wang et al., 2007). Bertoldi et al. (1998) in their study observed that the thermal coefficient of expansion for ABS prototype is much less as compared to bulk ABS. Further, they pointed that this occurs due to the filling of void spaces by the road material, which explains the warpage phenomena development. Furthermore, several researchers have tried to model the warpage behaviour in the form of mathematical model in extrusion based AM parts (Bellini and Guceri, 2003; Hutmacher et al., 2001; Mamadapur, 2007; Rodriguez et al., 2001, 2003b). Not only FDM based machines but other AM machines also suffers from warpage or distortion in parts. Some useful

studies that considered SLA (Jayanthi et al., 1994), SLS (Yang et al., 2002) and LOM (Sonmex and Hahn, 1998) based machines for the warpage studies in parts.

The next hurdle in the growth and development of FDM based machines as a mainstream manufacturing process can be hindered by geometric complexity. The geometric complexity can be identified by the level of geometrical features involved in a part, topology and assembly of individual components (Rodriguez-Toro et al., 2002). Further, Sukumar et al., (2008) performed a sequence of experiments for examining the geometrical complexity of products. They found that complexity in geometry was directly correlated with the continuous change in the curvature. The sharper and unexpected curves and profile result in increasing the part complexity. Moreover, parts and profiles with less or no symmetry were described as most complex objects. Finally, the number of holes, protrusions and intricate details as well increases the part complexity. Moreover, the ability of FDM machines to make fine details by presenting a benchmark geometry is characterized by different surface patterns (Armilotta, 2006). One unique study for evaluating the capability of FDM process to fabricate geometric free-form surfaces is performed for different anatomical parts (a skull and a mandible). The comparison of two replicas showed a difference of about 0.1 mm (El-Katatny et al., 2010).

Most of the FDM based machines are not used for industrial applications till date (Wohlers, 2014). The primary reason being the dimensional and geometrical inaccuracy in printing the parts (Kruth et al., 1998; Pei et al., 2011). The dimensional accuracy is being considered as key parameter for quality assessment in different industrial applications (Liou, 2007). The part inaccuracy can be elucidated by computer and mechanical aspects and is related to the approximation involved in surface tessellation and virtual model slicing (Wang et al., 2007). Several researchers have attempted to improve the dimensional accuracy of FDM machines by suitable adjustment in process parameters. Anitha et al., (2001) studied the factors that affect the quality and dimensional accuracy of the FDM parts. It was found that the layer thickness is an important factor in producing accurate parts. Thrimurthulu et al., (2004) studied build time and part quality and suggests that part deposition orientation is imperative in determining improved part quality. Boschetto et al., (2011) applied full factorial experiments for and predicted that layer thickness along with deposition angle

are critical parameters affecting the part accuracy. Singh (2014) studied the ability of FDM based machines to print polymer patterns used in casting applications. He further pointed that part orientation is significant in improving part accuracy. In addition, he also observed the advantage of support materials and capability to improve dimensional accuracy by post processing.

Tong et al., (2008) applied software based error compensation to FDM machines, which was earlier used for SLA part studies. After experimental trials, it was found that the dimensional accuracy has been improved and machine resolution is the key factor which can affect it. Sood et al., (2009) applied Taguchi orthogonal array experimental design integrated with artificial neural network (ANN) and predicted a non-linear relation among parameters for dimensional accuracy improvement. Further, profile error and part quality have been identified and modelled using statistical Taguchi design (Chang and Huang). Further, dimensional accuracy of different AM systems is characterized by proposing a benchmark part. It was found from experiments that maximum deviation of FDM based systems is 0.7 mm having a layer thickness of 0.254 mm (Ippolito et al., 1995). Furthermore, FDM process includes CAD modelling, toolpath generation, filament melting, extrusion, road width laying, solidification and filament drive. The process parameter setting, incidence of thermal stresses, post-processing, etc., all processes offers dimensional deviation. An accumulation of these process errors, unless controlled, may amount to 500–600 μm (Zhou et al., 2000; Johnson et al., 2011; Johnson et al., 2014). In particular, the outer dimension of an individual slice layer is upset due to filament road width. This issue is further compounded with print speed, slice thickness, build temperature, etc. The phase change of filament invariably brings in volume change and thermal stresses cause distortion, drives and controls lay positional errors.

Different studies showed improvement in the dimensional accuracies of FDM printers by comparing the accuracy, cost and surface roughness (Lotz et al., 2012). It was found that the average geometrical deviation between desktop and high-level AM printers for the case studies was about 0.7% (Lotz et al., 2013). Some literature showed how to estimate and compare the dimensional accuracy, process capability and tolerance of a 3D printed part (Islam et al., 2013). Researchers have worked on the error in printing the parts at different locations in the print volume (Stopp et al., 2008). Though the work was not done on FDM-based AM machine, it is well applicable here.

It was predicted that the deviation on an AM printed cylindrical part and accordingly made corrections in STL file before sending it to the machine. This gives designers an opportunity to review the design Moroni et al. (2014). Of late, it was studied that the dimensional deviation in build direction along height (Z) especially due to the nature of the support base and could achieve 50% improvement in Z error (Volpato et al., 2014). All these illustrations would help FDM owners to understand the capability of their machine well. All these demand a multi-parameter optimization and provision for error compensation.

2.1.3 Process parameter optimization in FDM process

Currently, with the growth in AM applications, several researchers have focused on improvement of these processes including FDM process. For FDM to become fully application based manufacturing process, it is required to produce superior part quality (geometrical and dimensional), at low manufacturing cost and with short product development time (Rayegani et al., 2014). Although FDM process has shown competence in fast product development but its full- fledged use is hindered by limited materials available in market (Levy et al., 2003; Pilipovic et al., 2009). To achieve these objective, it is important to suitably adjust the process parameters during part fabrication stage. Figure 16 shows the process parameters optimized by various researchers through the years for improved part quality. Several studies have been presented to determine optimum process parameter condition for improved quality products. In 2001, Anitha et al. investigated the influence of the FDM parameters on the quality characteristics of the prototypes. Taguchi technique was used to predict the response and it was found that layer thickness has inverse relation with surface roughness. Ahn et al. (2002) and Lee et al. (2005) applied design of experiment approach (DOE) approach to determine the influence of process parameters like raster angle, air gap and layer thickness on AM response of elastic performance. Thirumurthulu et al. (2004) used GA to determine the optimum part orientation in AM to minimize surface roughness and build time. Chockalingam et al. (2006) optimized stereolithography (SL) process parameters to achieve maximum part strength by applying design of experiments. Furthermore, a correlation between part strength and process parameters were established using DoE.

Ang et al., (2006) used DoE method to determine that air gap and raster angle as most critical parameters that have influence on the porosity and mechanical properties of ABS structures. Another similar study was performed by Horvath et al., (2007) for minimizing the surface roughness of ABS prototype. Raghunath and Pandey (2007) applied Taguchi method to improve the accuracy of SLS parts through shrinkage. They presented empirical models for predicting shrinkage along X, Y and Z direction using regression analysis. For proving the effectiveness of developed models, one case study is considered which shows effectiveness of developed models for improving the accuracy of prototypes. Zhang and Chou (2008) applied finite element analysis (FEA) model to predict the part distortion and residual stresses in FDM part by evaluating the effect of deposition parameters.

Moreover, Sood et al. (2009) applied gray relational analysis to minimize the dimensional accuracy of AM parts. It was also found that shrinkage is more along length and width direction in comparison to thickness of built part. Nancharaih et al. (2010) describes an experimental design methodology using Taguchi orthogonal array for determining optimum parameters for improved surface quality and accuracy in FDM parts. Sood et al. (2010) and (2012) studied the effect of process parameters on mechanical properties using RSM and sliding wear of the AM models. Phatak and Pande (2012) used GA to determine the optimum part orientation for improved part quality by minimizing the build time and material used. Further, empirical relationships between process parameters such as wire-width compensation, extrusion velocity, filling velocity, and layer thickness was established and prediction about dimensional accuracy and deformation of FDM fabricated ABS part using Taguchi method combined with fuzzy was performed (Peng and Zhang, 2012).

Recently, one study applied Taguchi experimental design to study the effect of process parameters like layer thickness, raster angle, orientation and air gap on FDM part accuracy by integrating Fuzzy logic and Mamdani method (Sahu et al., 2013). Guralla and Regalla (2014) used NSGA algorithm for optimization of part strength and volumetric shrinkage in the AM parts. Boschetto and Bottini (2014) developed a mathematical model of the filament based on deposition angle and layer thickness for predicting the obtainable part dimensions. All the aforesaid studies suggest that researchers have correlates AM process parameters with the dimensional accuracy,

surface roughness, strength, shrinkage improvement, mechanical properties and wear analysis in a part produced by AM. However, the correlation between process parameters and Geometric dimensioning and Tolerancing (GD&T) errors have not found yet for AM based parts.

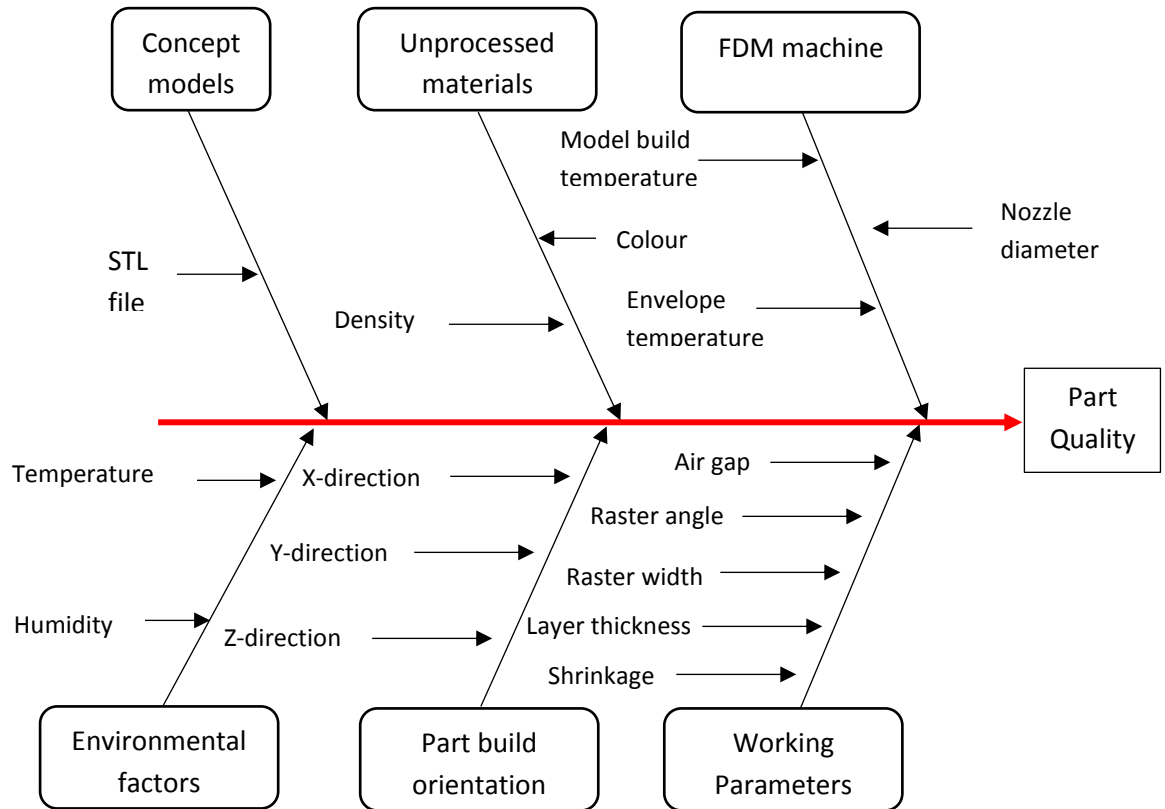


Figure 2.7 Fishbone diagram of FDM process parameters (Mohammed et al., 2015)

Table 2.2 Summary of process parameter optimization in FDM

Investigator	Year	Methods	Material	Output
Anitha et al.	2001	Taguchi Method and ANOVA	ABS	Surface roughness
Ahn et al.	2002	Full factorial design	ABS	Tensile strength, Compressive strength
Thirumurthulu et al.	2004	Genetic Algorithm (GA)	ABS	Surface finish and build time
Khan et al.	2005	Design of experiment	ABS	Elastic performance

Lee et al.	2005	Taguchi Method	ABS	Elastic performance
Chockalingam et al.	2006	Design of experiment	ABS	Part strength
Ang et al.	2006	Full factorial design	ABS	Compressive strength and porosity
Raghunath and Pandey	2007	Taguchi Method	ABS	Shrinkage
Horvath et al.	2007	Full factorial design	ABS	Surface roughness
Zhang and Chou	2008	Finite element analysis	ABS	Part distortion and residual stresses
Sood et al.	2009	Grey Relational Analysis	ABS	Dimensional Accuracy
Nancharaih et al.	2010	Taguchi and ANOVA method	ABS	Surface quality and dimensional accuracy
Sood et al.	2010, 2012	Response surface methodology	ABS	Mechanical Properties
Phatak and Pande	2012	Genetic Algorithm	ABS	Optimum part orientation
Peng and Zhang	2012	Taguchi method combined with fuzzy	ABS	Dimensional Accuracy and Deformation
Kumar and Regalla	2012	Full factorial design and ANOVA	ABS	Build time
Arivazhagan and Masood	2012	Lab experiments	ABS	Viscosity and modulus
Sahu et al.	2013	Taguchi method	ABS	Part Accuracy
Rayegani et al.	2014	Full factorial design and differential evolution	ABS	Tensile strength

Guralla and Regalla	2014	NSGA algorithm	ABS	Part strength and volumetric shrinkage
Boschetto and Bottini	2014	Optimization	ABS	Part Accuracy

2.2 Advances in 3D scanning systems and optimal parameter selection

In recent years, the use of contactless laser scanning devices is gaining an increasing interest for capturing the surface of real-world free form objects, widely applied in reverse engineering (RE) processes as well as quality inspection purposes. These devices provides millions of accurate three dimensional (3D) point data in short span of time making it a valuable alternative for scanning and measurement of industrial parts. The non-contact laser scanning system can provide sampled point data even for the complex free-form objects like curved surfaces. These non-contact scanning devices work on different principles including triangulation, time-of-flight, structured light and photogrammetry (Varady et al., 1997; Schwenke et. Al., 2002). Wang et al., (1999) developed a contactless scanning system having 4 axis for data acquisition. Furthermore, several researchers have developed scanning devices based on laser diode and CCD sensor for data acquisition of the objects surface using laser stripes (Yau et al., 2000; Chang and Chang, 2002). Chang and Chang developed an integrated approach for data capturing by using touch probe as well as laser scanner which are mounted on a CMM.

The non-contact devices are classified as active and passive system by Isgro et al., (2005). Active systems works on using light patterns on any scene to spot its position for measurement. Passive systems on the other hand, uses naturally occurring images formed by reflected light from a natural or man-made source, and they do not use any kind of energy to help the sensors. Nowadays, these contactless scanning systems have reached a good level of confidence for RE applications and laser scanners mainly based on triangulation principle are employed for inspection in industries (Lin et al., 2010; Jorge et al., 2011; Xu et al., 2011; Pathak et al., 2016).

Past studies suggests that the coordinate measuring machines (CMMs) were widely used for accurate shape, data acquisition and offers quality inspection process to conform the geometrical and dimensional tolerance specifications (Gao et al., 2006; Martinez et al., 2010). Mostly, the touch probe CMMs are used for acquiring point data

of primitive features like holes, slots, steps etc., as these features require only few sample points for their definition. However, the process of data acquisition with touch probe CMM is inherently slow, since the probe has to make contact at each point to be sampled. In addition, some studies have pointed that CMM data acquisition planning is a difficult and complex task, it become even prohibitive when any complex free-form surface is to be measured as it required higher sampling points (Elkott et al., 2002).

With increasing occurrence of free-form objects in industries, either for functional or aesthetic purposes, data acquisition becomes an important task for accurate inspection. Since, these are generally expensive parts and plays a vital role in final assembly, the complete part data measurement is imperative for effective functionalities (Curles, 1997; Lindau et al., 2013). However, CMM has incompetence in free-form surface measurement and non-contact scanners have capability of acquiring thousands of points in short span of time, together with increased accuracy in recent times. For all these reasons, the contactless laser scanners can be used for quality control of industrial components. A general arrangement of such a contactless laser scanning device is shown in Figure 2.8.

Since, the use of scanners with laser head are becoming increasingly common in other industrial fields also, it is essential to understand wisely different factors that can be chosen to get the best results. Besides the advancement in optical control of 3D laser scanners, there are many other factors that affects the quality and overall accuracy of scanned data (Lee and Chang, 2006; Ali et al., 2006; Mian et al., 2015). Feng et al.,

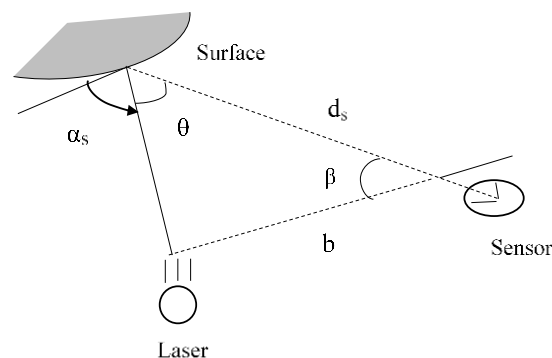


Figure 2.8 Laser triangulation principle (Curles, 1997), (α_s is incident scanning angle) (2001) predicted digitization error considering the effect of scan depth and projected angle on measurement accuracy. The prediction model developed calculates the systematic error having maximum deviation of 25 μm . Shuo and Dar has developed a

laser scanning system and suggested in their study that error compensation of the inclination angle data can be used to improve the precision of the system. Mian et al., (2015) performed experimental study and investigated the influence of different scanning factors on the final accuracy of the reverse engineered model. The scanning parameters they considered includes laser power, shutter time, measuring field and threshold for reflection. It was found that the laser power and shutter time are inversely related to the final accuracy of model. Threshold for reflection has major influence on the surface accuracy.

Several studies have been reported, which addresses different factors that are either related to acquisition instrument or scanning parameters. The factors that are related to acquisition device includes scanner resolution (Liang et al., 2016), field of view (Mian et al., 2015) and accuracy (Yin et al., 2014). Ghazali et al., (2011) reveals that scanner resolution significantly affects the accuracy of points captured by comparison of data points captured using 3D scanner with GPS observation. Subsequently, the factors addressed related to scanning factors includes laser power, shutter time and threshold for reflection (Ali et al., 2008). Their study found that the most important factor which affect the quality of point data acquired is laser power. Gestel et al., (2009) proposed a test method for laser scanners based on a planar test artefact. The study also addresses the systematic error evaluation which is based on in-plane, out-of-plane angle and scan depth effect. One similar study was reported, which investigated the influence of range and surface reflectance as the scanning parameters on the data acquisition (Tornincasa and Vezzetti, 2005). Additionally, some studies pointed out that ambient light conditions and scanned object characteristics are few other factors responsible for measurement accuracy. In the work of Lemes and Uzunovic (2009), the influence of ambient lighting on the quality of scan data is reported. An empirical relationship was established between object surface colors, ambient lighting and laser scan quality. Similarly, Blanco et al. (2008) in their study evaluates the effect of ambient light on the scanning process. It has been found that different type of light produce different results which is not uniform. Further, Voisin et al. (2007) in their study shows the influence of illumination (ambient light) on structured light based scanner performance. It was observed that the ambient light more or less affects the range accuracy depending on the original color.

A comparative study of laser scanning and touch probe CMM is reported, which suggested that final accuracy of scan part depends on the scanning strategy. The study suggested that single head orientation is preferable in comparison to multiple head orientation during scanning (Martinez et al., 2010). Few of the specific studies are based on studying the effects of laser intensity which depends on surface roughness. This study suggests that laser intensity is directly related to machining process and further wide range of intensities for maximum data acquisition were suggested (Cuesta et al., 2009). Further, Kaasalainen et al., (2010) pointed that target object moisture has an effect on the laser scanning performance and its output. In a continuing effort (Kaasalainen et al., 2011), effect of two important parameters such as incidence angle and range on the intensity measurement and radiometric calibration for different Terrestrial laser scanner (TLS) scanners were studied for establishing a correction scheme. In addition, few studies pointed out methods for data acquisition of transparent and shining surfaces. They suggested that providing coating sprays to the surface will be the solution for such objects. Further, it was clarified from results that only 5-15 μm variation in the actual surface is added (Mahmuda et al., 2011). Pesci and Teza, (2008) in their study evaluated the influence of surface irregularities (roughness) on the point data provided by laser scanning.

Most of the previous studies consider different factors of contactless scanning system to get accurate scanned surface. However, attempts to investigate the influence of scanned surface topology and local geometry have hardly been explored in literatures (Xi et al., 2001; Shiou and Ali, 2005; Uzunovic and Lemes, 2010; Mian et al., 2015). The effect of relationship among object, image, and the error of the measuring device have been studied (Xi and Shu, 1999). The study shows absolute error in terms of non-linear relation among precalibrating factors. This preceding error was also discussed in (Lee et al., 2002), and it was established that distance between laser head and object lead to out-of-plane error. The summary of all the literatures studied are shown in Table 2.3.

Table 2.3 Summary of published work on scanning parameters investigation

Investigator	Year	Scanner Type	Scanning Parameter	Output
Xi and Shu	(1999)	3-D line laser scanning	Object, image and absolute error	The study shows absolute error in terms of non-linear relation among precalibrating factors.
Feng et al.	(2001)	3D laser scanner	Scan depth and Projected angle	The study reveals that there exist a bilinear relationship of systematic error with the scan depth and the projected angle with maximum deviation of about 25 μm .
Lee et al.	(2002)	Laser scanner	Orientation and distance	distance between laser head and object lead to out-of-plane error
Shuo and Dar	(2006)	Position sensitive laser scanner	Inclination angle, error compensation	Error compensation of the inclination angle data can be used to improve the precision of the system
Voisin et al.	(2007)	Structured light scanner	Ambient light	It has been found that different type of light produce different results which is not uniform
Blanco et al.	(2008)	Laser 3D scanner	Ambient light	It has been found that different type of light produce different results which is not uniform
Ali et al.	(2008)	3D laser scanning	Depth of field, resolution, laser power	Effects of variation of laser power and resolution on data editing stages were identified.

Pesci and Teza,	(2008)	Laser scanner	surface irregularities	The influence of surface irregularities (roughness) on the point data is studied.
Gestel et al.	(2009)	Laser line scanning probe	Out-plane angle, in-plane angle, scan depth	Optimum process parameter results in systematic error of 10 μm .
Stefano and Enricho,	(2009)	3D laser scanning	Range and surface reflectance	Proposed a benchmark study for reverse engineering procedures.
Lemes and Uzunovic	(2009)	Desktop laser scanner	Light intensity, ambient light	The effect of ambient light is more when object surface is glossy white, and green.
Cuesta et al.	(2009)	Laser stripe scanner	Surface roughness	Laser intensity is directly related to machining process
Martinez et al.	(2010)	Laser scanning and touch probe	Head orientation	The study suggested that single head orientation is preferable in comparison to multiple head orientation during scanning
Kaasalainen et al.	(2010)	Terrestrial laser scanner	Target object moisture	Objects moisture has a direct effect on the laser scanning performance and its output.
Ghazali et al.	(2011)	3D laser scanning	Scanner resolution	Scanner resolution must be determined based on the spatial accuracy required in the project.

Kaasalainen et al.	(2011)	Terrestrial laser scanner	Range and incidence angle	The range and incidence angle influence on the intensity measurement for various TLS scanners were studied.
Mahmuda et al.	(2011)	3D laser scanner	Transparent object and coating sprays	They suggested applying coating sprays to the surface results in only 5-15 μm variation in the actual surface.
Mian et al.	(2015)	Laser line scanning probe	Laser power, measuring field, shutter time and threshold for reflection	The study reveals that threshold for reflection is main contributing factor for improved scanning performance.
Liang et al.	(2016)	Terrestrial laser scanner	Occlusion, Scanner resolution	The scanning resolution significantly impacts the quality of data captured in forests.

2.3 Surface reconstruction from point cloud data to accurate surface model

Lots of literature are available which suggest that the process of surface reconstruction from raw point data of an object is a challenging and important task in reverse engineering (Zhao et al., 2001; Dalmaso and Nerino, 2004). The primary reason being the use of curves for processes like surface fitting and parametrization (Tsai et al., 2008). On the other hand, recent advancements in structured light pattern and scanning technology has enhanced the process of surface reconstruction from unorganized point cloud data. The prime significance of these systems is the digitization time. The problem associated with these devices are concerned with missing data points, due to the occlusion phenomena and inaccurate surface generation because of the potential reflection of laser, results from a shiny object surface (Azvedo et al., 2009; 2010). Although, the data acquisition is accomplished from different angles and points

of view, both the part intricacy and the employed acquisition system (e.g. laser scanning) can be such that some regions of the outer surface are inaccessible. This may result in some dearth in the point cloud data and forming a set of holes in the generated triangle mesh. Figure 2.9 (a) displays the turbine blade data using a laser scanning system. Using the point of view 1 (b), the scanner is not capable to reach certain portions of the part, which is clearly evident from another point of view (c). This is due to the optical occlusion phenomenon (Varady et al., 1996). The presence of these undesired holes results in unexpected errors during the surface reconstruction (Pernot et al., 2007). Occlusion is the problem of blocking scanning laser by obstruction of surfaces. One of the methods to remove the occlusion problem is by using multiple scanning devices simultaneously (Koivunen, 1992).

As discussed in earlier sections, different industrial applications require models with free-form profiles such as turbine blades (Gao et al., 2006), vase (Li et al., 2002), gear wheel (Dubravcik and Kender, 2012) etc. As the shape of these objects are complex, it becomes a challenge to reconstruct the model either by using the non-uniform rational basis spline (NURBS) generation or other surface fitting methods. Many studies have been reported involving the use of NURBS curves and surfaces for data fitting of free-form objects (Yin, 2004; Zhongwei, 2004; Saini et al., 2015). However, the primary concern in developing 3D models using RE systems is the inconvenience in handling thousands of point data acquired by digitization of a physical object (Pardinas et al., 2008). The second problem arises in creating meshes which best explain the part surface. It is crucial to create triangle meshes that best fit the complex and free-form surfaces. At last, it is important for the RE tools to not only develop a complete digital model, but should also acquire the original design shape and geometry (Barbero, 2009; Kofman and Borribanbunpotkat, 2014). The general steps in RE methodology include the following steps (Soni et al., 2009; Thakur et al., 2009):

1. Raw point cloud data acquisition using touch probe or non-contact scanner.
2. Processing of the dense unorganized point data by proper registration, alignment and filtering of the noise data.
3. Mesh generation (triangulation of points), mesh decimation and optimization.
4. Surface reconstruction by surface fitting using curves and surfaces.
5. Feature based parametrization.

Initially, the point cloud acquisition performed using either contact based measurement devices like CMM or contactless optical devices like 3D scanner. However, during the data acquisition several practical problems arises (Raja and Fernandes, 2007). The calibration of the 3D scanner is an imperative and challenging task prior to data acquisition. The calibration is essential for determining parameters such as camera points, orientations of the image plane (Niola et al., 2011). Other issue is the accessibility of the different part of an object as shown in Figure 2.9. The primary reason being the topology and different configuration of the part scanned. Usually, a number of scans are required to capture different curvatures and features of the whole part by different orientations.

However, due to complex profiles and topology, it is difficult or sometimes impossible to acquire points of any specific regions like through holes (Maruyama et al., 1993). Next issue is occlusion which is discussed earlier. Occlusion is also introduced due to the fixturing used for parts during scanning. The raw point cloud data are acquired from different orientation and views, which results in inaccuracy in actual data (Ronnholm et al., 2007). Due to this reason, the acquired point data contains redundancy and noise, resulting in increased data size.

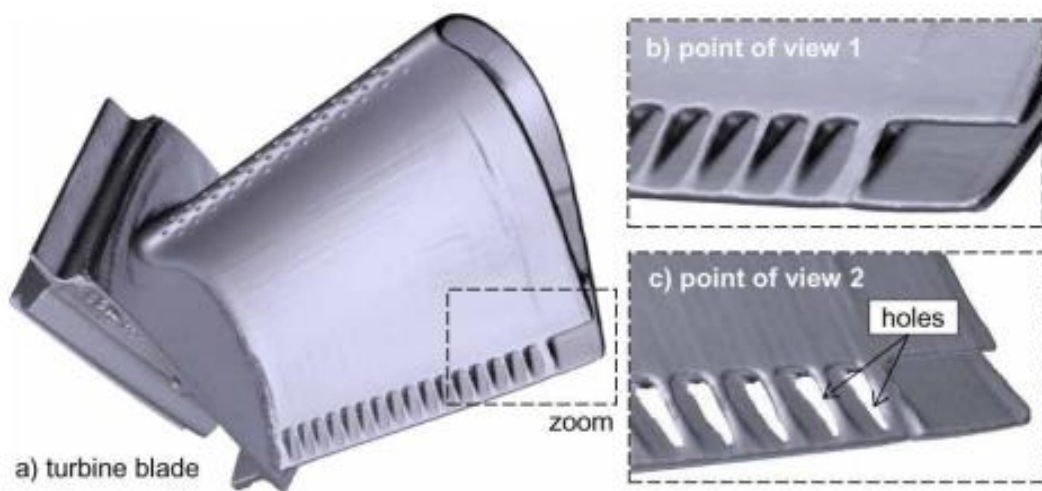


Figure 2.9 Point acquisition of (a) turbine blade (b) point of view 1 (c) point of view

The minimization of noise is a critical issue which is required to improve the accuracy of acquired point data. Noise filtering is an important step in processing of point cloud data and towards getting a parametric model. Sometimes, it is advisable to avoid the filtering step as the sharp edges tend to disappear and is replaced by smooth

edges. Many studies have been reported for noise elimination of point data (Peng et al., 2001; Pauly and Gross, 2001; Huang et al., 2010; Hu et al., 2006). Further, to maintain the accuracy of the actual design, it is also required to eliminate any unwanted outliers that are captured during scanning like any support or podium.

The point cloud data acquired by using multiple scans to oriented and aligned for proper registration (Grimm, 2005) and for full development of model. Multiple scan data are superimposed over each other using either automatic or N-point tools. For an accurate alignment of the point clouds, two or more point clouds patch must include as a minimum one common feature. One specific study (Minetola, 2012) was reported on the effect of appropriate alignment technique on the accuracy of product quality and inspection. The term alignment or registration refers to the transformation of scanned point cloud data from a local coordinate system that is interior to the measurement device into a global coordinate system that the user desires. To perform alignment, the operator usually identifies the geometric features in the scanned part that signifies the datum reference.

The remaining noise and redundancy are removed by using suitable point filtering techniques. Filtering is an important step that is used to reduce the redundant points. The suitable filtering technique can result in lowering the size of point data and help in easy handling and processing as shown in Figure 2.10. Data filtering has been studied by different researchers that are based on mathematical approximations (Vosselman, 2000; Axelsson, 2000). In addition, some studies also applied median and mean based filtering techniques for noisy point cloud data (Nuchter et al., 2004; Kobbelt and Botsch, 2004). These are the simplest and efficient filtering algorithm but can eradicate noise only if the noisy area occupy less than one half of the neighborhood area. Another common filtering technique used is Voxel Grid method, which removes noise by using a grid of 3D voxels (Martin et al., 1997). This method have some specific drawbacks such as sensitivity to noisy input spaces. Subsequently, all the existing data points are approximated and it does not represent the underlying surface accurately. In addition, some of the more work are reported in point filtering techniques (Tomasi and Manduchi, 1998; Wasza et al., 2011, Budak et al., 2011, Feng, 2009). However, the point cloud data using these filtering techniques is not able to remove the outliers and noise accurately. Also, their main focus will be on retaining surface details without considering the accuracy of point cloud data.

The next step is generation of triangle meshes which is commonly referred to as tessellation or triangulation. The primary purpose of mesh generation is to create the topology of each discrete point and obtain a linear surface according to actual object (Gibson, 2004; Waterman, 2004). Numerous triangulation methods have been proposed by researchers that are either Delaunay based (Okabe et al., 2009) or non – Delaunay based (Berg and Kreveld, 2000). Few of the methods present in literature based on the selection of a triangle from raw point cloud and adds it into the surface set. The two sets are both restructured, and follows to a dynamic principle from local to global. The methods are Ball Pivoting Algorithm (BPA) (Bernardini et al., 1999) and Delaunay-based Region-growing Algorithm (DBRB) (Kuo, 2005). These methods has inherent strength on development of surface mesh, though it appears not very firm by means of sampling uniformity degree to determine the scale of the influence region.

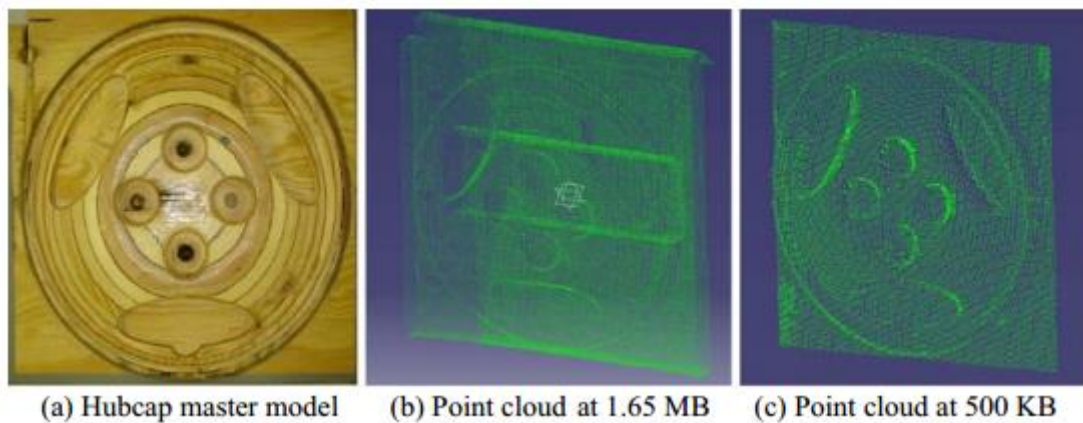


Figure 2.10 Hubcap master model and its point data after filtering (Soni et al., 2009)

The major drawback of these algorithm being the computation method of the influence region, which perhaps is the next hindrance on the efficiency of theses algorithm. Moreover, such algorithms are only applicable to surfaces without holes. Similarly, one more geometry based approach i.e. Voronoi diagrams is proposed by Dey and Goswami, (2006). Although, it has advantage of developing mesh using fine details, it is almost impossible to get a smooth surface in presence of noise. Further, after mesh generation, smoothing is the next step in RE process. Its main aim is to refine the mesh and can increase the quality and accuracy of surfaces. There are some algorithms available in literature that make use of Delaunay and Voronoi diagrams. The alpha shape (Yu, 1999) is heuristic approach that depends on the varying sampling density value.

Decimation is the next step of the refining process of triangle mesh by reducing the number of triangles (Grimm, 2005). Additionally, re-aligning the orientation of the triangular facets, which depends on the edge length of adjacent triangles, also represented as optimization. By using decimation, redundancy in points is removed with simplified meshes. This helps in minimizing the size of mesh file with increased quality and aids in easy and fast handling of points. Moreover, decimation is a challenging task and most of the research reported are for multi resolution rendering (Park et al., 2004; Duranleau et al., 2008). These algorithm are based on down sampling of points according to the surface details. One more algorithm was developed for decimation (Ma et al., 2013), which is Quad Tree based (QTB) and works by selecting a plane based area for point removal. The suitability of these algorithms presents a question mark on the accuracy of final mesh as it does not consider the holes and various details in the surface. Optimization is performed which may increase the number of triangles and hence used for providing sharpness to the mesh files. At last, surface reconstruction process is performed for the mesh by using techniques like feature extraction and surface fitting.

Several soft computing techniques are also used for surface reconstruction. Yu (1999) in its study used neural network for to get the point data coordinates. One more specific study (Wu, 2008) deals with construction of point data using a modified neural network. The simulated annealing algorithm integrated with radial basis function to solve the incomplete point cloud data problem, which helps in minimizing holes (Wu et al., 2008a, b). The genetic algorithm is another population based algorithm used for the curve and surface fitting (Galvez et al., 2007). In the study of Liu et al., (2005), shape reconstruction of an object is performed by using genetic algorithm for cost function minimization. Similarly genetic algorithm is used for easy handling of millions of point data (Xiaomin et al., 2007). Several studies show that particle swarm optimization performed better than genetic algorithm in finding the solution (Chandrasekran et al., 2009). This performance of particle swarm optimization is useful in the surface fitting using Bezier curves (Galvez et al., 2008). In the same context, differential evolution (DE) is used in minimizing the error in estimated and measured point data (Rekonas, 2008). They also concluded that results of DE are better as compared to particle swarm algorithm for surface and shape reconstruction. These algorithms are computationally efficient but often produced heuristics results that are

approximation and not exact. These drawbacks allow the need of software based data processing as an alternative and effective method especially for personal with less skill and expertise.

With the increasing computing abilities during the last decade, along with the growth and expansion of high-performance digital sensors and the significant software revolutions created by computer-based vision and visual perception research areas, have prolonged the difficult processing of a 3-D point cloud generation from a series of non-calibrated images to accurate surface reconstruction. The quality of the final surface model is of utmost importance especially when software are used for data processing and manipulation. So, it becomes important to examine the accuracy of the developed digital model with reference to the actual physical model. Several RE software tools are available that suits the requirements needed by design personnel and operators. Prior using difficult mathematical approximations, they attempt to obtain the desired accuracy of 3D models by regulating various key factors through continuous approximations using commercially available CAD application tools.

2.4 GD&T error evaluation and optimization

Manufacturing of a perfect part as per the drawing specifications is not possible, because of different errors developed during the manufacturing process. For proper functioning of the parts, it is essential to provide some tolerances. Form tolerances assigned to the features are functional, regardless of variation in their form. Assessment of these errors in manufactured parts is crucial to conform the tolerance specification. Various types of geometric form errors include straightness, circularity, cylindricity and flatness (Cogorno, 2006). These errors are related to the primitive geometric features which contribute significantly to the production of mechanical components such as assembly parts, injection molds and dies, transmission systems and gauges to achieve intended functionalities. In general practice, sometimes it becomes impractical to acquire variation over the whole surface. Consequently, only finite points are considered which represent features of the surface, and these points are used for evaluation of form errors. Earlier, coordinate measuring machines (CMMs) were used for acquiring 3D points off-line and for on-line inspection activities (Cui et al., 2007; Zhang, 2008; Wang et al., 2014).

Therefore, modelling of different geometric errors associated with manufactured parts is very important for high precision output. Traditionally, the least squares method (LSM) is the most common used technique for form error evaluation in industry because of its simplicity in computation and uniqueness in solution. However, LSM does not adhere to the standards and does not guarantee the minimum zone solution, which may lead to overestimation of tolerances. Therefore, potentially functional parts can be rejected, resulting in an economic loss (Samuel and Shunmugam, 2000). In 1980s, Murthy and Abdin (1980) were the first to implement mathematical programming methods like Monte-Carlo and spiral search technique for successful evaluation of different form errors (straightness, sphericity, circularity and flatness) using minimum zone method and the result shows better convergence than LSM method. Similarly, Shunmugam (1987) used simplex method for evaluating minimum average cylindricity deviation, in place of minimum zone solution. The objective function proposed is in the form of $f = |e_{max}| + |e_{min}| + \frac{1}{|e_{max}||e_{min}|}$. It was found that the results of minimum average deviation is better than the conventional least square method. Further, limitations of this technique are analyzed by Dawson (1992) for evaluating cylindricity. He also provided the discussion on different fitting techniques for cylindricity that includes MZC, minimum circumscribed circle (MCC) and maximum inscribed circle (MIC) along with their limitations. Prakasvudhisarn et al. (2003) applied support-vector regression technique which employs mathematical programming for minimizing the circularity zone.

In this regard, several algorithms were suggested to replace LSM, and the majority of them follow the minimum zone (MZ) principle. Wang et al., (1999) proposed a generalized non-linear optimization procedure for circularity evaluation based on a minimum radial separation criterion. Jywe et al. (1999) applied three different mathematical models to find the MCC, MIC, and MZC by directly resolving the simultaneous linear algebraic equations. Cheraghi et al., (2003) proposed criteria based on the least square cylinder, minimum circumscribed cylinder, and maximum inscribed cylinder for evaluation of cylindricity error. Endrias and Feng (2002) formulated an objective function which is a function of the rigid body coordinate transformation parameters.

The direct search algorithm and the downhill simplex search algorithm are employed to minimize the form tolerance objective function. Carr and Ferreira (1995) formulated straightness, flatness, and cylindricity as non-linear problems, and transformed them into a series of linear problems. Some algorithms that are available in numerical libraries but haven't been tried yet and are seem to be well applicable here are Hyper least squares (Kanatani and Rangarajan, 2011), iterative reweighted least square algorithm (Wang, 2004), discrete and linear Chebyshev approximation (Dhanish and Shunmugam, 1991) and finite-differences derivative descent approach (Gosavi and Phatak, 2006). A number of researchers have applied computational geometry mechanism for evaluation of minimum zone. In the late 1980s, Traband et al., applied a convex hull technique for evaluating the flatness error. In the same context, Huang et al., (1993, 1993) proposed a control plane rotation scheme (CPRS) for evaluation of minimum zone straightness and flatness. A computational geometry mechanism was used by Damodarasamy and Anand (1999), searching within varying polygon to produce great results.

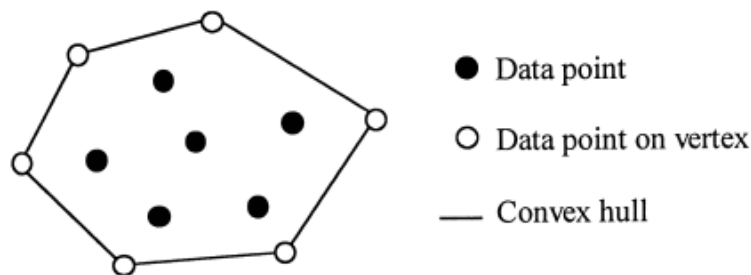


Figure 2.11 Convex hull around data points (Kim et al., 2000)

Similarly, a selective data-partitioning method for circularity error assessment was proposed by Rajagopal and Anand (1999). This was an iterative method which deals with partitioning the data points in four quadrants by applying three different methods. Lai and Wang (1988), Le and Lee (1991) and Kim et al. (2000) used a Voronoi-diagram method, which employs the concepts of convex hull as shown in Figure 2.11 to compute circularity. Roy and Zhang (1992) formulated a technique keeping in view all possible pairs of concentric circles for measuring the circularity error. Etesami and Qiao (1990) provide a Voronoi diagram to determine the centers of the maximum inscribed and the minimum circumscribed circles. Roy and Xu (1995) used a method that develops co-axial cylinders coupled with Voronoi diagrams for measuring cylindricity.

Over the years, researchers have applied several optimization techniques for form error evaluation. Venkaiah and Shunmugam (2007) introduced distinctive optimization algorithms such as numerical and computational geometry optimization approaches which are used for evaluation of circularity and cylindricity. Seun and Chang (1997) developed an interval bias linear neural-based approach with least mean squares learning algorithm for straightness and flatness assessment, and analysis. Weber et al. (2002) proposed a unified linear approximation technique for evaluating the form errors. The non-linear equation for individual form was linearized implementing Taylor expansion, and it was solved using linear programming. The numerical approaches are ubiquitous methods to solve optimization problems and are also computationally efficient. However, they may result in inaccurate results due to mathematical approximations. Furthermore, some of the researchers have reviewed different numerical methods for form error evaluation (Gosavi and Cudney, 2012; Moroni and Petro, 2008).

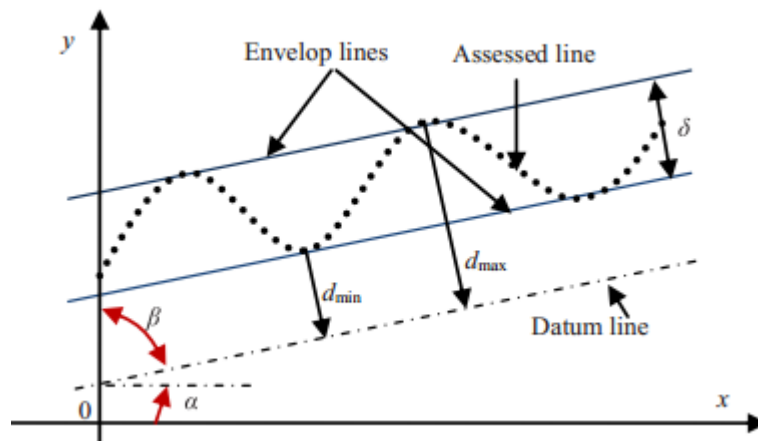


Figure 2.12. Straightness error evaluation (Cui et al., 2013)

On the contrary, with the evolution of computational intelligence, computational geometry approaches can identify minimum zone with certainty (Liu et al., 2011). Some of the nature-inspired optimization algorithms used for form tolerance evaluation are genetic algorithm (GA), ant colony optimization (ACO), particle swarm optimization (PSO) and artificial bee colony (ABC) (Liu et al., 2011; Andrea et al., 2011; Wen et al., 2010; Luo et al., 2012). Liu et al. (2011) in their study proposed an adaptive ant colony optimization (AACO) algorithm based on the foraging behaviour of ants in finding shortest paths. The experimental results show that AACO algorithm

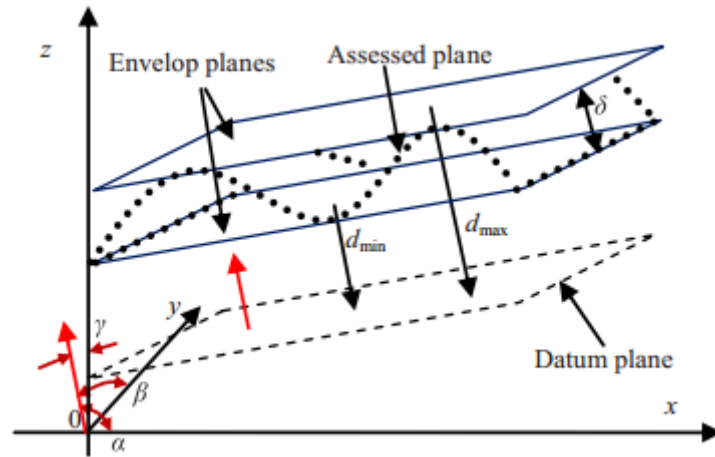


Figure 2.13. Flatness error evaluation (Cui et al., 2013)

is flexible and robust as compared to conventional techniques. One specific study on the application of GA algorithm was presented for evaluation of exact roundness error and to minimize computational time (Andrea et al., 2011). Similarly, Wen et al. (2010) presented a method which takes ideal cone as a particle for evaluating conicity and cylindricity. From results, it was observed that PSO not only is easy to use and flexible. Also, PSO evaluates conicity and cylindricity error more accurately as compared to genetic algorithm and immune algorithm (IM). Furthermore, Zhang and Wang (2011) applied hybrid ant colony and simplex search method for form error evaluation. The results are better than the results of traditional methods used earlier in literature and satisfactory in evaluation of form errors. An improved artificial bee colony algorithm proposed for accurate evaluation of axis straightness error was reported by Luo and Wang (2014).

In addition, Hu and Yong (2009) proposed improved genetic algorithm for evaluating cylindricity error. Use of GA was found more complicated than PSO in principle for the same work (Lai et al., 2000; Cui et al., 2007). For determining the cylindricity error, several other methodologies were developed with main aim to find the fine-tuned axis of cylinder and optimized it using simulated annealing algorithm (Chou and Sun, 2000). Recently, Wang et al., (2012) in their study applied differential evolution (DE) algorithm for flatness error evaluation. In comparison to other traditional methods, DE has the advantage of flexibility and simplicity. ACO is time consuming and its convergence time is also uncertain. ABC has slow convergence rate, quickly falls in local optima and with its use, it's hard to find the best out of all available feasible solutions (Rao and Savsani, 2012). For solving continuous problems, PSO has been

widely used due to simplicity of the concept with fewer parametric settings as compared to other population based optimization algorithms (Tseng et al., 2010; Lee and Lee, 2014; Li et al., 2014). However, classical PSO still has some disadvantages, such as weak local search ability that may lead to entrapment in local minimum solutions affecting the convergence performance that results in uncertainties in the outcomes obtained. In PSO, updation of the new solution is performed only over the existing one, without comparing which one is better. This behaviour is due to lack of exploitation capability in classical PSO, which makes it hard to find the best possible solution (Rao and Savsani, 2012). The above discussion on different techniques used for GD&T error evaluation is summarized in Table 2.4.

Table 2.4 Summary of methods used for geometric error evaluation

Investigator	Year	Methods	Type of Methods	Error evaluation
Murthy and Abdin	1980	Monte-carlo and Spiral search	Mathematical programming	straightness, circularity and flatness
Shunmugam	1987	Simplex method	Mathematical programming	Cylindricity deviation
Traband et al.	1989	Convex hull	Computational Geometry techniques	flatness
Dhanish and Shunmugam	1991	Chebyshev Approximation	Mathematical approximations	All form errors
Dawson	1992	Three fitting methods (MZC, MCC, MIC)	Mathematical programming	Cylindricity deviation
Huang et al.	1993	Control plane rotation scheme	Computational Geometry techniques	Straightness and flatness

Carr and Ferreira	1995	Linearization	Computational Geometry techniques	straightness, flatness, and cylindricity
Roy and Xu	1995	Voronoi diagram	Computational Geometry techniques	Cylindricity
Seun and Chang	1997	Neural based approach	Optimization algorithms	Straightness and flatness
Wang et al.	1999	minimum radial separation criterion	non-linear optimization	Circularity
Jywe et al.	1999	MZC, MCC, MIC	Mathematical programming	Cylindricity
Rajagopal and Anand	1999	selective data-partitioning	Computational Geometry mechanism	Form error
Kim et al. and Le and Lee	2000, 1992	Convex Hull	Voronoi-diagram method	Circularity
Lai et al.	2000	Genetic algorithm	Optimization algorithm	Cylindricity error
Chou and Sun,	2000	Simulated annealing algorithm	Optimization algorithm	Axis cylindricity error
Endrias and Feng	2002	direct search algorithm and the downhill simplex search	Mathematical programming	Form error
Weber et al.	2002	Linear programming	Numerical method	Form error

Prakasvudhisarn et al.	2003	Support vector machines	Mathematical programming	Circularity
Cheraghi et al.	2003	MZC, MCC, MIC	Mathematical programming	Cylindricity error
Venkaiah and Shunmugam	2007	numerical and computational geometry optimization	Optimization algorithm	Circularity and cylindricity error
Cui et al.	2007	Genetic algorithm	Optimization algorithm	Straightness and flatness
Hu and Yong	2009	Improved genetic algorithm	Optimization algorithm	Cylindricity error
Wen et al.	2010	Particle swarm optimization	Optimization algorithm	Cylindricity and conicity
Zhang and Wang	2011	ant colony and simplex search method	Hybrid algorithm	Form error
Liu et al.	2011	Adaptive ant colony optimization	Optimization algorithm	Form error
Andrea et al.	2011	Genetic algorithm	Optimization algorithm	Roundness error
Luo et al.	2012	Artificial bee colony	Optimization algorithm	Flatness
Wang et al.,	2012	Differential Evolution	Optimization algorithm	Flatness

Luo and Wang	2014	Improved artificial bee colony	Optimization algorithm	Axis straightness error
--------------	------	--------------------------------	------------------------	-------------------------

2.5 Inspection planning, procedures and development of benchmark part for scanner characterization

Nowadays, with the advancement in 3D optical data acquisition systems, laser sensor scanners have evolved in terms of resolution, measurement speed and accuracy making it suitable for inspection and quality control (Martinez et al., 2010). However, for successful industrial inspection, the inspectional planning strategy is of prime importance (Cho et al., 2005). In past years, significant research work has been done on inspection strategy and approach for contact and contactless based systems (Lee and Park, 2000; Prieto et al., 2002a, b; Son et al., 2002; Leopald et al., 2003; Li and Gu, 2004). In the mid-90s, Tarbox and Gottschlich (1995) presented a planning algorithm for complete coverage of object surface prior to inspection. Yau and Menq (1995) in their work reported a systematic inspection planning system using coordinate measuring machines. The work deals with providing the collision free inspection path for complex surfaces using simulation and experimental analysis. The results proved the effectiveness of the proposed system for the specific study of mold and dies.

Truco et al., (1997) reported a system for providing optimal sensor position planning for inspection purpose using feature object models. Similarly, Cowan and Kuvesi (1998) presented another study for generating automatic locations of sensor for capturing an object. One of the advantage of this approach is removal of occlusion as all the object surface lie within the sensor field of view. Zhang et al., (2000) proposed an inspection planning system procedure for CMM machines (Figure 2.14). However, the study has limitation that only six orientations have been considered for the touch probe. Furthermore, the study takes into consideration, the sampling number and point distributions for defining the sampling plan and sequence. Lee and Park (2000) proposed an algorithm for generating the scanning procedure that consists of scanning path and direction for a laser scanner, mounted on three axis transport mechanism. Prieto et al. (2002) presents a robust approach for providing an accurate 3D data

acquisition using high precision sensor and algorithm for tolerance control of industrial parts.



Figure 2.14 The inspection path planning for CMM (Zhang et al. 2000)

Similarly, Son et al., (2002) proposed a methodology for automated measuring system of free form surfaces. They also developed a software module that provides scanning path after considering different scanning parameters like view angle, depth of field, occlusion etc. The laser scanner used for this approach has four degrees of freedom and an automated rotary table with two degrees of freedom was used. Elkott et al., (2002) proposed a genetic algorithm for automatic selection of sampling algorithm. Experimental results shows that the proposed algorithm proves to be an effective tool to predict the sampling plans in CMM based inspection. In the work reported (Sheng et al., 2003a, 2003b), a methodology of recursive algorithm was developed considering the previous work sensor planning problems. Further, feasible viewpoints were generated satisfying the kinematics constraints.

Additionally, Li and Gu (2004) reported a comprehensive state of the art literature review on methodologies, techniques and various processes in inspection of free-form surfaces. They also presented discussions on commercially available inspection software, used in industries. Cho et al., (2005) proposed a feature based inspection planning for complex workpieces. The proposed approach for inspection planning is divided in two stages i.e. local and global inspection. Global inspection planning is performed by generating optimum sequence for features of the part. In contrast, for local inspection planning, features are divided into sub components and based on the number and position of sampling points an optimum sequence is determined (See Figure 2.15). A model based approach was proposed to find minimum camera locations during scanning which is based on cost function minimization resulting from inspection procedures (Ellenrieder and Komoto, 2005).

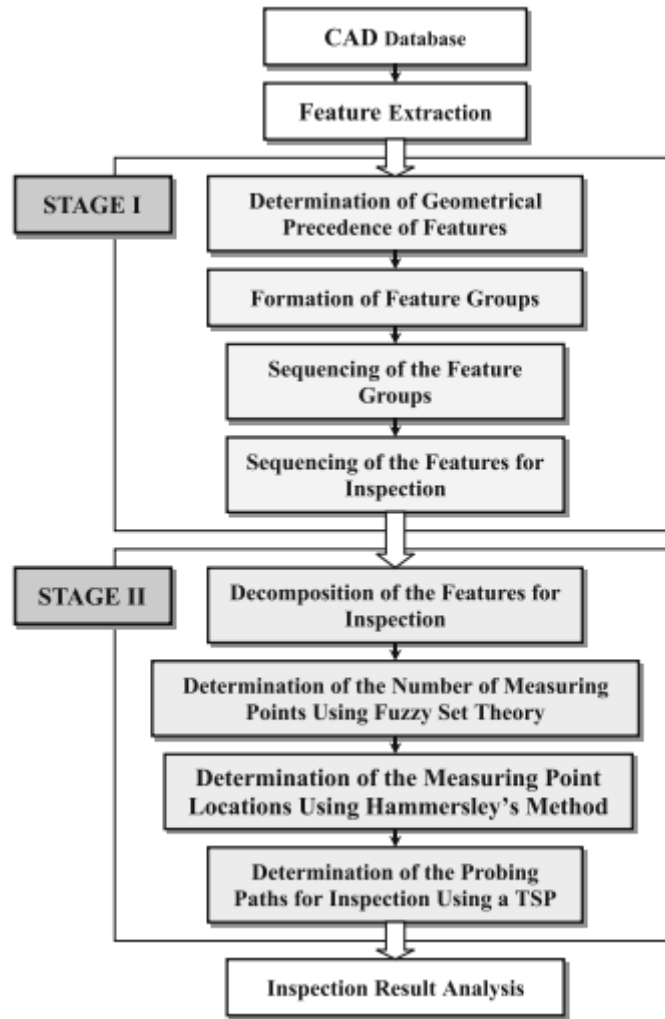


Figure 2.15 Integrated inspection planning strategy (Cho et al., 2005)

Derigent et al., (2006) reported a novel digitizing strategy which is based on the Minkovsky operation to compute the minimum set of directs required to scan an object. Martins et al., (2005) presented a collision free and efficient inspection framework on industrial scanning systems having 5 degree of freedom. Shi et al., (2007) presents a two stage inspection process using robot aided dimensional inspection system. One with off-line inspection and second using the feedback according to the point cloud measured. Similar survey was reported for computer aided inspection planning (CAIP) by dividing it into mainly two groups i.e. geometry based and tolerance based systems (Zhao et al., 2009). One of the CAIP systems was developed in the late 1980s, considering the characteristics of CMM, the geometry of the part inspected and the standards used to characterize them. The inspection planning system developed is shown in Figure 2.16.

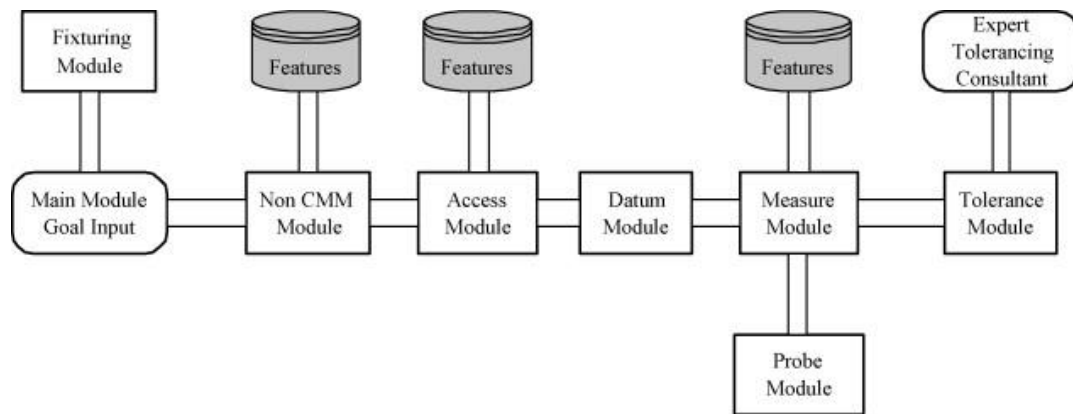


Figure 2.16 The Computer aided inspection planning system (Elmarghy and Gu, 1987)

Few research work also reported on-machine measurement (OMM) system combining touch probe and non-contact sensor. The inspection is performed on the machine tool directly (Kim et al., 1998; Nam and Chung, 1998). Besides, the touch probe and non-contact sensor, a hybrid type of system was used which integrates both the sensors (Lee et al., 2000). These systems have enhanced usefulness as compared to single inspection systems. The contact based sensor helps in precise measurement but are slow in process. The non-contact sensors lacks in precision measurement but are fast in point data acquisition. Mohib et al., (2009) also proposed a hybrid (contact/non-contact) inspection planning method that possesses the advantages of both systems. They also discussed about the sensor selection and inspection feature inspection applied to water pump housing of an automotive engine. The work performed by Souzani et al., (2006) addresses the problem of intelligent scanning in the perspective of reverse engineering. The new scan paths for an optimal digitizing are then calculated including optimal orientation search.

Moreover, Fernandez et al., (2007) presented an automatic process planning for scanning free-form surfaces by using laser stripe mounted on CMM machine. This study also considered the constraints imposed by both the contact as well as the laser based system. Martinez et al., (2009) reported a methodology of vision sensor planning system applied to the accuracy control of head lamp lenses. The study deals with finding the optimum viewpoints through a fuzzy set approach. In addition, genetic algorithm was also used for determining the distribution and number of viewpoints, which is demonstrated by the methodology on commercial sensors. Scott, (2009) presented a

multi-phase, model based procedure for planning of automated high reliability inspection or reconstruction considering laser scanning range cameras. Zhou et al., (2011) proposes a novel algorithm for freeform surface inspection planning. The deviation between actual geometry and nominal CAD model was generated using search based planning method. The proposed algorithm was tested using variety of the machined metal skin of aircraft. Zhao et al., (2012) proposed a hybrid inspection methodology combining the advantages of both touch trigger probe and laser scanner system (Figure 2.17). For tactile based measurements, the sampling strategy considers the measurement uncertainty calculated by simulation study. The scanning path is generated automatically considering the position and view angles of the laser scanner.

Although the above mentioned contactless measurement-based inspection systems are generally suggested for inspection and product quality control. These aforementioned studies are mainly concentrated on the stages of planning collision free scanning paths, processing raw point cloud data, aligning of the models and further deviation of the two models by comparisons. Till date, none of the reported studies have been able to present an effective inspection framework or procedure for the GD&T features in a product, including form, position and orientation tolerances.

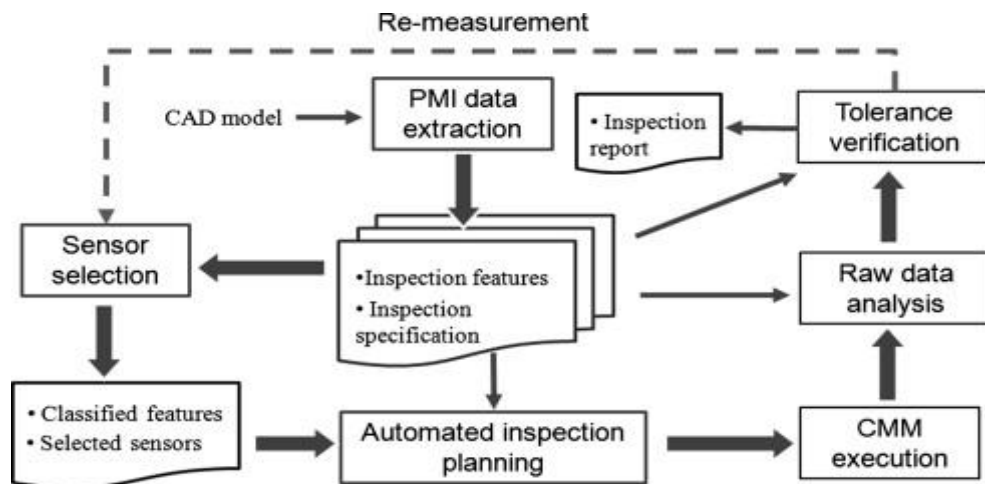


Figure 2.17 Inspection framework using CMM and laser scanner (Zhao et al., 2012)

The laser scanners are gaining importance due to the improved technical characteristics driven by research in metrology field (Estler et al., 2002). However, GD&T inspection is mostly performed by using contact based coordinate measuring machines (CMM) in industries (Feng et al., 2001; Yadong and Peihua, 2004). The main advantages of CMM are high measuring accuracy, point-to-point data acquisition and

well established calibration process. However, inspection planning using CMM is a complex and troublesome task, which requires skilled and experienced operator (Elkott et al., 2002). The CMM inspection is effective for certain types of parts but not suitable for soft materials, complex geometry especially free form shapes.

Furthermore, performing rapid data acquisition of part surface is one of the primary concern, which is even higher for large and complex parts. In industries, non-contact scanning systems are used as a tool for physical model restoration and development of complete and worn-out components (Bagci, 2009). Nowadays, contactless digitizing systems have realized an adequate level of assurance in reverse engineering field (Son et al., 2002; Carbone et al., 2001). Further, significant efforts have been made to improve the accuracy of non-contact scanning systems (Cuesta et al., 2008). However, the use of non-contact scanning instruments for industrial applications is impeded by investment particularly involving cost of instrument, software, training and timely maintenance.

Moreover, the laser scanner accuracy are one order magnitude less than the touch probe measurement. Consequently, it is more difficult to define the laser scanner accuracy as the standard and procedures used for characterizing CMM machines are not suitable for contactless scanners. Therefore, for effective characterization and development of non-contact scanning systems, some standardized parts and methodology are required for providing adequate metrological data and quality claims. To test the quality claims of products, very few methods and techniques are available with industries. In addition, the selection of best method is quite tricky as the best technique for one application might not work for other. The lack of appropriate inspection standard makes it difficult for selection of a suitable scanning system only based on information provided by the manufacturer. The metrological specification provided by the manufacturers are based on the different systems, methods and are provided in the non-standard format which are difficult to translate in the real life applications. Therefore, to investigate the potential offered by the non-contact scanning systems a common benchmark part and standard procedures are required. Such methods and benchmark parts will help the users in determining the strengths and weaknesses of a measuring system and hence in the adequate decision making process. In the same context, few examples of standards and guidelines provided for metrological verification using CMM is provided in the ISO 10360 and ISO 15530 (Kunzman et al.,

1997; Hansen and De Chiffre, 1997; Trapet et al., 2004). The summary of the above studies related to different inspection process planning are provided in Table 2.5.

Table 2.5 Summary of literatures on inspection process planning

Investigator	Year	Contact/ Non- contact	Features	Output
Elmarghy and Gu	1987	Touch probe CMM	Free-form part	The geometry of the part inspected and the standards used to characterize them
Tarbox and Gottschlich	1995	Non-contact laser scanner	Free-form surface	A set of sensing operations for completely measuring the object surface to be inspected
Yau and Menq	1995	Touch probe CMM	Complex free form surface	A systematic inspection planning for collision free inspection path for complex surfaces using simulation
Kim et al. ; Nam and Chung,	1998	touch probe and non- contact sensor	Industrial parts	The inspection is performed on the machine tool directly
Truco et al.	1997	non-contact scanner	Free form object	Optimal sensor position planning for inspection purpose
Cowan and Kuvesi	1998	non-contact scanner	Free-form object	Automatic locations of sensor for capturing an object
Zhang et al.	2000	Touch probe CMM	Free-form object	The study take into consideration the sampling number and point distributions for defining the sampling plan and sequence

Lee and Park	2000	Laser scanner	Free form object	Scanning path and direction for a laser scanner mounted on three axis transport mechanism
Lee et al.	2000	Hybrid system	Industrial parts	a hybrid type of system was used for inspection planning
Prieto et al.	2002	Laser scanner	industrial parts	A robust approach for providing an accurate 3D data acquisition using high precision sensor and algorithm for tolerance control
Son et al.	2002	Laser scanner	free form surfaces	a software module that provides scanning path after considering different scanning parameters was developed
Elkott et al.	2002	CMM based inspection		a genetic algorithm for automatic selection of sampling algorithm.
Sheng et al.	2003	Laser sensor	Free form surfaces	recursive algorithm was developed considering the previous work sensor planning problems
Li and Gu	2004	Laser scanner	free-form surfaces	state of the art literature review on methodologies, techniques and various processes in inspection of free-form surfaces
Cho et al.	2005	Laser sensor	Complex surfaces	Two stage approach for inspection planning is proposed i.e. local and global inspection

Ellenrieder and Komoto	2005	Laser scanner		model based approach was proposed to find minimum camera locations
Derigent et al.	2006	Laser scanner	Free form object	novel digitizing strategy which is based on the Minkovsky operation to compute the minimum set of directs required to scan an object
Martins et al.	2005	industrial scanning systems	Free form object	a collision free and efficient inspection framework on industrial scanning systems having 5 degree of freedom
Souzani et al.	2006	Laser scanner	Free form profile	problem of intelligent scanning in reverse engineering is addressed
Fernandez et al.	2007	CMM	Free-form surfaces	This study considered the constraints imposed by both the contact as well as the laser based system in inspection planning
Shi et al.	2007	Laser scanner	Free form object	presents a two stage inspection process using robot aided dimensional inspection system
Zhao et al.	2009	Laser scanner	Free form surface	computer aided inspection planning (CAIP) by dividing it into mainly two group
Mohib et al.	2009	Hybrid system	water pump housing	They also discussed about the sensor selection and inspection feature inspection

				applied to an automotive engine
Martinez et al.	2009	Commercial sensor	Complex surface	The study deals with finding the optimum viewpoints through a fuzzy set approach
Scott	2009	laser scanning range cameras		Presented a multi-phase, model based procedure for planning of automated high reliability inspection or reconstruction
Zhou et al.	2011	Laser scanners	aerospace applications	Proposes a novel algorithm for freeform surface inspection planning
Zhao et al.	2012	Hybrid system	Free form objects	The scanning path is generated automatically considering the position and view angles

Against this literature review, the present work has been undertaken to develop a novel inspection framework for effective and accurate inspection using contactless 3D scanning system with emphasis on GD&T features. The main focus of this work is to standardize the process of inspection in industries. In addition, the development of benchmark part will help the end users, manufacturing personnel and quality inspectors to characterize their measurement system prior to inspection.

2.6 The Knowledge Gap in Earlier Investigations

This exhaustive literature review presented above reveals the following knowledge gap that helped to set the objectives of this research work:

1. Though a lot of research work has been reported for inspection planning framework, the majority of the work has been done for CMM machines. This makes the inspection process slow, requiring adequate skill and expertise. Also, very few literature is available presenting the inspection planning for advance

manufacturing process i.e. Additive manufactured parts especially with GD&T features.

2. Several work has been reported on improving the scanner accuracy by optimizing the important scanning parameters. However, attempts to investigate the influence of scanned surface topology and local geometry have hardly been explored in literatures for improving the final accuracy. Furthermore, none of the literature reported used the nature-inspired algorithms like PSO and its modified variant for predicting the parameters.
3. As far as surface reconstruction is concerned, most of the work reported are using difficult mathematical approximations, which requires lot of skill and expertise, but only very few of them considered software based conversion. None of them have provided the critical parameters, there factors value and the path for accurate surface reconstruction.
4. GD&T is the main concern when design requirements were interpreted. However, the process relies heavily on human interaction. A more effective way of collecting and representing the GD&T error in metrology environment is needed.
5. Most of the work carried out for determination of GD&T error evaluation are based on the least square method that results in overestimation of tolerances. Very few of the literatures have used nature inspired algorithm for effective and accurate evaluation for form errors.
6. None of the literature have proposed any benchmark part for testing and evaluation of the scanner accuracy and the inspection framework.

2.7 Research objectives

The objectives of this research work are outlined as follows:

1. To overcome the limitations of traditional slow inspection planning procedures used in industries using CMM machines and replacing it with non-contact scanning based GD&T inspection framework for advanced manufacturing process like additive manufacturing.
2. To investigate the influence of scanned surface topology and local geometry (scanning distance and scanning angle) for improving the final accuracy of reverse engineered models using nature inspired algorithm.

3. To investigate the critical parameters, their factors value and the path for accurate surface reconstruction and improved accuracy of developed model.
4. To develop the mathematical model for effective and accurate evaluation of form error from the coordinated measured data obtained from CMM and 3D scanning and further optimized it using nature inspired algorithm like PSO.
5. To propose an improved variant of particle swarm optimization for more improved results in step 2 and 4.
6. To design and develop a benchmark part suitable for testing and evaluation of the scanner accuracy and the above developed inspection framework in step 1 for GD&T features.

2.8 Chapter summary

The chapter reviews the literature available on challenges and issues in additive manufacturing, scanning parameter optimization, surface reconstruction methods, GD&T error evaluation methods and various inspection frameworks. Based on the literature discussed, the research gap in the past research is determined and based on that objectives of the present work are determined.

CHAPTER 3

MINIMIZATION OF ADDITIVE MANUFACTURING CHALLENGES AND ISSUES

This chapter is focused on investigating different challenges and issues associated with AM produced parts. The main aim of this chapter is to improve the quality of the parts by suggesting and applying suitable corrective action. In AM, parts are produced from CAD model using STL format to handle and transfer data of a part. Additionally, AM can add multiple materials in a single part, and produce fully practical assembled mechanisms. The use of AM is useful in the field of automobile, biomedical, aerospace where unique feature components are required. One of the key characteristics of the AM systems is that lot of tutorials, blogs are available on the internet for sharing and exchanging ideas among users and developers to account for the betterment of the machine.

For the present study, three different AM machines are considered to examine significant similarities and differences among them. The three machines were the replicating rapid prototyper (RepRap II: Mendel) (<http://reprap.org>), the MakerBot CupCake CNC (<http://makerbot.com>) and the most popular Indian model 'aha!' ELAM machine Reality 3D version 2 (R3D2) (<https://ahagadgets.wordpress.com>, <http://www.aha3d.in/>). Although the three systems have somewhat different performance specifications as shown in Table 3.1, they hold the same layer by layer extrusion technology. One of the main advantages of all the systems is that the information about the hardware and software is easily available on the internet and blogs. It will help the end users to discuss the issues relating to these machines.

On the contrary, the key difference among the printers is in terms of cost, the aha! R3D2 is less expensive than the RepRap II and CupCake CNC, which makes it most affordable among the three. The part file for printing fed to R3D2 and CupCake CNC printer either by SD card or through USB but the RepRap only uses USB connection. The printing speeds of R3D2 and RepRap are comparable but the Cupcake has low printing speed. Another important factor to be considered is the print area, which is more in R3D2 as compared to the other two. The large print area will make

the use of R3D2 beneficial in terms of printing large products. Furthermore, the print resolution for R3D2 is 0.075 mm making it possible to construct minimal thickness edge or boundary of a part and hence provide better accuracy than the other two. Also, the construction of R3D2 is simple and robust rather than other two which looks complicated with the naked eye. Due to all these aforesaid advantages the R3D2 ELAM printer (see Figure 3.1) is considered for the present work to study the limitations of entry-level machines. While R3D2 used as an entry level machine, it must be elucidated that the results obtained from this paper do not aim to generalise the capabilities or limitations of other ELAM systems available in the market.

Table 3.1 Technical Specifications of ELAM systems

System	R3D2	RepRap	CupCake CNC
Cost	US\$ 700	US\$ 830	US\$ 750
Positioning	(X,Y,Z) three axis system	(X,Y,Z) three axis system	(X,Y,Z) three axis system
Input Type	SD card and USB	USB connection	SD Card and USB Connection
Print Dimensions(mm)	200 x 220 x 200	200 x 200 x 110	100 x 100 x 130
Printing Speed	8400 mm/min	9000 mm/min	5000 mm/min
Print Resolution (mm)	0.075	0.1	0.08
Materials	ABS, PLA	ABS, PLA, HDPE	ABS, PLA, HDPE, CAPA

3.1 Entry Level Additive Manufacturing (ELAM): Basics

The use of affordable AM machines is now locating its place in education where students can feel, fit and sense the fabricated objects. One of such low-cost ELAM machines was used as shown in Figure 3.1. One of the advantages of ELAM systems is that they can use open source slicing software such as Slic3r, Cura, kisslicer. Another

advantage is that these machines come with a single nozzle and the support material can be extruded through the same nozzle in a sparse manner. This cuts the cost of machine as wide choice of feedstock filaments are possible. It consists of a horizontally translating (x-y) heated bed platform with a usable build area of 200 mm x 220 mm and vertical translating (z-direction) extruder fitted with a nozzle. The maximum build height of the machine is 200 mm. The extrusion process is governed by a stepper motor with a feed of 1.7 mm diameter ABS filament into a heated 0.15 mm diameter nozzle. The R3D2 ELAM machine used to fabricate parts with a layer thickness of 0.075 mm.

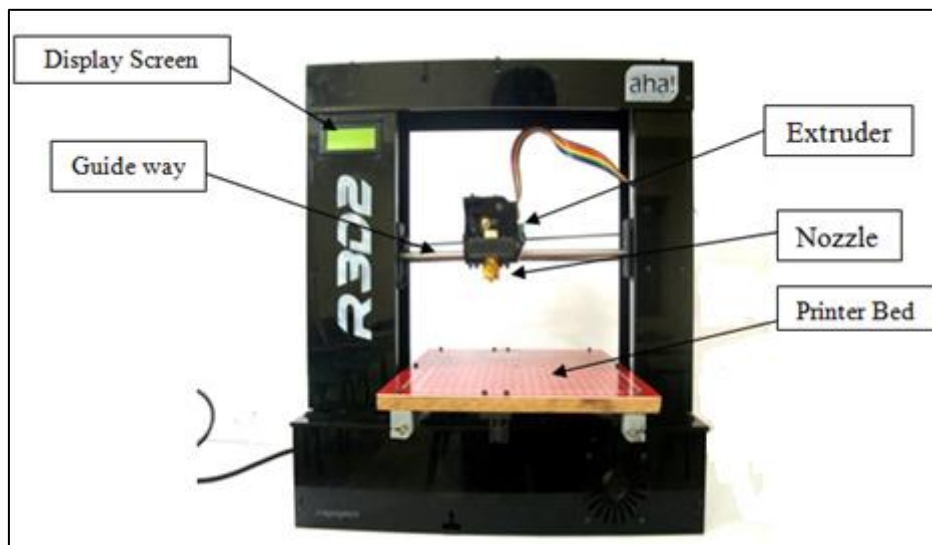


Figure 3.1 Schematic of R3D2 entry-level AM Printer

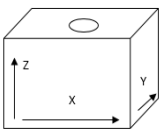
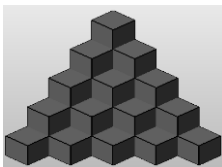
The process of printing the parts on R3D2 ELAM system begins with the CAD model saved in STL format. The surface defining the design must not contain any discontinuity (non-manifold edge). The part could be re-oriented and repaired for optimum print quality using Netfabb and MeshMixer. Slic3r software was used to slice the part with suitable layer thickness and for adjusting other print parameters before G-code generated. Initially, the extruder head and printer bed were heated to a predefined temp and then extruder head begins to extrude molten plastic to build prototype taking shape from bottom to top layer by layer. Acetone-ABS mixture is used on printer bed for effective part adherence. Acetone solution offers a satisfactory adhesion of the part on printer bed during the printing process.

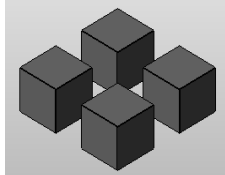

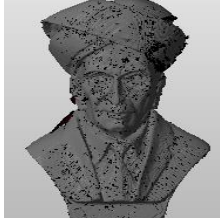
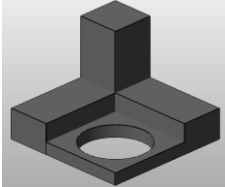
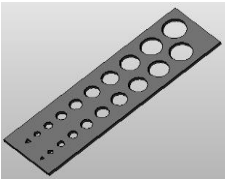
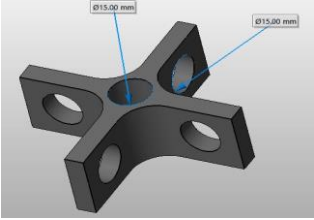
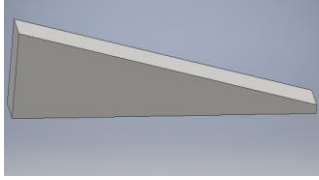
3.2 Objectives of the experiment

The elementary purpose of the experiments was to study the restrictions and challenges of an ELAM system when fabricating distinctive models and provide possible remedies for its minimization. The machine used for development of parts is an entry level AM machine, which works on an extruded filament basis. Regarding experimental limitations, only one trial was conducted for most model and thus the study does not really report the aspect of process variability. For providing consistency in the experiments, the ELAM machine was used with identical settings in terms of nozzle temp. (210°C), bed preheat temp. (60°C) and nozzle head speed (80 mm/s) with the single extrusion material (ABS) and bed surface during the trials. Additionally, all the trials were performed at the same time and at room temperature in a well-ventilated indoor space.

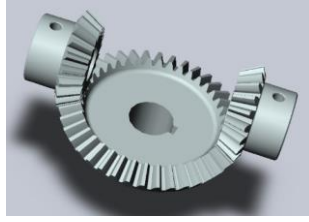
ELAM has an advantage of lower equipment cost processing cost and fast processing time. However, getting quality parts on entry level AM printer is always a big challenge. Ten CAD models were developed using Inventor software from Autodesk depending on its complexity. The significant features of the ten models are summarised in Table 3.2. They comprise of standard cubes with holes, Plane slab, stepped blocks, nested blocks, open cube, plate with different dia. holes, assembly parts and a statue. From the CAD models, the subsequent step was to manufacture them on the entry level R3D2 system and record any critical issues.

Table 3.2 CAD part fabrication using R3D2 printer

Models	Image	Features	Objective of Test	Affected Attributes
Standard Cubes with hole		Block, Hole, cylinder (Internal/ External Dimension)	To investigate dimensional accuracy	Linear Dimension, circularity, diameter
Stepped blocks		Object & parasites quality	To investigate whether extruder is injecting adequate material or not. (E steps/mm)	Surfaces, Edges, Ceilings

Multiple Cubes		Blocks in series (printing of multiple objects-intermittent printing)	To investigate the accuracy in printing multiple parts simultaneously	Aesthetics including upper surface and edges
Knuckle Joint		holes, protrusions and shafts	To investigate if fabricated parts could be assembled (relative accuracy/ Tolerance)	Assembly (Fit)
Sculpture Model - Visvesvaraya Statue		(Intricate profiles) Variation of curvature, Intricate details	To study minute features formed with or without support structures.	Minute details like Eyes, ears
Open Cube		Open Cube, Holes	To investigate printer quality at varying speeds	Bottom Surface
Plate with different dia. holes		Discontinuous – printing (breaks)	To investigate whether varying hole size can be printed in one part	Quality of Internal surface (internal nesting)
Cutter of grinder		Holes along three mutually perpendicular planes i.e. along x, y and z directions	To investigate the best axis or plane for printing circular holes.	Holes internal diameter and circularity
Ramp plate		Slope	To investigate angular deviation	Wedge and slope

Bevel Gears



Number of protrusions

To investigate if the parts can be fabricated with sufficient accuracy to allow meshing

Gears meshing

3.3 Fabrication of CAD models and Observed issues

Standard Cubes with hole

Dimensional Accuracy

Standard cube model having simplest of geometry with overall dimensions 30 x 30 x 30 mm³ (see Figure 3.2 (a) and (b)) and hole diameter of 10 mm printed on the ELAM R3D2 machine to understand about its resolution and accuracy. The cube was printed six times to examine the repeatable accuracy of the ELAM. The objective was to investigate the dimensional accuracy which includes linear dimensions along x, y, z-axis and diameter as well as the circularity (Figure 3.3 (a)) of the hole in the cube. Digital Vernier calliper with least count of 0.02 mm was used for measurement of linear dimensions. For diameter and circularity, touch probe Coordinate Measuring Machines (CMM) was employed as shown in Figure 3.3 (b) to have a greater level of accuracy in measurement.

The results of linear dimension, diameter and circularity measurement for all cubes was reported in Table 3.3. Figure 3.4 clearly shows the error distribution along the different axis. It was found that during printing, the dimensions along x and y direction are undersized as clearly seen in Figure 3.4 (a) and (b) all the error bars are below the nominal dimension (30 mm). Further, the dimension along z direction were oversized as seen in Figure 3.4 (c). The average dimensions along height was approximately 3% higher than average dimensions along x and y direction. From previous results, it was evident that linear dimension gets affected during printing with ELAM. Additionally, the dimensions in height was significantly higher than the length and width. Table 3.3 shows further that dimensional accuracy likewise different in the x, y and z axes i.e. -1.99%, -1.77% and 1.40% deviation respectively. The possible reason was high perimeter width setting in the slicer software, temperature difference on the bed surface and changes in environmental conditions. The flow rate settings for the perimeter was reduced in the slicing software and uniform temperature of the bed

surface was maintained. Also, the environmental conditions like humidity and temperature rise was maintained at suitable value. These factors can only minimise the dimensional inaccuracy as it is an inherent problem in the AM machines due to the approximations in STL file.

Circularity

According to ISO (ISO/DIS 1101-1996), the circularity tolerance (Figure 3.3(a)) is the minimum radial distance between two concentric circles enclosing the given feature. For defining a hole, measurement of six points on its circumference was performed using computer controlled touch probe CMM. The bar chart as depicted in Figure 3.4 (d) and 3.4 (e) indicate three issues,

1. The circularity of six circles measured at the top and bottom surface,
2. The difference between measured diameter and nominal diameter as diameter error,
3. The diameter error is shown as a percentage of nominal diameter.

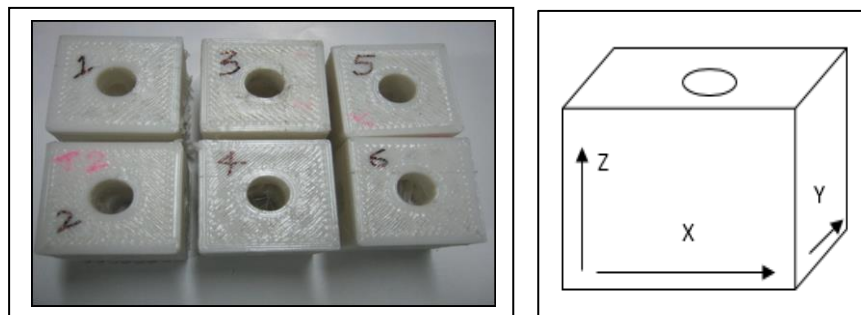


Figure 3.2 (a) 30x30x30 mm cube (b) Measurement direction for cube along x, y and z direction

Table 3.3 Linear Dimension, diameter and circularity measurement of standard size cube

S. No.	Along X (mm)	Along Y (mm)	Along Z (mm)	Top Surface		Bottom (Bed) Surface	
				Diameter	Circularity	Diameter	Circularity
1	29.80	29.52	30.74	9.5635	0.1209	9.3852	0.169
2	29.10	29.42	30.36	9.4711	0.1062	9.3531	0.4435
3	29.38	29.32	30.20	9.3225	0.1021	9.2304	0.4334
4	29.46	29.40	31.00	9.6998	0.1647	9.3527	0.3092
5	29.72	29.76	30.00	9.5291	0.1748	9.076	0.2622

6	29.84	29.42	30.20	9.657	0.2034	9.4254	0.2415
Avg	29.43	29.47	30.42	9.54	0.15	9.30	0.31
Nominal	30	30	30	10		10	
% deviation	-1.9	-1.77	1.40	4.6		6.96	

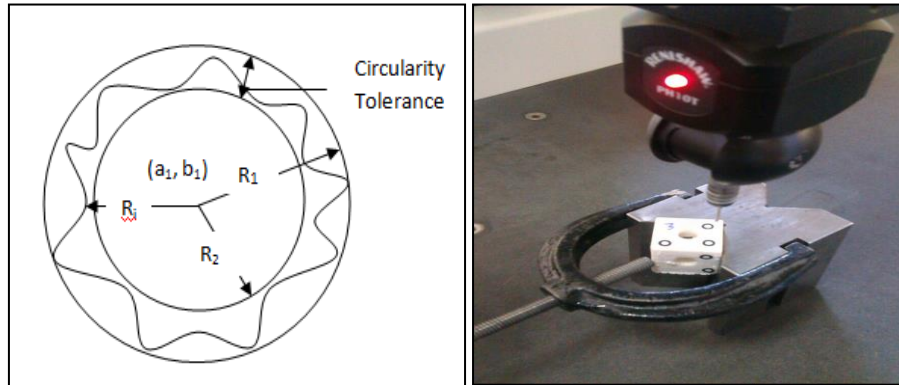
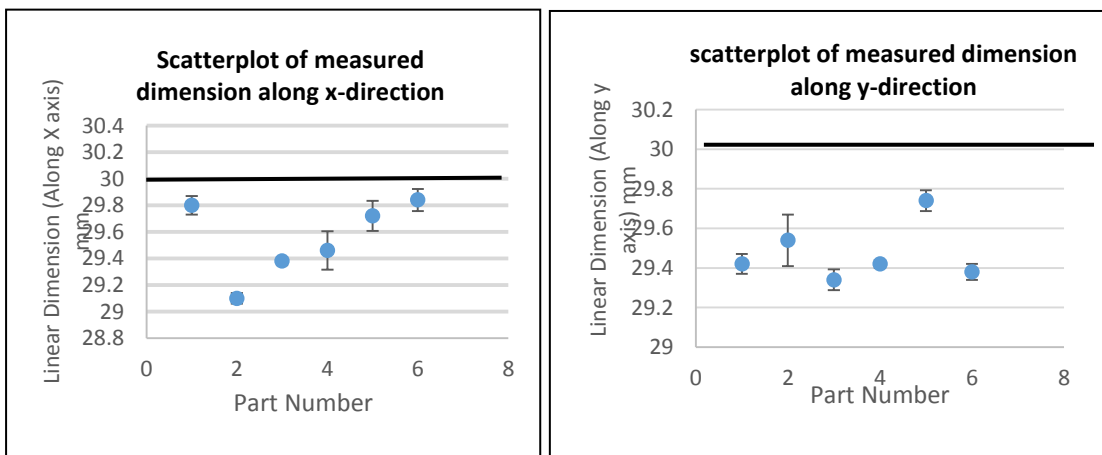


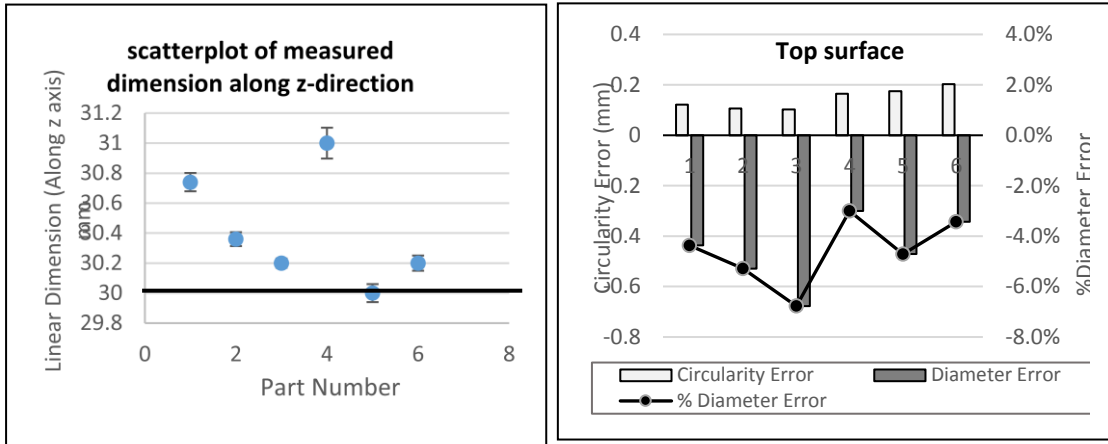
Figure 3.3. (a) Circularity Tolerance (b) CMM Measurement

The diameter errors were in accordance with the dimensional errors determined earlier. The negative diameter errors for both (top and bottom) surfaces were consistent with the conclusion that the part expanded and the wall thickness was increased. The percentage deviation of the diameter was higher at the bottom (bed) surface i.e. 6.96 than the top surface i.e. 4.6. The possible reason was contraction at the bottom surface due to the binding process between part materials and binding mixture on the printer bed surface. First layer is free to contract, but as we move from bottom to top the contraction decreased due to restriction by earlier printed layer. The last layer was most restricted which results in the least contraction, but still it was undersized in this case. The solution to minimize circularity and diameter error is same as that for the dimensional accuracy.



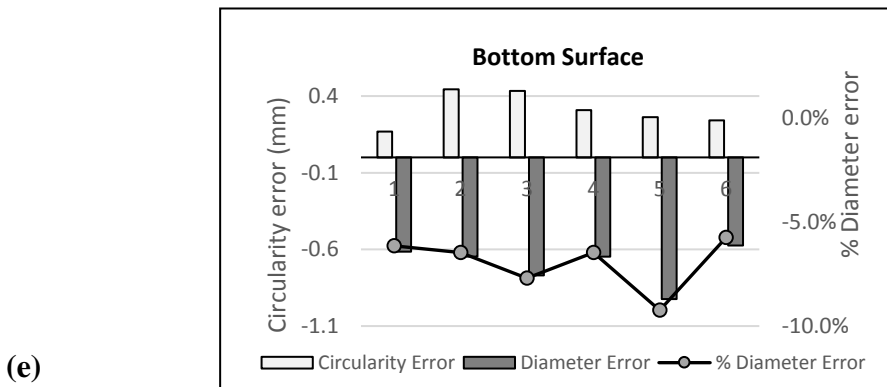
(a)

(b)



(c)

(d)



(e)

Figure 3.4 Variation of linear dimension, diameter and circularity for six standard cubes

Stepped Blocks

The stepped blocks contain a number of cubes stacks in series along x, y and z direction. The objective was to investigate whether the printer extruder injecting an adequate amount of material and the stepped block surfaces and edges are properly build. Owing to the relatively small surface area, no warping occurs but the upper surface of the stepped block shows some globbing appearance in which the top surface is not as precise and defined. As seen in Figure 3.5 (a) the material deposited at the top surface of the stepped blocks was not able to cool quickly enough to preserve its shape. The

most common cause was slow cooling process of the extruded plastic. The other possible reason includes printing at too high temperature, too many E-steps per mm of the extruder which makes printing process too fast and providing less time for solidifying each layer. A cooling fan for effective cooling of each layer was fitted on the head of the printer. Additionally, the print temperature was reduced down by 10-15 degrees. At last, the extruder steps per mm in the slicing software was also reduced by hit and trial. The earlier stepped blocks were made at 92 steps per mm. Thereafter, a number of trials were performed with reduced steps along with the possible solution discussed above. The best result were obtained at 85 steps per mm as shown in Figure 3.5 (b).

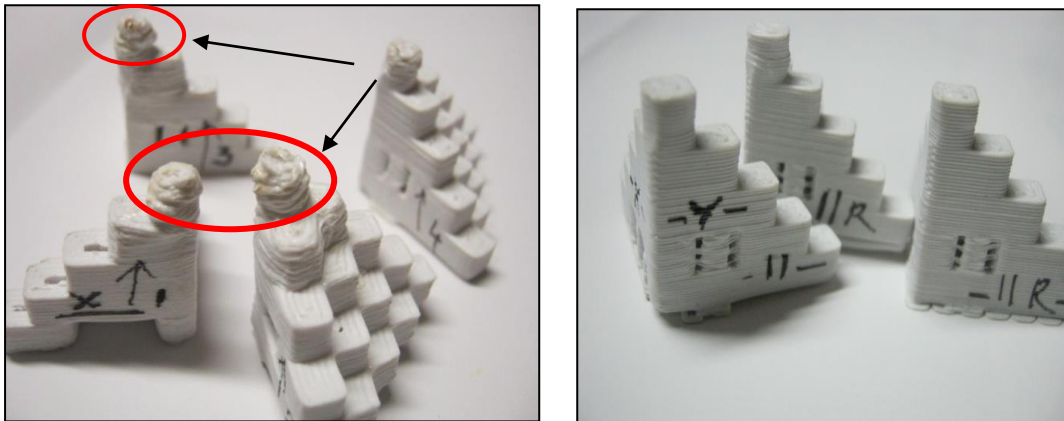
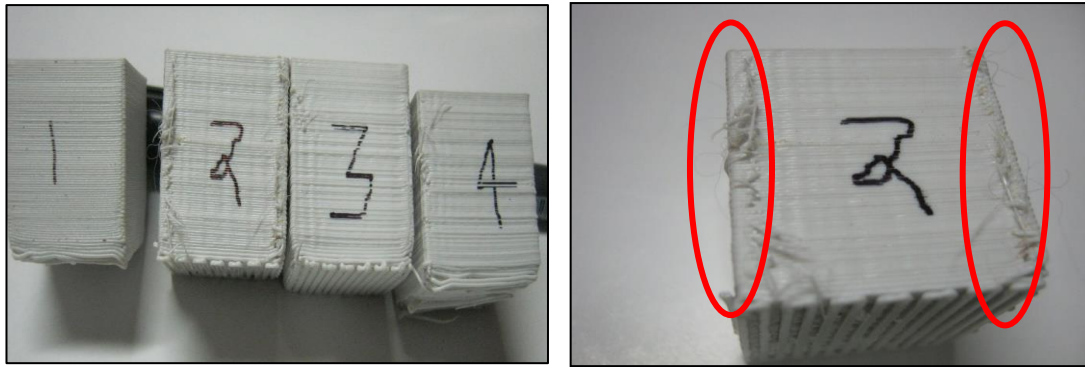


Figure 3.5 (a) Stepped blocks with globbing **(b)** Stepped blocks with clean surface

Multiple Cubes

In requirement of multiple copies of a part as one by one printing may take a lot of time. The objective was to investigate if these similar cubes can be printed simultaneously without any significant issue. The experiment showed that multiple cubes were printed in the same time, it takes for printing a single cube but the only issue is the occurrence of strings like appearance at the edges (see Figure 3.6 (a) and (b)). The possible reason was the large Z-offset distance of extruder from the bed resulting in the formation of threads due to poor adherence on the earlier printed layer. Also, disabled retraction setting in the slicer software makes the material drips out when the nozzle moves. The retraction setting was enabled in slicing software and Z-offset was reduced by 0.2 mm at a time, until strings formation stops. The problem was resolved by reducing the Z-offset by 0.6 mm in the motion settings of the printer itself. The result was satisfactory and multiple cubes were printed without any strings as shown in Figure 3.6 (c).



(a)

(b)



(c)

Figure 3.6 (a) Multiple cubes (b) Zoom view showing strings at the edges (c) Cubes with clean edges and surface

Knuckle Joint

The knuckle joint part consists of protrusions, holes and a shaft which categorised it as an intricate model. The objective was to examine whether the parts of knuckle joint could be assembled as a functional prototype. Despite the lengthwise dimension, no warping occurs in any part. The only problem found during the trial was undersized holes which results in a slight problem in the assembly of parts. As this problem is an inherent property of most of the printers, it is advisable to provide some tolerances in holes of 4-6 mm. After providing tolerances, parts were again built and assembled easily with no other issues observed (Figure 3.7).

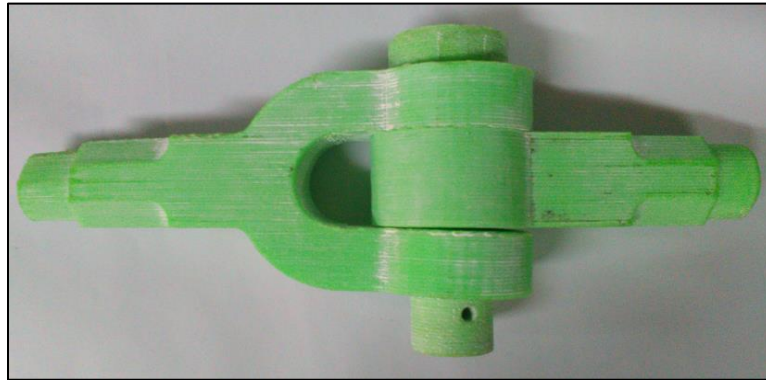


Figure 3.7 Assembled Knuckle Joint

Sculpture Model - Visvesvaraya Head

The complexity of the Visvesvaraya statue lays in having multiple variations of curvatures with very intricate surface details like eyes, ears, cheeks etc. It was observed that the statue geometry is slightly overhanging. The objective of the experiment was to examine if complicated and minute surfaces could be fabricated with or without the use of support structures. During the first trial, it was found that the part of the statue at the shoulder was slightly over hanged and without support structure it was not able to build. The solution was to provide support structures at the shoulder overhangs. So the final model was built with the support structure, the eyes are not clear as these are tiny, otherwise the other small features were built easily (Figure 3.8). The only issue to look after was removal of support material so that it does not affect surface finish and quality. Due to the removal of support structures surface blemishes appears on the surface. This positive outcome will make printing of overhang structures possible.



Figure 3.8 Sculpture model of Visvesvaraya

Open Cube

The open cube models having simplest of geometry with overall dimensions 90 x 90 x 90 mm³ were printed on the R3D2 machine. The objective was to investigate the maximum speed up to which it can print the parts adequately. The open cubes were printed by varying speed of extruder i.e. 80, 100 and 120 mm per sec. The first part made with 80 mm per sec speed shows no distortion, but the second and third part had significant distortion with maximum warpage is shown in part made with 120 mm per sec speed (Figure 3.9).

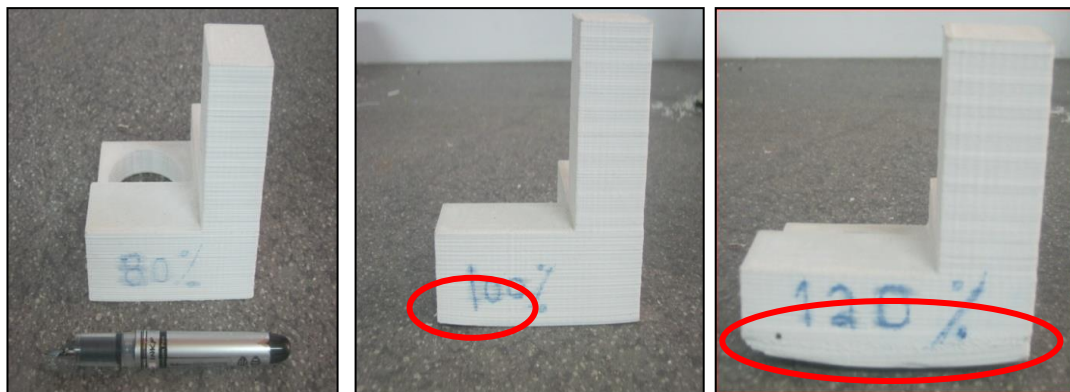


Figure 3.9 (a) 80mm/s speed (b) 100 mm/s speed with little distortion (c) Part with 120 mm/s speed with maximum warpage

Warpage occurred due to a variety of reasons. The primary reason was significant difference in temperature of the bed and first layer of the part, resulting in development of internal stresses which causes warpage. The other possible reasons include unclean bed surface, improper adhesion, too low bed temperature. Brim or raft up to 3-4 mm was used for minimising warpage in slicing software so that job gripped on the bed surface. Another solution performed was maintaining of the bed temperature just below ‘glass transition temperature’ of plastic which helped in keeping the first layer flat. The bed surface was properly cleaned before each run and ABS-acetone sticky solution was used evenly on bed surface for enhancing the job grip. Further, the cubes were built with 100 and 120 mm/s using raft or brim at the bottom surface which shows satisfactory results (Figure 3.10).

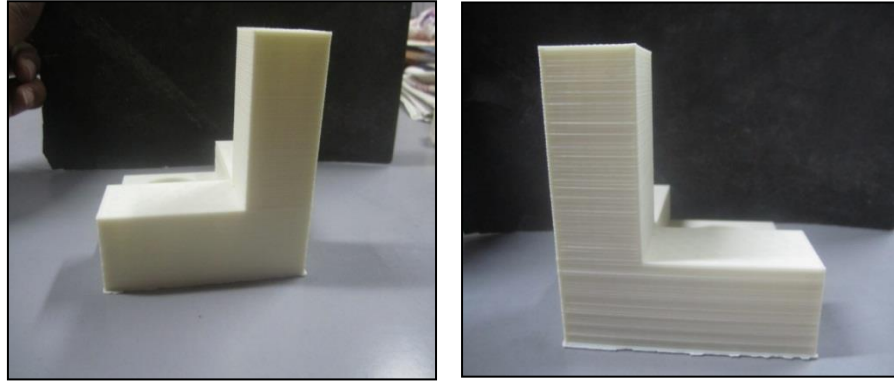


Figure 3.10 Open cubes printed with raft having no warpage

Calibration plate with varying diameter holes

The calibration plate contains several holes of varying diameter. The objective was to investigate whether the varying diameter holes are built using ELAM accurately. The result showed that plate is built with undersized holes and numerous ‘threads’ were formed at each hole called oozing of the extruder. As the hot head moves to a different location for deposition, it loses or leaks some material on the way that creates the unwanted small strings. The primary cause for the oozing is disabled retraction setting and the excess temperature of the extruder when moving from one location to other. This can be seen in the calibration plate (Figure 3.11) showing threads of ABS filament across the holes. The possible solution is reduction in extruder temperature and adjusting the retraction length of the extruder to 5 mm. There are also options in the software as Prime, Purge etc to control the so called leak of nozzle around the print part –known as Ooze.

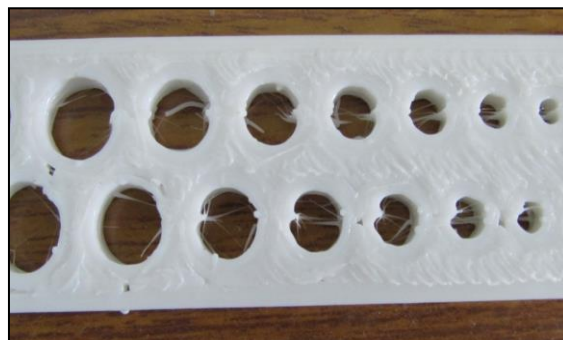


Figure 3.11 Calibration plate showing oozing defect

Grinder Cutter

Grinding cutter with holes along x, y and z axis is used in this study for investigating the best axis or plane for printing circular holes. Ten parts were printed using different settings of printer and the circularity values were measured for each axis. The bar charts in Figure 3.12 (a) depicts that holes printed in XY plane (along Z-axis) shows minimum circularity deviation. On the contrary, the circularity deviation in XZ plane (along y-axis) shows the maximum deviation for all ten parts. The result suggests that it is better to print holes along Z-axis rather than printing along X and Y axis for improved results. Subsequently, the orientation of the part on AM machine becomes an important factor. Additionally, the graph clearly shows that average circularity deviation does not exceed 0.2 mm which is in accordance with the earlier results.

Ramp Plate

The ramp plate was the next part printed to investigate the angular deviation for wedge feature fabrication. The angular tolerance is defined as the maximum allowable deviation from a specified angle. Figure 3.13 shows the location of angles that were measured. Nine parts (three for each angle) were printed to get the better repeatability for the measurement of angles. The part angles were measured using computer controlled touch probe CMM. Figure 3.14 shows the uniformity in the sign of angles of all the printed parts. Due to less amount of data it is difficult to provide reasons for this trend. However, the graph shows that the angular tolerance is within 0.65° for all the three angles.

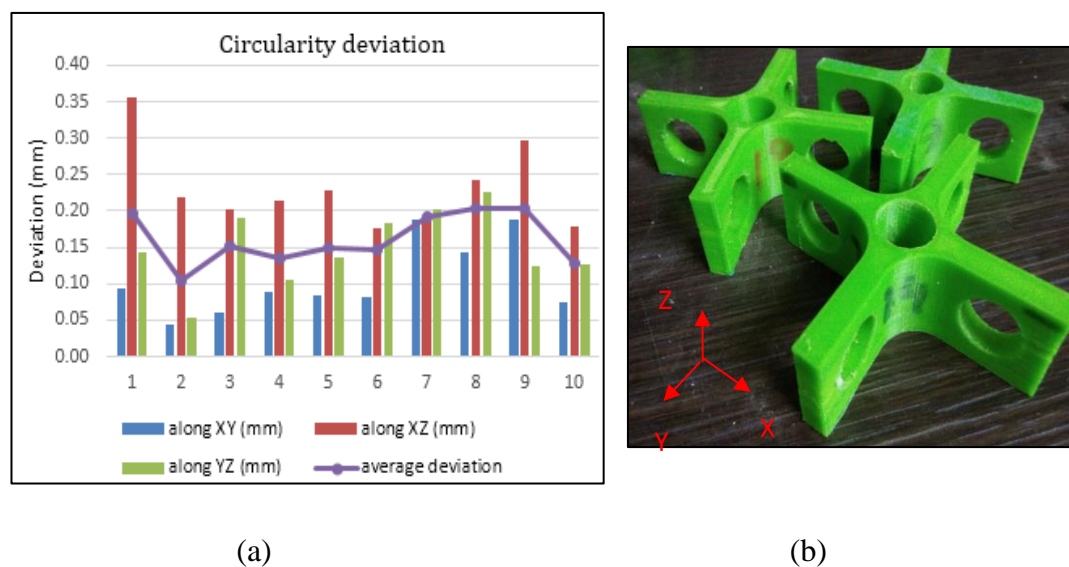


Figure 3.12 (a) Circularity deviation of ten holes **(b)** 3D printed grinding cutters

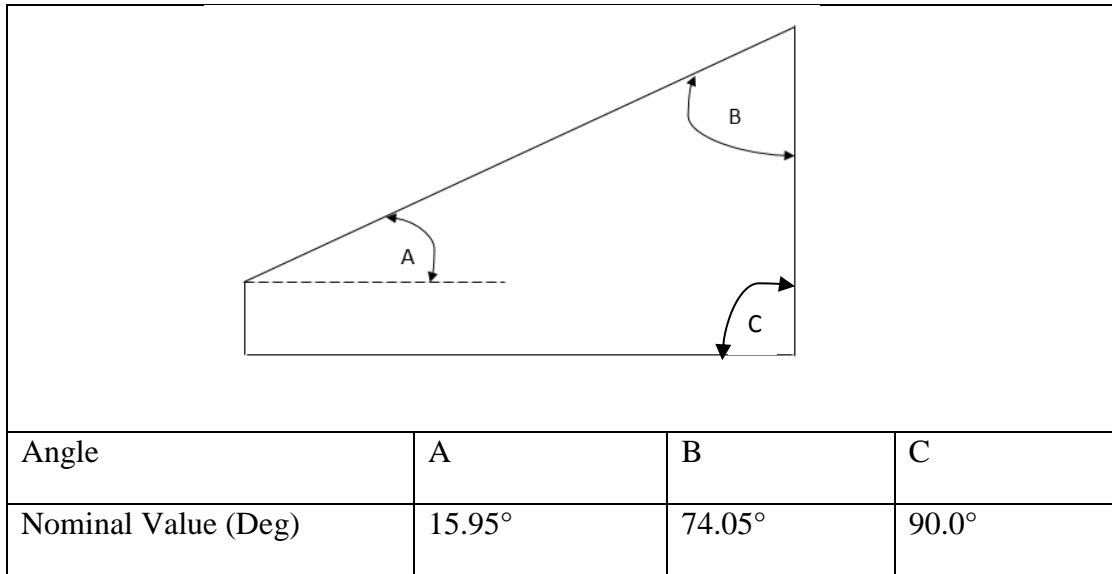


Figure 3.13 Position of measure angles in ramp plate for angular deviation

Bevel Gear System

The bevel gear model possesses high level of rotational symmetry with smallest of difference in surface curvature. However, the model intricacy rests on more number of protrusions and holes. The prime objective was to examine whether the parts could be produced with adequate accuracy that would allow the gears to mesh. The developed models were free from any major issues, only small blemishes were occurred on the some teeth of the gears as shown in Figure 3.15. Finally, the bevel gears were assembled together having proper meshing of the teeth.

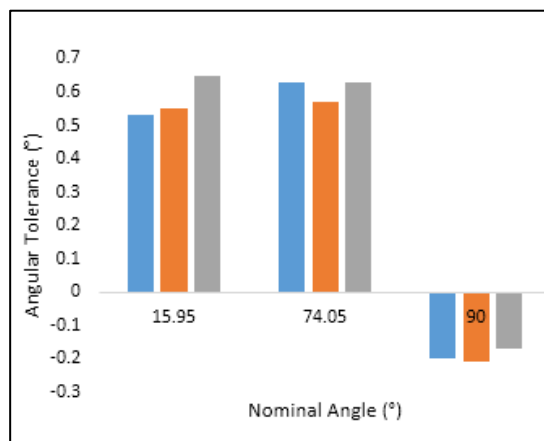


Figure 3.14 Angular tolerance of parts printed with different angles

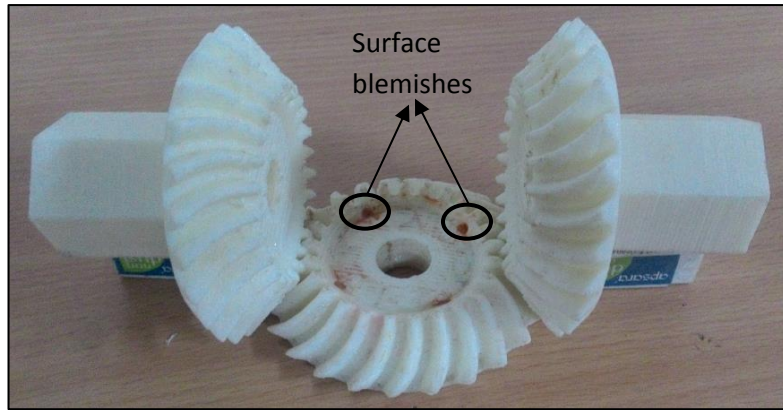


Figure 3.15 Bevel gear model with small surface blemishes

3.3 Summary of Issues found and Actions performed

This section summarises various issues encountered during development of proposed CAD parts using R3D2 ELAM machine. Further, the possible causes and suitable corrective action to be taken for minimising these issues were proposed based on the experiments conducted and the observations made (Table 3.4). This table will provide a helpful lead for the users and machine developers to improve the machine further.

3.4 GD&T error minimization

In recent times, due to emergence of advance manufacturing technologies, the market situation has become extremely competitive and volatile. To sustain in such competitive market, it is imperative to not only produce low cost product but also with high quality and shorter development time. To achieve the aforesaid objectives in flexible manufacturing industries, they are forced to use advanced manufacturing tools and machines such as Rapid prototyping (RP).

Additive manufacturing (AM) is a rapid growing tool that belongs to RP technologies. Although RP has shown competence in fast product development but its full- fledged use is hindered by limited materials available in market [Levy et al., 2003; Pilipovic et al., 2009]. To improve its sustainability in market, its performance needs to be improved. One way of improving the performance of any process is by suitably adjusting and optimizing its process parameters so that improved quality products may be fabricated.

Table 3.4 Problem, cause and corrective action

Model	Problems Found	Possible cause	Actions performed or recommendations
Standard Cube with Hole	Inaccuracy in Linear Dimensions	Inaccurate flow rate of printer, temperature difference on the printer bed, raster on the bed, environmental factors like increase humidity, excessive dust and temperature.	Flow rate of the printer was reduced gradually and different thickness wall or linear dimensions were printed for accurate flow rate of printer. For better accuracy wall thickness was kept an integral multiple of road width. Bed temperature was kept fixed, trials were performed in fully AC room to reduce moisture and keep away dust.
	Diameter, Circularity Error	Contraction at the bottom surface due to the binding process between part materials and binding mixture on the printer bed surface. G01 G-codes setting in the Slic3r software used was for approximated line segments.	Flow rate was adjusted and bed temperature was kept fixed. Kisslicer and Cura software used generate G02, G03 arc codes.
Stepped Blocks	Deposition defect	Primary reason is slow cooling process of the extruded plastic. Printing at too high temperature, too many E-steps per mm of the extruder which makes printing process too fast and providing less time for solidifying each layer.	Proper cooling was achieved by mounting a fan on the extruder head. Extruder temperature was reduced down by 10-15 degrees.
Multiple Cubes	Oozing Defect and strings like artefact	Large Z-offset and disabled retraction setting in the slicer software makes the material drips out when the nozzle moves.	The retraction setting was enabled in slicing software and Z-offset was reduced by 0.2 mm at a time, until strings formation stops at 0.6 mm.
Sculpture Model - Head	Surface Blemishes	Indolent removal of support material	Support material was removed by dipping the part in acetone solution.
Open Cubes	Warpage Error	Significant difference in temperature of the bed and first layer of the part, unclean bed surface, improper adhesion, too low bed temperature.	Brim or raft up to 3-4 mm was used for minimizing warpage in slicing software. Bed temperature was maintained just below 'glass transition temperature' of plastic which helped in keeping the first layer flat. The bed surface was properly cleaned before each run and ABS-acetone sticky solution was used which helped in minimizing the warpage.
Knuckle Joint	Under sizing of holes	Resolution of the machine in X Y Z movements, positional error etc.	Appropriate tolerances provided and the parts were assembled.
Calibration Plate	Oozing and strings formation	The primary cause is disabled retraction setting and the excess temperature of the extruder when moving.	Adequate temperature of extruder and high speed of retraction provided.
Grinder Cutter	Circularity error along x, y and z axis	Resolution of the machine in X Y Z movements	Result suggests that it is better to print holes along Z-axis rather than printing along X and Y axis for improved results.

3.4.1 Material and Methods

The quality and accuracy of any part produced using AM process typically depends on its process parameters. This study considered four important process parameters bed temperature (A), nozzle temperature (B), Infill (C), layer thickness (D) to study their effects on circularity (C_1) and flatness (F_1 and F_2). The circularity was measured for the hole and flatness was measured for the two surfaces as shown in Figure 3.16. The factors and their levels under which tests were carried out are given in Table 3.5. They are defined as follows:

- Bed Temperature (T_b): It is the temperature of printing bed. Its value changes for different material and adhesion of part depend on its correct setting.
- Nozzle Temperature (T_n): It is the temperature of the extruder.
- Infill (I): It is defined as the quantity of material injected inside the part. Optimum material inside the part can improve part quality with less waste of material.
- Layer Thickness (L): It is the thickness of each deposited slice. It is known that lower the layer thickness, better the part quality.

However, the number of experiments could be large when considering more parameters and levels. Taguchi orthogonal array is a good method to reduce the number of experiments According to Taguchi's design of experiments, for four parameters and three levels L_9 Taguchi orthogonal array (Jiang et al., 2010) was selected (Table 3.6). A 3D solid model of test part (Figure 3.16) is modelled in Creo parametric software and exported as stereolithography (STL) file. Further, STL file is imported in open source Slic3r AM

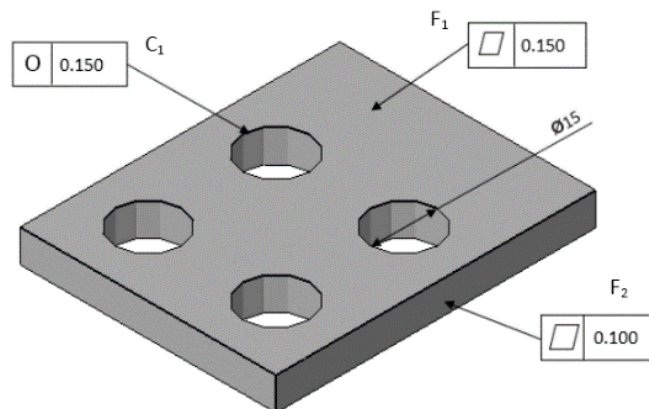


Figure 3.16. Test sample for GD&T error analysis. (All dimensions in mm)

software for G-code generation. The control parameters were set as per experimental plan (Table 3.6) and three parts per experiment were performed using Aha! R3D2 AM machine. The parts were manufactured using digital ABS material. Three readings for all the responses were taken per sample and average is taken and represented in Table 3.6. GD&T errors were measured using a computer controlled coordinate measuring machine (CMM).

Table 3.5 Factors and their levels

Factor	Symbol	Level			Unit
		1	2	3	
Bed temp. (T_b)	A	110	125	140	°C
Nozzle temp. (T_n)	B	200	215	230	°C
Infill (I)	C	20	25	30	%
Layer thickness (L)	D	0.2	0.3	0.4	mm

Table 3.6 Experimental run using L_9 orthogonal array

Exp. No.	Factors				Responses		
	A	B	C	D	C_1 (mm)	F_1 (mm)	F_2 (mm)
1	1	1	1	1	0.0925	0.1251	0.0439
2	1	2	2	2	0.0810	0.1290	0.0735
3	1	3	3	3	0.0688	0.1221	0.1051
4	2	1	2	3	0.1350	0.1142	0.0845
5	2	2	3	1	0.1380	0.2176	0.0867
6	2	3	1	2	0.0964	0.0765	0.0823
7	3	1	3	2	0.1878	0.1950	0.1232
8	3	2	1	3	0.1426	0.1030	0.1049
9	3	3	2	1	0.1736	0.1959	0.1144

3.4.2 Development of mathematical model

The AM parameter correlation with the circularity and flatness response were obtained using statistical regression analysis with the help of Minitab 16 software. During regression it is assumed that process parameters and response were linearly related to each other. The input factors of Bed temperature (°C), Nozzle temp. (°C), Infill (%) and layer thickness (mm) were used as the independent factors in the regression analysis. The final predictive mathematical model in terms of actual factors is as follows:

$$\text{Circularity, } C_1 = -0.0805 + 0.00291 * T_b - 0.000850 * T_n + 0.00210 * I - 0.0962 * L \quad (3.1)$$

$$\text{Flatness, } F_1 = -0.018 + 0.00131 * T_b - 0.000443 * T_n + 0.00767 * I - 0.332 * L \quad (3.2)$$

$$\text{Flatness, } F_2 = -0.291 + 0.00133 * T_b + 0.000558 * T_n + 0.00293 * I + 0.0757 * L \quad (3.3)$$

3.4.3 Checking the model accuracy

For testing the accuracy of developed model ANOVA analysis technique was used. According to ANOVA, if the calculated p-value is less than 0.05, the developed model is significant. Otherwise, p-value greater than 0.1 means the model is insignificant. However, for this study, the p-value is less than 0.05 for all three models. Hence, the developed models are significant.

Table 3.7 ANOVA for the Circularity (C_1) model

Source	df	Sum of Squares	Mean Square	F-value	p-value Prob > F	
Model	4	0.01360	0.00340	57.84	0.001	significant
Residual	4	0.000235	0.000059			
Total	8	0.013835				
R-Squared = 98.3 %			R-Squared (adj) = 96.6%			

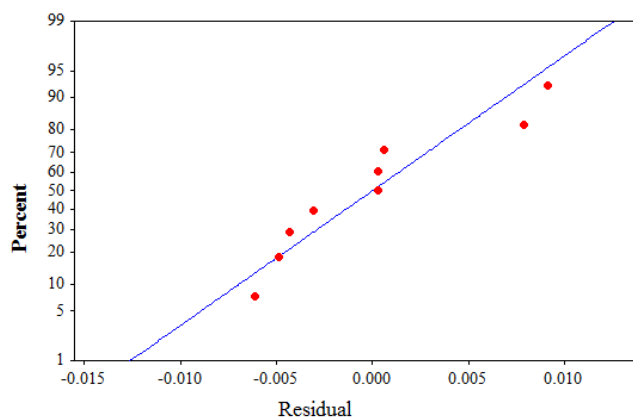
Source	df	Sum of Squares	Mean Square	F-value	p-value Prob > F	
Model	4	0.018012	0.004503	21.27	0.006	significant
Residual	4	0.000847	0.0002117			
Total	8	0.018858				
R-Squared = 95.5 %			R-Squared (adj) = 91.6%			

Table 3.8 ANOVA for the Flatness (F_1) model

Table 3.9 ANOVA for the Flatness (F_2) model

Source	df	Sum of Squares	Mean Square	F-value	p-value Prob > F	
Model	4	0.044542	0.0111355	27.26	0.004	significant
Residual	4	0.0001634	0.0000408			
Total	8	0.0447054				
R-Squared = 96.5 %			R-Squared (adj) = 92.9%			

Furthermore, to further test the adequacy of fitted regression model, determination coefficient (R^2) was determined. For present study, the value of R^2 and adj. R^2 for developed models is more than 80% and 70% respectively. This shows that these models are highly significant (Ramasamy et al., 2002). The results of ANOVA analysis for three models were shown in Table 3.7, 3.8 and 3.9. Additionally, the normal probability graphs of the response factors has been plotted as shown in Figure (3.17-3.19). The plot clearly



shows that the regression model is fairly well fitted to the observed values as the residuals were located on a straight line.

Figure 3.17 Normal plot residuals for Circularity C_1

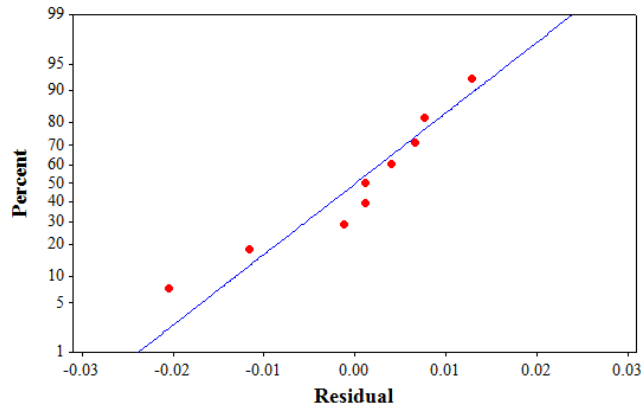


Figure 3.18 Normal plot residuals for Flatness F_1

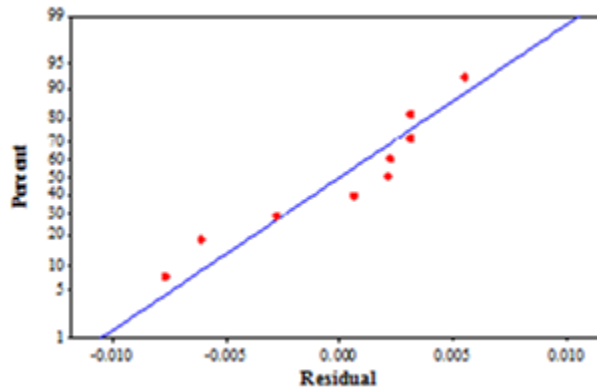


Figure 3.19 Normal plot residuals for Flatness F_2

3.5 Multi-objective optimization

The objective of the present study is to minimize circularity (C_1) and flatness (F_1 and F_2) errors, which is formulated using regression analysis technique. The objectives are function of decision variables viz. bed temperature (T_b), nozzle temperature (T_n), infill (I) and Layer Thickness (L). The empirical relation obtained between input and output parameters obtained from regression analysis were used as functional equations. The objective functions are given below:

Objective 1 = min. C_1

Objective 2 = min. F_1

Objective 3 = min. F_2

A weighted method was used for combining all objectives into a single objective. To overcome any significant difference in the different objectives the function corresponding to every AM performance output is normalized by dividing each function with their individual optimal values obtained in single objective optimization. Now, the weighted objective function now becomes:

$$\text{Minimize } Z = (w_1 * f_1 + w_2 * f_2 + w_3 * f_3) \quad (3.4)$$

where f_1 = Normalized function for C_1

f_2 = Normalized function for F_1

and f_3 = Normalized function for F_2

with the parameter feasible ranges:

$$110 \leq T_b \leq 140 \text{ (}^\circ\text{C)}$$

$$200 \leq T_n \leq 230 \text{ (}^\circ\text{C)}$$

$$20 \leq I \leq 30 \text{ (\%)}$$

$$0.2 \leq L \leq 0.4 \text{ (mm)}$$

Here, w_1 , w_2 and w_3 are the three weighting factors applied to normalized C_1 , F_1 and F_2 respectively. The weighting factors were selected in such a manner that the sum of three is equal to one. Matlab R2014a was used to write program of particle swarm optimization for determining optimum process parameters with minimum circularity and flatness errors by multi-objective optimization. The basic particle swarm optimization is a population based method suggested by Kennedy and Eberhart in 1995. For running optimization, the selected PSO parameters are given in Table 3.10.

Table 3.10. PSO parameters

S. No.	Parameters
1	Population size = 50
2	Max. iteration = 100
3	Simulation runs = 20

$$4 \quad C_1, C_2 = 2.1, 2.1$$

$$5 \quad W_{\text{start}}, W_{\text{end}} = 0.9, 0.4$$

After performing PSO, optimum process parameters were shown in Table 3.11, with different weighting factors. For the present study, case-1 provides optimum results with minimization of all GD&T objective functions. The minimized value of the objective function is 0.0761 with $w_1 = 0.35$, $w_2 = 0.35$ and $w_3 = 0.3$. Hence, case 1 is recommended as it give minimal values of circularity and flatness errors with process parameters as:

$$T_b=133.37^\circ\text{C}, T_n=201.32^\circ\text{C}, I = 20.13\%, L = 0.12 \text{ mm.}$$

Table 3.11 Optimal process parameters with different weighting factors

Control factors	Optimal AM condition			
	Case 1	Case 2	Case 3	Case 4
	$w_1=0.35$	$w_1=0.50$	$w_1=0.25$	$w_1=0.25$
	$w_2=0.35$	$w_2=0.25$	$w_2=0.50$	$w_2=0.25$
	$w_3=0.30$	$w_3=0.25$	$w_3=0.25$	$w_3=0.50$
T_b (°C)	133.37	114.39	134.93	111.17
T_n (°C)	201.32	214.01	226.25	226.40
I (%)	20.13	23.06	22.12	20.44
L (mm)	0.12	0.26	0.25	0.26
C_1 (mm)	0.0611	0.0794	0.0982	0.0828
F_1 (mm)	0.0692	0.0742	0.1167	0.0938
F_2 (mm)	0.0712	0.0851	0.1376	0.1201

3.6 Case study

A 30 mm x 30 mm x 30 mm cube with 10 mm hole was taken as a case study (see Fig. 3.20 (a)), for experimental verification of the predicted optimized process parameters by PSO.

Six cubes were printed by entry level AM machine with the same process parameters as shown in Fig. 3.20 (b). The case study was measured for flatness and circularity using computer controlled Coordinate Measuring Machine (CMM). One part was measured three times and average of the three trials was noted. The result for the case study part is shown in Table 3.12. As shown in Table 3.12, the predicted and experimental values of circularity and flatness are in proximity, which confirms that the developed model is correct.

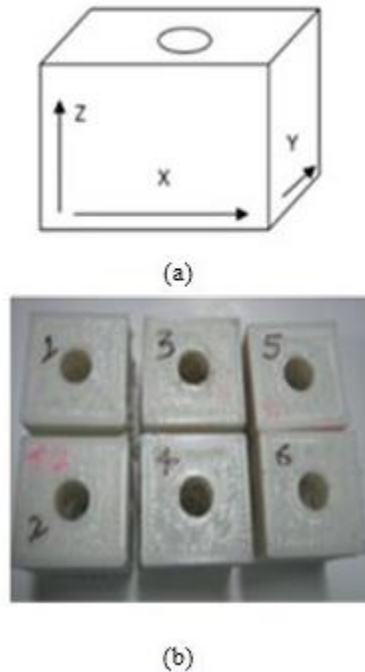


Figure 3.20 (a) Case study (b) Cubes printed with AM machine

Table 3.12 Experimental validation of the developed model

	Predicted	Experimental					
T_b (°C)	133.37	133					
T_n (°C)	201.32	201					
I (%)	20.13	20					
L (mm)	0.12	0.12					
F (mm)	0.069	0.081	0.071	0.077	0.072	0.079	0.072
C (mm)	0.061	0.072	0.063	0.066	0.065	0.061	0.062

3.7 Chapter Summary

This chapter discusses various issues related to AM machines and the corrective actions to eliminate these issues for producing improved quality products. From the models printed as part of current evaluation it was observed that only one out of ten revealed warping symptoms. The warping occurred only in open cubes between the part and the bed surface. Further, it was eliminated by employing factors like, heated printing bed, applying strong ABS-acetone adhesive on printing bed, proper cleaning of printer platform, use 'raft or brim' with large surface area which helps in proper binding of part with bed surface.

The other important observation noticed during current trials was improper deposition of material at the surface leading to the formation of globs and blobs like artefact. This can affect the aesthetics of the built parts. The possible reason for the occurrence of this issue was high E-steps per mm which causes large amount of plastic to extrude. Determination of adequate steps per mm depends upon the skills of the operator and by printing minimum thickness wall is one of the solution. Similar to formation of blobs, strings and threads produced was also one of the important issue. During printing multiple copies of an object, it is important for extruder to print adequately and properly. Formation of strings and threads are governed by more Z-offset distance between bed and extruder. Also, lesser retraction speed of extruder is one of the contributing factor. The solution provide in the current trials shows satisfactory results which include reducing Z-offset distance and increasing retraction speed.

Additionally, this chapter deals with the optimal AM part production with minimum GD&T error so that part build by AM can be functional and used in industrial applications. For that, optimum process parameters were found out for minimum GD&T error. Linear analytical models were developed for circularity and flatness using regression technique in terms of process parameters. Further, the mathematical models were optimized by multi-objective optimization using PSO. At last, a simple case study is used for experimental confirmation of the developed model. The adopted methodology will help the AM users in producing parts with high geometrical accuracy and bring more sustainability in AM parts for engineering applications as a functional components.

CHAPTER 4

DATA ACQUISITION USING OPTIMUM SCANNING PARAMETER

This chapter presents the determination of important process parameters during scanning of physical objects. On the basis of the scanned objects morphology, two important process parameters are specified namely scanning angle and distance of the laser beam from the part surface. Experiments have been performed with different scanning conditions using full factorial design. A mathematical prediction model for estimating the standard deviation of the final surface is developed in terms of the above scanning parameters using response surface methodology (RSM). Furthermore, analysis of variance (ANOVA) has been employed to establish the statistical significance of the scanning parameters and the developed model. In addition, it has been observed that the measured and predicted standard deviations are well in agreement, which confirms the effectiveness of the developed model. The mathematical model is further optimized using a modified particle swarm optimization (MPSO) algorithm, which is proposed in this chapter. It is important to optimize the standard deviation to determine the optimal condition for scanning for improved output of point cloud data. Finally, two realistic non-trivial case studies are considered for validation of the proposed methodology. This methodology provides the optimal combination of morphological process parameters with considerable reduction in standard deviation for final scanned surface models.

With increasing usage of free-form objects in industries, either for functional or aesthetic purposes, data acquisition becomes an important task for accurate inspection. Since, these parts are generally expensive and play a vital role in the final assembly, the complete part data measurement is imperative for effective functionalities (Huang et al., 2013; Lindau et al., 2013). However, CMMs exhibits incompetence in free-form surface measurement while non-contact scanners have the capability of acquiring thousands of points in a short span of time, together with increased accuracy, as reported in recent times. For all these reasons, the contactless laser scanners are used for quality control of industrial

components. A general arrangement of such a contactless laser scanning device is shown in Figure 4.1.

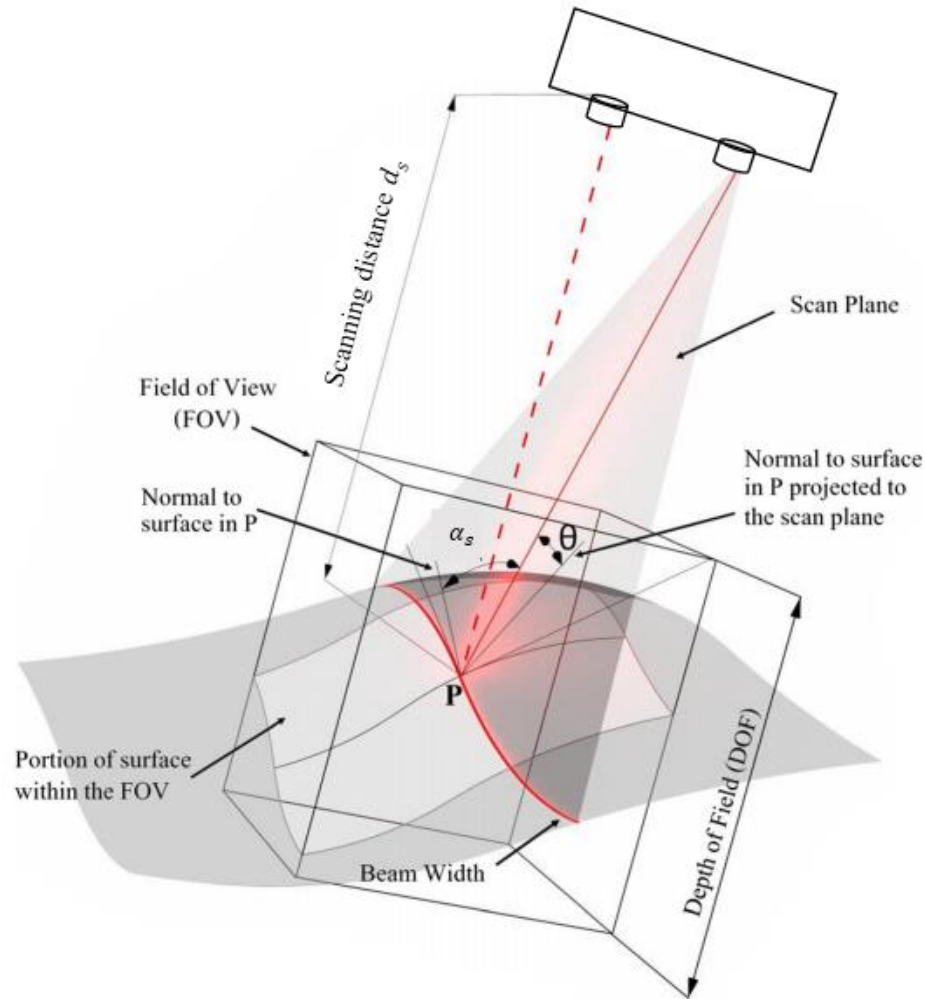


Figure 4.1 Laser triangulation principle (α_s is incident scanning angle)

4.1 Adopted methodology for optimal scanning parameter evaluation

A cuboid block made of steel with dimensions of 100 mm by 40 mm by 25 mm and coated with white powder (for effective scanning of surface) is used to study the correlation among scanning angle, scanning distance and standard deviation of errors. The block is chucked in a three jaw rotary head, which rotated from 0° to 90° in successive order with 5° increment each time. The data acquisition system used for the experiments is Steinbichler's blue light 3D scanner. After each scan at every 5° , the surface was reconstructed using

COMET Plus software. This procedure was repeated at different scan distances, ranging from 60 mm to 130 mm, with an increment of 10 mm. The outline of the proposed methodology for investigating optimum scanning parameters is shown in Figure 4.2.

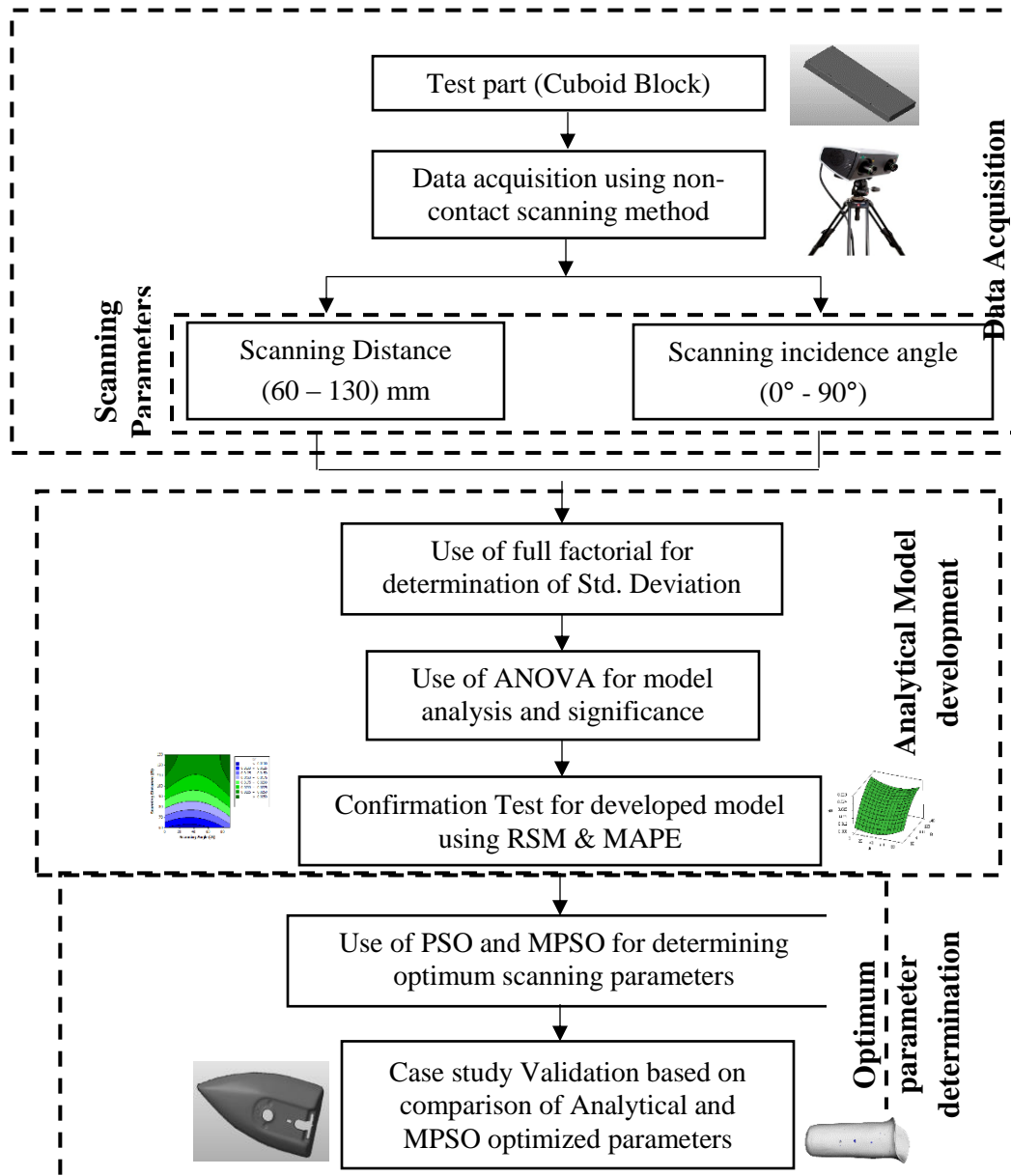


Figure 4.2 Adopted methodology for optimum scanning parameters determination

The methodology begins with scanning the object (cuboid block) using non-contact scanning system. The scanning is performed using different settings of scanning distance and scanning angle as described in framework using full factorial design. Afterwards, standard deviation is noted for each point cloud data acquired. Further, ANOVA analysis is performed for determining the model significance and analysis. The RSM technique is

used for determining the analytical model of standard deviation in terms of scanning parameters. The confirmation test is performed using MAPE factor by comparing the experimental results with the RSM results for chosen values. For optimization of scanning parameters, two nature inspired algorithms are used i.e. PSO and MPSO. The results of these algorithm helps in finding the parameters for which the standard deviation is minimum. Finally, two non-trivial case studies are taken to validate the adopted methodology.

4.2 Experimental tests and results

The blue light 3D scanner uses a source of a narrow band of blue light to generate a reflection stripe on the scanned surface that captures the topological information. For the experimental trials the laser beam captured a limited portion of the part in one shot characterized by a cuboidal volume. The obtained results based on the above procedure is shown in Figure 4.3. As clearly seen in the figure, the standard deviation shows a decreasing trend for scanning angle in the range of 25° to 55° and progressively increases after that. Additionally, low values of scanner-object distance show low standard deviation. Evidently, it is clear that low distance and low scanning angle will provide optimum results. These results will be used in the next section for setting of design model.

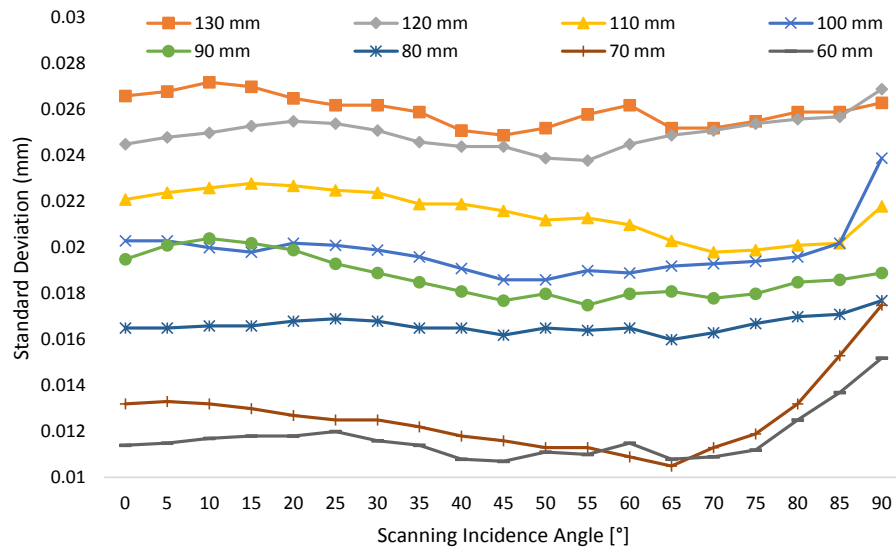


Figure 4.3 Standard deviation of various measurements at different incidence angles

4.3 ANOVA analysis and mathematical model development

In this study, general full factorial design consisting of 152 experimental runs with two replicas has been considered. The experimental runs were taken at 8 levels of distance and 19 levels of scanning incidence angle. The design of experiments was used for the ANOVA analysis and for development of appropriate mathematical design model. The mathematical model creation and analysis of experimental data was performed using Design-Expert software version 8.0.7.1. The response surface methodology (RSM) is used to develop cubic mathematical models for the purpose of predicting standard deviation values. The RSM is a collection of statistical and mathematical techniques that can be used in prediction and explanation of the existing relationship between input process parameters and output response (Myers et al., 2004). The relationship between input variables (scanning distance (d_s) and scanning angle (α_s)) and the output responses (standard deviation (Y)) can be expressed as:

$$Y = F(d_s, \alpha_s) \quad (4.1)$$

where F is the response function. A third order polynomial equation to approximate the response (Y) is expressed below for k factors:

$$Y = \beta_0 + \sum \beta_i X_i + \sum \beta_{ii} X_i^2 + \sum \beta_{ij} X_i X_j + \sum \beta_{iij} X_i^2 X_j + \sum \beta_{iii} X_i^3 \quad (4.2)$$

where β_0 , β_i , β_{ii} , β_{ij} , β_{iij} are the coefficients for model intercept, linear, quadratic and cubic terms respectively and the X_i represents input parameters.

The relative significance of control factors on standard deviation was examined using ANOVA. The response surface and contour plots are shown in Figure 4.4(a-b). The plot shows that minimum standard deviation value is achieved at a scanning distance of 60 mm with incidence angle between 30° to 50°. The results of ANOVA for cubic response surface method are tabulated in Table 4.1 which indicates that model is significant.

The higher F-value of 418.915 indicates that the model is significant. There is only 0.01% chance that such a high model F-value may have occurred due to noise. Additionally, the higher value of the determination coefficient ($R^2 = 98.02\%$) indicates that only less than 1.98% of the total variations in standard deviation (SD) are not clarified by the model. The higher value of adjusted determination coefficient (adjusted $R^2 = 96.33\%$)

assures significance of the model. Further, an equation was developed based for standard deviation in terms of actual factors and their interactions as shown in eqn. (4.3):

$$\begin{aligned} \text{Standard Deviation (SD)} = & -0.0576974 + 2.25839E - 03 * A + 2.97338E - \\ & 04 * B - 6.50794E - 06 * A * B - 2.80612E - 05 * A^2 + 3.09753E - 06 * \\ & B^2 - 3.34713E - 08 * A^2 * B + 4.30682E - 08 * A * B^2 + 5.53254E - 08 * \\ & A^3 + 7.23063E - 08 * B^3 \end{aligned} \quad (4.3)$$

Table 4.1 ANOVA results for chosen cubic model

Source	Degree of freedom (df)	Sum of squares (SS)	Mean Square (MS)	F-value	P-value probability > F	
Model	9	2.85E-03	3.167E-04	418.92	< 0.0001	Significant
A - Scanning Distance	1	2.62E-04	2.62E-04	346.56	< 0.0001	
B - Scanning Incidence Angle	1	3.74E-05	3.74E-05	49.47	< 0.0001	
AB	1	2.40E-05	2.40E-05	31.75	0.0001	
A ²	1	2.81E-05	2.81E-05	37.17	< 0.0001	
B ²	1	2.37E-05	2.37E-05	31.35	0.0001	
A ² B	1	2.83E-06	2.83E-06	3.74	0.1601	
AB ²	1	8.51E-06	8.51E-06	11.26	0.0151	
A ³	1	7.73E-06	7.73E-06	10.22	0.0246	
B ³	1	2.89E-05	2.89E-05	38.23	< 0.0001	
Residual Error	143	10.82E-05	7.56E-07			
Total	152	2.95E-03				
Standard Deviation =9.066E-04			R ² = 98.02%			
			Adjusted R ² = 96.33%			

Confirmation test for the developed design model

For testing the accuracy of the developed design model, fifteen scanning distance and scanning incidence angle values were randomly chosen. The random values were chosen from the surface plot shown in Figure 4.4 (b) and verified against the data obtained from cuboid block measurement in Figure 4.3. The results of the comparison were depicted in Figure 4.5. As seen in Figure 4.5, the difference between the measured and predicted standard deviation value is much less. The mean absolute percentage error (MAPE) has been used as a metric for evaluating the performance of developed model.

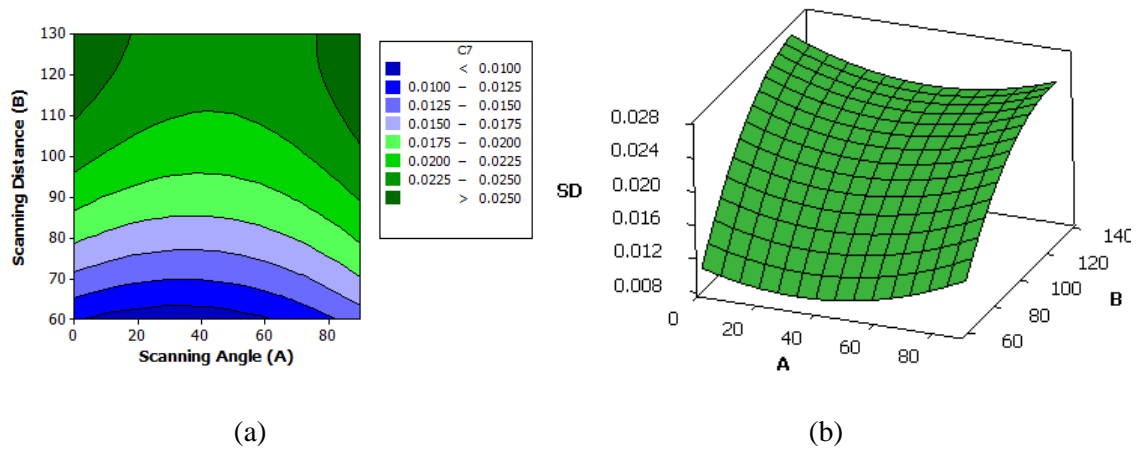


Figure 4.4 (a) Contour plot of angle-distance (b) Surface plot of angle-distance relation

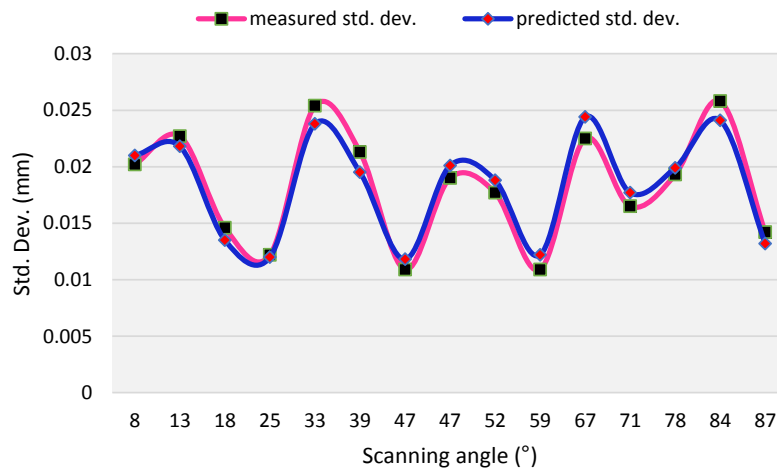


Figure 4.5 Measured and predicted standard deviation of randomly chosen distance-angle values

$$MAPE = \frac{1}{N} \sum_{k=1}^N \frac{|F_k - A_k|}{A_k} = 0.063683 \quad (4.4)$$

where F_k is forecasted or predicted value and A_k is the corresponding actual measured value. The MAPE output of 6.36% is acceptable which indicates the values predicted by the developed model are in accordance with the measured values.

4.4 Modified particle swarm optimization (MPSO) and optimization problem formulation

In the present study, developed mathematical model of the standard deviation was minimized to achieve optimum values of scanning distance and scanning incidence angle. This is required for achieving improved accuracy of final reverse engineered surfaces. Over the years, researchers have applied different optimization techniques for solving various real life applications. The main reason is the demand for global optimum solution among a number of local optimum solutions available. Moreover, these problems have large search space and are multi-dimensional, making it suitable to use numerical optimization algorithm rather than analytical methods. The main purpose of these techniques is to find the optimal values of design variables with the optimized values of the objective function, which are either minimization or maximization. After formulating the mathematical problem using design variables, it can be solved by using either traditional or evolutionary optimization algorithms. Moreover, in most of the cases, the optimization problems are non-differentiable. Consequently, the traditional optimization algorithm like gradient methods cannot be used for solving these problems. For, solving these problems, several modern nature inspired algorithms have been proposed for finding optimum solutions to the real life problems.

The nature-inspired optimization algorithms are becoming increasingly common in engineering applications since they rely on simple concepts are easy to use, can find global optima easily and do not require gradient information of objective function. Some of the most popular nature inspired algorithm includes Genetic Algorithm (GA) (Holland, 1992), Particle Swarm Optimization (PSO) (Kennedy and Eberhart, 1995), Differential Algorithm (DA) (Storn and Price, 1997), Bacteria Foraging Optimization (BFO) (Passino, 2002),

Artificial Bee Colony (ABC) (Karaboga and Basturk, 2007), Firefly algorithm (FA) (Yang, 2010) etc. These algorithms solve the problem by mimicking the natural or physical phenomena. The main advantage of these algorithms is that they can find global optimum solutions with less computational effort for large optimization problems.

In order to improve the performance of these nature inspired algorithms, the controlling parameters like population size and number of generations play a significant role along with the strategy for the initialization of the population of the algorithm. Moreover, there are no specific rules for specifying the values of these controlling parameters, it purely depends upon the user experience and problem description. Similarly, the performance can also be improved by balancing the exploration and exploitation ability of the algorithm (Mahdavi et al., 2007; Niu and Xiao, 2012). PSO is one such nature inspired optimization technique developed by Kennedy and Eberhart. This algorithm has been used for finding optimum solution of many real life problems. In solving real life applications, it was found that GA is more complicated than PSO in principle for the same work (Lai et al., 2000). In addition, ACO is time-consuming and its convergence time is also uncertain. ABC has slow convergence rate, quickly falls in local optima and with its use, it's hard to find the best out of all available feasible solutions (Rao and Savsani, 2012). For solving continuous problems, PSO has been widely used due to simplicity of the concept with fewer parametric settings as compared to other population-based optimization algorithms (Tseng et al., 2010; Lee and Lee, 2014; Li et al., 2014). However, classical PSO still has some disadvantages, such as weak local search ability that may lead to entrapment in local minimum solutions affecting the convergence performance that results in uncertainties in the outcomes obtained. In PSO, updation of the new solution is performed only over the existing one, without comparing which one is better. This behavior is due to lack of exploitation capability in classical PSO, which makes it hard to find the best possible solutions (Rao and Savsani, 2012).

A modified algorithm for particle swarm optimization (MPSO) has been proposed in this chapter to improve the exploitation capability for effective form error evaluation. The genesis of the proposed algorithm is based on the generation of new improved particle (candidate solution) position using the difference in the global and local best positions. An efficient greedy selection procedure is employed for obtaining better position between the

newly generated and the existing position based on the fitness value. Five benchmark test functions are used to verify the robustness and efficiency of the proposed algorithm.

The exploitation ability directly influences the quality of results, as it is an essential property for any swarm based heuristic optimization technique. The modified variant will help in overcoming the classical PSO drawback of slow convergence due to lack in exploitation abilities.

4.4.1 Definition of different terms used

Swarm: population size or number of particles

Search space: an area specified by lower and upper bound of the design variables

Particle: individual swarm which is a potential solution of the problem

pbest (personal best): It is the personal best position attained by the particle so far

gbest (global best): It is the best position attained by any particle in the entire swarm.

Exploration: Searching in entire search space to find optimal solution

Exploitation: searching around already existing solution and make refinement to get optimal solution

Candidate solution: It is defined as available solutions in search space that satisfy all constraints.

Convergence: It is the process of moving all particles to an optimum solution in search space through successive iterations.

Accuracy: It defines the quality of the best solution and how close the results are to each other for different runs.

Termination Criteria: It is the stopping criteria of the algorithm either by reaching maximum number of iterations or specified time.

Parameters used in the algorithm

k: individuals of population $k \in \{1, 2 \dots n\}$

j: components of an individual $j \in \{1, 2 \dots D\}$

m: number of variables

n: population size of swarm particles

w: inertia parameter

w_{min} :	minimum value of inertia parameter, 0.4
w_{max} :	maximum value of inertia parameter, 0.9
c_1 and c_2 :	accelerating coefficients
LB & UB:	lower bound and upper bound (within which variables may vary)
rand [0,1]:	uncorrelated and uniformly generated random number between 0 and 1
maxiter:	maximum number of iterations for which objective function will be evaluated
f_0, f_1 :	initial fitness/objective function and new fitness/objective function after velocity and position are updated
f_2 :	final objective function in the current iteration

4.4.2 Standard particle swarm optimization algorithm

The basic particle swarm optimization is a population based method suggested by Kennedy and Eberhart in 1995. PSO is modeled after the simulation of social behavior of birds in a flock (Kennedy and Eberhart, 1995; Eberhart and Kennedy, 1995). PSO is initialized by distributing each particle randomly in a D-dimensional search space. The performance of each particle is measured using a fitness or objective function which depends on the optimization problem. Each particle k is represented by the following information:

- x_k , the current position of the particle k
- v_k , current velocity of the particle k
- p_k , personal best position of the particle k
- g_k , global best position of the particle k

The personal best position signifies the best position that particle k has been at so far. Here, velocity v_k acts like a vector which helps in guiding the particle from one position to another with updated velocity and position at every iteration. The update in the personal best position of k^{th} particle with time step t can be expressed as eq. 4.5:

$$\begin{aligned}
 p_k(t+1) &= p_k(t), & \text{if } f(x_k(t+1)) \geq f(p_k(t)) \\
 & x_k(t+1), & \text{if } f(x_k(t+1)) < f(p_k(t))
 \end{aligned}
 \tag{4.5}$$

The psychological assumptions of particle swarm theory are general: in their search for consistent cognitions, individuals will tend to retain their own best beliefs, and will also

consider the beliefs of their colleagues. Adaptive change results when individuals perceive that others' beliefs are better than their own (Kennedy, 1997). The below equation is divided in three parts. First is inertia part described by $w \cdot v_k(t)$, used for providing motion to the algorithm. Second part is cognitive component $rand[0,1] \cdot (p_k(t) - x_k(t))$, which is based on individual knowledge and experience. The third and last part $rand[0,1] \cdot (g_k(t) - x_k(t))$, known as social component based on individual interaction with their neighbors. New position and velocity for k^{th} particle is updated at every iteration and expressed as Eqn. 4.6 and 4.7:

$$v_k(t + 1) = v_k(t) + c_1 \cdot r_1 \cdot (p_k(t) - x_k(t)) + c_2 \cdot r_2 \cdot (g_k(t) - x_k(t)) \quad (4.6)$$

$$x_k(t + 1) = x_k(t) + v_k(t + 1) \quad (4.7)$$

r_1 and r_2 are two statistically independent and uniformly distributed random numbers within given interval $[0,1]$. The acceleration coefficients c_1 and c_2 are also important parameters in PSO. c_1 pulls the particle towards the local best position whereas c_2 pulls the particle towards the global best and the sum of these two should be greater than 4 and less than 4.2 ($4 \leq (c_1 + c_2) \leq 4.2$) (Shi and Eberhart, 1999). So for balancing exploration and local convergence, the value of c_1 and c_2 is taken 2 each. $p(t)$ is the best position parameter of an individual particle and $g(t)$ is global best position parameter of entire swarms. Shi and Eberhart (Eberhart and Shi, 2001) introduced an inertia weight w into the velocity updating of the PSO that helps in controlling the scope of the search. Often, w decreases linearly from 0.9 to 0.4 over the whole iteration. Here, whole iteration is the maximum iteration needed to get the final result. The velocity updation with inertia weight is shown in Eq. 4.8.

$$v_k(t + 1) = w \cdot v_k(t) + c_1 \cdot r_1 \cdot (p_k(t) - x_k(t)) + c_2 \cdot r_2 \cdot (g_k(t) - x_k(t)) \quad (4.8)$$

The different steps of basic PSO are as follows (Kennedy and Eberhart, 1995) (see Figure 4.6):

Step 1: Define the PSO parameters and randomly generate a population with initial position ($x_k = x_{k1}, x_{k2}, \dots, x_{kD}$) and velocity ($v_k = v_{k1}, v_{k2}, \dots, v_{kD}$) of all the particles in the entire search space.

Step 2: Evaluate the objective (fitness) function (f_0) of each particle. The lower the objective function value is, the better the corresponding particle performs.

Step 3: Update or change the velocity and position of each particle according to relative positions from local best ($pbest$) and global best ($gbest$) using eqns. (4.6) or (4.8) and (4.7).

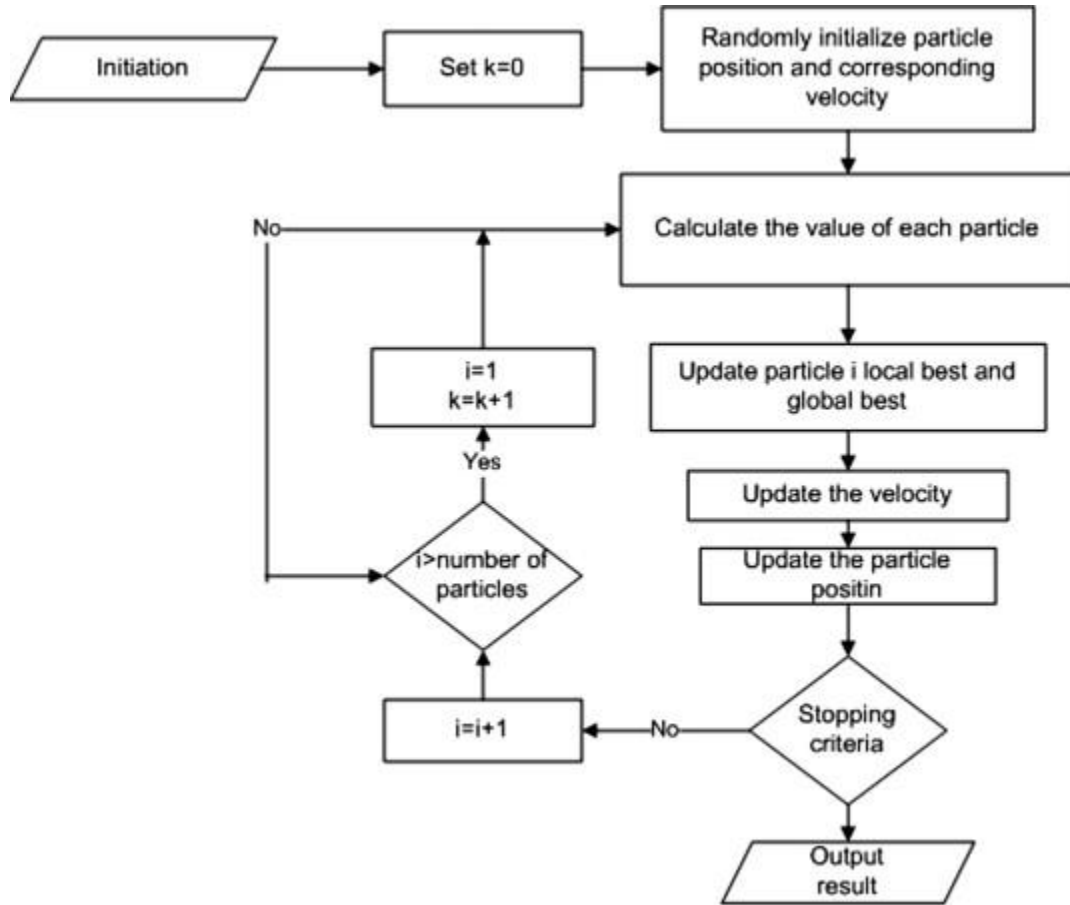


Figure 4.6 Flowchart of classical particle swarm optimization (PSO)

Step 4: Applying boundary constraints on design variables so that the value of design variables lie within the lower bound (LB) and upper bound (UB) and particle doesn't fly outside search space.

$$\begin{aligned}
 & \text{if } x(k,j) < LB(j); \quad x(k,j) = LB(j); \\
 & \text{else if } x(k,j) > UB(j); \quad x(k,j) = UB(j)
 \end{aligned}$$

Step 5: Again, fitness function for each particle is calculated. If the current objective function value is less than the previous p_{best} value then p_{best} is replaced by the current position.

Step 6: If the current objective function value is less than the previous g_{best} value then g_{best} is replaced by the current position.

Step 7: The termination criteria is checked and go to step 3, if it is not met. The termination criteria could be either max. iteration or good objective or fitness value.

It is observed from the above steps that basic PSO performs exploration in step 3 using equation (4.6) and (4.7) by generating new solutions in the search space. However, the exploitation part is nowhere seen in the algorithm, as selection mechanism is missing in PSO. In PSO, only updation of new solution takes place without comparing which one is better. So, basic PSO has only explorative tendency and it lacks the exploitation ability. Therefore, in order to overcome this limitation a modified PSO algorithm is presented here.

4.4.3 Modified particle swarm optimization (MPSO) algorithm

A new variant of PSO is proposed in this paper for the effective form error evaluation. The exploration and exploitation capabilities are two important factors that are considered during design of an optimization algorithm. Exploitation refers to the use of existing information whereas the exploration means generation of new solution in the search space. In PSO, an old solution is replaced by the new one without really comparing which one is better (Rao and Savsani, 2012). This shows the lack in exploitation capability of PSO and has only exploration tendency which makes it hard to find the best possible solutions (like in this case minimization of form error).

Because of the lack in exploitation strategy, classical PSO still have some disadvantages, such as weak local search ability and may lead to entrapment in local minimum solutions. To overcome all these problems, the modified variant of PSO algorithm generates new swarm position and fitness solution based on the new search equations (4.9) and (4.10):

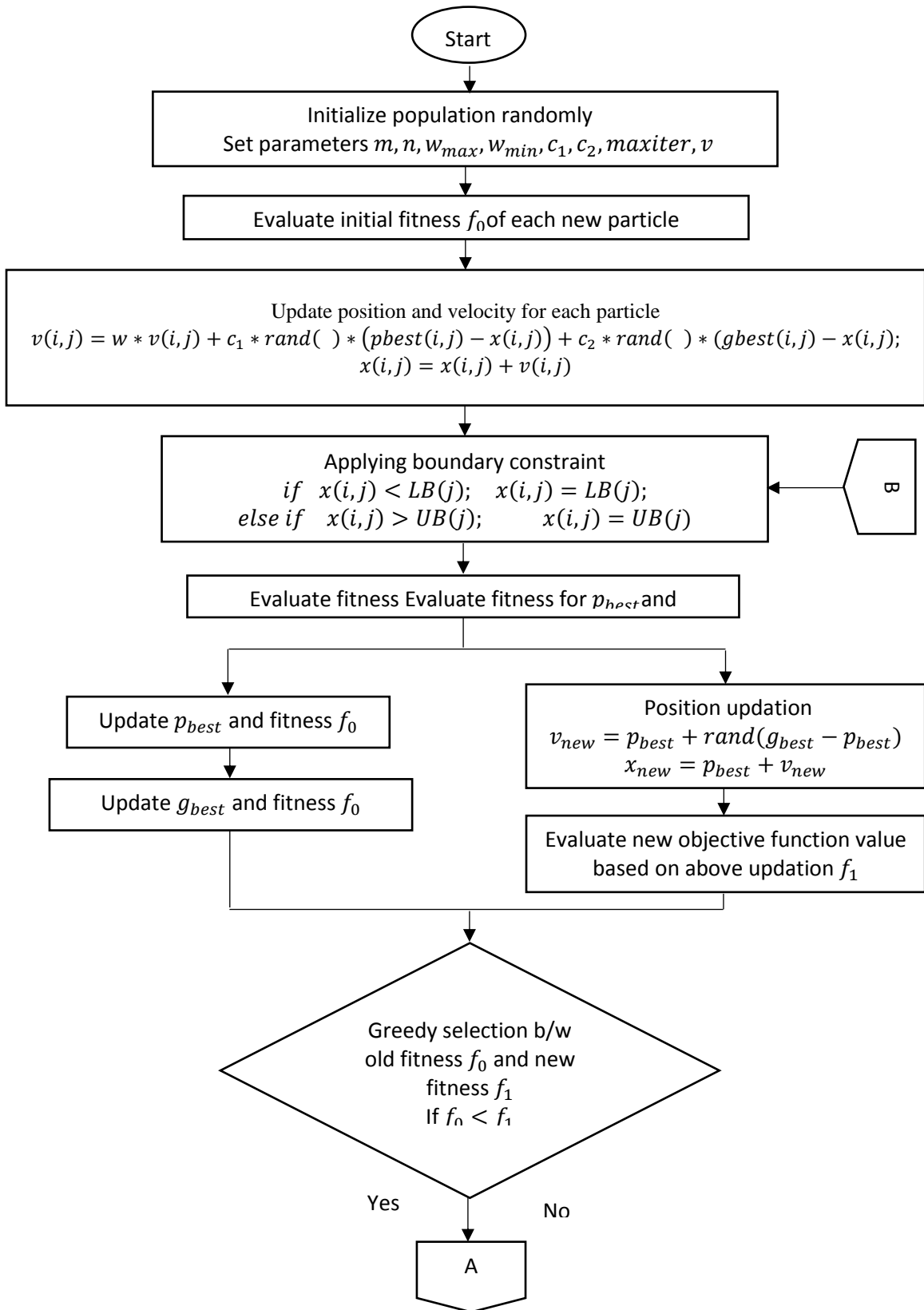
$$v_{new} = p_{best} + rand[0,1] \cdot (g_{best} - p_{best}) \quad (4.9)$$

$$x_{new} = p_{best} + v_{new} \quad (4.10)$$

where p_{best} is the particle best position, g_{best} is the particle global best position. $rand[0,1]$ is the random number generator between 0 and 1 that controls the rate at which the population evolves. The random number generator typically is initialized by this parameter, allowing to yield different values at each trial. The best solutions in the current population are very useful sources that can be used to improve the convergence performance. Also, Eq. (4.9) can drive the new candidate solution only around the best solution of the previous iteration. Therefore, the proposed search and updation equations described by Eq. (4.9) and (4.10) can increase the exploitation capability of the classical PSO.

Any selection strategy in the algorithm is usually considered as exploitation, as the fitness solution of the individual is used to determine whether or not an individual should be exploited. Therefore, the MPSO particle swarms employ greedy selection procedure among two parallel fitness functions to update the best candidate solution which also helps in improving the exploitation ability of the algorithm. The flowchart of proposed modified PSO algorithm is shown in Figure 4.7.

MPSO begins with step 1 of basic PSO algorithm and remain same till step 5. Afterwards, an additional path for generating new solution by position and velocity updation is introduced in the algorithm using equation (4.9) and (4.10). This additional path will provide an extra option for velocity and position updation besides the basic updation used in PSO, providing new objective function (f_1). Both the path runs independently for each iteration. The best particle with minimum fitness or objection function will be chosen for next iteration using greedy selection procedure. A greedy selection scheme is used for selection of best solution among two possible solution (the new solution and the old one) and the better one is preferred for inclusion in population based on the fitness or objective function value. In this way, the information of a good particle of the population is distributed among the other particles due to greedy selection scheme applied and thus enhancing the exploitation ability of the algorithm. Further, the final objective function is updated as f_2 with corresponding position of the best particle and is used in the next iteration. At last, the termination criteria is checked and go to step 3, if it is not met.



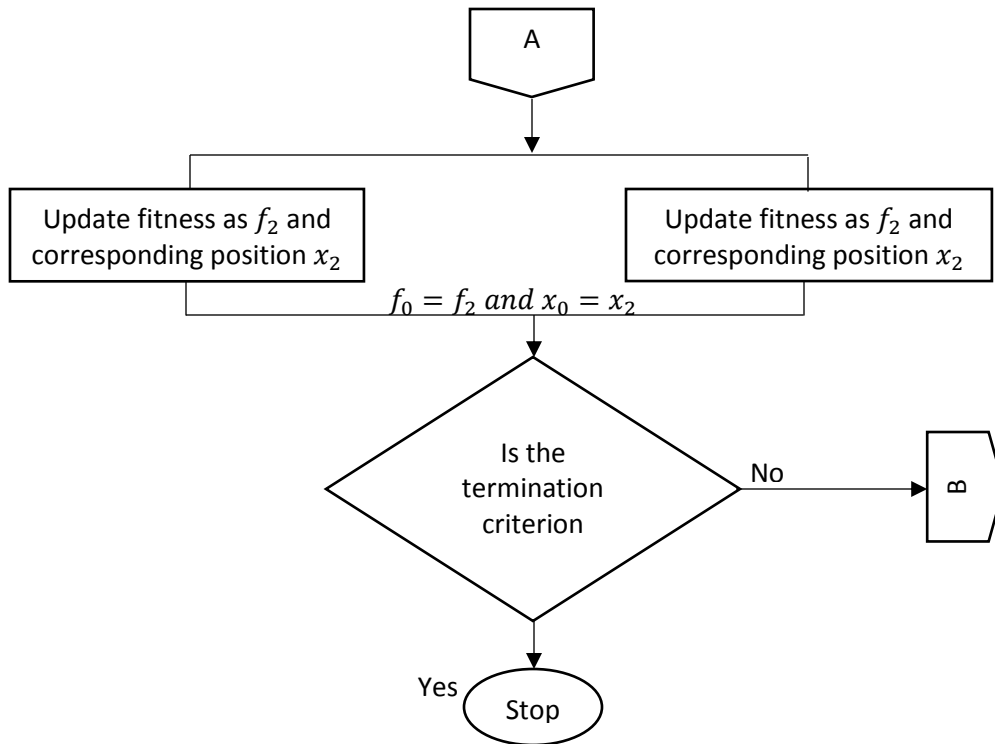


Figure 4.7 Flowchart of modified particle swarm optimization (MPSO) algorithm

4.4.4 Numerical Examples

In order to prove the effectiveness of the proposed MPSO algorithm and testify its applicability in evaluating accurate form error evaluation, five benchmark test functions are selected. These benchmark functions aim for a global minimum value and the commonly used to test any newly proposed algorithm or variant of an existing one. The test functions to be minimized include unimodal functions, multimodal functions having many local optima and multimodal function having local optima in the pre-defined search space. Results obtained using the MPSO algorithm are compared with the results of GA and basic PSO. The five test functions are defined as follows:

1. Benchmark Function 1

The sphere function (Rao and Patel, 2013) is defined as follows:

$$f_1(x) = \sum_{i=1}^D x_i^2$$

The function has a unique global minimum value of $\mathbf{0}$, and the search space is $-100 < x_i < 100$.

2. Benchmark Function 2

The Rosenbrock parabolic valley function (Rao and Patel, 2013) is defined as follows:

$$f_2(x) = \sum_{i=1}^{D-1} 100(x_i^2 - x_{i+1})^2 + (1 - x_i)^2$$

The function has a unique global minimum value of $\mathbf{0}$, and the search space is $-2 < x_i < 2$

2. The visualization of sphere and Rosenbrock function is shown in Figure 4.8

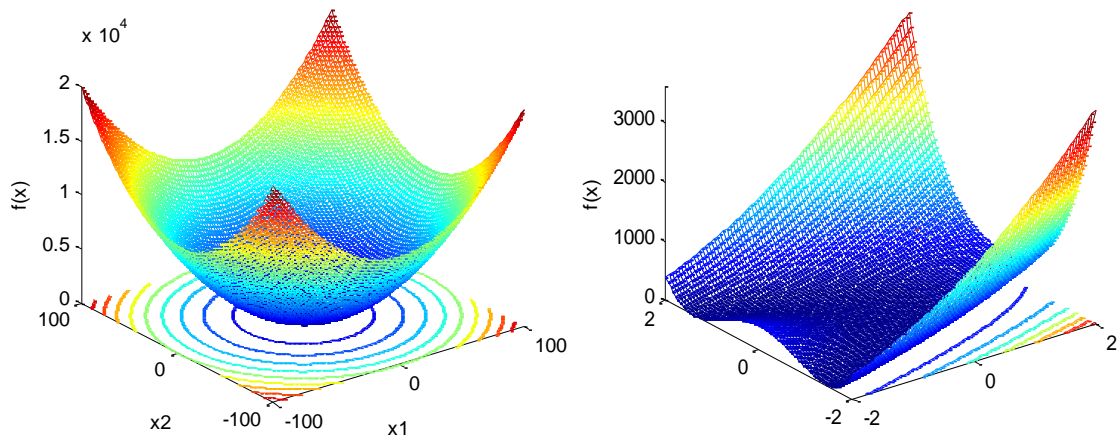


Figure 4.8 Visualization of (a) sphere (b) Rosenbrock parabolic valley benchmark function

3. Benchmark Function 3

The Powell Quartic function was proposed by MJD Powell in 1962 (Powell, 1962). It is a unimodal test function which is used to test the convergence performance and optimization effectiveness of the new optimization algorithms for several variables. The Powell Quartic function is defined as follows:

$$f_3(x_1, x_2, x_3, x_4) = (x_1 + 10x_2)^2 + 5(x_3 - x_4)^2 + (x_2 - 2x_3)^4 + 10(x_1 - x_4)^4$$

The function has a unique global minimum value of $\mathbf{0}$ and the search space is $-4 < x_i < 5$ where $(i = 1, 2, 3, 4)$.

4. Benchmark Function 4

It is a generic sample of non-linear multi-modal function. It was proposed by Rastrigin. Analytically, it represents very hard problem due to its large search space and its large number of local minima. The Rastrigin function (Rao and Patel, 2013) is defined as follows:

$$f_4(x) = \sum_{i=1}^D [x_i^2 - 10 \cos(2\pi x_i) + 10]$$

The function has many local minima and a unique global minimum value of **0** as depicted below in Figure 4.9. The search space is $-5.12 < x_i < 5.12$ within which the x_i variable will search the optimum solution. This function can be used for testing the ability of new optimization algorithms in searching and escaping from the local extreme points.

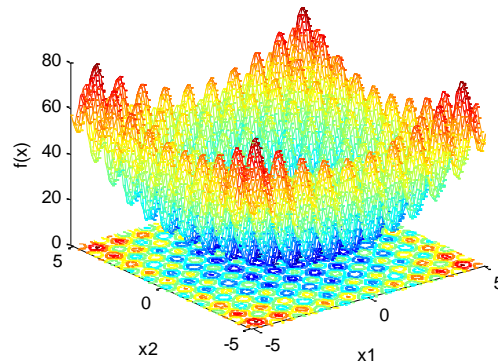


Figure 4.9 Visualization of Rastrigin benchmark function

5. Benchmark Function 5

The two-dimensional Goldstein-Price function (Rao and Patel, 2013) is defined as follows:

$$f_5(x_1, x_2) = [1 + (x_1 + x_2 + 1)^2(19 - 14x_1 + 3x_1^2 - 14x_2 + 6x_1x_2 + 3x_2^2)] \cdot [30 + (2x_1 - 3x_2)^2(18 - 32x_1 + 12x_1^2 + 48x_2 - 36x_1x_2 + 27x_2^2)]$$

The global minimum value of the function is **3** and the search space is $-2 < x_i < 2$ where ($i = 1, 2$). The visualized description is shown in Figure 4.10.

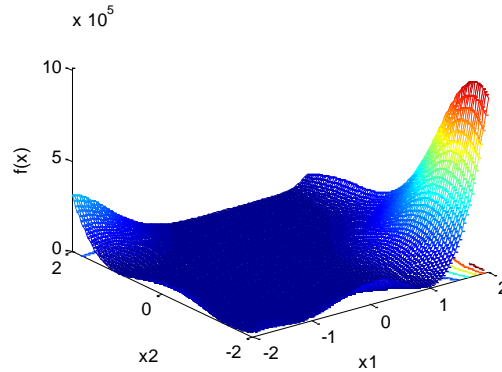


Figure 4.10 Visualization of Goldstein-Price benchmark function

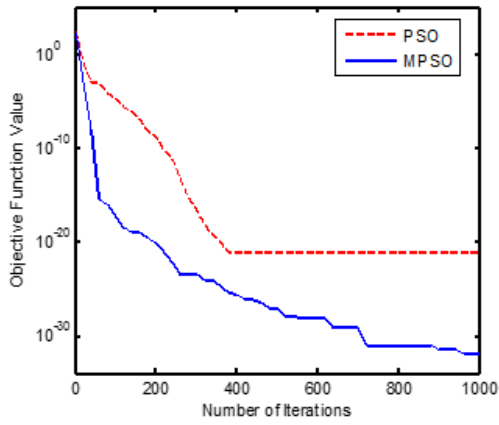
Since, the GA, PSO and MPSO algorithms are all stochastic in nature, it is not reasonable to compare their performance by optimizing these functions only one time. To reduce the stochastic influence, each algorithm optimized each function for 30 times. The numerical results are averaged over 30 trials for each benchmark function. The average number of function evaluations (number of population \times average number of iteration) is set to 50000 for Sphere and Rosenbrock function, while 25000 for Powell and Rastrigin function with 5000 for Goldstein-Price function respectively. In all cases, population size is set to 50. The dimension, D of the Sphere, Rosenbrock and Rastrigin function is 6, for Powell and Goldstein-Price function it is 4 and 2 respectively. For GA, the crossover and mutation probabilities are set to 0.8 and 0.1 respectively. For PSO and MPSO, the values of all the common parameters used are same.

The optimization results for all the three algorithms are shown in Table 4.2. The mean and standard deviation for evaluations on all the test functions is shown in Table 4.2 which also exhibit the effectiveness and precision of the proposed algorithm. The average number of function evaluations reflects the convergence rate of the algorithm. For benchmark function 4 and 5, the proposed MPSO takes less number of function evaluations to find the global optimum without trapping in local minima. The curves for PSO and MPSO are drawn to show the progress of average best values in Figure 4.11. f_1, f_2 and f_3 are unimodal functions primarily used to test the optimization accuracy and performance of the algorithm. For multimodal functions f_4 and f_5 with more local minima points, it was found that the MPSO algorithm shows capability of escaping from local minima to provide global optimization. As clearly seen from the results in Table 4.2 and the convergence

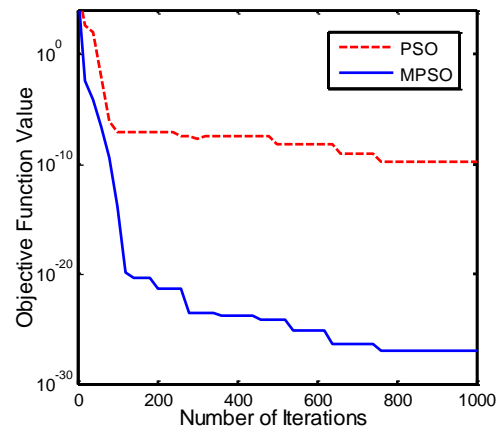
graphs in Figure 4.11, for all benchmark functions, MPSO outperforms classical PSO in optimization accuracy, function evaluations and convergence. Therefore, proposed MPSO can be applied for effective evaluation and optimization of minimum zone form error.

Table 4.2 Comparison of simulation results for benchmark functions

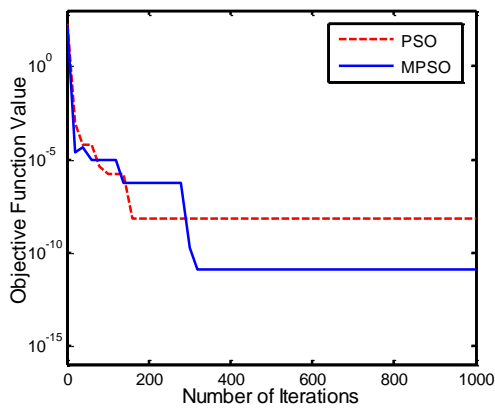
Benchmark Function	Algorithm	Best	Mean	Std. Deviation	Avg Number Func Eval
1	GA	2.76836E-10	2.198E-08	4.598E-08	50000
	PSO	6.4135E-22	9.237E-21	6.862E-21	50000
	MPSO	1.1276E-32	1.007E-30	5.997E-30	50000
2	GA	1.92E-07	3.22E-06	0.001115	50000
	PSO	1.53E-10	2.79E-9	3.95E-9	50000
	MPSO	3.915E-27	1.582E-26	4.442E-26	50000
3	GA	4.28389E-07	0.002459	0.0067926	25000
	PSO	1.93E-9	3.79E-07	4.11E-07	25000
	MPSO	3.77E-14	1.09E-11	8.287E-11	25000
4	GA	5.6318E-4	0.596975	0.9806	25000
	PSO	1.581E-8	6.818433	6.3046	25000
	MPSO	0	0	0	6450
5	GA	3.0000	5.3875	8.4599	5000
	PSO	3.0074	3.3621	0.3974	1250
	MPSO	3.0000	3.0000	2.26E-9	1000



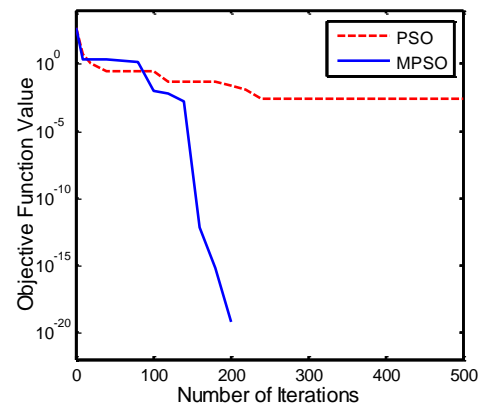
f_1



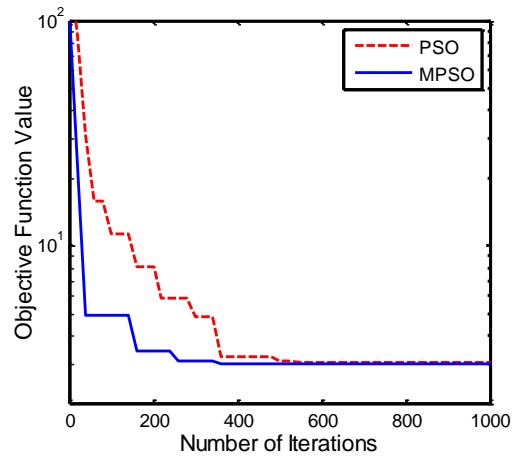
f_2



f_3



f_4



f_5

Figure 4.11 Convergence for benchmark function using PSO and MPSO

Identification of design variables

Developed cubic design model for standard deviation in Eq. (4.3) is composed of two important parameters i.e. scanning distance (d_s) and scanning incidence angle(α_s). These two parameters are taken as the design variables.

Objective function and constraints

For improving the final accuracy of reverse engineered surface models, the standard deviation in Eq. (4.1) needs to be minimized subject to constraints expressed as $60 \leq d_s \leq 130$ and $0^0 \leq \alpha_s \leq 90^0$. Now the optimization problem is formulated as:

$$\begin{aligned} \text{Minimize } f(d_s, \alpha_s) = & -0.0576974 + 2.25839E - 03 * d_s + 2.97338E - 04 * \alpha_s \\ & -6.50794E - 06 * d_s * \alpha_s - 2.80612E - 05 * d_s^2 + 3.09753E - 06 * \alpha_s^2 \\ & -3.34713E - 08 * d_s^2 * \alpha_s + 4.30682E - 08 * d_s * \alpha_s^2 + 5.53254E \\ & -08 * d_s^3 + 7.23063E - 08 * \alpha_s^3 \end{aligned}$$

Subject to $60 \leq d_s \leq 130$ and $0^0 \leq \alpha_s \leq 90^0$.

For framing and solving the optimization problem, a computer code was developed in Matlab R2014a for the objective function and modified PSO was implemented as the solver. The MPSO program employed different settings of PSO parameters to predict the values of scanning angle and distances and obtain minimized values of standard deviation of reverse engineered 3D models. For proving the effectiveness of the proposed MPSO algorithm, its results are compared with those obtained from the standard PSO algorithm. The parameters for both the algorithms are set as: c_1 and $c_2 = 2.05, w_{max} = 0.9, w_{min} = 0.4$, number of population size =10.

The results predicted for minimized standard deviation using PSO and proposed MPSO for optimized values of scanning angle and distance are shown in Table 4.3. Although, it must be noted that the results provided are not standard values of distance and incidence angle. The MPSO predicted results for nearest values of scanning distance and incidence angle are taken from Figure 4.5. The optimized variables are corresponding to the minimum standard deviation (as shown by bold). It can be seen from Table 4.3 that the

predicted values of standard deviation for reverse engineered 3D model by MPSO algorithm shows significant improvement over PSO results as well as the RSM method by 6.7% and 27.6% respectively. The convergence graph of MPSO algorithm in comparison to basic PSO is shown in Figure 4.12. It is observed from Figure 4.12 that MPSO algorithm requires only 30 iterations to converge to the optimum solution as compared to basic PSO which requires about 60 iterations. The minimized values of standard deviation confirms that the proposed MPSO algorithm provides improved results. This will enhance the final accuracy and quality of the scanned surface model and hence the result of RE process will be improved.

Table 4.3 Comparison of std. dev. prediction using Analytical, PSO and MPSO results

S No.	Scanning Distance Prediction			Scanning angle prediction			Std. Dev. Predicted		
	Anlytical	PSO	MPSO	Analytical	PSO	MPSO	Analytical	PSO	MPSO
1	95	93.97	93.02	8	7.22	7.17	0.0210	0.0171	0.0161
2	110	110.56	108.48	13	11.01	12.64	0.0218	0.0208	0.0195
3	75	73.44	77.12	18	18.02	19.49	0.0135	0.0140	0.0135
4	67	66.91	68.81	25	23.75	23.84	0.0120	0.0093	0.0085
5	125	123.40	126.95	33	31.15	31.66	0.0238	0.0219	0.0217
6	117	117.73	116	39	37.94	39.56	0.0195	0.0154	0.0150
7	61	60.47	61.55	47	48.45	47.37	0.0118	0.0101	0.0101
8	102	101.76	104.87	47	47.30	48.57	0.0201	0.0170	0.0154
9	77	77.82	77.61	52	53.10	50.22	0.0188	0.0155	0.0145
10	70	69.81	68.93	59	58.56	58.65	0.0122	0.0120	0.0120

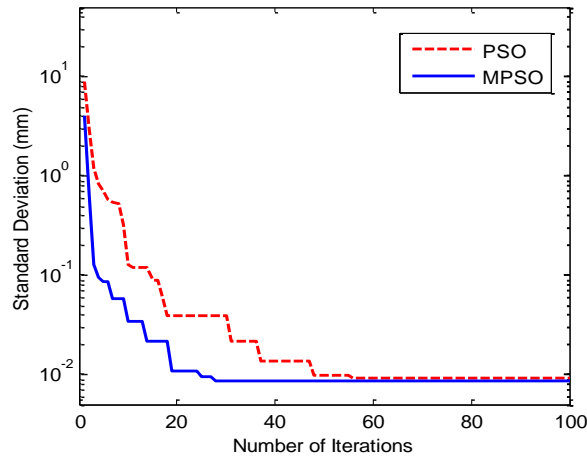


Figure 4.12 Convergence of MPSO for optimization of scanning process

4.5 Case Study Validation

The adopted methodology for optimum scanning parameters was tested by using two real life case studies: first of an electric iron part and second of a prosthetic socket part as shown in Figure 4.13 (a) and 4.14 (a).

Case study 1

This first case study was appropriate for the current investigation due to its continuously changing slope. Also, the presence of curvature makes it highly useful due to changing incidence angle and distance. To test the validity, three scanning trials were performed. One without considering any scanning parameters, secondly by considering developed analytical model values and lastly by using optimized MPSO values. For all the three cases, the case study parts were scanned and the surface was reconstructed using RE processes. Afterwards, inspection was performed using INSPECT PLUS software where the average deviation and standard deviation were calculated and compared with those from the actual CAD model.

From Table 4.4, optimized parameters were used for both analytical and MPSO optimized samples. As clearly seen from Figure 4.13 (b), the average and standard deviation were 0.06875 mm and 0.07495 mm respectively for the scanned case study using analytical model parameters. From all the three trials, it was evident that scanning distance

and scanning incidence angle have considerable influence on final part quality of RE surface irrespective of the number of point data as shown in Table 4.4. It can be seen in Table 4.4 that the scanned model optimized by MPSO algorithm achieved best values for average deviation and standard deviation among all the three samples. The % reduction in standard deviation after MPSO optimization is 21.6%.

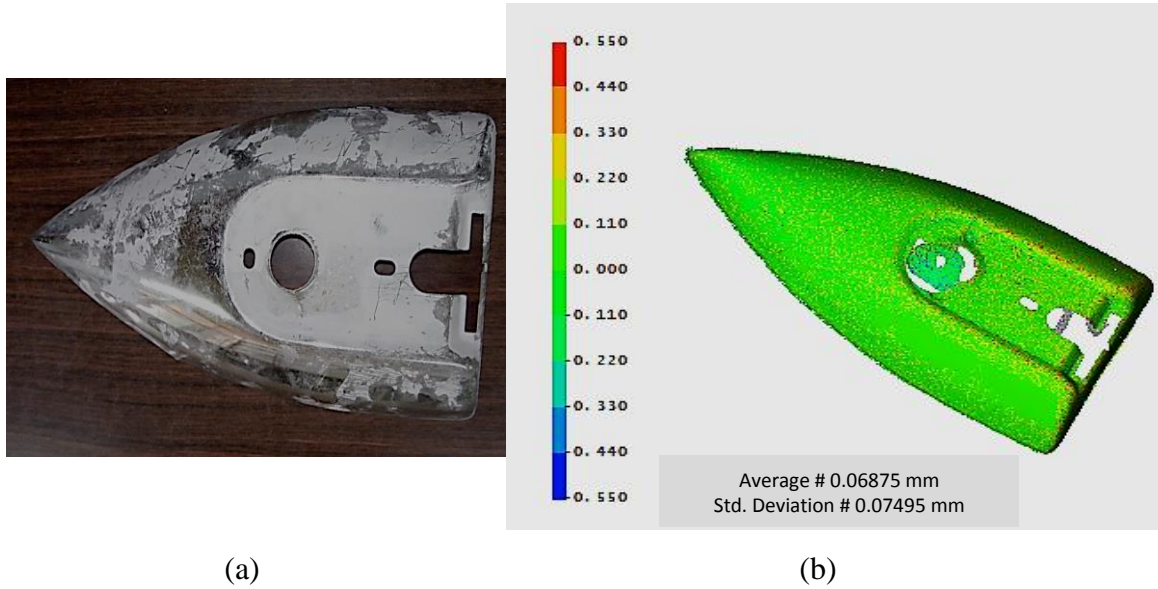


Figure 4.13 (a) Case study (b) Optimized parameters result using developed analytical model

Table 4.4 Case study results for three RE models of case study 1

	Default Parameters	Analytical	MPSO optimized
No. of Points	2,61,583	2,60,718	2,60,576
Average deviation (mm)	0.08871	0.06875	0.06624
Std. Deviation (mm)	0.09112	0.07495	0.07146
% reduction	-	17.75	21.6

Case study 2

The second case study selected was of a trans-tibial prosthetic socket as shown in Figure 4.14 (a). The socket is an appropriate case study for the validation because of the continuous changing slope and curvature. For validation of the proposed methodology, the socket was scanned three times. Once with default scanning parameters, secondly by considering developed analytical model values and lastly by using MPSO optimized parameter values. For all the three trials, the case study parts were scanned and surface was reconstructed using various RE processes. Further, inspection is performed using INSPECT PLUS software where the average deviation and standard deviation were calculated and compared with the actual CAD model values.

From Table 4.5, it can be concluded that the final accuracy of surface models have been improved using parameter values of developed analytical model and optimized MPSO algorithm. One important observation from the two case studies was the reduction in point cloud data of case studies which will help in easy and efficient handling of data. The results for optimized parameters using developed analytical model are shown in Figure 4.14 (b) using Steinbichler INSPECT PLUS software. The percentage reduction in standard deviation using analytical and MPSO were 9.24 % and 11.77 % respectively.

Table 4.5 Case study results for three RE models of case study 2

	Default Parameters	Analytical	MPSO optimized
No. of Points	3,10,413	3,05,252	3,03,959
Average deviation (mm)	0.03381	0.02992	0.02722
Std. Deviation (mm)	0.03510	0.03187	0.03097
% reduction	-	9.24	11.77

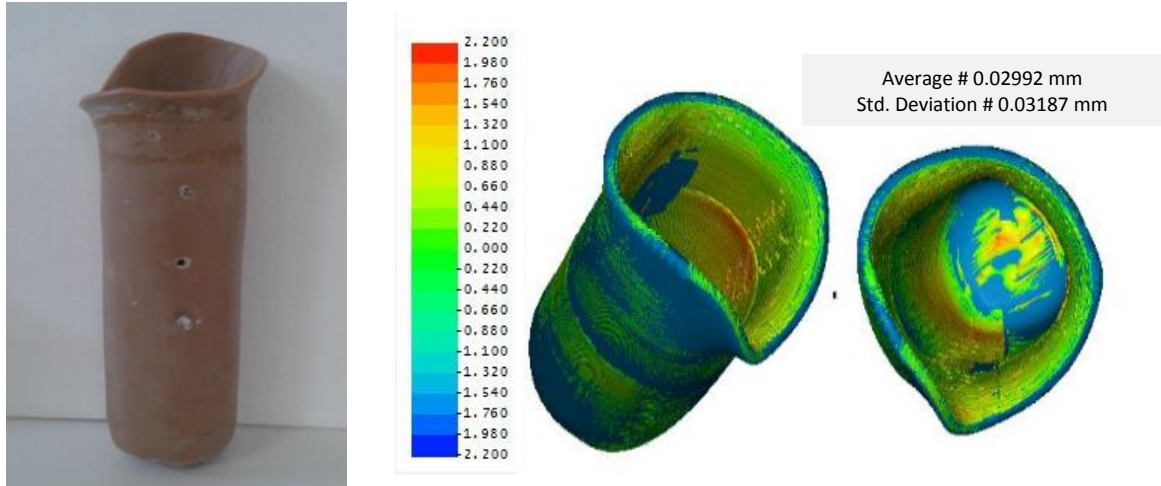


Figure 4.14 (a) Case study 2 **(b)** Optimized parameters result using developed analytical model

4.6 Chapter summary

This chapter identified and explained that morphology of scanned surface is an important factor to be considered for high quality output in 3D scanning processes. Based on surface morphology, two critical parameters were identified and their influence on final accuracy of scanned model was studied. An analytical model for standard deviation of final scanned model based on RSM and ANOVA was developed. It was observed that scanning distance must be as close to the object as possible within 70 mm to be precise and angle must be below 50° for improving final results of RE process. These optimized parameters values helped in reducing the standard deviation of the final surface model and hence will increase the accuracy of CAD model. In addition, an efficient optimization methodology using modified particle swarm optimization (MPSO) was proposed for providing optimum scanning distance and incidence angle values. The convergence graph shows effectiveness and robustness of the proposed MPSO algorithm. For validation of the proposed methodology two real-life case studies were considered. The results of analytical model and its optimization were obtained and evaluated. It was seen that the standard deviation of the final reverse engineered models significantly reduced by 21.6% and 11.77%.

CHAPTER 5

METHODOLOGY FOR ACCURATE SURFACE RECONSTRUCTION

This chapter focusses on providing accurate path of surface reconstruction form unorganized raw point cloud data. For this purpose, two commercially available software CATIA and Solidworks are employed.

5.1 Introduction

Reverse engineering (RE) begins with acquisition of 3D point cloud from the external surface of an actual product. Various methods are available for obtaining different data shape where each one of these works on a different principle to acquire the point data from the part surface, usually known as digitalization. Traditionally, common methods used for constructing digital human body models or free-form shapes are based on structured light pattern and 3D scanner methods. The prime significance of these systems are the digitization time, capturing an accurate profile of a surface and ease of use. The problem associated with these devices is concerned with missing data points, due to the occlusion phenomena and inaccurate surface generation because of the potential reflection of laser results from a shiny object surface (Rengachary and Benzel, 1999).

The primary concern in developing 3D models using RE systems is the inconvenience in handling thousands of point data acquired by digitization of a physical object (Roca-Pardinas et al., 2008). The second problem arises in creating meshes which best explain the part surface (Pernot et al., 2007). At last, it is important for the RE tools to not only develop a complete digital model, but should also acquire the original design shape and geometry.

3D models with free-form profiles are extensively used in various medical applications such as surgery planning, customized inserts and biomechanical work. In the same context, the design and development of prosthesis socket is a challenge due to the complex geometry of the stump which differs from one amputee to another. The precision of the produced 3D model is of utmost importance for the outcome of the result, particularly

when different software process the captured point data. So, it becomes important to examine the accuracy of the developed digital model with reference to the actual physical model. Several RE software tools are available that suits the requirements needed by design personnel and operators. Prior using difficult mathematical approximations, they attempt to obtain the desired accuracy of 3D models by regulating various key factors through continuous approximations using commercially available CAD application tools.

5.2 Study Model

The present study focuses on accurate 3D surface generation of a complex profile. This free-form surface is generated from a Plaster of Paris (PoP) socket model of an amputee. The external dimensions of the socket are 105 mm (maximum diameter) with a height of 252 mm. The complete PoP socket model and 3D scanning arrangement are shown in Figure 5.1.



Figure 5.1 The Plaster of Paris socket model (left), 3D scanning arrangement (right)

5.3 Point clouds digitization

The case study was scanned using a non-contact blue light scanner (Steinbichler's COMET L3D). The mean acquisition rate of COMET L3D scanner is about 50,000 points per second. The version used in this study for data acquisition has a resolution of 1 Mpx and

1170 x 880 pixels. The complete acquisition of the case study takes about 15 scans, which are taken from different orientations. The socket was placed on a rotary table which makes the scanning process more efficient and faster. The complete digitization process for handling the point clouds was controlled by the 3D scanner software (COMET PLUS). To change the point of view between one scan and the next one, the part was fixed in the working volume and the scanner location was changed. No additional data processing was needed, since the RE software merges multiple scans in one point cloud either automatically or by manually selecting N points. For effective scanning and identification of previous scans, tie points are placed on the socket surface uniformly. The 3D point cloud was exported in IGES format and the raw data of the socket composed of 11,585 points.

5.4 RE tools application

RE systems goal is to transform unorganized 3D point clouds into a surface replica with desired precision and accuracy. There are generally two segments available in these systems: one module converts the raw data into a triangle mesh and second module reconstruct digital surface model from a triangle mesh file. The present study employed two different CAD tools: CATIA V5R16 and SolidWorks 2010. For CATIA study, mesh file is created using the Digitized Shape Editor module. The surface models were reconstructed using Quick Surface Reconstruction and Scanto3D modules. After data capturing, three important steps include:

Step 1 - Processing of unorganized 3D point data. The outliers associated with point cloud data were removed followed with the use of adaptive and homogeneous filtering techniques applied with different percentages. The initial point data captured comprise all the geometric features of the object. The initial raw points consist of higher amount of noise produced as a result of the 3D scanning process. Consequently, huge amount of data size is produced and for effective handling and processing of this data, a suitable filtering technique is applied which results in reducing the redundant points without losing object original geometry.

Step 2 – Development of triangle meshes and processing. The development of triangle meshes is popularly known as tessellation. It is a process to build triangles by

joining three neighbouring points and replicates the same procedure until a network is formed to create a definite, lucid and consistent triangulated surface (Gibson, 2004). In general, the initial raw mesh consists of sharp boundaries and non-manifold vertices, all these discrepancies need to be rectified to guarantee accurate surface generation. Further, it is essential that the meshes are cleaned and refined. The residual unwanted triangle meshes removed and created holes are filled. Occasionally, the triangle meshes are extremely dense which enhances difficulty in handling and processing the file data. The solution to this problem is re-meshing and decimation of the mesh file. Smoothing the mesh, moreover, helps in improving the accuracy of the generated surface model.

Step 3 – Generation of surface model and feature identification. The accuracy of socket surface model was analysed using the parameters including mean deviations (AD), maximum deviation and standard deviation. Three different techniques were employed for the surface reconstruction from a triangular mesh file: feature recognition, surface fitting and NURBS surface patching. Subsequently, for regular features or prismatic profiles, not many software applications are available that allow semi or fully-automated procedure for recognition of various features, which highly depends on the intricacy of the shape. Several individual surfaces are linked resulting in an approximate global surface with automatic creation of arbitrary topology. The surface fitting technique was not applied in the current work. Since the development of each surface fit to characterize the complete surface of a part requires sufficient user expertise that will definitely reflect in the outcome of the final result.

5.4.1 CATIA Methodology

First part of the current work was realized by means of the CATIA software. The organization of the performed process is shown in Figure 5.2. It includes critical parameters of the filtering process, the mesh generation process and the settings applicable for smoothing process prior to surface reconstruction. For free-form geometry, it is essential to carefully remove all outlier points manually after choosing initial point data of the concerned zone. The mesh file W signifies the default procedure employed without using any of filtering or smoothing techniques prior to surface reconstruction.

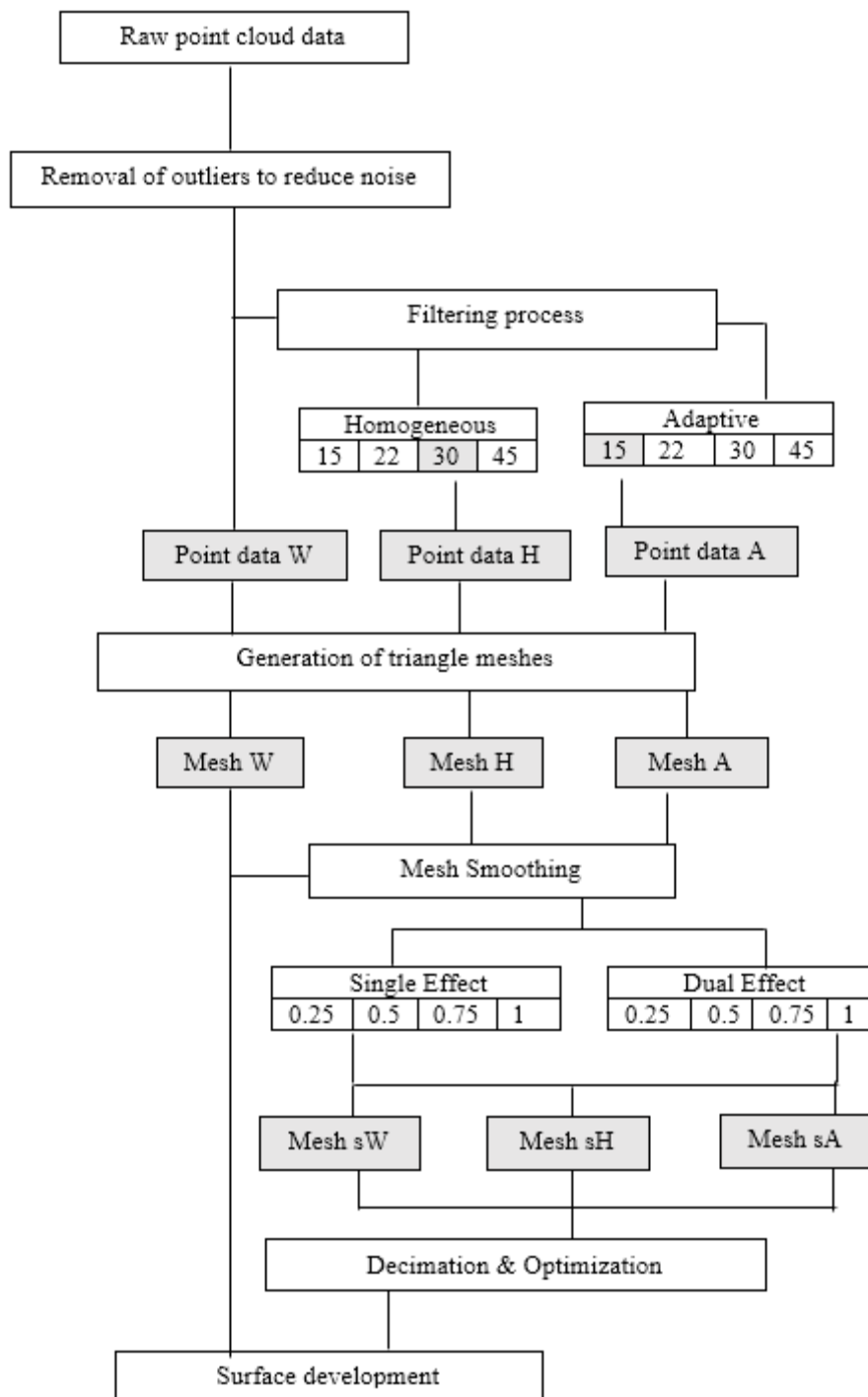


Figure 5.2 Flowchart of CATIA study

5.4.1.1 Filtering technique effect

The Digitized Shape Editor module was used for the reduction of noise and redundant points by using two different types of filtering criteria. The use of the adaptive filtering causes a reduction in the point data which is based on a chord height deviation analysis criteria. This technique helps in removing points from flat zones but preserves data close to the edges, boundaries and high curvature zones. The 3D point cloud was exported and the raw data of the socket model consisted of 11,585 points. Following results for number of faces, maximum deviation and mean deviation were obtained automatically after performing the individual filtering processes. The software provides deviation value of model in comparison to actual model without performing any individual processes.

The use of homogeneous filtering allows a uniform reduction in the point cloud data. Different point filtering percentages (15%, 22%, 30% and 45%) were applied to point data using both the filtering techniques. The default value taken by the software for filtering was 22% which was used as the control for comparison purpose. The resultant files were studied and examined using reduced points (%), number of faces, reduction in mean and maximum deviation. The best results were provided by the homogeneous filtering technique for mesh (H) with 30% of reduced points with a reduction in maximum deviation of 55.27% and mean deviation 25.67% (see Table 5.1). For the adaptive filter, mesh (A) with 15% of reduced points shows best results with a reduction in maximum deviation of 72.31% and in mean deviation 35.76% (Table 5.1).

Table 5.1 Filtering results for point data using homogeneous filter and adaptive filter

		Homogeneous				Adaptive			
Reduction	0%	15%	22%	30%	45%	15%	22%	30%	45%
Number of faces	124	108	122	101	94	120	115	105	87
		-12.90%	-1.61%	-18.55%	-24.19	-3.22%	-7.26%	-15.32%	-29.84%
Max. deviation	1.570	1.019	1.496	0.702	1.609	0.435	1.034	1.375	1.175
		-35.09%	-4.71%	-55.27%	2.49%	-72.31%	-34.12%	-12.43%	-25.13%
Mean. Deviation	0.950	0.760	0.810	0.601	0.851	0.310	0.833	0.900	0.882
		-20.05%	-14.76%	-25.76%	-10.45%	-35.76%	-12.35%	-5.31%	-7.13%

5.4.1.2 Mesh smoothing process analysis

The prime objective of mesh smoothing process is to enhance the accuracy of the reconstructed surface, which can be used by the operator input and shows global effects. There are two techniques available (single effect or the dual effect) for mesh smoothing from which the consumer can choose either of the ones. The importance of the single effect is that it will rub out the sharp edges present in the mesh resulting in the reduction of the volume of the object (shrinkage in the direction of the center of gravity of the object). The second technique lessens the distance between the surface and outliers, furthermore it also reduces the deletion of minor internal radius. Thus, results for maximum and mean deviation were obtained automatically after performing the individual smoothing processes using the smoothing module through the software.

For the analysis of the used smoothing techniques, both single and dual effects parameters used were 0.25, 0.5, 0.75 and 1 generating mesh W, mesh H and mesh A. Mesh W was realized without using any of the filtering technique. The developed meshes were analysed using the percentage of reduced points, the number of faces, and maximum and mean deviation. The finest accuracy results were achieved for smoothing technique used in mesh W (without any filtering). Best result obtained using double effect smoothing, 0.25 parameter for mesh W reduces the maximum and mean deviation to 62.15% and 25.71% respectively. For the mesh A (adaptive filter 15%), best results were obtained for single effect 0.75 smoothing with reduction of about 17.3% as maximum deviation and 25.5% as the mean deviation. Finally, for 30% homogeneous mesh H, best results were coming for the single effect smoothing with factor of 0.50. This shows an increment in maximum deviation of 7.2% and decrease in the mean deviation of 9.2%. Table 5.2 depicts the best outcomes for each of the mesh.

5.4.1.3 Decimation and optimization mesh process

As the resultant mesh sizes are large, it is better to represent it accurately with less number of triangles. The process of lowering the number of triangle mesh, which makes it suitable for processing and handling of the data, is known as decimation. It can be executed on the whole mesh or on any selected area of the mesh file. There are two types of decimation

available, the first is the chordal deviation method and the second is the edge length criterion. However, this study does not consider the decimation process as it can lead to a reduction in accuracy in regions with high curvature, also it may influence the outcome of the results. Next step is to optimize the triangle meshes as this process reallocates the triangles meshes. The usefulness of this process consists in obtaining homogeneity in meshes. This process performs edge split and collapses depending on whether the edge is too long or too short.

Table 5.2 Results obtained after smoothing effect

		Mesh W		Mesh A		Mesh H		
		Max. (1.5 mm)	Mean (0.9 mm)	Max. (0.425 mm)	Mean (0.31 mm)	Max. (0.702 mm)	Mean (0.601 mm)	
Single	0.25	1.323	0.719	0.392	0.292	0.774	0.576	
		-11.8%	-20.15%	-7.76%	-5.81%	10.23%	-4.22%	
	0.50	1.174	0.830	0.451	0.302	0.752	0.546	
		-21.73%	-7.74%	6.12%	-2.43	7.2%	-9.2%	
	0.75	1.092	0.674	0.351	0.231	0.840	0.644	
		-27.2%	-25.06%	-17.3%	-25.5%	19.71	7.23%	
	1.0	1.350	0.801	0.381	0.277	0.803	0.587	
		-10.0%	-11.24%	-10.35%	-18.37	14.47%	-2.35%	
	Dual	0.25	0.568	0.505	0.372	0.271	0.715	0.564
			-62.15%	-43.87	-12.47%	-12.58%	1.86	-6.12%
		0.50	0.782	0.593	0.447	0.320	0.772	0.614
			-47.87%	-34.11%	2.2%	3.1%	9.97%	2.24%
0.75		0.859	0.711	0.512	0.353	0.812	0.686	
		-42.73%	-22.0%	20.47%	13.87%	15.67%	14.21%	
1.0		1.142	0.860	0.435	0.291	0.873	0.765	
		-23.87%	-4.44%	2.35%	-6.13%	24.36%	27.32%	

The optimization operation has a tendency to change the shape of the digital model. Consequently, this chapter takes into consideration the point % to make a comparison between the initial mesh with the optimized mesh. The outcome of the result suggested that best results were obtained for mesh W with dual effect of 0.25. The results for the maximum and mean deviation are 0.875 mm and 0.069 mm respectively. For mesh H, single smoothing with 0.75 factor presents the best result with a maximum and mean deviation of 1.136 mm and 0.135 mm respectively. For mesh A, single effect smoothing with 0.75 shows mean and maximum deviations were 0.113 mm and 0.748 mm respectively.

5.4.1.4 Surface generation

The process of surface generation begins with triangle meshes. Generally, the complexity of the free-form structure of socket peripheral can be duplicated through automated reconstruction commands. In this chapter, the generation of the freeform surface was accomplished by the automatic setting of Surface Reconstruction module. The parameters that were analysed include output surfaces, the percentage of points within tolerance, maximum and average surface deviation. The key input factors include the average surface deviation and the surface detail. The methodology applied is shown in Figure 5.3.

One important input parameter set by the operator was the average surface deviation to achieve the desired accuracy of the surface generated. The outcome of setting this parameter shows some interesting results (see Figure 5.4). At a lesser value, it provides small surface deviation, but in contrast the number of surfaces generated also increases which in turn increases the size of data. The effect of another significant parameter, i.e. surface detail, is shown in Figure 5.5. With the increase in the surface details from 250 to 7500, a significant reduction is shown in the maximum and mean surface deviation. The variation shown was more evident up to a surface facet of 1250, and another noticeable result was observed in the increase in the number of surfaces beyond this value. The surface detail of 1250 appears to be the standard value as beyond which it seems that there was not any significant variation in the results. This means that after this reference value, there does not seem any additional benefits for increasing the refinement.

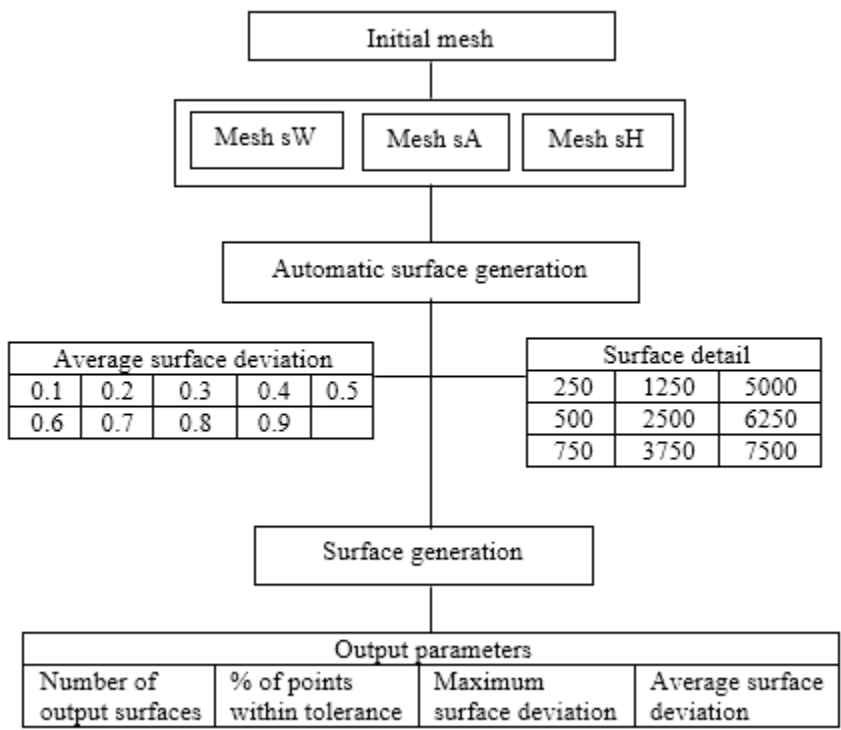


Figure 5.3 Methodology applied for surface generation

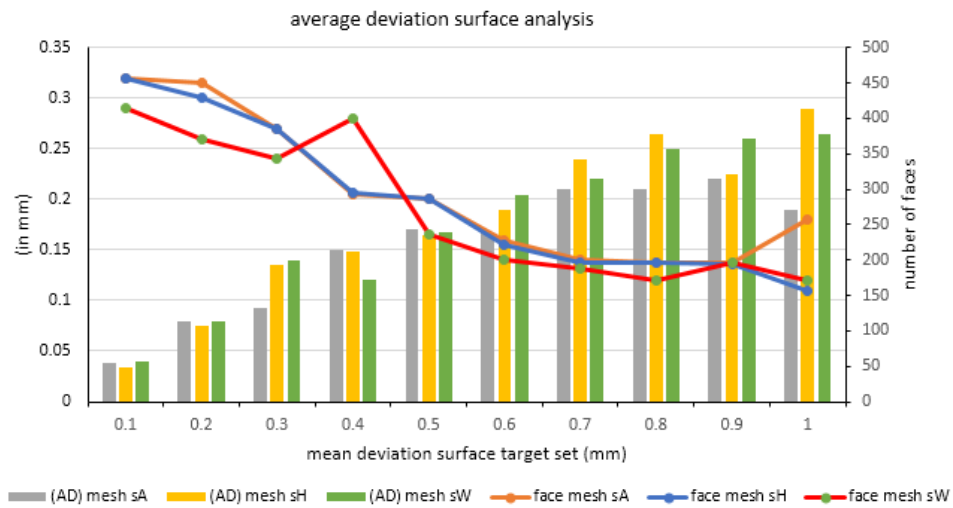


Fig. 5.4 Plot between mean deviation and number of faces

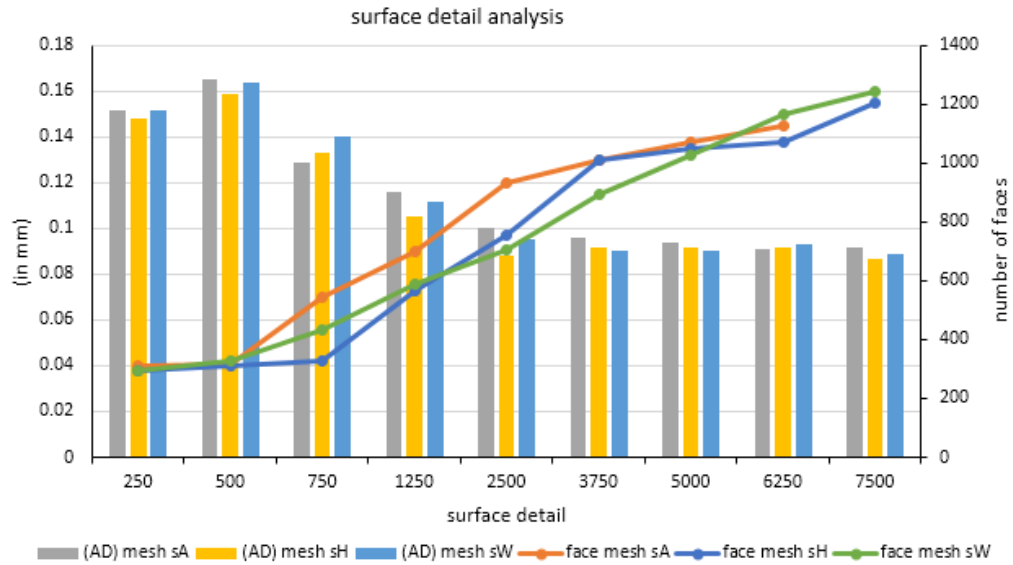


Figure 5.5 Plot between mean deviation, surface detail and number of surfaces

5.4.2. Solidworks study

The second part of this study was performed by employing the Solidworks using the ScanTo3D add-in. The usefulness of this add-in is that it is easy in use and can be used in an automatic way by simply varying few optional parameters. The performed methodology using Solidworks is shown in Figure 5.6 and one can see slight difference comparatively to the CATIA software study. The process of removing outliers and noise is employed on all the point clouds and does not appear to have a significant influence on the overall accuracy as the mean and standard deviation have minimal variation.

Next step was to use the process of filtering which will be applied on the entire point clouds. The command used in the software to filter out point clouds was the “simplification” command by employing curvature based, random, uniform and hybrid based criteria. The 3D point cloud was exported and the raw data of the socket model consists of 11,585 points. Following results for number of faces, maximum and min. deviation were obtained automatically after performing the individual filtering processes. The outcome of filter process is reported in Table 5.3. From the results, it is clear that the curvature based filter and hybrid-based filter have shown significant variation having a

reduction factor of 30% and 15% respectively. In both the cases, a substantial reduction in the maximum and minimum deviation was witnessed.

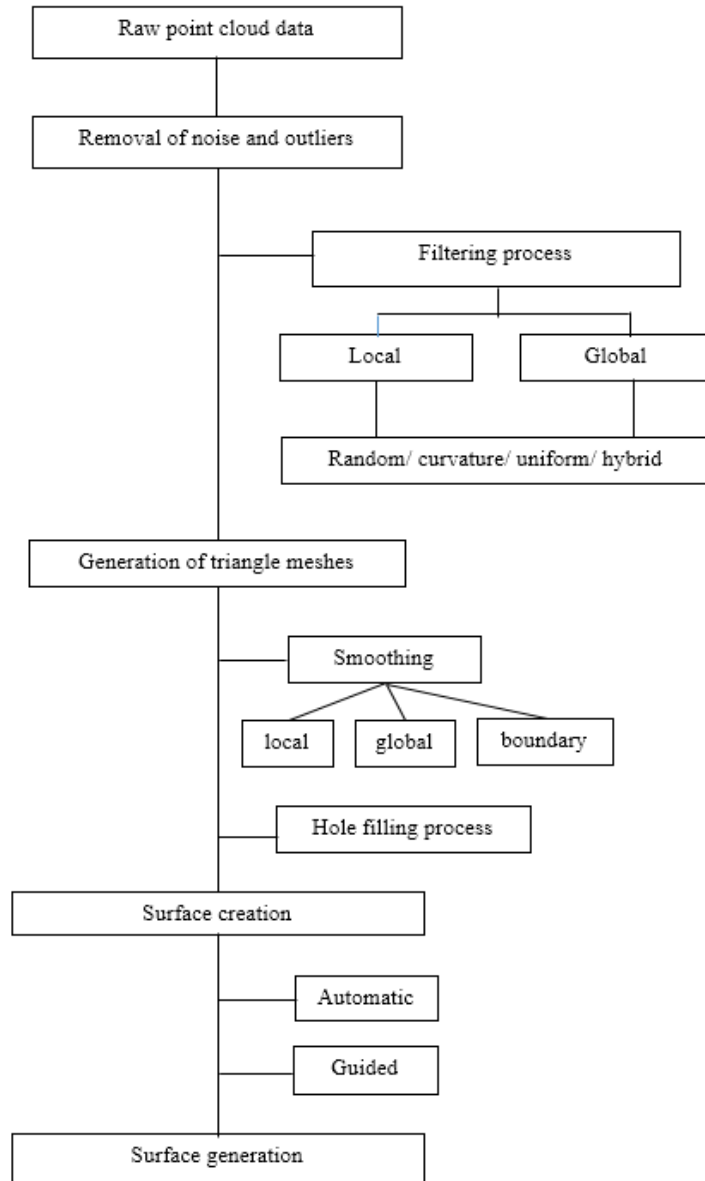


Fig. 5.6 Proposed methodology for Solidworks study

The next step is smoothing of triangle meshes which was performed through three dissimilar criteria: local, global and boundary smoothness. The smoothing process assumes 0 (zero) value for no smoothing and a value of 10 for maximum smoothing with results reported in Figure 5.7. As seen in Figure 5.7, the outcome of the results shows a declining

trend for the maximum deviation. The results for the minimum deviation are slightly varying as compared to maximum deviation. The max. deviation values begins from 0 and then stabilizes at 6. One value for the minimum deviation shows a significant variation for the factor 3, which is a particular extreme point present in the mesh file without any effect in the analysis of the results.

Table 5.3. Filtering process output for point cloud data

		Random			Curvature			Uniform			Hybrid		
reduction	0%	15%	30%	45%	15%	30%	45%	15%	30%	45%	15%	30%	45%
Number of faces	124	112	103	80	145	118	92	150	122	110	131	110	72
		-9.68%	-	-35.48%	16.94%	-	-	25.81%	17.33%	-1.61%	-	5.64%	-
Max. deviation	1.57	1.34	0.86	3.87	1.28	0.57	3.95	1.42	0.76	1.06	0.72	0.95	0.55
		-	-	146.5%	-	-	151.6%	-9.55%	-51.6%	-32.5%	-	39.5%	-
Min. deviation	-0.65	-0.85	-0.98	-1.97	-0.68	-1.27	-1.03	-0.59	-1.54	-0.67	-0.47	-0.72	-0.64
		30.88%	50.8%	203.07%	4.61%	95.4%	58.5%	-9.23%	136.9%	3.07%	-27.7%	10.8%	-1.5%
Std. deviation	0.097	0.094	0.098	0.156	0.091	0.083	0.154	0.104	0.098	0.097	0.088	0.098	0.098
		-3.09%	1.03%	60.8%	-6.2%	-	58.8%	7.21%	1.03%	0.0%	-9.3%	1.03%	1.03%

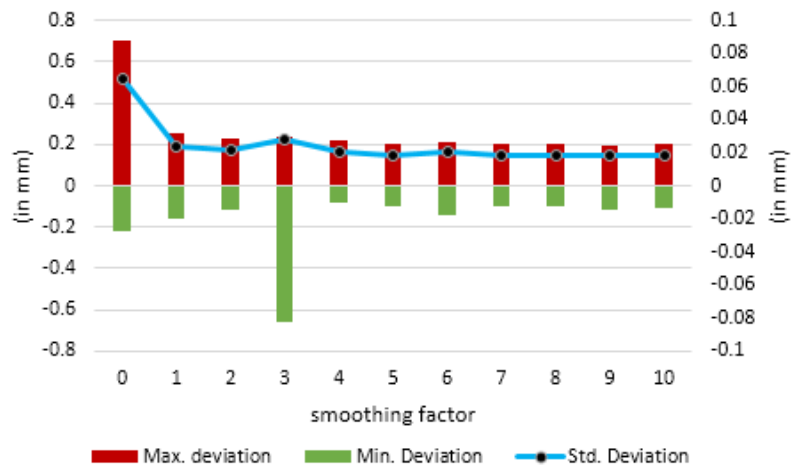


Fig. 5.7 Plot for smoothing factor effect

The used add-in directly converts the triangle mesh file to a solid model through the Automatic Creation command. Also, the guide creation command is sometimes used to generate sub-meshes which directly fit the surface. The final step performed was generation of part-surface by means of surface command with an increase of surface detail factor from 0 to 20. The default factor value used by software was 10. Consequently, two mesh files were considered, one with best results of filtering and smoothing and another mesh without filtering or smoothing effects (curvature filter 30% and smoothing factor 4). Five different conditions were selected (2, 6, 10, 14, 18) and the result depicts how the surface accuracy increases with the increment of the detail factor.

5.5 Results and discussion

For investigation on the real implications of the proposed methodology for producing accurate models, comparison of the SolidWorks model and the CATIA model with the actual model was performed. The developed prosthetic models using both software are shown in Figure 5.8. The comparison of models was implemented using a computer controlled CMM (INSPECS RUBY 564 CMM). For effective comparison, 3-2-1 rule was used to perform suitable alignment. The importance of 3-2-1 rule is that it restricts six degrees of freedom available for the models in space that helps in effective alignment.

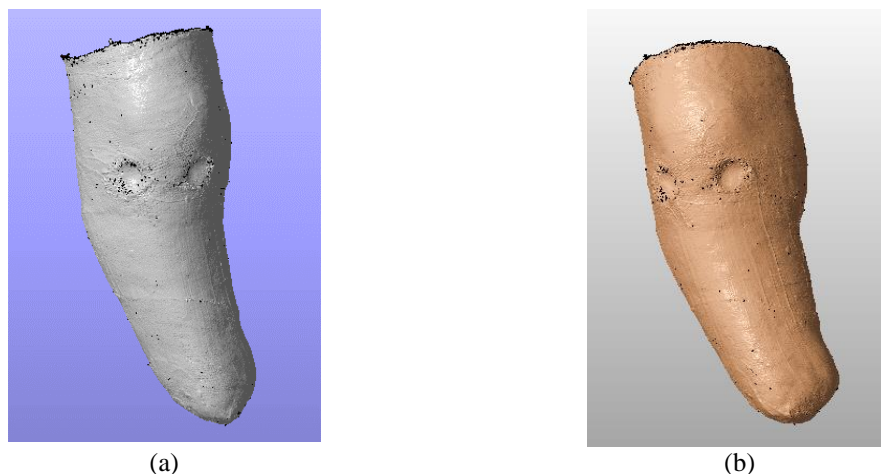


Figure 5.8 Developed model using (a) CATIA V5 (b) Solidworks software

The next step is to measure the external surface of prosthesis socket physical model in sixty random positions using probe tip of 2 mm diameter. Lastly, the deviation of the measured values of the actual model were compared with the digital model of RE. The

nominal values at different original model points were considered as reference values and then comparative results for the six dissimilar 3D models were reported in Table 5.4. The result shows that surfaces developed by applying extra-fine command in both the software have a comparable accuracy (85% CATIA against 81.7% points for Solidworks within the tolerance zone of ± 0.2 mm).

Table 5.4. Comparison of the reconstructed models

CATIA				Solidworks		
	Coarse	Fine	Very Fine	Coarse	Fine	Very Fine
Filtering	None	Homogeneous 30%	Homogeneous 30%	None	Curvature 30%	Curvature 30%
Smoothing	None	None	Single effect (0.5)	None	None	10%
Optimization	None	None	Yes	None	None	None
Measured Points	60	60	60	60	60	60
Points out of tolerance	33	25	9	20	14	11
Efficiency	45%	58.33%	85%	66.67%	76.67%	81.67%
Max. deviation	0.517	0.647	0.302	0.287	0.289	0.297
Min. deviation	-0.669	-0.517	-0.408	-0.447	-0.421	-0.403
Std. deviation	0.237	0.216	0.145	0.152	0.148	0.149

One significant difference reported in comparison of both software kinds was in the model development using default parameters. The Solidworks result is better than the CATIA result for default value, but it cannot be linked with the inaccuracy of the CATIA, it is because of higher extent of the automatic commands employed in Solidworks

(ScanTo3D). The prime objectives of this study includes the assessment of the accuracy of digital 3D models developed by RE procedure and determination of the key factors which influence the freeform, and dimensional and geometric accuracy. The investigation of absolute accuracy is very problematic since the only reference available for a user is the original model. However, the digital and the actual models were used to compare the dimensional deviations at each corresponding points. The Hausdorff-distance criteria were used for determining the differences in the two models. The Hausdorff distance is a measure defined between two point sets representing a CAD model and an actual model. In the past, it has been used to search images for instances of a model that has been translated or translated and scaled by finding transformations that bring a large number of model features close to image features, and vice versa. The Hausdorff distance is reliable even when the model contains multiple objects, noise, spurious features, and occlusions.

The methodology presented shows that inexperienced users have an extra advantage in working on instinctive and automated tools like ScanTo3D and a digitized shape editor. On the contrary, a skilled user can help in improving the quality and accuracy of digital models generated using vigilant selection of different point processing parameters using a variety of CAD tools. The software used in this study have better flexibility in selecting different point processing parameters. The accuracy obtained for the developed model in this study is in accordance with published literature results (Lin et al., 2005), for the use in medical applications and in FEM analysis.

5.6 Summary

For accurate surface reconstruction, two unified solutions using different CAD methodologies for modelling and analysing a freeform surface from a raw unorganized point cloud is proposed. In the first approach, the digital model was generated with default settings of the used software. For second approach, the developed digital model was based on the user's expertise to achieve an upgraded and enhanced surface model. The proposed methodologies are useful in capturing the original surface model accurately and improving the conventional reverse engineering process appropriately.

CHAPTER 6

GD&T ERROR EVALUATION USING PSO AND MPSO

This chapter presents the optimization problem formulation for determining different geometric dimensioning and tolerancing (GD&T) errors like straightness, flatness, circularity and cylindricity in the parts. GD&T tolerances are applied to the most basic geometric features that contribute significantly to different mechanical components such as rotational parts, assembly part, and injection molds to achieve desired functionalities. The form of any individual feature controlled by size tolerances. The GD&T error were evaluated using advanced evolutionary algorithm like basic particle swarm optimization (PSO) and an improved variant of PSO i.e. MPSO, which was proposed in this thesis earlier.

6.1 Minimum zone straightness formulation

By measuring a line element of a surface, the measured data points obtained are represented as $D_i(x_i, y_i)$ where $(i = 1, 2, 3 \dots n)$. Then, the minimum zone solution of straightness error is calculated by finding two parallel lines minimally distant from each other that enclose all data points as shown in Figure 6.1, which also defines the smallest feasible region. These lines are represented by $y = mx + c_1$ and $y = mx + c_2$ where m, c_1 and c_2 are coefficients. If x and y coordinates are known then c_1 and c_2 become a function of x , where m is the slope of line. Now, the shortest distance, d between these two lines can be calculated by as shown in Eqn. (6.1):

$$d = \frac{|c_1 - c_2|}{\sqrt{1 + m^2}} \quad (6.1)$$

The above equation is written in the form of $h(m) = d_{max} - d_{min}$ i.e., straightness error as Eqn. (6.2):

$$d = \frac{\max(y_i - mx_i) - \min(y_i - mx_i)}{\sqrt{1 + m^2}} \quad (6.2)$$

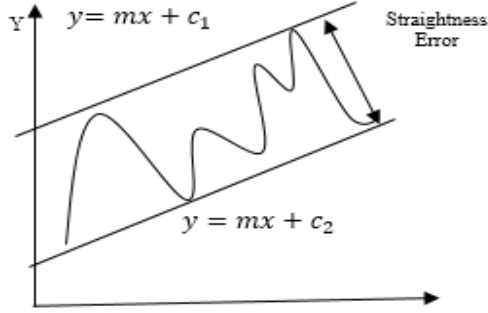


Figure 6.1 Straightness error by minimum zone method

The distance d , between two parallel lines is a function of m . Now, the minimum zone straightness error objective/fitness function can be expressed as Eqn. (6.3):

$$f(m) = \min\left(\frac{\max(y_i - mx_i) - \min(y_i - mx_i)}{\sqrt{(1 + m^2)}}\right) \quad (6.3)$$

where (x_i, y_i, z_i) are 3D point data measured by CMM. The above objective function is a function of m . Accordingly, using PSO and its proposed variant, m is calculated for which the value of the above expression is minimum.

6.2 Minimum zone flatness formulation

For calculating minimum zone flatness error, the two parallel planes are represented by $z = mx + by + c_1$ and $z = mx + by + c_2$, where x, y, z are coordinates and m, b, c_1 and c_2 are coefficients. Similar to straightness, the flatness error can be represented as Eqn. (6.4):

$$\frac{\max(z_i - mx_i - by_i) - \min((z_i - mx_i - by_i))}{\sqrt{(1 + m^2 + b^2)}} \quad (6.4)$$

where x, y and z are coordinates of point data and m and b are the optimization variables. So the objective/fitness function for minimum zone flatness error is given by Eqn. (6.5)

$$f(m, b) = \min\left(\frac{\max(z_i - mx_i - by_i) - \min(z_i - mx_i - by_i)}{\sqrt{(1 + m^2 + b^2)}}\right) \quad (6.5)$$

This is a function of m and b . Consequently for solving the above objective function by searching the value of m and b for which the objective function $f(m, b)$ is minimum.

6.3 Minimum zone circularity formulation

According to ISO (ISO, 1996), circularity is defined as the minimal radial distance between two concentric circles containing the whole data points. Assume all the given data points $D_I(x_i, y_i)$ where $(i = 1, 2, 3 \dots n)$ lie on or between the two concentric circles as shown in Figure 6.2.

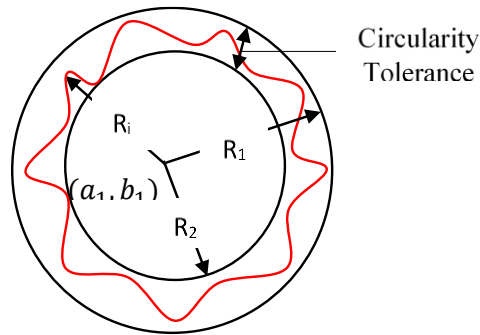


Figure 6.2 Schematic for determining circularity error using MZC

Then the minimum radial separation between these two concentric circles is known as minimum zone solution, and the middle circle is the minimum zone circle (MZC). With the centre of MZC is (a_1, b_1) , the radial distance R_i between data point $D_I(x_i, y_i)$ and the centre is given by Eqn. (6.6)

$$R_i = \sqrt{(x_i - a_1)^2 + (y_i - b_1)^2} \quad (6.6)$$

Now the objective/fitness function for circularity evaluation using MZC is expressed as Eqn. (6.7)

$$f(a, b) = \min(R_{max} - R_{min}) \quad (6.7)$$

Subject to $R_1 \leq R_i \leq R_2$. The above objective function will depend on a_1 and b_1 .

6.4 Minimum zone cylindricity formulation

As per the ISO definition, cylindricity error is the minimal normal gap between two coaxial cylinders which encloses all the data points. The axis of coaxial cylinder can be specified by any random point $P_0(x_0, y_0, z_0)$ which defines its position and the direction cosine of the axis as l, m and n as shown in Figure 6.3.

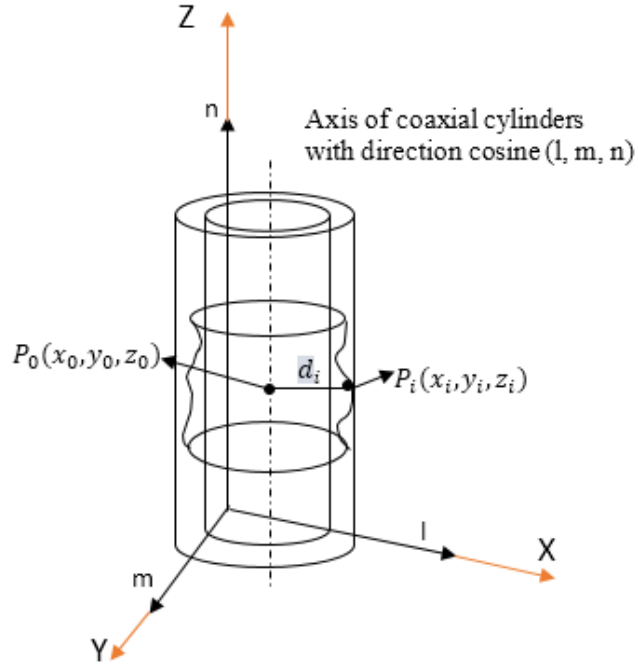


Figure 6.3 Schematic for determining cylindricity error using MZC

So the axis can be represented by Eqn. (6.8)

$$\frac{x - x_0}{l} = \frac{y - y_0}{m} = \frac{z - z_0}{n} \quad (6.8)$$

The normal distance d_i between the measured point $P_i(x_i, y_i, z_i)$ on surface of cylinder and the axis is given by Eqn. (6.9):

$$d_i = \sqrt{\frac{a^2 + b^2 + c^2}{l^2 + m^2 + n^2}} \quad (6.9)$$

where $a = (y_i - y_0) \cdot n - (z_i - z_0) \cdot m$

$b = (z_i - z_0) \cdot l - (x_i - x_0) \cdot n$

$c = (x_i - x_0) \cdot m - (y_i - y_0) \cdot l$

The objective/fitness function for minimum zone cylindricity is given by Eqn. (6.10):

$$f(x_0, y_0, z_0, l, m, n) = \min(\max(d_i) - \min(d_i)) \quad (6.10)$$

where x_0, y_0, z_0, l, m and n are decision variables of the objective function.

6.5 Experimental implementation

Before evaluation of the form tolerances based on measured data, various examples from literature are taken for evaluating the form tolerance and the proposed algorithm robustness and effectiveness is verified. A set of data points are taken from literature (Cui et al., 2013; Wen et al., 2012; Lei et al., 2014; Chou and Sun, 2000; Carr and Ferreira, 1995) for straightness, flatness, circularity and cylindricity. As GA, PSO and MPSO algorithms are stochastic in nature, consequently the results are not repeatable. For this reason, all algorithms are run 25 times independently with similar parameters to evaluate these datasets. Further, average of these 25 datasets are taken for providing reliable estimate of the accuracy in results. The algorithm is programmed and implemented in MATLAB R2014a. The parameters used for PSO and MPSO optimization techniques are shown in Table 6.1.

Practical Examples (Straightness)

For the purpose of comparison, four examples available in literature (Cui et al., 2013) are selected. The real data points measured using CMM for straightness evaluation are shown in Appendix A with allowable tolerance of 0.00165 inch. Table 6.2 shows the results presented in literature (Cui et al., 2013) along with the solution provided by the proposed MPSO algorithm. For example 1, it is observed that minimum zone straightness error obtained by LSM is 0.0017, Optimization Technique Zone (OTZ) (Weber et al., 2002) is 0.0017, Linear Approximation Technique (LAT) (Weber et al., 2002) is 0.0017, GA (Cui et al., 2007) is 0.001672 and PSO (Cui et al., 2013) is 0.001711. While the minimum zone straightness error obtained by the proposed MPSO is 0.00160. If the allowable straightness tolerance is 0.00165 inch, all the algorithms except the MPSO algorithm overestimates the tolerances and hence results in rejection of good parts. This signifies the importance of the proposed algorithm in accurate evaluation of minimum zone tolerance and also helps in

preventing the rejection of good part based on product specifications. This will further help in minimizing the economic loss occurred in manufacturing of part.

Table 6.1 Parameters used for PSO and MPSO

S. No.	PSO and MPSO parameters
1	Swarm Size: 50
2	Maximum Number of iterations: 100
3	$c1, c2 = 2.05, 205$
4	$w_{start}, w_{end} = 0.9, 0.4$

The result shows that MPSO algorithm has higher computational accuracy and its optimization result surpassed those from the other methods and from LSM. The iterative curve for PSO and MPSO is shown in Figure 6.4 (a-d) confirming the better performance and efficiency of the proposed MPSO algorithm. For further confirmation and testing of MPSO, the bootstrap methodology is employed for example 1 to prove better convergence of MPSO. The dataset size is taken upto 500 points. The result of the comparison between PSO and MPSO algorithm upto 500 data points is shown in Figure 6.5. From Figure, it is observed that average straightness error shows a minimum with dataset size of 150 and no further significant decrease beyond that. The MPSO result is still better in comparison with basic PSO.

Table 6.2 Results of straightness Evaluation (inch)

Examples	LSM	OTZ (Weber et al., 2002)	LAT (Weber et al., 2002)	fmincon	Non-linear least square	GA (Cui et al., 2007)	PSO (Cui et al., 2013)	MPSO
1	0.0017	0.0017	0.0017	0.00172	0.0017	0.001672	0.001711	0.00160
2	0.0015	0.0014	0.0014	0.00148	0.00149	0.001428	0.001401	0.00139
3	0.0049	0.0047	0.0047	0.0047	0.0048	0.004687	0.004706	0.00468
4	0.0025	0.0023	0.0023	0.0023	0.0024	0.002266	0.002291	0.00215

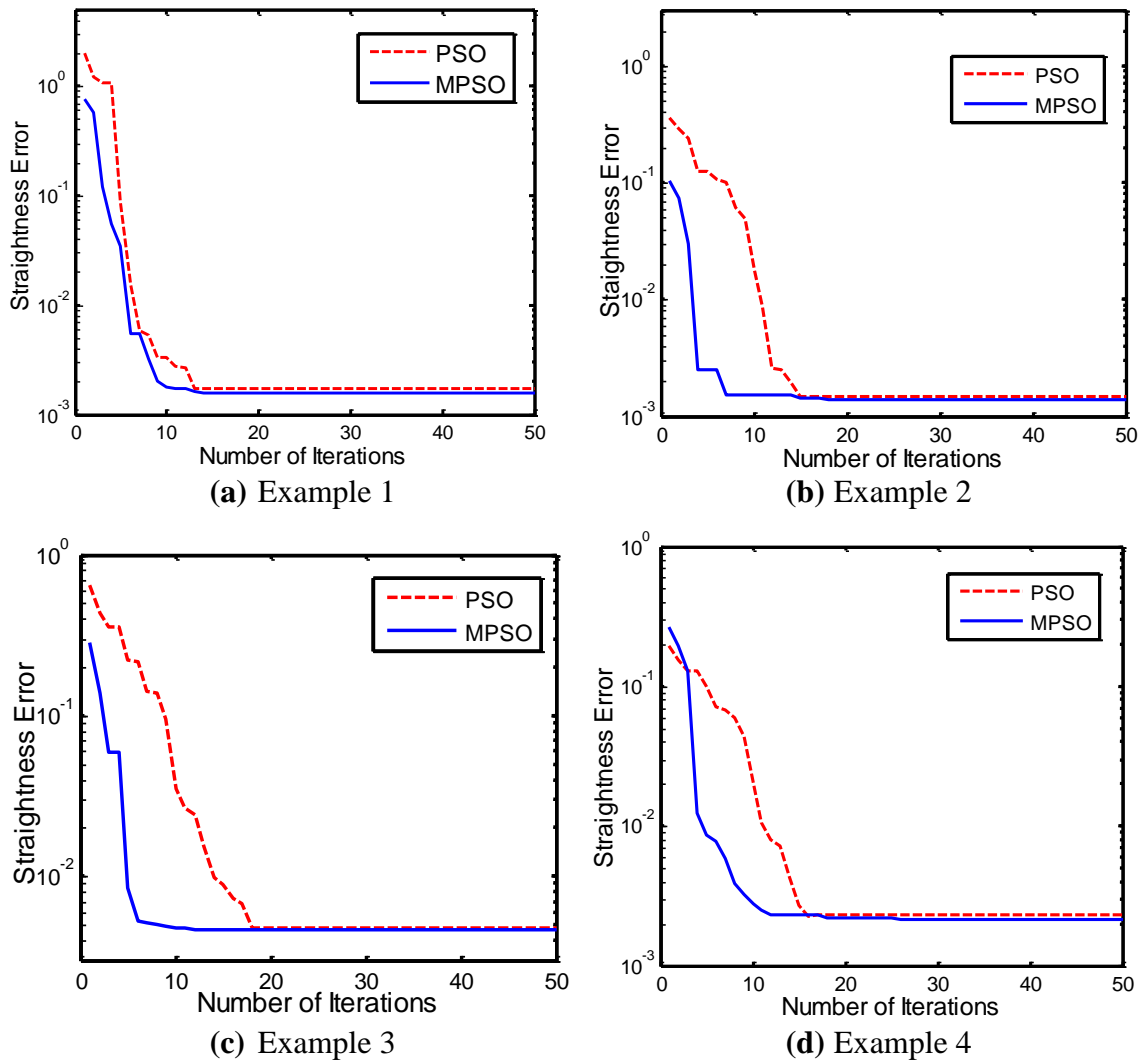


Figure 6.4 Convergence of PSO and MPSO algorithm for straightness error evaluation

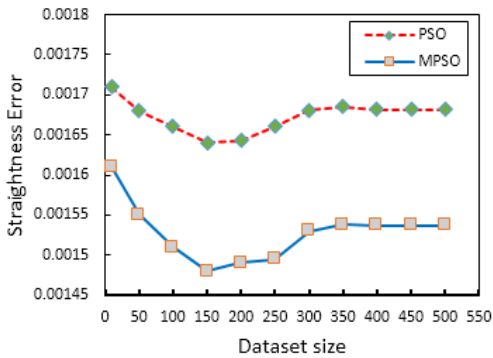


Figure 6.5 Average Straightness error versus dataset size ($0 < \text{dataset} < 500$) using bootstrap methodology for example 1

Practical Examples (Flatness)

The sampling data available in literature (Wen et al., 2012) are selected as shown in Appendix B with 25 data points for each measurement. A plane part with length and width of 140 mm and 120 mm respectively is considered with allowable tolerance of 0.018 mm. For part inspection, it is important to follow an appropriate sampling strategy. The sampling strategy suggests selection of exact location for each measurement points. Two sampling data sets are taken which means location of points are same for both measurements. The results for flatness error evaluation is tabulated in Table 6.3 It is observed that the minimum zone flatness error obtained by the proposed MPSO for 2 times sampling are 0.0174 and 0.0178 respectively with a mean of 0.0176. The result is of practical significance as the allowable maximum tolerance is 0.018 mm, with GA and PSO providing 0.0187 mm tolerance.

On the contrary, the result of MPSO is 0.0176 mm, which is under the allowable tolerance limit. This result shows that the good part may get rejected if LSM, GA and PSO algorithm is used, due to overestimation of flatness. Also, it is well in agreement with the results reported in literature (Wen et al., 2012) and far better than those obtained by LSM. The iterative curves when making assessment of flatness for PSO and MPSO are shown in Figure 6.6 (a-b). It clearly shows that MPSO has faster convergence and higher optimization accuracy compared to standard PSO algorithm. For further confirmation and testing of MPSO, the dataset size is resampled using bootstrap methodology and taken upto 500 points for experimental trials. The result of the comparison between PSO and MPSO algorithm upto 500 data points is shown in Figure 6.7. From Figure 6.7, it is clearly seen that average flatness error shows a minimum for dataset size of 200 and no further significant decrease is observed beyond that.

Table 6.3 Results of Flatness Evaluation (mm)

Examples	Allowable Tolerance	LSM	fmincon	Non-linear least square	Improved GA	PSO	MPSO
1 st time sampling	0.018	0.0219	0.0195	0.0194	0.0184	0.0184	0.0174

2 nd time sampling	0.018	0.0229	0.0211	0.0195	0.0189	0.0189	0.0178
Mean	0.018		0.0203	0.01945	0.0187	0.0187	0.0176

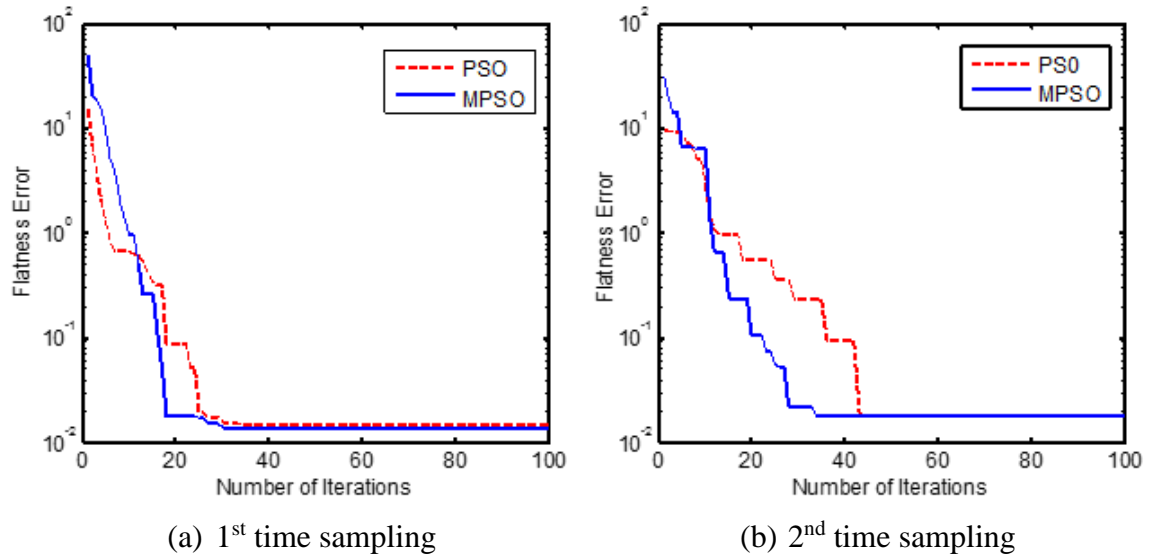


Figure 6.6 Convergence of PSO and MPSO algorithm for Flatness error evaluation

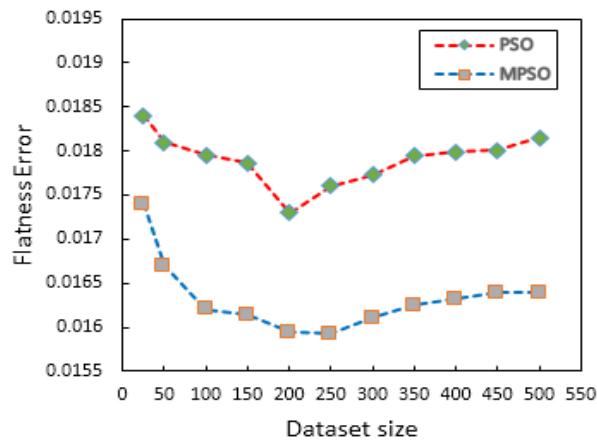


Figure 6.7 Average Flatness error versus dataset size ($0 < \text{dataset} < 500$) using bootstrap methodology

Practical Examples (Circularity)

A bearing ring part is measured using CMM with PC-DMIS software. The coordinates of all measured points are shown in Appendix C. The results are tabulated in Table 6.4. It is observed that the minimum zone circularity error obtained by the least square circle (LSC),

Minimum Zone Circle (MZC) and Geometric Approximating Searching Algorithm (GASA) (Lei et al., 2014) for example 1 are 0.0259, 0.0250 and 0.0244 respectively. While the circularity error obtained by the proposed MPSO is 0.02335.

Standard PSO is also used to calculate the minimum zone circularity error for comparison with the proposed MPSO. It can be seen that the roundness error for MPSO shows better results than LSC, MZC and standard PSO and comparable to GASA results. Similarly, for example 2, the MPSO algorithm outperforms the other mentioned methods available in literature. Figure 6.8 (a-b) shows the searching process of PSO and MPSO with iteration. Obviously, the convergence and optimization accuracy of MPSO is higher than standard PSO, which indicates that MPSO reaches to the optimum value earlier than standard PSO. Further validation of MPSO is performed using the bootstrap methodology by multiplication of the experimental data for example 1. The dataset size is taken upto 500 points. The result for 500 data points is shown in Figure 6.9. From Figure, it is observed that average circularity error shows a minimum with dataset size of 200 and no further significant decrease beyond that.

Table 6.4 Results of Circularity Evaluation

Example	LSC (Lei et al., 2014)	MZC	GASA (Lei et al., 2014)	Fmincon	Non-linear least square	PSO	MPSO
1	0.0259	0.0250	0.0244	0.0251	0.0249	0.02508	0.0233
2	-	0.038231	0.038231	0.03801	0.0382	0.03823	0.0372

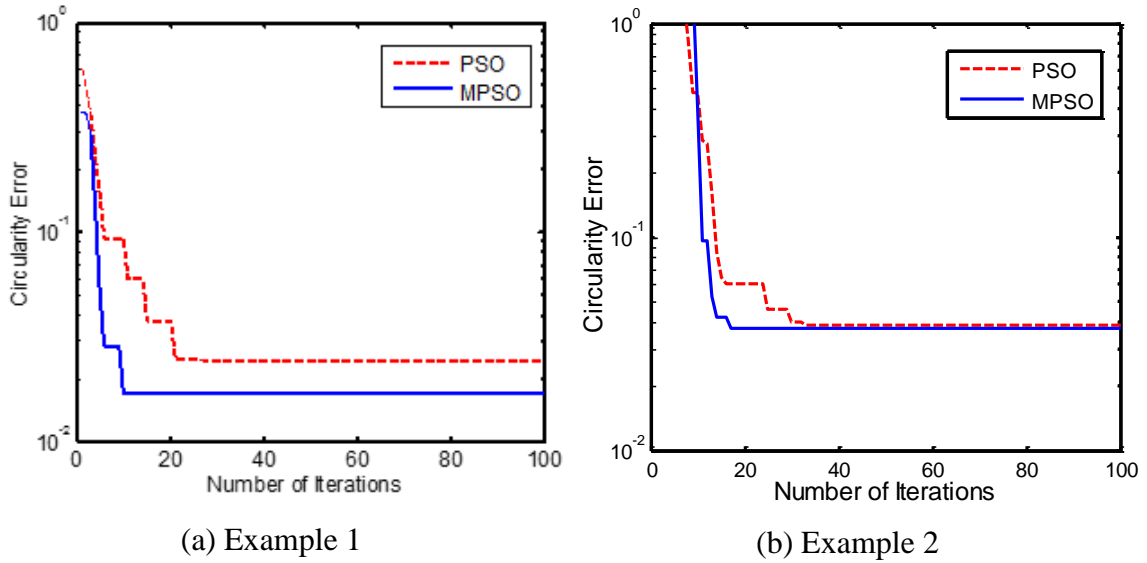


Figure 6.8 Convergence of PSO and MPSO algorithm for Circularity error evaluation

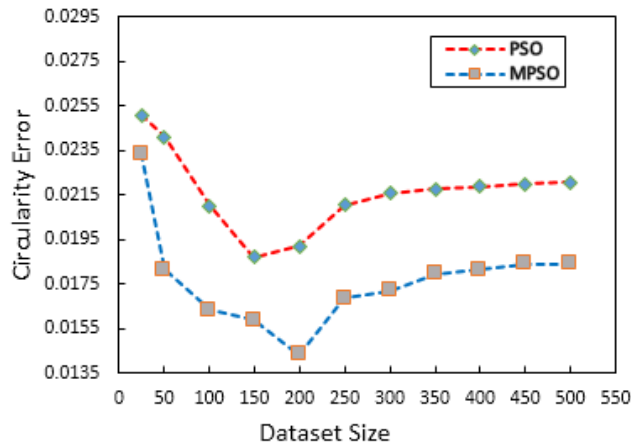


Figure 6.9 Average Circularity error using bootstrap methodology

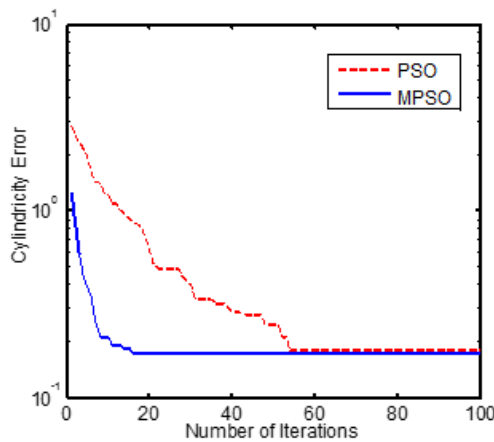
Practical Examples (Cylindricity)

For cylindricity evaluation, two different sampling data available in literature (Wen et al., 2010) are selected. The coordinates of all measuring points are shown in Appendix D. From Table 6.5, it is observed that for sample data 1 minimum zone cylindricity error attained by method (Chou and Sun, 2000), by (Carr and Ferreira, 1995), PSO (Wen et al., 2010) and LSM are 0.184590, 0.183960, 0.174635 and 0.212829 respectively. 0.20254 and 0.18396 respectively. While, the cylindricity error obtained by proposed MPSO is 0.173520, which is in agreement with the previous literature results. Also, for second

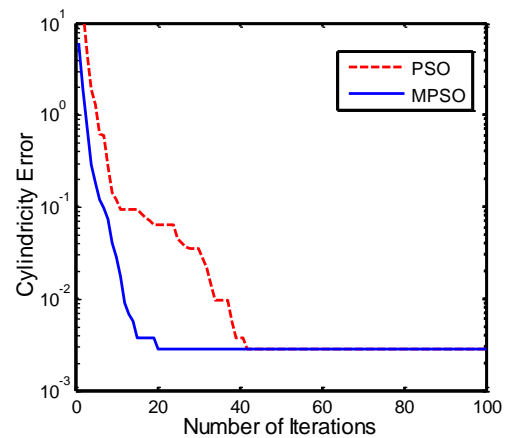
example data cylindricity error by MPSO is 0.002782 in comparison to GA (Lai et al., 2000) and PSO (Wen et al., 2010) values of 0.002788 and 0.002788 respectively. Evidently, MPSO algorithm results are comparable with the previously published literatures. The iteration curves of PSO and MPSO with iteration in search of minimum zone cylindricity error is shown in Figure 6.10 (a-b). The Figure 6.17 (a-b) clearly depicts the fast convergence and effectiveness of the proposed MPSO in comparison to standard PSO. For further confirmation and testing of MPSO, the bootstrap methodology is employed by multiplication of used experimental data for example 1. The dataset size is taken upto 500 points. The result of the comparison between PSO and MPSO algorithm upto 500 data points is shown in Figure 6.11. From Figure 6.11, it is observed that average cylindricity error shows a minimum dataset size of 200 and no further significant decrease beyond that.

Table 6.5 Results of Cylindricity Evaluation

Example	LSM	Literature		fmincon	Non-linear least square	PSO (Wen et al., 2010)	Proposed MPSO
1	0.212829	0.184590 (Chou and Sun, 2000)	0.183960 (Carr and Ferreira, 1995)	0.1832	0.01921	0.174635	0.165120
2	0.037162	-	0.002788 (Lai et al., 2000)	0.0032	0.00334	0.002788	0.002782



(a) Example 1



(b) Example 2

Figure 6.10 Convergence of PSO and MPSO algorithm for Cylindricity error evaluation

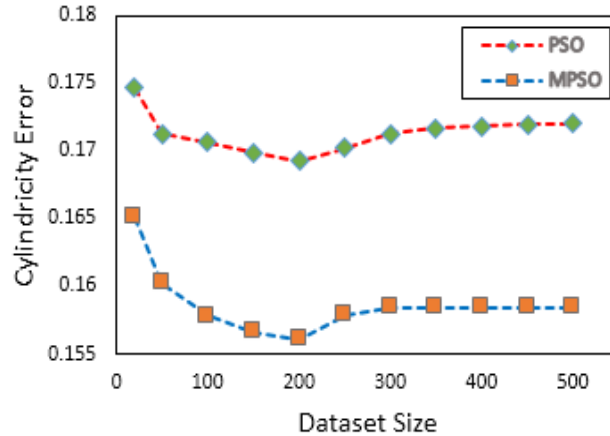


Figure 6.11 Average Cylindricity error versus dataset size ($0 < \text{dataset} < 500$) using bootstrap methodology

6.6 Summary

This chapter deals with the determination of different GD&T error that incurred during manufacturing of the part. A simple objective function for form tolerance evaluation was formulated as an unconstrained optimization problem. Numerical examples have been illustrated to verify form errors from coordinate data effectively. Compared to conventional or existing heuristics optimization methods, the proposed MPSO algorithm not only has the advantage of a simple realization in computers and good flexibility, but it was shown to have improved the form error evaluation accuracy. The traditional techniques for form error evaluation generally convert the non-linear objective function into a linear one thus embedding more assumptions function. However, the implementation of the proposed MPSO algorithm can ensure that direct form error can be evaluated without any conversion. Consequently, this algorithm could be implemented for inspection and form error evaluation on CMMs.

CHAPTER 7

DEVELOPMENT OF FRAMEWORK FOR ACCURACY CONTROL AND CONTACTLESS INSPECTION

This chapter presents an iterative and effective inspection framework to investigate the accuracy and capability of contactless laser scanning systems in terms of free-form and GD&T control. For testing and validating the proposed framework a standard benchmark part with typical features conforming to different families of geometrical dimensioning and tolerancing (GD&T) is proposed. The benchmark part designed consists of various canonical features widely used in an engineering and industrial applications. Surface reconstruction of the benchmark model performed using different reverse engineering software used in chapter 5 (COMET PLUS, CATIA v5 and Solidworks Scan-to-3D), and results are analyzed to study the correlation between various critical parameters. The need of suitable alignment technique prior to contactless inspection and the second part presents the optimization problem formulation for determining different geometric dimensioning and tolerancing (GD&T) errors like straightness, flatness, circularity and cylindricity in the parts. One of the important step in the non-contact inspection procedure using the 3D scanner is the correct localization of the datum reference frame. This step would help in the effective alignment of the acquired point data.

This work takes into consideration various 3-2-1 alignment approach and investigates its influence on the inspection results. The result provides an evidence that an incorrect description of the product reference frame can lead to erroneous estimation of actual part deviations. Considering the contact based measurement as a reference, different models developed were analyzed and compared in terms of geometrical and dimensional tolerance. The proposal of standard benchmark part and methodology for GD&T verification will provide a simple way of performance evaluation for various contactless laser-scanning systems. This chapter proposes an effective inspection framework and further validating the techniques used in previous chapters on a benchmark part for free-form and GD&T features.

7.1 Introduction

The geometrical dimensioning and tolerancing (GD&T) inspection is used to examine the conformity of manufactured parts with the defined part specification. Often, GD&T inspection is performed using contact based coordinate measuring machines (CMM) in industries (Lee et al., 1997). The main advantages are high measuring accuracy, point-to-point data acquisition and well established calibration process. However, inspection planning using CMM is a complex and troublesome task, which requires skilled and experienced operator (Elkott et al., 2002). The CMM inspection is effective for certain types of parts but not suitable for soft materials, complex geometry especially free form shapes. Furthermore, performing rapid data acquisition of part surface is one of the primary concern, which is even higher for large and complex parts. In industries, non-contact scanning systems are used as a tool for physical model restoration and development of complete and worn-out components. Nowadays, contactless digitizing systems have realized an adequate level of assurance in reverse engineering field. Further, significant efforts have been made to improve the accuracy of non-contact scanning systems. However, the use of non-contact scanning instruments for industrial applications is impeded by investment particularly involving cost of instrument, software, training and timely maintenance.

For effective characterization and development of non-contact scanning systems, some standardized parts and methodology are required for providing adequate metrological data and quality claims. To test the quality claims of products, very few methods and techniques are available with industries. In addition, the selection of best method is quite tricky as the best technique for one application might not work for other. The lack of appropriate inspection standard makes it difficult for selection of a suitable scanning system only based on information provided by the manufacturer. The metrological specification provided by the manufacturers are based on the different systems, methods and are provided in the non-standard format which are difficult to translate in the real life applications.

Therefore, to investigate the potential offered by the non-contact scanning systems a common benchmark part and standard procedures are required. Such methods and

benchmark parts will help the users in determining the strengths and weaknesses of a measuring system and hence in the adequate decision making process. In the same context, few examples of standards and guidelines provided for metrological verification using CMM is provided in the ISO 10360 and ISO 15530 (Kunzmann et al., 1990; Hansen and De Chiffre, 1997; Trapet et al., 2004).

Focusing on the metrological aspect, this chapter presents an innovative benchmark part and a methodology to evaluate the suitability and effectiveness of the non-contact scanning systems for GD&T inspection of parts. Additionally, the proposed benchmark part will serve as a standard tool in examining whether workpieces meet a set of tolerance specifications as defined using GD&T terminology. In the same context, a comparative study between non-contact scanning system and touch probe CMM has been performed by taking CMM as reference. The reason for taking CMM as reference is its repeatability and precision of measurement. The benchmark part is scanned and virtual model is developed, which is compared with the model developed using CMM. The accuracy of two systems (contact vs non-contact) has been analyzed by performing comparisons between the reconstructed benchmark surfaces. Different scanning orientations were considered and the best is suggested for accurate results. In addition, the influence of different reverse engineering (RE) software, used in the processing of raw point data to a reconstructed surface, has also been considered.

7.2 Development of Framework for accuracy control and contactless inspection

Based on the results obtained so far according to the adopted methodology, an iterative and effective framework is proposed in Figure 7.1 for GD&T features and free-form surface verification of contactless laser scanning systems. The framework consist of different elements described by previous chapters. The framework is mainly divided in two stage i.e. Stage 1 (Digitization and surface reconstruction) and Stage 2 (Inspection). This framework will be helpful to the laser scanner end users in verifying the accuracy of their scanning device provided by the manufacturers. The framework features and its components are explained below:

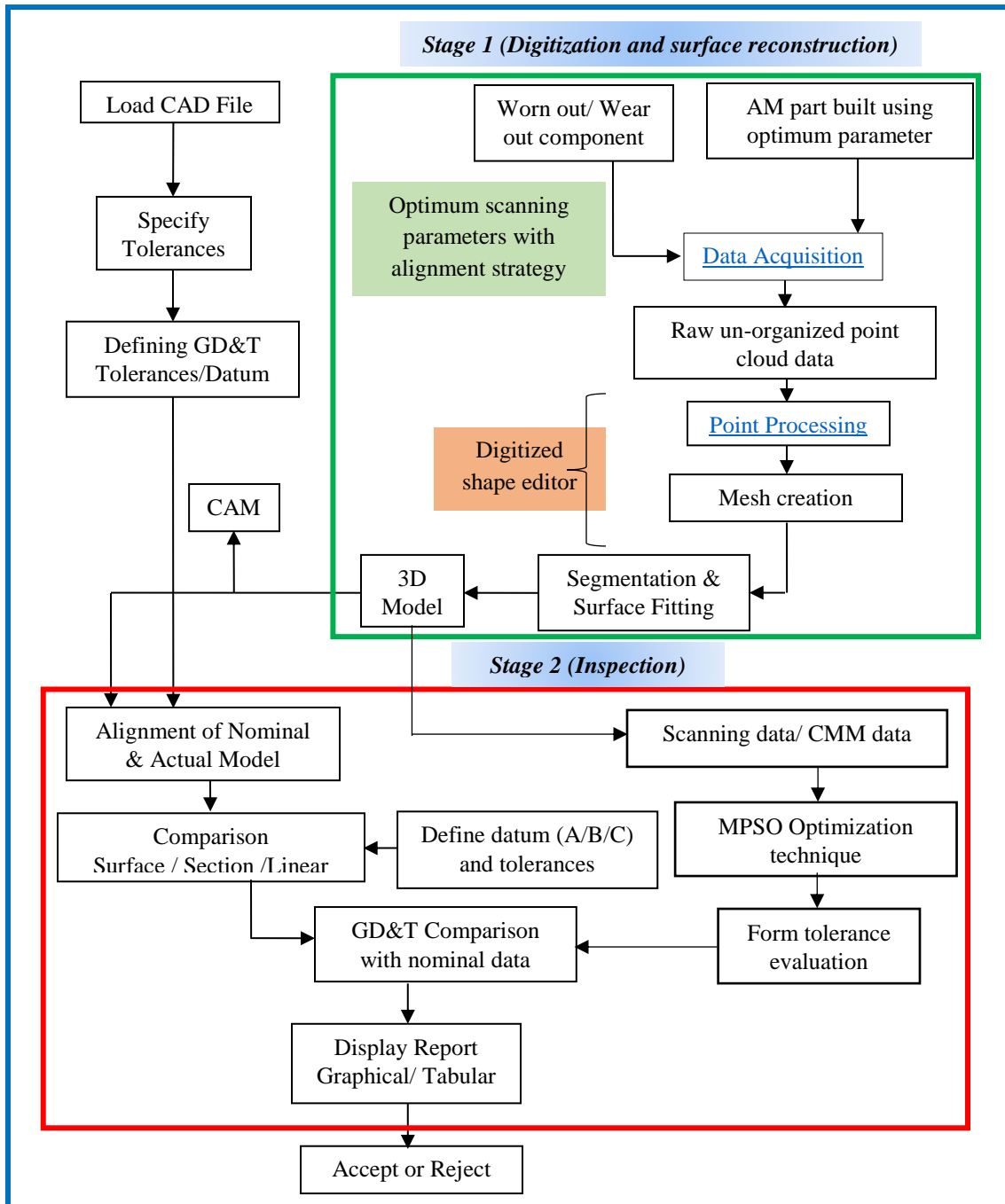


Figure 7.1 Proposed framework for GD&T features and free-form surface verification in contactless scanning system

Stage 1 (Digitization and surface reconstruction)

Stage 1 deals with the formulation of surface model from a physical component. In industries, most of the manufactured components need to be inspected so that they can perform the intended function without failure—demanding least skill. The starting point of this stage deals with the data acquisition strategy—selecting a scanner, preparing the part to be scanned and performing actual scanning to capture the information that describes all geometric features of the manufactured component like slots, hole, steps etc. 3D scanners capture the surface cloud point, which helps in defining the complete geometry of the manufactured part. 3D cloud points are point coordinates in space with x, y and z coordinates which provide complete information about the features of the product. After data acquisition, point cloud data processing is done which includes removal of noise, reducing the number of points etc. Reducing the number of points is an important process which is known as filtering, that helps in proper handling of the data and increasing the speed of processing. During scanning, to capture complete features of a component it is required to take multiple scans. Due to multiple scans, captured data include the intended data and also the noise part in the surroundings. So it is essential to remove this noise as it will unnecessarily slow down the process of point processing. Captured data needs to be filtered to remove unwanted and noise data (Malamsa et al., 2003). As multiple scans are needed to capture data over the entire surface, and the data obtained from different views have to be integrated. Registration process is used to determine the transformation of data from two different scans, so that data can be integrated under similar coordinate system. Integration is the process of creating a single surface representation from the sample points of two or more range images (Turk and Levoy, 1994). The next step is segmentation which refers to a process to pluck out the selected regions of interest from the rest of data using automated or manual techniques. After all, the above steps 3D surface model is created which may either be used for Computer Aided Manufacturing (CAM) or for the inspection process.

Stage 2 (Inspection)

Inspection of manufactured component is an important aspect of industry quality program. Second stage of this framework is concerned with the inspection processing of

the manufactured component. Inspection practice starts with importing the actual/nominal CAD model into the INSPECT PLUS software. To perform GD&T inspection, it is important to define datum first. After specifying datum and GD&T tolerances in the actual CAD model of the part, import the scanned model of the part to the INSPECT PLUS software. After importing both the nominal and scanned file in the software, the next step is to align the two models. Correct alignment is an important task as it can change the inspection results drastically. There are few options available for correct aligning like 3-2-1 aligning, automatic pre alignment and best fit alignment. In 3-2-1 alignment, three planes, two vectors and one point are created on the nominal part and the corresponding planes, vectors and point are created on the actual model. After aligning of the models is done, actual part is ready for inspection. GD&T inspection is performed over different geometrical features like plane, holes, slots, cylinder, etc. Report in tabular and graphical format is produced for GD&T tolerances like straightness, flatness, circularity, cylindricity, angularity, parallelism etc. It displays GD&T tolerances, surface and section reports, which will be very helpful for industries. After getting all the reports, it becomes an easy task to check whether the geometrical features on the parts are within tolerance or not. This leads to decision on acceptance or rejection of the part.

7.3 Case study validation

In the present study, two different sensors were used. For contact based measurement, a touch probe tip of 2 mm on an INSPECS RUBY 564 CMM model, fitted with an indexable swinging head. The touch trigger probe having resolution of 0.5 μm was used. The volumetric length measuring accuracy MPEE of the machine according to ISO-10360-2 is $2.5 + L/350 \mu\text{m}$, where MPEE is the abbreviation for maximum permissible error for length measurement and L is the measured length. For non-contact measurement, Steinbichler COMET L3D contact less scanning system was used. The version of COMET scanner used in this study for data capturing has a resolution of 1170 x 880 dpi available (Table 7.1). It is imperative to highlight that the accuracy of the CMM is approximately one order of magnitude higher than the non-contact scanning systems. Therefore, the CMM measurement is used as reference for the geometries of benchmark part. Different software were used for the accurate surface reconstruction from unorganized point clouds. The

software used particularly includes COMET PLUS, CATIA v5 and Solidworks. The 3D scanner default software for surface reconstruction is COMET PLUS. CATIA v5 software considered here has good prominence in industry for various modelling and analysis application. The third software used for surface reconstruction is Solidworks Scan-to-3D, which is widely used for reverse engineering applications in industries. Finally, INSPECT PLUS software is used for quality control and inspection of free-form surface and GD&T comparison. Figure 7.1 depicts the methodology adopted for the comparison of touch probe CMM and non-contact scanning results for GD&T verification of laser scanners.

Table 7.1 COMET L3D scanner parameters (Steinbichler, 2016)

S. No.	Scanner Parameters	Value	Unit
1	Camera Resolution	1170 x 880	dpi
2	Measuring Field	100	mm ³
3	Measuring Volume	92 x 69 x 60	mm ³
4	Point to point distance	100	µm
5	Fastest measurement time	2.5	sec

7.3.1 Benchmark Part Design

The accuracy of data acquisition systems can be easily evaluated when standard geometric entities are scanned in a single view. Commonly, the non-contact scanners involve multiple scans for complete capturing of complex parts. The number of views depend on the existence of occlusion in the features of the component. Due to multiple scans, each point cloud needs to aligned and merged for develop a complete model of the object. These two process (aligning and merging) results in some errors due to superposition of multiple point data. However, the contactless scanning system need to produce accurate models even after combining multiple point cloud data in one for proving their effectiveness in quality control.

From quality control perspective, the existence of typical classic features is indispensable, since form errors and other geometrical tolerances are defined using them. The proposed benchmark parts was designed with reference to canonical GD&T features

used in regular engineering components. The test part designed includes different artifacts and primitives which are specifically selected to characterize variety of dimensions and geometries defined by GD&T control. The overall dimensions of the benchmark part are 120 x 120 x 33 mm³ (see Figure 7.2). The size of benchmark part was determined to make it portable and fit into the working area of small contact based and contactless scanning systems. Additionally, the proposed standard artefacts have sufficient optical and geometrical features for providing error introduced by laser scanner with reference to contact based systems.

The following classic geometries appear in the proposed benchmark parts:

- An outer cylinder (OC), of 5 mm high. The cylinder has a diameter of 25 mm.
- Three similar blocks with flat surfaces (FS), that are parallel and perpendicular to the part base. The dimensions of each block is 20 x 10 x 10 mm.
- Five inner cylinders (IC). The biggest (IC1) has a diameter of 20 mm, the second (IC2) has a diameter of 15 mm. The third (IC3) and fourth (IC4) has dia. of 12 and 10 mm respectively. The smallest (IC5) cylinder is in between the four ICs having dia. of 5 mm.
- A stair step (SS) having five steps of equal size. The height of each step is 4 mm.

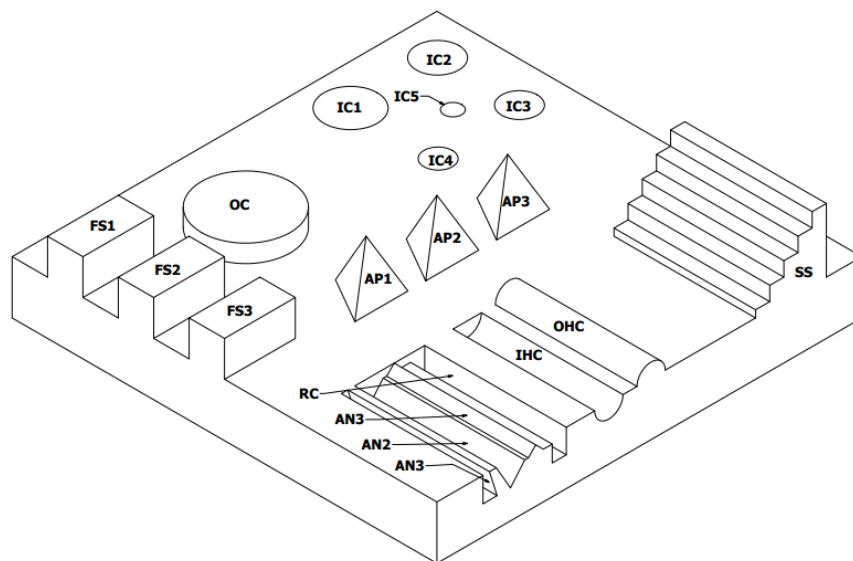


Figure 7.2 Proposed benchmark part with nomenclature

- Three triangular pyramids (TP). The side faces of TP1 are tilted to the apex of the pyramid with angle of 63.4° . For TP2 side faces are inclined at 61.7° . In third pyramid TP3, side faces are tilted with angle 60° .
- Two half-cylinders (HC). The outer half cylinder (OHC) and inner half cylinder (IHC) both has a radius of 4 mm.
- A rectangular notch (RC), having depth of 6.75 mm from part top surface. The width of the notch is 4 mm.
- Three angular Notches (AN). The first (AN1) has angle of 90° . The second (AN2) and third (AN3) notch has angle of 70° and 72.6° .

In this work, the manufacturing of the proposed benchmark part is carried out using dual extruder rapid prototyping (RP) machine. The RP machine used has an enclosed chamber that helps in limiting the influence of environmental conditions like moisture, dust etc. The machine has a positional accuracy of 2.8 microns. The benchmark part was not finished manually but using acetone finishing to improve the part quality and get it close to its CAD model. For contactless scanning, a thin layer of white powder is sprayed on the benchmark part for effective optical scanning of the part. In past research (Mahmuda et al., 2011), it was verified that such layer doesn't affect the results of non-contact measurements. Additionally, it helps in converting the reflective surface to suitable one for optical scanning. Whatever may be the colour of the part, the white powder helps in improving the contrast of the object's surfaces with respect to the contactless instrument.

7.3.2 Common reference system definition (Contact and non-contact)

For effective and accurate comparison, it is imperative to define the common reference system for part alignment in contact as well as non-contact systems with minimum error (Yau et al., 2000; Wolf et al., 2000). For contact based measurement, a part reference system was used. However, in case of non-contact digitization, the 3D point cloud data acquired are related to the machine reference system. In literature, quite a few methods are available to perform the part alignment (Van Gustel et al., 2008; Martinez et al., 2008). This work considered one of the most common methods used in the literature by

positioning three equal size spheres on the benchmark part (see Figure 7.3) and scanning them along with the surface of the part. Further, the sphere surfaces were reconstructed and their centers and the distance between their centers are used to establish the common reference system. Since the accuracy of the reconstructed surface is greatly influenced by registration, so the error in the sphere measured data must be evaluated. The comparison of the spheres surface is performed using the INSPECT PLUS software. For characterization of contactless scanner, it is required to consider the CMM measurement as reference and the scanner measurement as test values. For effective alignment the center of the sphere sampled using CMM is matched with center of sphere captures using scanner as shown in Figure 7.4.

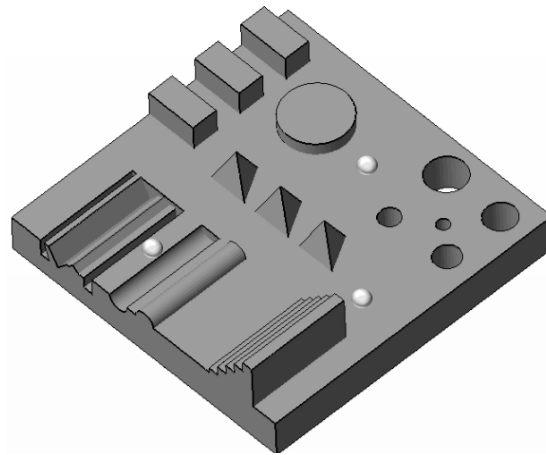


Figure 7.3 Benchmark part with three similar spheres for establishing common reference system

From Figure 7.4, it is observed that the coordinate value sampled from CMM are different from laser coordinate value especially along z axis. In addition, the radius of the three sphere seems to be different. For confirming, radius of the three spheres (16.5 mm diameter) placed over benchmark part is measured using touch probe CMM and laser scanner. For contact less scanning, different head orientation strategies were adopted which results in 2, 4, 6 and 10 scans for each sphere. The results are reported in Figure 7.5. It was found that the radius of the spheres are changing irrespective of whether only two or more scans are performed. However, one important observation was the decrease in the radius of the all the sphere as the number of scans are increasing. The difference in the radius of

sphere when using 2 scans and 10 scans is in the range of 15-20 μm . This difference is quite insignificant and it is closer to the reference values of the contact based CMM system.

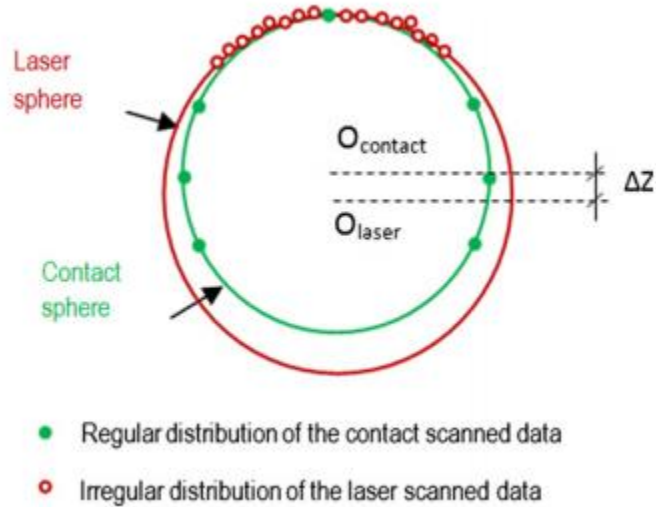


Figure 7.4 Sphere matching for part alignment

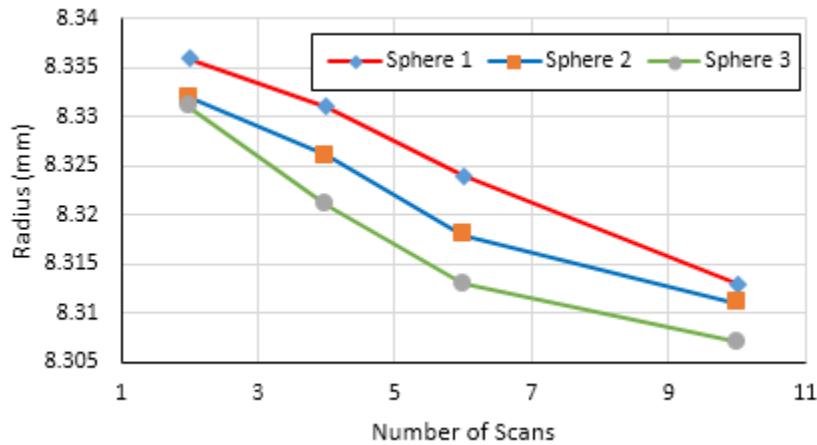


Figure 7.5 Sphere radius variation for part alignment

7.3.3 Non-Contact digitization strategy

The first and foremost step of the non-contact scanning process is to define optimum scanning parameters. As discussed and shown in previous chapters the scanning parameters can significantly influence the final results of the scanned model. The optimum parameter values will help in acquiring maximum point cloud data with minimum dispersion. The

scanning distance and scanning incidence angle are fixed at 60 mm and 40-45° respectively for improved scanner output. These optimal scanning distance and scanning angle values were earlier calculated in the previous chapters. The COMET PLUS software was used for matching of scans, scanning paths and building up of the surface model. Further, two different head orientation techniques for part scanning was used. First strategy deals with fixing the head of the scanner at one place using minimum rotation and rotating the table by 5° and capturing the part. The second strategy deals with moving the scanner head orientation and scanning individual components of the part, thus removing the occlusion. The next important step is the processing of unorganized raw point clouds. The redundant points were removed manually using the cutting tools provided in the COMET PLUS interface. Finally, the point cloud data are exported in STL format for surface reconstruction in the next stage.

7.3.4 Surface reconstruction using different software

Three different software interface are used for accurate surface reconstruction from unorganized raw point cloud data.

- COMET PLUS
- CATIA v5 (Digitized shape editor, quick surface reconstruction module)
- Solidworks (Scan-To-3D)

Initially, the benchmark part surface was reconstructed using touch probe CMM point data and considered as reference model for further comparison. Once all the point clouds are imported in the CAD interface, these are grouped according to the different features they belong to (cylinders, pyramids, blocks etc.). The process of surface reconstruction is simpler and faster for point clouds acquired using contact method. The possible reason being the uniform dispersion of point data at each surface. On the contrary, in contactless scanning the major concern is in determining the edges and boundary of the part surface and the dispersion of point data across the surface boundary. In addition, the points along the half cylinders and rectangular notches are difficult to determine and discriminate. Each of the region is fitted based on the adjacent region point data using the suitable algorithm in each CAD software.

The surface reconstruction process in CATIA v5 and Solidworks Scan-To-3D is taken from adopted methodology in the chapter 5. The process of surface development in COMET plus is performed using its default settings. The advantage of using the earlier path provided in chapter 5, being the less time requirement to develop an accurate surface. Also, less number of steps and factors are need to be changed or altered. The path used for surface reconstruction in digitized shape editor module (CATIA v5) and Scan-To-3D (Solidworks) is shown in Figure 7.6. Among the three software used, CATIA v5 and Solidworks produced surface appropriately and accurately as shown in Figure 7.7.

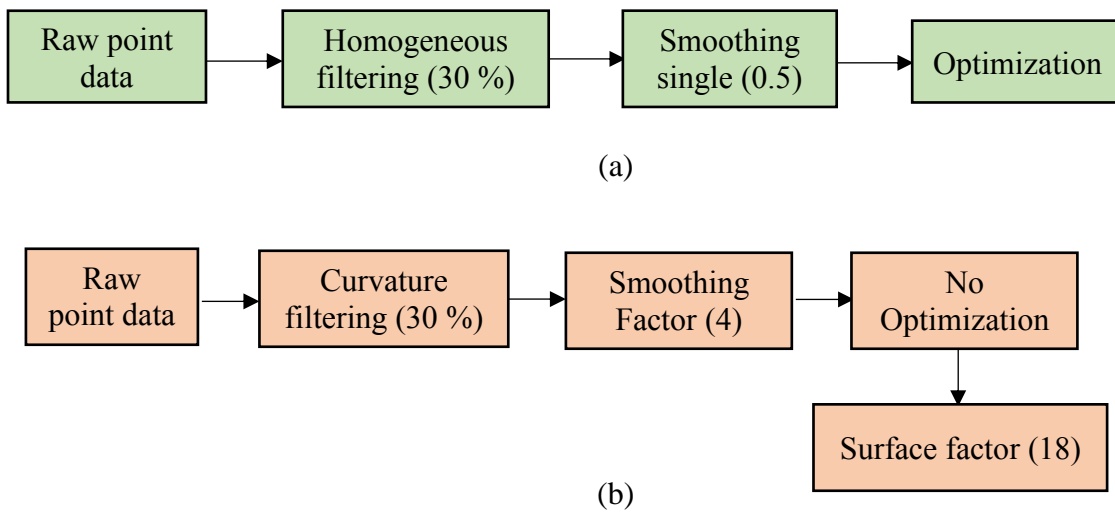


Figure 7.6 Path for accurate surface reconstruction (a) CATIA v5 (b) Solidworks

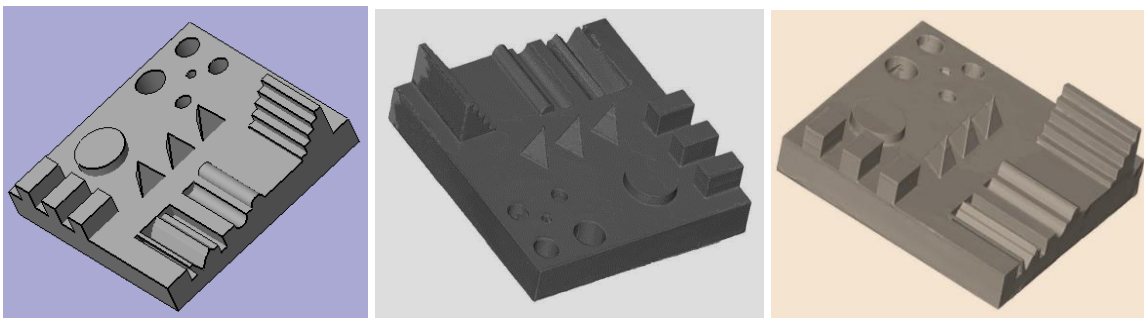


Figure 7.7 Surface model (a) CATIA v5 (b) COMET PLUS (c) Scan-to-3D

7.4 Importance of correct alignment technique

Prior to inspection, it is imperative to show the importance of correct alignment technique for effective and actual comparison. An AM part is picked for case study and a blue light L3D scanner was chosen for scanning and contactless inspection. The scanning device helps in retrieving the point cloud data that represents the complete geometry of the AM part. Subsequently, dissimilar inspection alignments were performed on the scanned point cloud by choosing various points for the evaluation of the similar reference frame. The outcome of the inspection process were affected by the selection of points and it was assessed in the following ways:

1. Differently aligned point data were inspected using INSPECT PLUS software.
2. Point to point inspection of actual part using CMM.

The first case considers average distance as a measure for comparing two scanned point cloud, but it does not provide information about which one is better and accurate representation of the actual product. For CMM inspection, the scanned point cloud coordinates are considered as the reference values for the point to point measurement of the original part. Subsequently, the deviation between the actual part and its scanned model is evaluated, allowing to differentiate the utmost perfect representation of the AM part. A CMM is used, as it has higher accuracy than the non-contact scanning for inspection.

This work performs 3-2-1 alignment for defining the datum on scanned point data of the case study. Subsequently, 3-2-1 approach was repeated five times by choosing dissimilar points at every single time on the same features. The proposed methodology for the current work using point to point contact based measurements is shown by the flow diagram in Figure 7.8. Selection of different points on the same aligned feature leads to the definition of the dissimilar reference system. Due to different alignment, various aligned data correspond to different surfaces, although the data is same. Once the repetitions of the alignments are done, ten dissimilar aligned scanned point data were compared among themselves to calculate the deviation of the complete point data. Consequently, sixty dispersed scanned points were carefully chosen on each differently-aligned point cloud. For the next stage of CMM inspection, the coordinates of these chosen points were treated as reference values. Therefore, it becomes possible to calculate the inaccuracy in the

different-aligned scanned data with reference to the actual physical product and not with a hypothetical virtual model like STL. The alignment of the part on the CMM was performed systematically and carefully in the similar mode as for the scanned data to evade any inaccuracies.

Case Study

The case study chosen was a traditional stepped bar which is fabricated by AM for scanning purpose (Figure 7.9 (a)). The test part was manufactured using FDM machine taking a layer thickness of 0.175 mm of ABS plastic. The overall dimension of the part is 152.4 mm x 38.1 mm x 25.4 mm and its surface was neither cleaned nor polished after fabrication, not to change the staircase effect. Staircase effect arises due to the layer by layer process and this effect is not present in the model STL file. The case study was scanned using Steinbichler's COMET L3D - blue light scanner. The mean acquisition rate of COMET L3D scanner is about 50,000 points per second. The version used in this study for data acquisition has a resolution of 1 Mpx and 1170 x 880 pixels. The complete acquisition of the case study takes about 40 scans, taken at different orientations with scanning distance of about 65 mm.

Reference Frame Definition

Once data acquisition is completed, the next step was to define part reference frame using the 3-2-1 method on scan data which is as shown in Figure 7.9 (b) and the steps includes:

1. Three points (circle mark) were selected on the third step with a hole to define the z-direction and its origin.
2. Two points (trapezium mark) were selected at the side plane to define the x-direction and y-direction origin.
3. One point (square mark) was selected at the front plane or back plane to define x-direction origin.

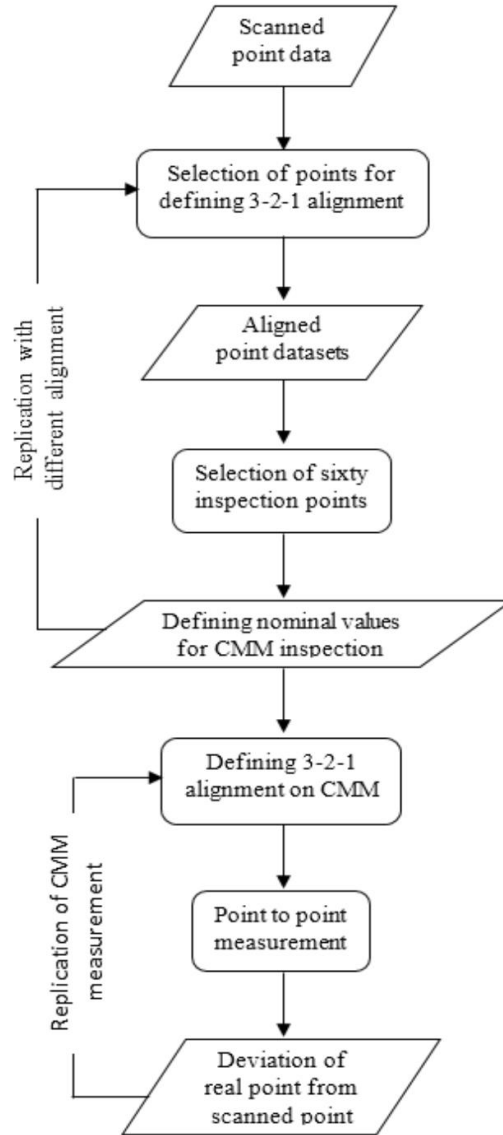


Figure 7.8 Proposed flowchart of the experimental procedure

The 3-2-1 method was repeated five times on the COMET scan data. At each repetition, different points were selected on the aligning features (top plane, side plane and front plane) as shown on top left loop of the Figure 7.8. In RE software environment, the 3-2-1 alignment was performed by the operator manually by selecting the points with a mouse click. While performing this operation, an error was deliberately introduced to increase the variation amid two differently allied scan point data. The variation among the differently aligned scan point data can be seen visually checked by superimposing the point

clouds. In this study, five differently-aligned point data are presented for comparison due to the repetitions of the different reference system.

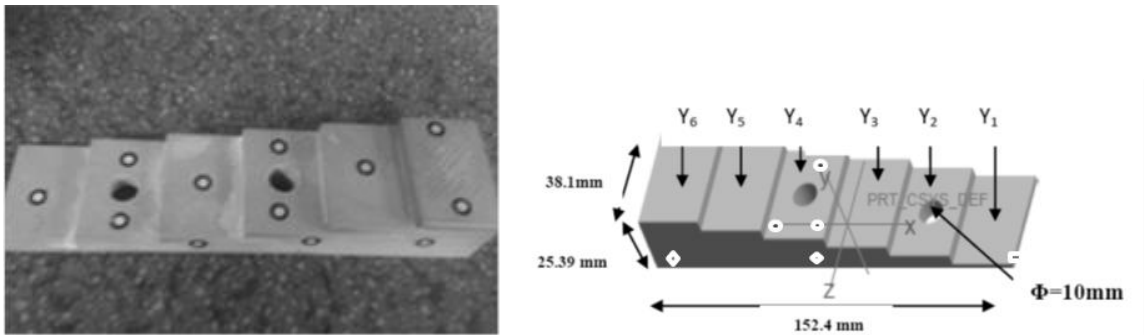


Figure 7.9. (a) Stepped bar (AM part) selected as case study (b) Definition of part reference frame

Result and Discussion

The above five point clouds with different alignment were compared to the theoretical STL model by means of Steinbichler's INSPECT PLUS software. For comparison, the CAD model of the scanned part was used as a reference. On the contrary, this study uses the STL file as a reference for comparison with the scan data, and it does not consider the deviation associated with the slicing operation. Here, the deviation obtained is the summation of AM process error, digitization process errors and alignment errors. Table 7.2 shows the average deviation in the distance from the reference STL and the standard deviation spreading of distance for the five different-aligned point data. In opposition, use of CAD model as reference will enhance the deviation in Table 7.2, due to the error introduced by slicing. Meanwhile, looking at each column, the difference between two consecutive rows would not have varied as it is only due to the alignment error. AM process error, slicing error and digitization error will remain constant.

The first line of Table 7.2 shows the best-fit rule comparison with the theoretical STL model which provides the least distance, but it is not repeatable if the scan data changes. Using a fixed reference (i.e. the STL file), there are chances of identifying the similarity among the different alignments of the similar scan data. For instance, the

Table 7.2 Differently aligned point data comparison of COMET (in mm)

S. No	Different Alignment	Average Distance	Standard Deviation
1	Best Fit vs STL	0.14	0.12
2	1 st Alignment vs STL	0.23	0.19
3	2 nd Alignment vs STL	0.23	0.19
4	3 rd Alignment vs STL	0.28	0.22
5	4 th Alignment vs STL	0.27	0.23
6	5 th Alignment vs STL	0.24	0.21

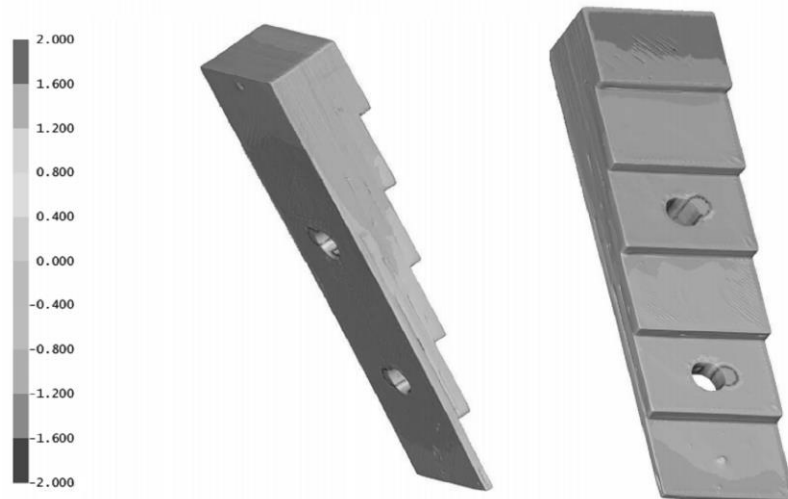


Figure 7.10 Deviation chart of COMET data 1st alignment vs. the theoretical STL model alignments 1 and 2 for COMET data are similar, since the absolute average distance is 0.23 mm and the standard deviation is 0.19 mm for both of them. Moreover, the 3rd alignment represents the worst case having maximum deviation. The comparisons results can also be visualized as colored distance deviation chart in Figure 7.10. Additionally, each of the five different aligned point clouds of COMET scanner was compared in a group of two by means of INSPECT PLUS software. The results of the comparative analysis were shown

in Table 7.3. As clearly seen in Table 7.3, the comparison depicts that the difference in average distance is below 0.08 mm which is less than the declared accuracy of the scanner.

Table 7.3 Comparison of differently aligned point data (in mm)

S. No	Alignments	Average Distance	Standard Deviation
1	1 st Alignment vs 2 nd Alignment	0.07	0.06
2	1 st Alignment vs 3 rd Alignment	0.03	0.02
3	1 st Alignment vs 4 th Alignment	0.04	0.03
4	1 st Alignment vs 5 th Alignment	0.06	0.04
5	2 nd Alignment vs 3 rd Alignment	0.04	0.03
6	2 nd Alignment vs 4 th Alignment	0.03	0.02
7	2 nd Alignment vs 5 th Alignment	0.05	0.04
8	3 rd Alignment vs 4 th Alignment	0.05	0.04
9	3 rd Alignment vs 5 th Alignment	0.04	0.02
10	4 th Alignment vs 5 th Alignment	0.03	0.02

CMM Inspection

For additional examination and confirming the results obtained from the software based comparisons, sixty dispersed points were carefully chosen at approximately same locations of each differently-aligned point cloud. For inspection, each of the points was selected in INSPECT PLUS software by choosing with the mouse. The inspection software redeems and shows each point of the data as three coordinates (i.e. x, y, z) and the surface of test part was shown by cosines of normal. The surface normal is calculated by taking into account all the triangles sharing particular point as a common vertex. Consequently, the coordinates (i.e. x, y and z) of the points were fixed as reference values for point to point inspection of the AM part and the programming for CMM probe route with an approaching direction that was equivalent to the point normal. For obtaining similar results from the

CMM inspection, sixty points were selected in similar positions as on the COMET scan data.

The sample set was inspected by a probe tip of 2 mm on a INSPECS RUBY 564 CMM model that was fitted with an indexable swinging head and a touch trigger probe whose resolution is 0.5 μm . The volumetric length measuring accuracy MPEE of the machine according to ISO-10360-2 is $2.5 + L/350\mu\text{m}$, where MPEE is the abbreviation for maximum permissible error for length measurement and L is the measured length.

The point-to-point measurement were repeated four times on the nominal values of individually different aligned point clouds. Prior to each replication, the physical alignment of the AM part on the RUBY CMM was repeated. For doing this, the 3-2-1 approach was performed by choosing the same points with the touch probe as was used for the point clouds alignment. Therefore, the CMM alignment of the part in each repetition does not change. Instead, the nominal coordinates of the inspection points are different for each point cloud but do not vary for the four repetitions. The results of the inspection of COMET data are shown in Table 7.4. The values in the table show the average absolute distance and standard deviation between the nominal position of the point clouds of the sixty inspected points and their actual position on the physical AM part.

The point clouds captured by the scanner with different alignment are having a total average distance greater than 0.20 mm. For COMET data, all the values are similar and very close to 0.25 mm. The highest value is observed for the 3rd alignment which is about 0.29 mm. Consequently, the choice of the points for the 3rd alignment was crucial, because the greater average distance of the alignment 3 depends on the part datum reference only.

Table 7.4 CMM inspection results with 3-2-1 alignment of COMET data (mm)

	Average Distance (Standard Deviation)			
	1st Trial	2nd Trial	3rd Trial	4th Trial
1 st Alignment	0.24(0.26)	0.26(0.26)	0.25(0.27)	0.23(0.25)
2 nd Alignment	0.25(0.27)	0.24(0.26)	0.26(0.28)	0.25(0.26)
3 rd Alignment	0.27(0.29)	0.29(0.32)	0.29(0.31)	0.28(0.30)

4 th Alignment	0.27(0.29)	0.25(0.28)	0.28(0.30)	0.27(0.29)
5 th Alignment	0.26(0.28)	0.24(0.26)	0.25(0.27)	0.25(0.27)

Further examination and analysis of results can be presented in terms of the absolute error distribution. Three instances are taken for the second trial of CMM measurements for the alignment 2, alignment 3 and alignment 4 of COMET data as shown in Figure 7.11, 7.12 and 7.13. The straight vertical dashed line as indicated on the graphs represents the average distance in mm. It can be observed that the bar charts for alignment 2 and alignment 4 of COMET point cloud (Figure 7.11, Figure 7.13) indicate a decreasing trend: the spreading becomes thinner as the distance value increases since the points are less for which the absolute distance is high. This is more reasonable and common trend for a spreading of inspection results that are non-uniform. However, the results are not influenced by systematic errors or singularities. On the contrary, for alignment 3 (Figure 7.12) bar chart shows the different trend which is more of a uniform type. The distance distribution is analogous and high for most of the point data of 3rd alignment since the distance distribution is also influenced by the worst description of the part reference frame.

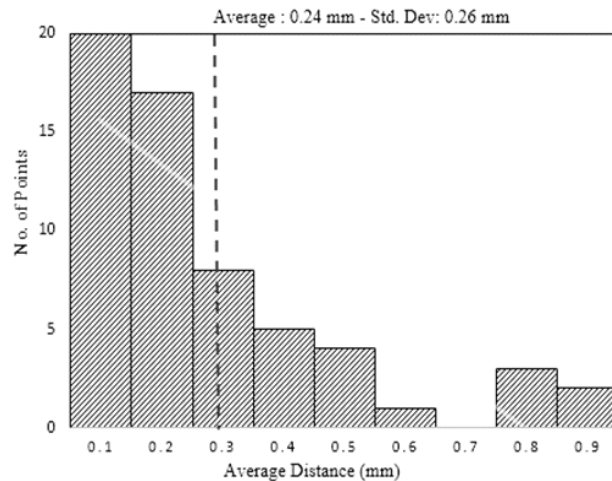


Figure 7.11 Average distance distribution for second replication in 2nd alignment of COMET data

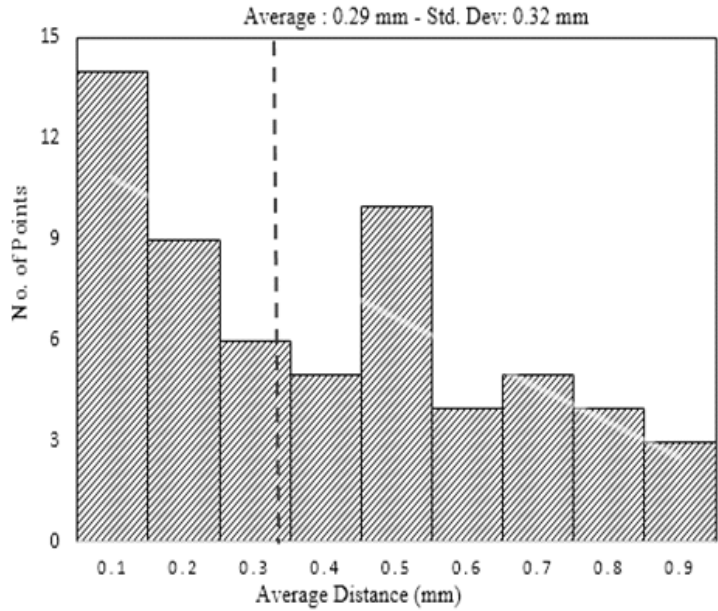


Figure 7.12 Average distance distribution for second replication in 3rd alignment of COMET data

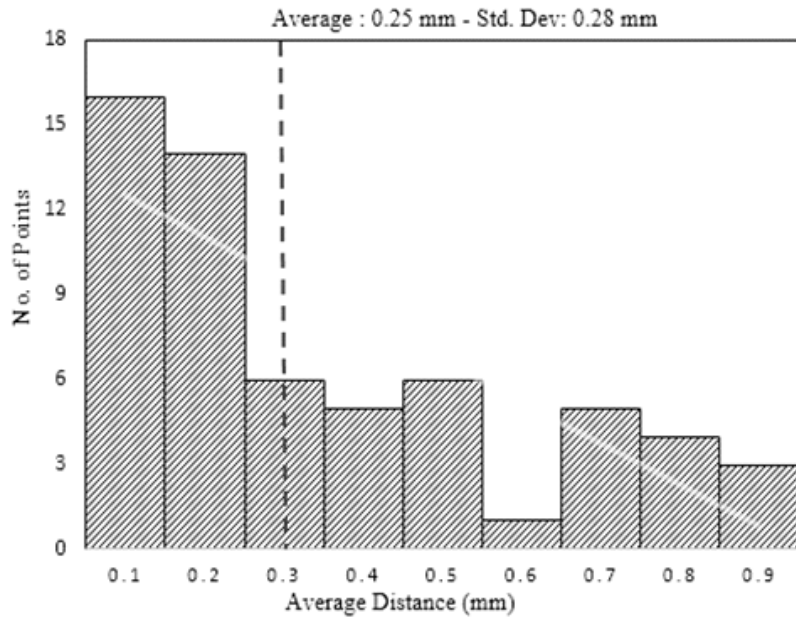


Figure 7.13 Average distance distribution for second replication in 4th alignment of COMET data

Overall, both the comparisons (software-based and CMM inspection) of different-aligned point clouds reveals that the selection of the points on part features during defining

the part reference frame can affect the results of non-contact inspections, which leads to incorrect evaluations. The impact is more evident if the accuracy and quality of the scan data are worse, as for the 3rd alignment and 4th alignment. However, the large number of points obtained from 3D scanner does not necessarily signify an advantage. The results of this investigation depict that in 3-2-1 alignment the inspection results are changing by simply varying the point selection on an aligning feature. Therefore, the optimal selection of the points for defining correct alignment and part reference frame is important, otherwise erroneous deviations will occur in the outcome of the inspection results. After optimal point selection, it is required to determine various GD&T error in the component.

7.5 Comparison of developed surface models

The INSPECT PLUS software application by Steinbichler is used for inspection of the surface reconstructed in the previous section. The surface as well as GD&T deviations are compared and results are presented. The surface and average deviations are displayed by the software in the form of coloured maps. The average deviations are simply the distance between a set of corresponding point data acquired in a given area of the part. Beginning with the importing of the CAD and scanned data in software, the next step is proper alignment. For effective comparison, 3-2-1 rule was used to perform suitable part alignment. The importance of 3-2-1 rule is that it restricts six degrees of freedom available for the models in space that helps in effective alignment. The main purpose of alignment is to bring the scanned data reference frame (X, Y and Z) to the CAD data reference frame and origin. Figure 7.14, 7.15 and 7.16 shows the average deviation between the surface reconstructed using contact point data (reference) and contactless point data using three chosen software applications.

From figure 7.14, it was found that the surface reconstruction is performed most accurately by CATIA v5 and the average deviation did not exceed 18 μm . All the individual features are reconstructed with absolute precision and improved accuracy. On the contrary, the COMET PLUS results are opposite to the CATIA as clearly seen from Figure 7.15.

The average deviation is around 2.5 times as compared to the CATIA v5 results. The holes, rectangular notches and the half cylinders edges are not reconstructed appropriately by the

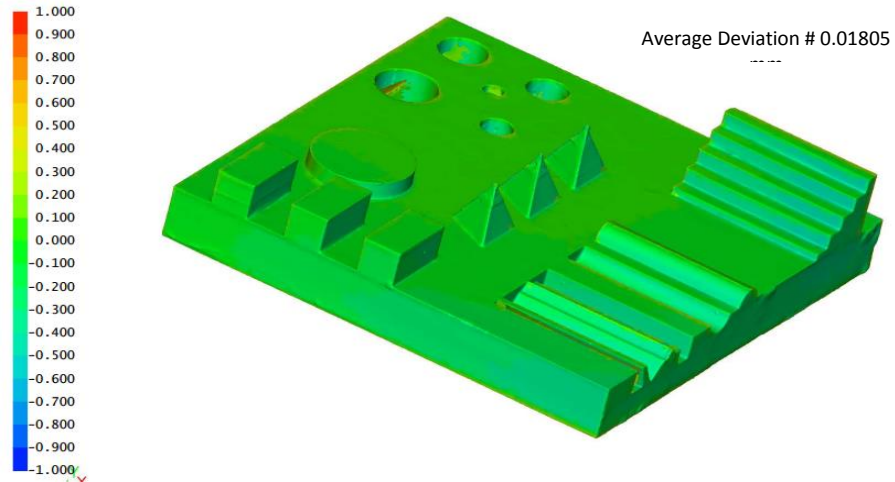


Figure 7.14 Average deviation comparison using contact and non-contact (CATIA v5) scanning

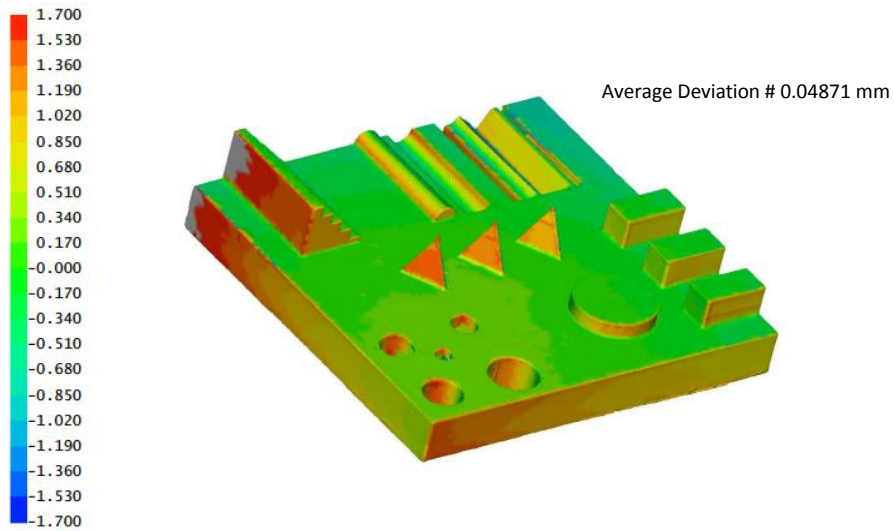


Figure 7.15 Average deviation comparison using contact and non-contact (COMET PLUS) scanning

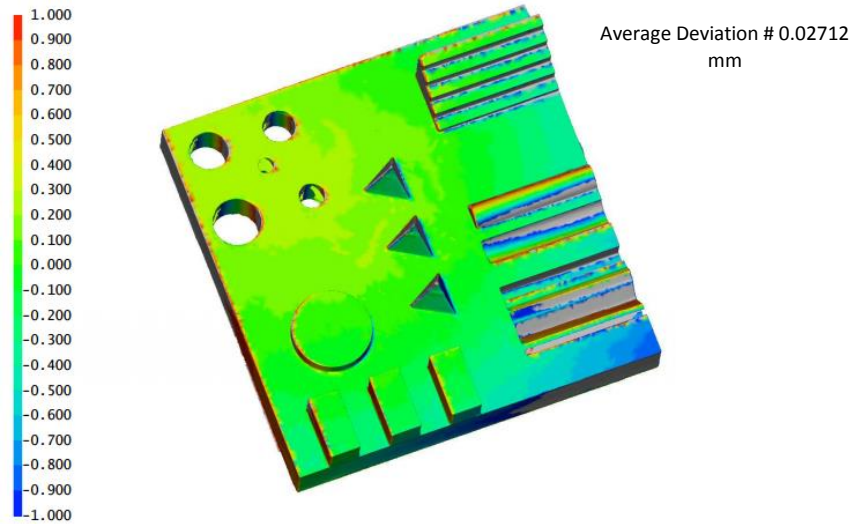


Figure 7.16 Average deviation comparison using contact and non-contact (Solidworks) scanning

default COMET PLUS software application. The main reason being the scarcity of point data in these regions. In Solidworks Scan-To-3D module, the average deviation value is in between the CATIA and COMET PLUS which is approximately 27 μm . The main deviation arises along the edges of the individual features like rectangular and circular blocks. After the above comparison in contact point data and contactless acquired point data, it is clear that point data dispersion (variation) is more in contactless scanning. Moreover, irrespective of the higher amount of data acquired, point data dispersion causes decrement in accuracy of the developed surface model. In addition, different software applications are useful in minimizing the deviation of scan data from the actual CAD model by applying various algorithms inbuilt in them.

7.6 GD&T comparison of reconstructed surface models

In this section, GD&T comparison (flatness, cylindricity, parallelism, perpendicularity, angularity) along with the distance comparison was performed using INSPECT PLUS software application. The results of the distance comparison including the horizontal and vertical plane are shown in Figure 7.17. The vertical plane distances are marked as d_1 , d_2 and d_3 respectively, while the horizontal plane distances are marked as d_4 , d_5 and d_6 . From Figure 7.17 (b), it was observed that CATIA and Solidworks results for vertical planes are having very minimum deviation from CMM data. The exact value of deviation

is approximately 6 μm , which is negligible as compared to the test data of CMM. However, the results of default COMET data is worst, similar to the earlier results of 3D deviations. The variation in the maximum and minimum deviation for COMET PLUS software is around 40 μm .

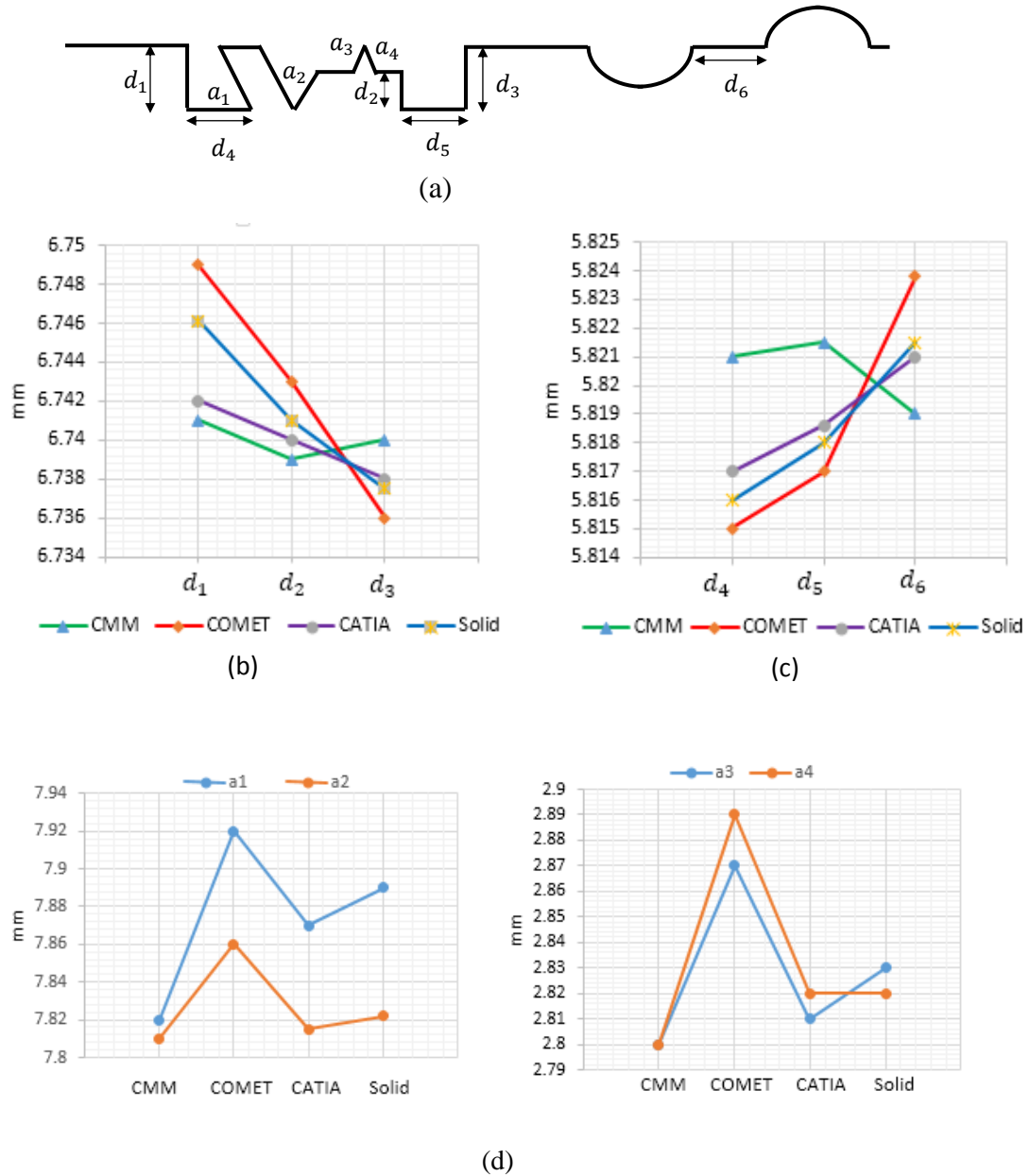


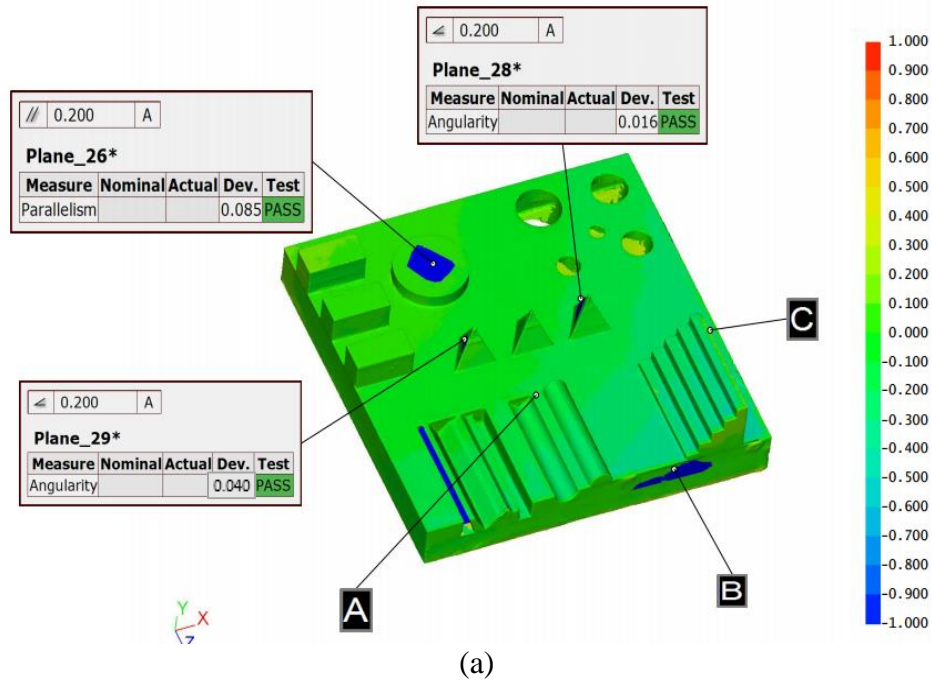
Figure 7.17 (a) Distance comparison of benchmark part for (b) vertical (c) horizontal planes (d) angular planes

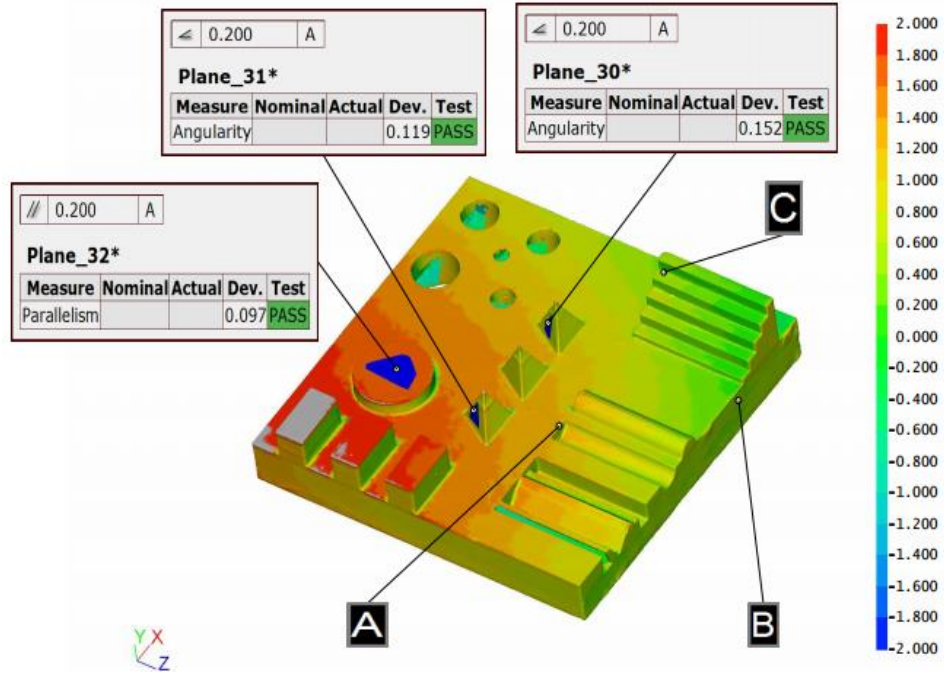
Furthermore, the comparison results for horizontal planes are reported in Figure 7.17 (c). The results displayed shows that the deviation increases nearly two times to 11 μm for chosen horizontal planes. Moreover, the distance d_4 and d_5 shows significant variation for CATIA, Solidworks and COMET reconstructed surface. The possible reason being the scarcity and incomplete point data captured during the scanning of these inner notches. The positive deviation of d_6 distance is because of the good quality of points acquired during scanning of flat surface. Similar to the previous results, the COMET surface deviation is worst among the three application software results. Further, the angular dimension are marked as a_1 , a_2 , a_3 and a_4 . Figure 7.17 (d) shows the result of angular dimension measurement and comparison of different application with contact based CMM measurement. The angular distance a_1 comparison with CMM test data shows significant difference in the contactless data captured. The CATIA result itself shows difference of nearly 35 μm and Solidworks result shows deviation of approximately 55 μm . The primary reason being the non-availability of adequate number of point clouds due to occlusion phenomena. In contrast, the deviation for angular distance a_2 has reduced inversely reporting only 10 μm difference. The COMET results are also have improved accuracy with deviation of 30 μm . There are no significant differences for angular distances a_3 and a_4 as the upper surface points are of good quality and large in number.

Seeing the above results, the CATIA application software is providing the best output. So, for GD&T comparison study, the default software of Steinbichler i.e. COMET PLUS results are compared with CATIA v5 results. Moreover, GD&T comparison of COMET PLUS and CATIA v5 reconstructed surface for the complete benchmark part is presented in Figure 7.18 and 7.19. Figure 7.20 illustrates the angularity and parallelism comparison at the angular pyramids and outer cylinder respectively. The angularity1 angularity2 is measured for angular pyramid AP_1 and AP_3 with reference to datum plane A. The parallelism1 is measured for outer cylinder OC with reference to datum A. The Figure 7.18 (a) depicts the CATIA results having the parallelism1, angularity1 and angularity2 values are 0.085, 0.016 and 0.040 mm respectively. The default parameters COMET results are illustrated in Figure 7.18 (b). It is observed that parallelism1, angularity1 and angularity2 values are 0.115, 0.152 and 0.092 mm respectively. It is clearly found that these GD&T errors have significantly reduced using CATIA v5 application.

Overall, the percentage improvement is around 12.3%, 66.38% and 89.47% for adopted CATIA methodology.

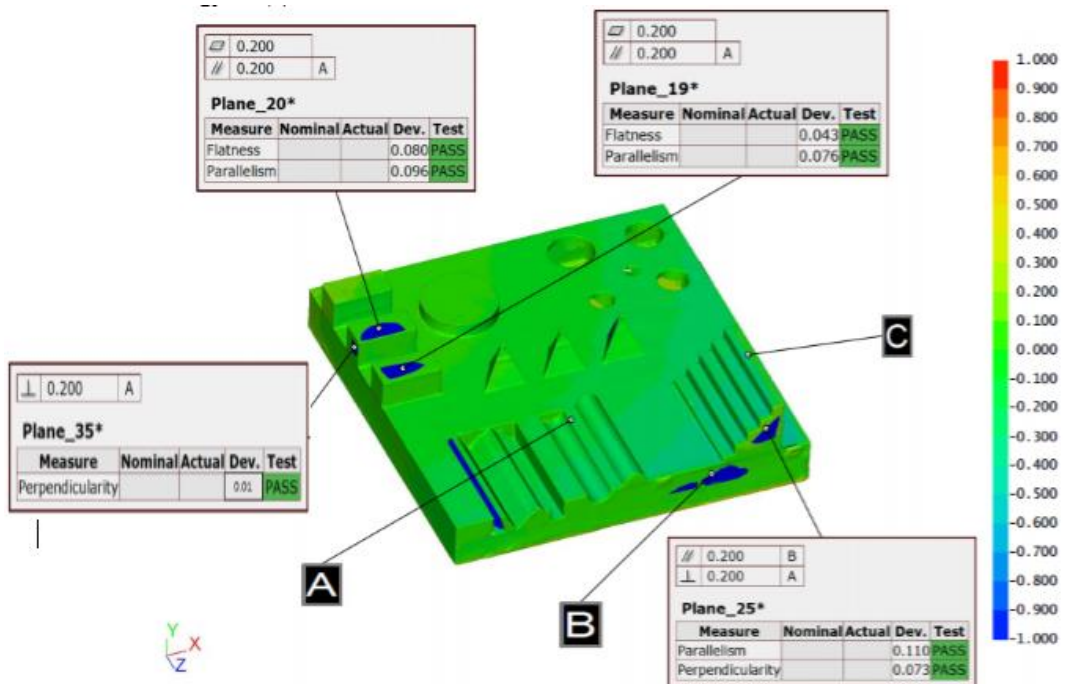
Similarly, Figure 7.19 (a-b) shows the GD&T error results for flatness, parallelism and perpendicularity. Flatness1 and flatness2 are measured for blocks of flat surfaces FS₂ and FS₃. The parallelism2 error is measured for FS₂ block with reference to datum A. At last the perpendicularity error is also measured for FS₂ block with reference to datum A. It is observed that Flatness1, flatness2 and parallelism2 values are 0.043, 0.096 and 0.01 mm respectively. Similar to the previous results, it is clearly found that these GD&T errors have significantly reduced using CATIA v5 application. Overall, the percentage improvement is around 20%, 38% and 77% respectively for adopted CATIA methodology.





(b)

Figure 7.18 GD&T results for (a) CATIA and (b) COMET PLUS developed surface



(a)

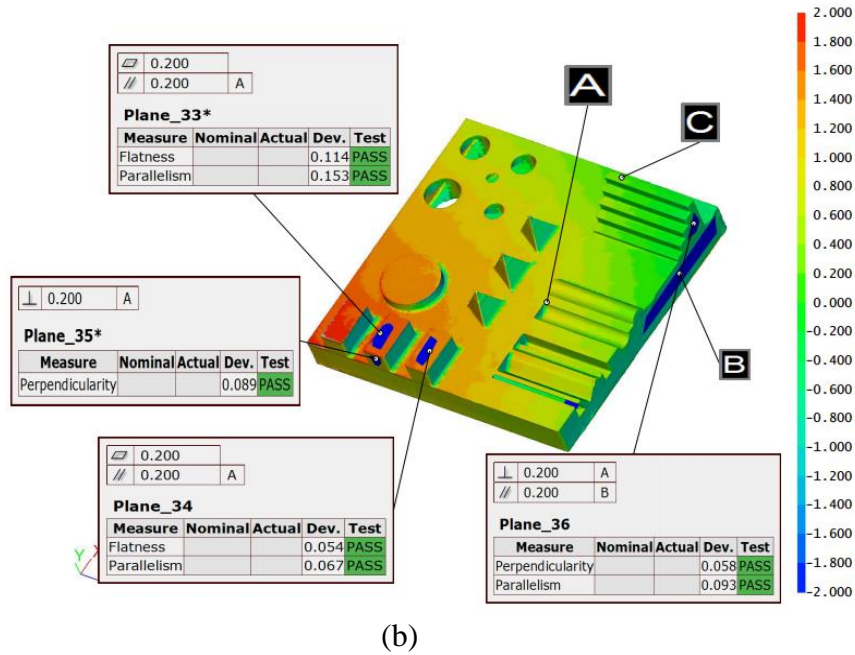


Figure 7.19 GD&T results 2 (a) CATIA and (b) COMET PLUS developed surface

Finally, circularity measurement was performed for five inner cylinders IC₁, IC₂, IC₃, IC₄ and IC₅. The CMM point data is easily acquired and cylinders are reconstructed easily. However, the laser point cloud are not acquired adequately, especially in the vertical direction of the cylinder. So the surface reconstruction was become possible when a multi-oriented strategy was considered, acquiring the vertical point data.

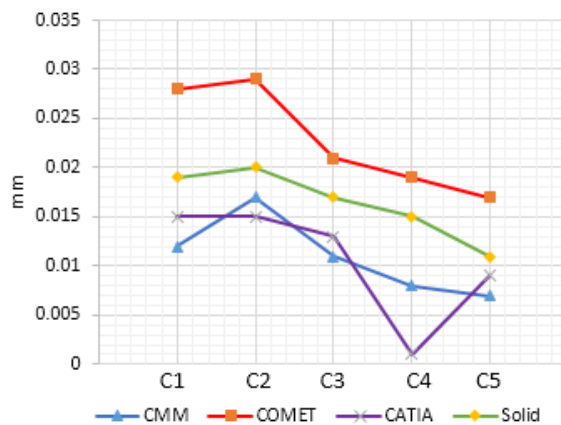


Figure 7.20 Circularity comparison of the reconstructed surface

The results of CATIA v5 and Solidworks comparison with CMM data are illustrated in Figure 7.20. It was found that the circularity is decreasing as the size of hole is decreasing. The possible reason being less number of points are required for reconstructing small holes. Finally, all GD&T results are reported in Table 7.5, with the percentage improvement by considering adopted methodology.

Table 7.5 Results of GD&T comparison

S.No.	Parameter	Unit	Adopted Methodology (CATIA v5)	COMET PLUS	% improvement
1.	Average deviation	mm	0.20	1.70	52.9%
2.	Parallelism 1	mm	0.085	0.097	12.3%
3.	Angularity 1	mm	0.040	0.119	66.38%
4.	Angularity 2	mm	0.016	0.152	89.47%
5.	Flatness1	mm	0.080	0.114	29.82%
6.	Flatness2	mm	0.043	0.054	20.37%
7.	Parallelism 2	mm	0.096	0.153	37.25%
8.	Perpendicularity	mm	0.01	0.089	77.52%
9.	Circularity1	mm	0.015	0.028	46.42%
10	Circularity2	mm	0.015	0.029	48.27%

7.7 Summary

This chapter presents an iterative framework that would be a handy tool to quality inspectors as it provides the systematic guideline to be followed in an automated dimensional inspection system using contactless scanning systems. For validating the proposed framework a novel benchmark part consisting of canonical features for the GD&T verification of contactless laser scanning. Since, very few methodologies and standard parts are available for metrological verification and testing of non-contact sensor

system, particularly for GD&T features. The proposed inspection framework and benchmark part was designed keeping in mind the common features used in industries and it will prove to be an effective reference tool which have almost all available GD&T features. For accurate comparison and measuring deviations of contactless scanners acquired data, contact based touch probe CMM sampling data is taken as reference. From CAD point of view, CATIA v5 application software (digitized shape editor module) has best results in comparison to Solidworks (scan-to-3D) and default software of scanner COMET PLUS.

CHAPTER 8

CONCLUSION AND FUTURE WORK

This thesis presents a novel framework for accuracy control and contactless inspection for parts with free-form surface and GD&T features using reverse engineering approach. The proposed framework is divided into two stages. The first stage is digitization and surface reconstruction, while the second stage is inspection. The two stages include different components and important features, from manufacturing to inspection of the industrial parts, which are discussed in the chapters of the thesis. Based on the work performed and results obtained, this thesis is divided into mainly five parts.

The first part of the thesis discussed and describes about the classical particle swarm optimization (PSO) and the proposed modified particle swarm optimization (MPSO) algorithm. The terms used in the proposed MPSO algorithm are also discussed. One simple numerical example is considered for understanding and demonstrating the working of PSO and MPSO algorithm. The effectiveness and accuracy of the proposed MPSO algorithm is tested by solving five standard benchmark functions. The second part of the thesis discussed about the manufacturing issues related to AM machines and corrective actions are suggested accordingly to improve the quality of the part. The issues discussed in this part is related to dimensional accuracy, warpage, oozing, surface blemishes and circularity. The main purpose of this part is to know the issues arises during manufacturing of the part and suggests corrective action to improve the quality of the AM parts. So that industrial parts can be produced conforming to the actual dimensions and tolerances provided in the design stage. For the same reason and improving the GD&T canonical features accuracy, the process parameters of the AM process are optimized using PSO algorithm. The results reported provides the optimal AM process condition to produce parts with minimized GD&T error so that part build by AM can be acceptable during inspection and quality control. These parts will be functional and can be used in industrial applications for long time.

The next part of the thesis deals with determining the important process parameters during 3D laser scanning of physical objects to improve the accuracy of point cloud data captured. Based on the surface morphology, scanning distance and scanning incidence angle are the two important scanning parameters that are ignored till date in the literature. The standard deviation of the acquired point data is considered as response, which is analytically modelled in terms of scanning distance and scanning angle along with their interactions. The response surface methodology (RSM) is used for developing cubic model and for the validation of the results. Further, the developed model is optimized by using MPSO algorithm for determining optimum process parameters. It was found that the MPSO results are better than the analytical and experimental results with minimum standard deviation. The optimum scanning distance and scanning angle are 70 mm to be precise and angle must be below 50° respectively for improving final results of RE process. It was seen that the standard deviation of the final reverse engineered models significantly reduced by 21.6% and 11.77%. In addition, for accurate surface reconstruction two unified solutions using different CAD methodologies for modelling and analysing a freeform surface from a raw unorganized point cloud is proposed. The two application software used are CATIA v5 and Solidworks. The proposed methodologies are useful in capturing the original surface model accurately and improving the conventional reverse engineering process appropriately.

The fourth part of the thesis comes in the second stage of the proposed framework which shows the significance of correct selection of points during alignment for effective and accurate inspection. This study assesses the influence of 3-2-1 method for aligning of the scanner point clouds in the same Cartesian reference frame prior to inspection. Several dissimilar points were selected on each aligning feature for each repetition with the purpose of examining the effect of point selection with respect to inspection results. The process of describing the reference frame for non-contact inspection is very quick, and it takes very little time. Additionally, a simple objective function for form tolerance evaluation was formulated as an unconstrained optimization problem for exact evaluation of GD&T error using the proposed MPSO algorithm. Several real life numerical problems have been illustrated to calculate GD&T errors from coordinate data effectively. Compared to conventional or existing heuristics optimization methods, the proposed MPSO algorithm

not only has the advantage of a simple realization in computers and good flexibility, but it was shown to have improved the form error evaluation accuracy.

The last and fifth part of this theses aims to provide a step-by-step inspection framework, beginning with the manufacturing of the AM part to the inspection which will serve as a handy tool to the end users and quality inspectors as it provides the systematic guideline to be followed in an automated geometrical and dimensional inspection system using contactless scanning systems. To test and validate the methodology adopted in the previous four stages a novel benchmark part is proposed which is aimed to verify the contactless laser scanner accuracy provided by the manufacturers. The benchmark part consists of canonical features commonly used in mechanical components in industries and is will be highly helpful in GD&T verification of contactless laser scanning. For accurate comparison and measuring deviations of contactless scanners acquired data, contact based touch probe CMM sampling data is taken as reference.

On the basis of work carried out in this thesis, following conclusions have been reported in the five parts of this thesis as,

1. This work proposes a novel inspection planning framework for eliminating conventional CMM inspection planning requiring skill and expertise and provides a way for inspection of soft materials like AM parts.
2. This work proposes an improved variant of classical particle swarm optimization named as modified particle swarm optimization (MPSO). The proposed algorithm overcomes the insufficiency of the classical PSO in terms of a weak exploitation behaviour by introducing an improved solution search equation based on the best solution of the previous iteration. Additionally, a greedy selection procedure is added to further improve the exploitation ability of the classical PSO.
3. This work produced accurate parts by minimizing various challenges, issues and by process parameter optimization of AM machines.
4. The work addresses the significance of two 3D scanning parameters (scanning angle and scanning distance) previously ignored in the literature. The effect of these parameters on the final accuracy of capture point data using non-contact laser scanning is also studied.

5. This work provided an alternating and optimum path for accurate surface reconstruction from raw unorganized point cloud data using two commercial software. In addition, it investigates the critical parameters and their factors value for accurate surface reconstruction and improved accuracy of developed model.
6. A simple objective function for GD&T error was formulated as an unconstrained optimization problem. Further, the minimum zone objective function was minimized using nature inspired algorithm like GA, PSO and MPSO.
7. The MPSO algorithm is further used in optimizing morphological scanning parameter and GD&T form error. Compared to conventional or existing heuristics optimization methods, the proposed MPSO algorithm not only has the advantage of a simple realization in computers and good flexibility, but it was shown to have improved evaluation accuracy.
8. This work also proposes a benchmark part having prismatic features for GD&T inspection and non-contact scanner characterization. The proposal of standard benchmark part and methodology for GD&T verification will provide a simple way of performance evaluation for various contactless laser-scanning systems.

Scope for Future work

This research work has given rise to some useful directions which forms the future scope of research. They are as follows:

1. This study proposes the novel inspection framework and takes a step towards making the inspection process fully automatic. So, the next step will be to automatize the procedure described in the proposed framework by converting the steps into an algorithm for automatically extracting information from CAD to achieve an integrated GD&T-RE system.
2. Application of other advanced single and hybrid nature inspired optimization techniques for determining optimum scanning parameters and GD&T error evaluation.
3. Application of the proposed framework and adopted methodologies in inspection of components produced by other manufacturing processes.

4. Need to explore other scanning parameters that affect the final output of the reverse engineered models. Also, in response surface roughness is the key parameter that need to be considered while scanning any object.
5. It will be interesting to see the effect of number of input point cloud data, number of triangles in polygon model and noise reduction on the final accuracy of reverse engineered surfaces.
6. Application of advanced computational tools like Fuzzy sets and neural network will be highly interesting for optimum scanning parameters and optimizing form error.

References

- American Society of Mechanical Engineers. (2009). ASME Y14. 5-2009: Dimensioning and Tolerancing: Engineering Drawing and Related Documentation Practices. ASME.
- Annex Business Media (2016) Study: 3D printing saves weight fuel in aerospace design. Available online at: <http://www.design-engineering.com/study-3d-printing-saves-weight-fuelin-aerospace-design-136069/>.
- Ahn, S. H., Montero, M., Odell, D., Roundy, S., & Wright, P. K. (2002). Anisotropic material properties of fused deposition modeling ABS. *Rapid prototyping journal*, 8(4), 248-257.
- Ahn, D., Kim, H., & Lee, S. (2009). Surface roughness prediction using measured data and interpolation in layered manufacturing. *Journal of materials processing technology*, 209(2), 664-671.
- Ali, F., Chowdary, B. V., & Imbert, C. A. C. (2008). Part design and evaluation through reverse engineering approach. In *The 2008 IAJC-IJME International Conference*.
- Ang, K., Fai Leong, K., Kai Chua, C., & Chandrasekaran, M. (2006). Investigation of the mechanical properties and porosity relationships in fused deposition modelling-fabricated porous structures. *Rapid Prototyping Journal*, 12(2), 100-105.
- Anitha, R., Arunachalam, S., & Radhakrishnan, P. (2001). Critical parameters influencing the quality of prototypes in fused deposition modelling. *Journal of Materials Processing Technology*, 118(1), 385-388.
- Armillotta, A. (2006). Assessment of surface quality on textured FDM prototypes. *Rapid Prototyping Journal*, 12(1), 35-41.
- ASTM, A. (2012). F2792-12 Standard terminology for additive manufacturing technologies. *ASTM International*.
- Azevedo, T. C., Tavares, J. M. R., & Vaz, M. A. (2009). 3D object reconstruction from uncalibrated images using an off-the-shelf camera. *Advances in computational vision and medical image processing*, 117-136.
- Azevedo, T. C., Tavares, J. M. R., & Vaz, M. A. (2010). Three-dimensional reconstruction and characterization of human external shapes from two-dimensional images using volumetric methods. *Computer methods in biomechanics and biomedical engineering*, 13(3), 359-369.
- Bradley, C., & Currie, B. (2005). Advances in the field of reverse engineering. *Computer-Aided Design and Applications*, 2(5), 697-706.

- Bandyopadhyay, A., & Bose, S. (Eds.). (2015). *Additive manufacturing*. CRC Press.
- Banerjee, R., Collins, P. C., Genc, A., & Fraser, H. L. (2003). Direct laser deposition of in situ Ti–6Al–4V–TiB composites. *Materials Science and Engineering: A*, 358(1), 343-349.
- Barbero, B. R. (2009). The recovery of design intent in reverse engineering problems. *Computers & Industrial Engineering*, 56(4), 1265-1275.
- Bartolo, P., Domingos, M., Gloria, A., & Ciurana, J. (2011). BioCell Printing: Integrated automated assembly system for tissue engineering constructs. *CIRP Annals-Manufacturing Technology*, 60(1), 271-274.
- Bellini, A., & Güçeri, S. (2003). Mechanical characterization of parts fabricated using fused deposition modeling. *Rapid Prototyping Journal*, 9(4), 252-264.
- Berg, M., Van Kreveld, M., Overmars, M., & Schwarzkopf, O. C. (2000). Computational geometry. In *Computational geometry* (pp. 1-17). Springer Berlin Heidelberg.
- Bernard, A., & Fischer, A. (2002). New trends in rapid product development. *CIRP Annals-Manufacturing Technology*, 51(2), 635-652.
- Bernardini, F., Mittleman, J., Rushmeier, H., Silva, C., & Taubin, G. (1999). The ball-pivoting algorithm for surface reconstruction. *IEEE transactions on visualization and computer graphics*, 5(4), 349-359.
- Bertoldi, M., Yardimci, M. A., Pistor, C. M., Güçeri, S. I., & Sala, G. (1998). Mechanical characterization of parts processed via fused deposition. In *Proceedings of the 1998 solid freeform fabrication symposium* (pp. 557-565).
- Bian, W., Li, D., Lian, Q., Li, X., Zhang, W., Wang, K., & Jin, Z. (2012). Fabrication of a bio-inspired beta-Tricalcium phosphate/collagen scaffold based on ceramic stereolithography and gel casting for osteochondral tissue engineering. *Rapid Prototyping Journal*, 18(1), 68-80.
- Bochmann, L., Bayley, C., Helu, M., Transchel, R., Wegener, K., & Dornfeld, D. (2015). Understanding error generation in fused deposition modeling. *Surface Topography: Metrology and Properties*, 3(1), 014002.
- Boschetto, A., Giordano, V., & Veniali, F. (2013). 3D roughness profile model in fused deposition modelling. *Rapid Prototyping Journal*, 19(4), 240-252.
- Boschetto, A., & Bottini, L. (2014). Accuracy prediction in fused deposition modeling. *The international journal of advanced manufacturing technology*, 73(5-8), 913-928.

- Buchbinder, D., Schleifenbaum, H., Heidrich, S., Meiners, W., & Bültmann, J. (2011). High power selective laser melting (HP SLM) of aluminum parts. *Physics Procedia*, *12*, 271-278.
- Budak, I., Sokovic, M., & Barisic, B. (2011). Accuracy improvement of point data reduction with sampling-based methods by Fuzzy logic-based decision-making. *Measurement*, *44*(6), 1188-1200.
- Calvert, P. (2001). Inkjet printing for materials and devices. *Chemistry of materials*, *13*(10), 3299-3305.
- Carr, K., & Ferreira, P. (1995). Verification of form tolerances part I: basic issues, flatness, and straightness. *Precision Engineering*, *17*(2), 131-143.
- Chandrasekaran, M., Muralidhar, M., Krishna, C. M., & Dixit, U. S. (2010). Application of soft computing techniques in machining performance prediction and optimization: a literature review. *The International Journal of Advanced Manufacturing Technology*, *46*(5-8), 445-464.
- Chang, D. Y., & Chang, Y. M. (2002). A freeform surface modelling system based on laser scan data for reverse engineering. *The International Journal of Advanced Manufacturing Technology*, *20*(1), 9-19.
- Chartier, C., Bastide, S., & Lévy-Clément, C. (2008). Metal-assisted chemical etching of silicon in HF-H₂O₂. *Electrochimica Acta*, *53*(17), 5509-5516.
- Chartrain, N. A., Williams, C. B., & Whittington, A. R. (2016). Engineering Tissues with Bioprinting. *BioProcess Int*, *14*(10).
- Cheraghi, S. H., Jiang, G., & Ahmad, J. S. (2003). Evaluating the geometric characteristics of cylindrical features. *Precision Engineering*, *27*(2), 195-204.
- Chockalingam, K., Jawahar, N., Ramanathan, K. N., & Banerjee, P. S. (2006). Optimization of stereolithography process parameters for part strength using design of experiments. *The International Journal of Advanced Manufacturing Technology*, *29*(1), 79-88.
- Choi, J. W., Kim, H. C., & Wicker, R. (2011). Multi-material stereolithography. *Journal of Materials Processing Technology*, *211*(3), 318-328.
- Chopra, K., Mummery, P. M., Derby, B., & Gough, J. E. (2012). Gel-cast glass-ceramic tissue scaffolds of controlled architecture produced via stereolithography of moulds. *Biofabrication*, *4*(4), 045002.

- Chou, S. Y., & Sun, C. W. (2000). Assessing cylindricity for oblique cylindrical features. *International Journal of Machine Tools and Manufacture*, 40(3), 327-341.
- Chua, C. K., Leong, K. F., & Lim, C. S. (2010). *Rapid prototyping: principles and applications*. World Scientific.
- Cogorno, G. R. (2006). Geometric dimensioning and tolerancing for mechanical design. McGraw-Hil.
- Cooper, K. (2001). *Rapid prototyping technology: selection and application*. CRC press.
- Crump, S. S. (1992). *U.S. Patent No. 5,121,329*. Washington, DC: U.S. Patent and Trademark Office.
- Cuesta, E., Rico, J. C., Fernández, P., Blanco, D., & Valiño, G. (2009). Influence of roughness on surface scanning by means of a laser stripe system. *The International Journal of Advanced Manufacturing Technology*, 43(11), 1157-1166.
- Cui, C., Li, B., Huang, F., & Zhang, R. (2007). Genetic algorithm-based form error evaluation. *Measurement science and technology*, 18(7), 1818.
- Cui, C., Li, T., Blunt, L. A., Jiang, X., Huang, H., Ye, R., & Fan, W. (2013). The assessment of straightness and flatness errors using particle swarm optimization. *Procedia CIRP*, 10, 271-275.
- Curless, B. (1997). *New methods for surface reconstruction from range images* (Doctoral dissertation, Stanford University).
- Dalmasso, P., & Nerino, R. (2004, September). Hierarchical 3D surface reconstruction based on radial basis functions. In *3D Data Processing, Visualization and Transmission, 2004. 3DPVT 2004. Proceedings. 2nd International Symposium on* (pp. 574-579). IEEE.
- Damodarasamy, S., & Anand, S. A. M. (1999). Evaluation of minimum zone for flatness by normal plane method and simplex search. *IIE transactions*, 31(7), 617-626.
- Dawson, D. J. (1992). Cylindricity and its measurement. *International Journal of Machine Tools and Manufacture*, 32(1-2), 247-253.
- Dey, T. K., & Goswami, S. (2006). Provable surface reconstruction from noisy samples. *Computational Geometry*, 35(1-2), 124-141.
- Dhanish, P. B., & Shunmugam, M. S. (1991). An algorithm for form error evaluation—using the theory of discrete and linear Chebyshev approximation. *Computer Methods in Applied Mechanics and Engineering*, 92(3), 309-324.

- Dúbravčík, M., & Kender, Š. (2012). Application of reverse engineering techniques in mechanics system services. *Procedia Engineering*, 48, 96-104.
- Duranleau, F., Beaudoin, P., & Poulin, P. (2008, May). Multiresolution point-set surfaces. In *Proceedings of Graphics Interface 2008* (pp. 211-218). Canadian Information Processing Society.
- El-Katatny, I., Masood, S. H., & Morsi, Y. S. (2010). Error analysis of FDM fabricated medical replicas. *Rapid Prototyping Journal*, 16(1), 36-43.
- Elkott, D. F., Elmaraghy, H. A., & Elmaraghy, W. H. (2002). Automatic sampling for CMM inspection planning of free-form surfaces. *International Journal of Production Research*, 40(11), 2653-2676.
- Elliott, A. M., Ivanova, O. S., Williams, C. B., & Campbell, T. A. (2013). Inkjet printing of quantum dots in photopolymer for use in additive manufacturing of nanocomposites. *Advanced Engineering Materials*, 15(10), 903-907.
- Endrias, D. H., & Feng, H. Y. (2003). Minimum-zone form tolerance evaluation using rigid-body coordinate transformation. *Journal of Computing and Information Science in Engineering*, 3, 31-38.
- Es-Said, O. S., Foyos, J., Noorani, R., Mendelson, M., Marloth, R., & Pregger, B. A. (2000). Effect of layer orientation on mechanical properties of rapid prototyped samples. *Materials and Manufacturing Processes*, 15(1), 107-122.
- Etesami, F., & Qiao, H. (1990). Analysis of two-dimensional measurement data for automated inspection. *Journal of Manufacturing systems*, 9(1), 21-34.
- Feng, H. Y., Liu, Y., & Xi, F. (2001). Analysis of digitizing errors of a laser scanning system. *Precision Engineering*, 25(3), 185-191.
- Feng, Y., Ji-xian, Z., Li, Z., & Jing-xiang, G. (2009, May). Urban DEM generation from airborne LiDAR data. In *Urban Remote Sensing Event, 2009 Joint* (pp. 1-5). IEEE.
- Frazier, W. E. (2014). Metal additive manufacturing: a review. *Journal of Materials Engineering and Performance*, 23(6), 1917-1928.
- Gálvez, A., Iglesias, A., Cobo, A., Puig-Pey, J., & Espinola, J. (2007). Bézier curve and surface fitting of 3D point clouds through genetic algorithms, functional networks and least-squares approximation. *Computational Science and Its Applications-ICCSA 2007*, 680-693.
- Gans, B. J., Duineveld, P. C., & Schubert, U. S. (2004). Inkjet printing of polymers: state of the art and future developments. *Advanced materials*, 16(3), 203-213.

- Gao, J., Gindy, N., & Chen, X. (2006). An automated GD&T inspection system based on non-contact 3D digitization. *International journal of production research*, 44(1), 117-134.
- Gausemeier, I. J., & Echterhoff, N. (2011). Thinking ahead the Future of Additive Manufacturing-. *Future Applications*.
- Gibson, D. C. (2004). *Parametric feature recognition and surface construction from digital point cloud scans of mechanical parts*.
- Gibson, I., Rosen, D. W., & Stucker, B. (2010). *Additive manufacturing technologies* (Vol. 238). New York: Springer.
- Gibson, I., Rosen, D., & Stucker, B. (2014). *Additive manufacturing technologies: 3D printing, rapid prototyping, and direct digital manufacturing*. Springer.
- González-Jorge, H., Riveiro, B., Armesto, J., & Arias, P. (2011). Standard artifact for the geometric verification of terrestrial laser scanning systems. *Optics & Laser Technology*, 43(7), 1249-1256.
- Gosavi, A., & Phatakwala, S. (2006). A finite-differences derivative-descent approach for estimating form error in precision-manufactured parts. *Journal of Manufacturing Science and Engineering*, 128(1), 355-359.
- Gosavi, A., & Cudney, E. (2012). Form errors in precision metrology: a survey of measurement techniques. *Quality Engineering*, 24(3), 369-380.
- Gridlogics Technologies Pvt Ltd (2014) 3D printing-Technology insight report, www.patentiSIGHTPro.com. Accessed 16 Jul 2014.
- Grimm, T. (2005). Magic, Mystique, and Myth. *Desktop Engineering*, 10(12), 32-37.
- Gurralla, P. K., & Regalla, S. P. (2014). Multi-objective optimisation of strength and volumetric shrinkage of FDM parts: a multi-objective optimization scheme is used to optimize the strength and volumetric shrinkage of FDM parts considering different process parameters. *Virtual and Physical Prototyping*, 9(2), 127-138.
- Himmer, T., Nakagawa, T., & Noguchi, H. (1997, August). Stereolithography of ceramics. In *International Solid Freeform Fabrication Symposium, Austin, TX* (pp. 363-369).
- Horvath, D., Noorani, R., & Mendelson, M. (2007). Improvement of surface roughness on ABS 400 polymer using design of experiments (DOE). In *Materials Science Forum* (Vol. 561, pp. 2389-2392). Trans Tech Publications.

- Huang, P., & Pretzsch, H. (2010). Using terrestrial laser scanner for estimating leaf areas of individual trees in a conifer forest. *Trees*, 24(4), 609-619.
- Huang, S. H., Liu, P., Mokasdar, A., & Hou, L. (2013). Additive manufacturing and its societal impact: a literature review. *The International Journal of Advanced Manufacturing Technology*, 1-13.
- Hutmacher, D. W., Schantz, T., Zein, I., Ng, K. W., Teoh, S. H., & Tan, K. C. (2001). Mechanical properties and cell cultural response of polycaprolactone scaffolds designed and fabricated via fused deposition modeling. *Journal of Biomedical Materials Research Part A*, 55(2), 203-216.
- Ibrahim, M., Otsubo, T., Narahara, H., Koresawa, H., & Suzuki, H. (2006). Inkjet printing resolution study for multi-material rapid prototyping. *JSME International Journal Series C Mechanical Systems, Machine Elements and Manufacturing*, 49(2), 353-360.
- Ingole, D., Madhusudan Kuthe, A., Thakare, S. B., & Talankar, A. S. (2009). Rapid prototyping—a technology transfer approach for development of rapid tooling. *Rapid Prototyping Journal*, 15(4), 280-290.
- Ippolito, R., Iuliano, L., & Gatto, A. (1995). Benchmarking of rapid prototyping techniques in terms of dimensional accuracy and surface finish. *CIRP Annals-Manufacturing Technology*, 44(1), 157-160.
- Isagro, F., Odone, F., & Verri, A. (2005, July). An open system for 3D data acquisition from multiple sensor. In *Computer Architecture for Machine Perception, 2005. CAMP 2005. Proceedings. Seventh International Workshop on* (pp. 52-57). IEEE.
- Islam, M. N., Boswell, B., & Pramanik, A. (2013). An investigation of dimensional accuracy of parts produced by three-dimensional printing. In *Proceedings of the world congress on engineering* (Vol. 1, pp. 3-5).
- Islam, M. N., Pramanik, A., & Slamka, S. (2016). Errors in different geometric aspects of common engineering parts during rapid prototyping using a Z Corp 3D printer. *Progress in Additive Manufacturing*, 1(1-2), 55-63.
- Jayanthi, S., Keefe, M., & Gargiulo, E. P. (1994, August). Studies in stereolithography: influence of process parameters on curl distortion in photopolymer models. In *Solid Freeform Fabrication Symposium 1994* (pp. 250-258). University of Texas, Austin.
- Johnson, W. M., Rowell, M., Deason, B., & Eubanks, M. (2011, August). Benchmarking evaluation of an open source fused deposition modeling additive manufacturing system. In *Proceeding of the 22nd annual international solid freeform fabrication symposium* (pp. 197-211).

- Johnson, W., Rowell, M., Deason, B., & Eubanks, M. (2014). Comparative evaluation of an open-source FDM system. *Rapid Prototyping Journal*, 20(3), 205-214.
- Jywe, W. Y., & Liu, C. H. (1999). The min–max problem for evaluating the form error of a circle. *Measurement*, 26(4), 273-282.
- Kaasalainen, S., Ahokas, E., Hyypä, J., & Suomalainen, J. (2005). Study of surface brightness from backscattered laser intensity: Calibration of laser data. *IEEE Geoscience and Remote Sensing Letters*, 2(3), 255-259.
- Kaasalainen, S., Jaakkola, A., Kaasalainen, M., Krooks, A., & Kukko, A. (2011). Analysis of incidence angle and distance effects on terrestrial laser scanner intensity: Search for correction methods. *Remote Sensing*, 3(10), 2207-2221.
- Kai Chua, C., Fai Leong, K., Sing Lim, C., & Thien Vu, T. (2010). Multimedia courseware for teaching of rapid prototyping systems. *Rapid Prototyping Journal*, 16(2), 80-89.
- Kakinuma, Y., Mori, M., Oda, Y., Mori, T., Kashihara, M., Hansel, A., & Fujishima, M. (2016). Influence of metal powder characteristics on product quality with directed energy deposition of Inconel 625. *CIRP Annals-Manufacturing Technology*, 65(1), 209-212.
- Kanatani, K., & Rangarajan, P. (2011). Hyper least squares fitting of circles and ellipses. *Computational Statistics & Data Analysis*, 55(6), 2197-2208.
- Kim, D. S., Kim, D., & Sugihara, K. (2001). Voronoi diagram of a circle set from Voronoi diagram of a point set: I. Topology. *Computer Aided Geometric Design*, 18(6), 541-562.
- Kobbelt, L., & Botsch, M. (2004). A survey of point-based techniques in computer graphics. *Computers & Graphics*, 28(6), 801-814.
- Kofman, J., & Borribanbunpotkat, K. (2014). Hand-held 3D scanner for surface-shape measurement without sensor pose tracking or surface markers: A compact hand-held 3D scanner simultaneously projecting multiple light lines is presented, enabling 3D surface-shape measurement without requiring sensor tracking or surface markers. *Virtual and Physical Prototyping*, 9(2), 81-95.
- Koivunen, V. (1992). Robust signal restoration and local estimation of image structure.
- Krishna, B. V., Xue, W., Bose, S., & Bandyopadhyay, A. (2008). Functionally graded Co–Cr–Mo coating on Ti–6Al–4V alloy structures. *Acta biomaterialia*, 4(3), 697-706.
- Kruth, J. P. (1991). Material increment manufacturing by rapid prototyping techniques. *CIRP Annals-Manufacturing Technology*, 40(2), 603-614.

- Kruth, J. P., Leu, M. C., & Nakagawa, T. (1998). Progress in additive manufacturing and rapid prototyping. *CIRP Annals-Manufacturing Technology*, 47(2), 525-540.
- Kruth, J. P., Mercelis, P., Van Vaerenbergh, J., Froyen, L., & Rombouts, M. (2005). Binding mechanisms in selective laser sintering and selective laser melting. *Rapid prototyping journal*, 11(1), 26-36.
- Ke, Y. L., Xiao, Y. X., & Li, J. X. (2001). The research of reverse engineering CAD modeling technique. *J Comput aid Design Graph*, 13(6), 570-5.
- Kuo, C. C., & Yau, H. T. (2005). A Delaunay-based region-growing approach to surface reconstruction from unorganized points. *Computer-Aided Design*, 37(8), 825-835.
- Laeng, J., Stewart, J. G., & Liou, F. W. (2000). Laser metal forming processes for rapid prototyping-A review. *International Journal of Production Research*, 38(16), 3973-3996.
- Lai, K., & Wang, J. (1988, May). A computational geometry approach to geometric tolerancing. In *16th North American manufacturing research conference* (pp. 376-379).
- Lai, H. Y., Jywe, W. Y., & Liu, C. H. (2000). Precision modeling of form errors for cylindricity evaluation using genetic algorithms. *Precision Engineering*, 24(4), 310-319.
- Lam, C. X. F., Mo, X. M., Teoh, S. H., & Hutmacher, D. W. (2002). Scaffold development using 3D printing with a starch-based polymer. *Materials Science and Engineering: C*, 20(1), 49-56.
- Le, V. B., & Lee, D. T. (1991). Out-of-roundness problem revisited. *IEEE Transactions on Pattern Analysis and Machine Intelligence*, 13(3), 217-223.
- Lee, C. T., & Lee, C. C. (2014). On a hybrid particle swarm optimization method and its application in mechanism design. *Proceedings of the Institution of Mechanical Engineers, Part C: Journal of Mechanical Engineering Science*, 228(15), 2844-2857.
- Lee, G., Mou, J., & Shen, Y. (1997). An analytical assessment of measurement uncertainty in precision inspection and machine calibration. *International Journal of Machine Tools and Manufacture*, 37(3), 263-276.
- Lee, K. H., & Park, H. P. (2000). Automated inspection planning of free-form shape parts by laser scanning. *Robotics and Computer-Integrated Manufacturing*, 16(4), 201-210.

- Lee, K. H., Park, H., & Son, S. (2001). A framework for laser scan planning of freeform surfaces. *The international journal of advanced manufacturing technology*, 17(3), 171-180.
- Lee, M., Dunn, J. C., & Wu, B. M. (2005). Scaffold fabrication by indirect three-dimensional printing. *Biomaterials*, 26(20), 4281-4289.
- Lee, B. H., Abdullah, J., & Khan, Z. A. (2005). Optimization of rapid prototyping parameters for production of flexible ABS object. *Journal of materials processing technology*, 169(1), 54-61.
- Lee, S. J., & Chang, D. Y. (2006). A laser sensor with multiple detectors for freeform surface digitization. *The International Journal of Advanced Manufacturing Technology*, 31(5), 474-482.
- Lemeš, S., & Zaimović-Uzunović, N. (2009, October). Study of ambient light influence on laser 3D scanning. In *Proceedings of the 7th International Conference on Industrial Tools and Material Processing Technologies*.
- Leong, K. F., Cheah, C. M., & Chua, C. K. (2003). Solid freeform fabrication of three-dimensional scaffolds for engineering replacement tissues and organs. *Biomaterials*, 24(13), 2363-2378.
- Levy, G. N., Schindel, R., & Kruth, J. P. (2003). Rapid manufacturing and rapid tooling with layer manufacturing (LM) technologies, state of the art and future perspectives. *CIRP Annals-Manufacturing Technology*, 52(2), 589-609.
- Li, L., Schemenauer, N., Peng, X., Zeng, Y., & Gu, P. (2002). A reverse engineering system for rapid manufacturing of complex objects. *Robotics and Computer-Integrated Manufacturing*, 18(1), 53-67.
- Li, Z., Tian, G., Cheng, G., Liu, H., & Cheng, Z. (2014). An integrated cultural particle swarm algorithm for multi-objective reliability-based design optimization. *Proceedings of the Institution of Mechanical Engineers, Part C: Journal of Mechanical Engineering Science*, 228(7), 1185-1196.
- Liang, X., Kankare, V., Hyypä, J., Wang, Y., Kukko, A., Haggrén, H., ... & Holopainen, M. (2016). Terrestrial laser scanning in forest inventories. *ISPRS Journal of Photogrammetry and Remote Sensing*, 115, 63-77.
- Lin, S. C., Douglass, M. J., Holdaway, S. J., & Floyd, B. (2010). The application of 3D laser scanning technology to the assessment of ordinal and mechanical cortex quantification in lithic analysis. *Journal of Archaeological Science*, 37(4), 694-702.

- Lindau, B., Lindkvist, L., Andersson, A., & Söderberg, R. (2013). Statistical shape modeling in virtual assembly using PCA-technique. *J. Manuf. Syst*, 32(3), 456-463.
- Liou, F. W. (2007). *Rapid prototyping and engineering applications: a toolbox for prototype development*. CRC Press.
- Lin, H., & Peng, Y. (2009, July). Evaluation of cylindricity error based on an improved GA with uniform initial population. In *Control, Automation and Systems Engineering, 2009. CASE 2009. IITA International Conference on*(pp. 311-314). IEEE.
- Lindemann, C., Jahnke, U., Moi, M., & Koch, R. (2012). Analyzing product lifecycle costs for a better understanding of cost drivers in additive manufacturing. In *23th Annual International Solid Freeform Fabrication Symposium—An Additive Manufacturing Conference. Austin Texas USA 6th-8th August*.
- Lipson, H. (2011). The shape of things to come: frontiers in additive manufacturing. *Frontiers of Engineering*, 33-44.
- Liu, Y., Yang, H., & Wang, W. (2005, June). Reconstructing B-spline Curves from Point Clouds--A Tangential Flow Approach Using Least Squares Minimization. In *Shape Modeling and Applications, 2005 International Conference* (pp. 4-12). IEEE.
- Liu, J., Wang, G. L., & Pan, X. D. (2011). Minimum-zone form tolerance evaluation for cylindrical surfaces using adaptive ant colony optimization. *Journal of Computational Information Systems*, 7(12), 4480-4490.
- Lotz, M. S., Pienaar, H., & De Beer, D. J. (2012, September). Optimisation of entry-level 3D printers to improve the quality of printed products. In *Proceedings of the South African Telecommunications Networks and Applications Conference* (pp. 2-5).
- Lotz, M. S., Pienaar, H. C. V. Z., & de Beer, D. J. (2013, September). Entry-level additive manufacturing: Comparing geometric complexity to high-level machines. In *AFRICON, 2013* (pp. 1-5). IEEE.
- Luo, J., Wang, Q., & Fu, L. (2012). Application of modified artificial bee colony algorithm to flatness error evaluation. *Guangxue Jingmi Gongcheng(Optics and Precision Engineering)*, 20(2), 422-430.
- Luo, J., & Wang, Q. (2014). A method for axis straightness error evaluation based on improved artificial bee colony algorithm. *The International Journal of Advanced Manufacturing Technology*, 71(5-8), 1501-1509.

- Mahmud, M., Joannic, D., Roy, M., Isheil, A., & Fontaine, J. F. (2011). 3D part inspection path planning of a laser scanner with control on the uncertainty. *Computer-Aided Design*, 43(4), 345-355.
- Malone, E., & Lipson, H. (2007). Fab@ Home: the personal desktop fabricator kit. *Rapid Prototyping Journal*, 13(4), 245-255.
- Mamadapur, M. S. (2007). *Constitutive modeling of fused deposition modeling acrylonitrile butadiene styrene (ABS)* (Doctoral dissertation, Texas A&M University).
- Martínez, S., Cuesta, E., Barreiro, J., & Alvarez, B. (2010). Methodology for comparison of laser digitizing versus contact systems in dimensional control. *Optics and Lasers in Engineering*, 48(12), 1238-1246.
- Maruyama, M., & Abe, S. (1993). Range sensing by projecting multiple slits with random cuts. *IEEE Transactions on Pattern Analysis and Machine Intelligence*, 15(6), 647-651.
- Mian, S. H., Mannan, M. A., & Al-Ahmari, A. (2015). Accuracy of a reverse-engineered mould using contact and non-contact measurement techniques. *International Journal of Computer Integrated Manufacturing*, 28(5), 419-436.
- Minetola, P. (2012). The importance of a correct alignment in contactless inspection of additive manufactured parts. *International Journal of Precision Engineering and Manufacturing*, 13(2), 211-218.
- Mohamed, O. A., Masood, S. H., & Bhowmik, J. L. (2015). Optimization of fused deposition modeling process parameters: a review of current research and future prospects. *Advances in Manufacturing*, 3(1), 42-53.
- Moroni, G., Polini, W., & Semeraro, Q. (1998). Knowledge based method for touch probe configuration in an automated inspection system. *Journal of Materials Processing Technology*, 76(1), 153-160.
- Moroni, G., & Petro, S. (2008). Geometric tolerance evaluation: A discussion on minimum zone fitting algorithms. *Precision Engineering*, 32(3), 232-237.
- Moroni, G., Syam, W. P., & Petrò, S. (2014). Towards early estimation of part accuracy in additive manufacturing. *Procedia CIRP*, 21, 300-305.
- Mott, M., & Evans, J. R. G. (1999). Zirconia/alumina functionally graded material made by ceramic ink jet printing. *Materials Science and Engineering: A*, 271(1), 344-352.
- Mueller, B., & Kochan, D. (1999). Laminated object manufacturing for rapid tooling and patternmaking in foundry industry. *Computers in Industry*, 39(1), 47-53.

- Murr, L. E., Gaytan, S. M., Ramirez, D. A., Martinez, E., Hernandez, J., Amato, K. N., & Wicker, R. B. (2012). Metal fabrication by additive manufacturing using laser and electron beam melting technologies. *Journal of Materials Science & Technology*, 28(1), 1-14.
- Murthy, T. S. R., & Abdin, S. Z. (1980). Minimum zone evaluation of surfaces. *International Journal of Machine Tool Design and Research*, 20(2), 123-136.
- Naing, M. W., Chua, C. K., Leong, K. F., & Wang, Y. (2005). Fabrication of customised scaffolds using computer-aided design and rapid prototyping techniques. *Rapid Prototyping Journal*, 11(4), 249-259.
- Nancharaiah, T., d Ranga Raju, V. R., & Raju, R. (2010). An experimental investigation on surface quality and dimensional accuracy of FDM components.
- Navangul, G., Paul, R., & Anand, S. (2013). Error minimization in layered manufacturing parts by stereolithography file modification using a vertex translation algorithm. *Journal of Manufacturing Science and Engineering*, 135(3), 031006.
- Nayak, C., Singh, A., Chaudhary, H., & Tripathi, A. (2016). A novel approach for customized prosthetic socket design. *Biomedical Engineering: Applications, Basis and Communications*, 28(03), 1650022.
- Noorani, R. (2006). *Rapid prototyping: principles and applications*. John Wiley & Sons Incorporated.
- Nuchter, A., Surmann, H., Lingemann, K., Hertzberg, J., & Thrun, S. (2004, April). 6D SLAM with an application in autonomous mine mapping. In *Robotics and Automation, 2004. Proceedings. ICRA'04. 2004 IEEE International Conference on* (Vol. 2, pp. 1998-2003). IEEE.
- Okabe, A., Boots, B., Sugihara, K., & Chiu, S. N. (2009). *Spatial tessellations: concepts and applications of Voronoi diagrams* (Vol. 501). John Wiley & Sons.
- Pandey, P. M., Thrimurthulu, K., & Reddy*, N. V. (2004). Optimal part deposition orientation in FDM by using a multicriteria genetic algorithm. *International Journal of Production Research*, 42(19), 4069-4089.
- Pardiñas, J., Lorenzo, H., Arias, P., & Armesto, J. (2008). From laser point clouds to surfaces: Statistical nonparametric methods for three-dimensional reconstruction. *Computer-Aided Design*, 40(5), 646-652.

- Park, S. I., Smith, M. J., & Mersereau, R. M. (2004). Improved structures of maximally decimated directional filter banks for spatial image analysis. *IEEE Transactions on Image Processing*, 13(11), 1424-1431.
- Pathak, V. K., Singh, A. K., Sivadasan, M., & Singh, N. K. (2016). Framework for automated GD&T inspection using 3D scanner. *Journal of The Institution of Engineers (India): Series C*, 1-9.
- Pauly, M., Gross, M., & Kobbelt, L. P. (2002, October). Efficient simplification of point-sampled surfaces. In *Proceedings of the conference on Visualization'02* (pp. 163-170). IEEE Computer Society.
- Pei, E., Ian Campbell, R., & de Beer, D. (2011). Entry-level RP machines: how well can they cope with geometric complexity?. *Assembly Automation*, 31(2), 153-160.
- Peng, A., & Xiao, X. (2012). Investigation on reasons inducing error and measures improving accuracy in fused deposition modeling. *Advances in Information Sciences and Service Sciences*, 4(5).
- Peng, A. H. (2012). Research on the interlayer stress and warpage deformation in FDM. In *Advanced Materials Research* (Vol. 538, pp. 1564-1567). Trans Tech Publications.
- Pernot, J. P., Moraru, G., & Véron, P. (2007). Repairing triangle meshes built from scanned point cloud. *Journal of Engineering Design*, 18(5), 459-473.
- Pesci, A., & Teza, G. (2008). Terrestrial laser scanner and retro-reflective targets: an experiment for anomalous effects investigation. *International Journal of Remote Sensing*, 29(19), 5749-5765.
- Phatak, A. M., & Pande, S. S. (2012). Optimum part orientation in rapid prototyping using genetic algorithm. *Journal of manufacturing systems*, 31(4), 395-402.
- Pilipović, A., Raos, P., & Šercer, M. (2009). Experimental analysis of properties of materials for rapid prototyping. *The International Journal of Advanced Manufacturing Technology*, 40(1-2), 105-115.
- Prakasvudhisarn, C., Trafalis, T. B., & Raman, S. (2003). Support vector regression for determination of minimum zone. *TRANSACTIONS-AMERICAN SOCIETY OF MECHANICAL ENGINEERS JOURNAL OF MANUFACTURING SCIENCE AND ENGINEERING*, 125(4), 736-739.
- Raja, V., & Fernandes, K. J. (Eds.). (2007). *Reverse engineering: an industrial perspective*. Springer Science & Business Media.

- Ram, G. J., Yang, Y., & Stucker, B. E. (2006). Effect of process parameters on bond formation during ultrasonic consolidation of aluminum alloy 3003. *Journal of Manufacturing Systems*, 25(3), 221-238.
- Ram, G. D., Robinson, C., Yang, Y., & Stucker, B. E. (2007). Use of ultrasonic consolidation for fabrication of multi-material structures. *Rapid Prototyping Journal*, 13(4), 226-235.
- Rao, R. V., & Savsani, V. J. (2012). *Mechanical design optimization using advanced optimization techniques*. Springer Science & Business Media.
- Rekanos, I. T. (2008). Shape reconstruction of a perfectly conducting scatterer using differential evolution and particle swarm optimization. *IEEE Transactions on Geoscience and Remote Sensing*, 46(7), 1967-1974.
- Rodríguez, J. F., Thomas, J. P., & Renaud, J. E. (2001). Mechanical behavior of acrylonitrile butadiene styrene (ABS) fused deposition materials. Experimental investigation. *Rapid Prototyping Journal*, 7(3), 148-158.
- Rodríguez, J. F., Thomas, J. P., & Renaud, J. E. (2003). Mechanical behavior of acrylonitrile butadiene styrene fused deposition materials modeling. *Rapid Prototyping Journal*, 9(4), 219-230.
- Rodríguez-Toro, C., Tate, S., Jared, G., & Swift, K. (2002, January). Shaping the complexity of a design. In *ASME 2002 International Mechanical Engineering Congress and Exposition* (pp. 641-649). American Society of Mechanical Engineers.
- Rönholm, P., Honkavaara, E., Litkey, P., Hyypä, H., & Hyypä, J. (2007). Integration of laser scanning and photogrammetry. *International Archives of Photogrammetry, Remote Sensing and Spatial Information Sciences*, 36(3/W52), 355-362.
- Rossi, A., Antonetti, M., Barloscio, M., & Lanzetta, M. (2011). Fast genetic algorithm for roundness evaluation by the minimum zone tolerance (MZT) method. *Measurement*, 44(7), 1243-1252.
- Roy, U., & Xu, Y. (1995). Form and orientation tolerance analysis for cylindrical surfaces in computer-aided inspection. *Computers in Industry*, 26(2), 127-134.
- Roy, U., & Zhang, X. (1992). Establishment of a pair of concentric circles with the minimum radial separation for assessing roundness error. *Computer-Aided Design*, 24(3), 161-168.
- Raghunath, N., & Pandey, P. M. (2007). Improving accuracy through shrinkage modelling by using Taguchi method in selective laser sintering. *International journal of machine tools and manufacture*, 47(6), 985-995.

- Rajagopal, K., & Anand, S. (1999). Assessment of circularity error using a selective data partition approach. *International journal of production research*, 37(17), 3959-3979.
- Rayegani, F., & Onwubolu, G. (2014). Fused deposition modelling (FDM) process parameter prediction and optimization using group method for data handling (GMDH) and differential evolution (DE). *International Journal of Advanced Manufacturing Technology*, 73.
- Sachs, E., Cima, M., Brecht, J., Curodeau, A., Fan, T., & Brancazio, D. (1992). CAD-casting: direct fabrication of ceramic shells and cores by three-dimensional printing. *Manufacturing Review(USA)*, 5(2), 117-126.
- Sahu, R. K., Mahapatra, S. S., & Sood, A. K. (2013). A study on dimensional accuracy of fused deposition modeling (FDM) processed parts using fuzzy logic. *Journal for Manufacturing Science & Production*, 13(3), 183-197.
- Saini, D., Kumar, S., & Gulati, T. R. (2015). Reconstruction of free-form space curves using NURBS-snakes and a quadratic programming approach. *Computer Aided Geometric Design*, 33, 30-45.
- Samuel, G. L., & Shunmugam, M. S. (2000). Evaluation of circularity from coordinate and form data using computational geometric techniques. *Precision Engineering*, 24(3), 251-263.
- Schwendner, K. I., Banerjee, R., Collins, P. C., Brice, C. A., & Fraser, H. L. (2001). Direct laser deposition of alloys from elemental powder blends. *Scripta Materialia*, 45(10), 1123-1129.
- Schwenke, H., Neuschaefer-Rube, U., Pfeifer, T., & Kunzmann, H. (2002). Optical methods for dimensional metrology in production engineering. *CIRP Annals-Manufacturing Technology*, 51(2), 685-699.
- Sherwood, J. K., Riley, S. L., Palazzolo, R., Brown, S. C., Monkhouse, D. C., Coates, M., ... & Ratcliffe, A. (2002). A three-dimensional osteochondral composite scaffold for articular cartilage repair. *Biomaterials*, 23(24), 4739-4751.
- Shin, K. H., Natu, H., Dutta, D., & Mazumder, J. (2003). A method for the design and fabrication of heterogeneous objects. *Materials & Design*, 24(5), 339-353.
- Shiou, F. J., & Lai, Y. C. (2005). Development of a non-contact multi-axis reverse engineering measurement system for small complex objects. In *Journal of Physics: Conference Series* (Vol. 13, No. 1, p. 178). IOP Publishing.
- Shunmugam, M. S. (1987). New approach for evaluating form errors of engineering surfaces. *Computer-Aided Design*, 19(7), 368-374.

- Singh, R. (2014). Process capability analysis of fused deposition modelling for plastic components. *Rapid Prototyping Journal*, 20(1), 69-76.
- Sirrine, J. M., Pekkanen, A. M., Nelson, A. M., Chartrain, N. A., Williams, C. B., & Long, T. E. (2015). 3D-printable biodegradable polyester tissue scaffolds for cell adhesion. *Australian Journal of Chemistry*, 68(9), 1409-1414.
- Snelling, D., Blount, H., Forman, C., Ramsburg, K., Wentzel, A., Williams, C., & Druschitz, A. (2013). The effects of 3D printed molds on metal castings. In *International solid freeform fabrication symposium*.
- Son, S., Park, H., & Lee, K. H. (2002). Automated laser scanning system for reverse engineering and inspection. *International Journal of Machine Tools and Manufacture*, 42(8), 889-897.
- Song, B., Dong, S., Deng, S., Liao, H., & Coddet, C. (2014). Microstructure and tensile properties of iron parts fabricated by selective laser melting. *Optics & Laser Technology*, 56, 451-460.
- Sonmez, F. O., & Hahn, H. T. (1998). Thermomechanical analysis of the laminated object manufacturing (LOM) process. *Rapid Prototyping Journal*, 4(1), 26-36.
- Soni, K., Chen, D., & Lerch, T. (2009). Parameterization of prismatic shapes and reconstruction of free-form shapes in reverse engineering. *The International Journal of Advanced Manufacturing Technology*, 41(9), 948-959.
- Sood, A. K., Ohdar, R. K., & Mahapatra, S. S. (2009). Improving dimensional accuracy of fused deposition modelling processed part using grey Taguchi method. *Materials & Design*, 30(10), 4243-4252.
- Sood, A. K., Ohdar, R. K., & Mahapatra, S. S. (2010). Parametric appraisal of mechanical property of fused deposition modelling processed parts. *Materials & Design*, 31(1), 287-295.
- Sood, A. K., Equbal, A., Toppo, V., Ohdar, R. K., & Mahapatra, S. S. (2012). An investigation on sliding wear of FDM built parts. *CIRP Journal of Manufacturing Science and Technology*, 5(1), 48-54.
- Standard, A. S. T. M. (2012). F2792. 2012. Standard Terminology for Additive Manufacturing Technologies. West Conshohocken, PA: ASTM International. See www.astm.org.(doi: 10.1520/F2792-12).
- Steinbichler, (2016) Accessed on 16 sept, 2016 <http://optotechnik.zeiss.com/produkte/3d-digitalisierung/comet-13d>

- Stopp, S., Wolff, T., Irlinger, F., & Lueth, T. (2008). A new method for printer calibration and contour accuracy manufacturing with 3D-print technology. *Rapid Prototyping Journal*, 14(3), 167-172.
- Stucker, B. R. E. N. T. (2012). Additive manufacturing technologies: technology introduction and business implications. In *Frontiers of Engineering: Reports on Leading-Edge Engineering From the 2011 Symposium*, National Academies Press, Washington, DC, Sept (pp. 19-21).
- Suen, D. S., & Chang, C. N. (1997). Application of neural network interval regression method for minimum zone straightness and flatness. *Precision Engineering*, 20(3), 196-207.
- Sukumar, S. R., Page, D. L., Koschan, A. F., & Abidi, M. A. (2008, June). Towards understanding what makes 3D objects appear simple or complex. In *Computer Vision and Pattern Recognition Workshops, 2008. CVPRW'08. IEEE Computer Society Conference on* (pp. 1-8). IEEE.
- Sun, W., Starly, B., Nam, J., & Darling, A. (2005). Bio-CAD modeling and its applications in computer-aided tissue engineering. *Computer-Aided Design*, 37(11), 1097-1114.
- Tay, B. Y., Zhang, S. X., Myint, M. H., Ng, F. L., Chandrasekaran, M., & Tan, L. K. A. (2007). Processing of polycaprolactone porous structure for scaffold development. *Journal of materials processing technology*, 182(1), 117-121.
- Thakur, A., Banerjee, A. G., & Gupta, S. K. (2009). A survey of CAD model simplification techniques for physics-based simulation applications. *Computer-Aided Design*, 41(2), 65-80.
- Thrimurthulu, K., Pandey, P. M., & Reddy, N. V. (2004). Optimum part deposition orientation in fused deposition modeling. *International Journal of Machine Tools and Manufacture*, 44(6), 585-594.
- Tomasi, C., & Manduchi, R. (1998, January). Bilateral filtering for gray and color images. In *Computer Vision, 1998. Sixth International Conference on* (pp. 839-846). IEEE.
- Tong, K., Amine Lehtihet, E., & Joshi, S. (2003). Parametric error modeling and software error compensation for rapid prototyping. *Rapid Prototyping Journal*, 9(5), 301-313.
- Tong, K., Joshi, S., & Amine Lehtihet, E. (2008). Error compensation for fused deposition modeling (FDM) machine by correcting slice files. *Rapid Prototyping Journal*, 14(1), 4-14.
- Tornincasa, S., & Vezzetti, E. (2005). Feasibility study of a reverse engineering system benchmarking. *Proceedings of ADM-Ingegraf*.

- Traband, M. T., Joshi, S., Wysk, R. A., & Cavalier, T. M. (1989). Evaluation of straightness and flatness tolerances using the minimum zone. *Manufacturing Review*, 2(3), 189-195.
- Tsai, J. H., & Wang, J. H. (1999). Using self-creating neural network for surface reconstruction. In *Systems, Man, and Cybernetics, 1999. IEEE SMC'99 Conference Proceedings. 1999 IEEE International Conference on* (Vol. 4, pp. 886-890). IEEE.
- Tseng, K. Y., Zhang, C. B., & Wu, C. Y. (2010). An enhanced binary particle swarm optimization for structural topology optimization. *Proceedings of the Institution of Mechanical Engineers, Part C: Journal of Mechanical Engineering Science*, 224(10), 2271-2287.
- Vaezi, M., Chianrabutra, S., Mellor, B., & Yang, S. (2013). Multiple material additive manufacturing—Part 1: a review: This review paper covers a decade of research on multiple material additive manufacturing technologies which can produce complex geometry parts with different materials. *Virtual and Physical Prototyping*, 8(1), 19-50.
- Van Gestel, N., Cuypers, S., Bleys, P., & Kruth, J. P. (2009). A performance evaluation test for laser line scanners on CMMs. *Optics and Lasers in Engineering*, 47(3), 336-342.
- Varady, T., Martin, R. R., & Cox, J. (1997). Reverse engineering of geometric models—an introduction. *Computer-Aided Design*, 29(4), 255-268.
- Venkaiah, N., & Shunmugam, M. S. (2007). Evaluation of form data using computational geometric techniques—Part II: Cylindricity error. *International Journal of Machine Tools and Manufacture*, 47(7), 1237-1245.
- Voisin, S., Foufou, S., Truchetet, F., Page, D., & Abidi, M. (2007). Study of ambient light influence for three-dimensional scanners based on structured light. *Optical Engineering*, 46(3), 030502-030502.
- Volpato, N., Aguiomar Foggiatto, J., & Coradini Schwarz, D. (2014). The influence of support base on FDM accuracy in Z. *Rapid Prototyping Journal*, 20(3), 182-191.
- Walczyk, D. F., & Yoo, S. (2009). Design and fabrication of a laminated thermoforming tool with enhanced features. *Journal of Manufacturing Processes*, 11(1), 8-18.
- Waterman, P. (2004). 3 D Data At Work. *Desktop Engineering*, 9(11), 18-21.
- Vosselman, G. (2000). Slope based filtering of laser altimetry data. *International Archives of Photogrammetry and Remote Sensing*, 33(B3/2; PART 3), 935-942.

- Wang, M., Cheraghi, S. H., & Masud, A. S. (1999). Circularity error evaluation: theory and algorithm. *Precision Engineering*, 23(3), 164-176.
- Wang, G. J., Wang, C. C., & Chuang, S. H. (1999). Reverse engineering of sculptured surfaces by four-axis non-contacting scanning. *The International Journal of Advanced Manufacturing Technology*, 15(11), 800-809.
- Wang, M. Y. (2004). Form error evaluation: an iterative reweighted least squares algorithm. *Journal of manufacturing science and engineering*, 126(3), 535-541.
- Wang, J., & Shaw, L. L. (2006). Fabrication of functionally graded materials via inkjet color printing. *Journal of the American Ceramic Society*, 89(10), 3285-3289.
- Wang, C. C., Lin, T. W., & Hu, S. S. (2007). Optimizing the rapid prototyping process by integrating the Taguchi method with the Gray relational analysis. *Rapid Prototyping Journal*, 13(5), 304-315.
- Wang, M., Xi, L., & Du, S. (2014). 3D surface form error evaluation using high definition metrology. *Precision Engineering*, 38(1), 230-236.
- Wasza, J., Bauer, S., & Hornegger, J. (2011, November). Real-time preprocessing for dense 3-D range imaging on the GPU: defect interpolation, bilateral temporal averaging and guided filtering. In *Computer Vision Workshops (ICCV Workshops), 2011 IEEE International Conference on* (pp. 1221-1227). IEEE.
- Weber, T., Motavalli, S., Fallahi, B., & Cheraghi, S. H. (2002). A unified approach to form error evaluation. *Precision engineering*, 26(3), 269-278.
- Wen, X. L., Huang, J. C., Sheng, D. H., & Wang, F. L. (2010). Conicity and cylindricity error evaluation using particle swarm optimization. *Precision Engineering*, 34(2), 338-344.
- Williams, C. B., Cochran, J. K., & Rosen, D. W. (2011). Additive manufacturing of metallic cellular materials via three-dimensional printing. *The International Journal of Advanced Manufacturing Technology*, 53(1), 231-239.
- Wilson, J. M., Jones, N., Jin, L., & Shin, Y. C. (2013). Laser deposited coatings of Co-Cr-Mo onto Ti-6Al-4V and SS316L substrates for biomedical applications. *Journal of Biomedical Materials Research Part B: Applied Biomaterials*, 101(7), 1124-1132.
- Wilson, J. M., Piya, C., Shin, Y. C., Zhao, F., & Ramani, K. (2014). Remanufacturing of turbine blades by laser direct deposition with its energy and environmental impact analysis. *Journal of Cleaner Production*, 80, 170-178.

- Wimpenny, D. I., Bryden, B., & Pashby, I. R. (2003). Rapid laminated tooling. *Journal of Materials Processing Technology*, 138(1), 214-218.
- Wohlers, T. (2014). 3D Printing and Additive Manufacturing State of the Industry Annual Worldwide Progress Report. *Wohlers Report*.
- Wohlers, T. T., & Caffrey, T. (2015). *Wohlers report 2015: 3D printing and additive manufacturing state of the industry annual worldwide progress report*. Wohlers Associates.
- Wong, K. V., & Hernandez, A. (2012). A review of additive manufacturing. *ISRN Mechanical Engineering*, 2012.
- Wu, F. (2008, October). Surface reconstruction method based on GRNN. In *Intelligent Computation Technology and Automation (ICICTA), 2008 International Conference on* (Vol. 1, pp. 262-265). IEEE.
- Wu, H. X., Dong, H. X., & Su, J. Q. (2008, December). 3D reconstruction from section plane views based on self-adaptive neural network. In *Intelligent Information Technology Application, 2008. IITA'08. Second International Symposium on* (Vol. 3, pp. 84-88). IEEE.
- Wu, X. M., Li, G. X., & Zhao, W. M. (2008, August). Incomplete points cloud data surface reconstruction based on neural network. In *Intelligent Information Hiding and Multimedia Signal Processing, 2008. IIHMSP'08 International Conference on* (pp. 913-916). IEEE.
- Xi, F., & Shu, C. (1999). CAD-based path planning for 3-D line laser scanning. *Computer-Aided Design*, 31(7), 473-479.
- Xi, F., Liu, Y., & Feng, H. Y. (2001). Error compensation for three-dimensional line laser scanning data. *The International Journal of Advanced Manufacturing Technology*, 18(3), 211-216.
- Xiaomin, C., Junchuan, W., & Qiaoguan, W. (2007, August). Leak-mending and recruitment of incomplete points data in 3D reconstruction based on genetic algorithm. In *Natural Computation, 2007. ICNC 2007. Third International Conference on* (Vol. 5, pp. 259-263). IEEE.
- Xie, D., Zhang, H., Shu, X., Xiao, J., & Cao, S. (2010). Multi-materials drop-on-demand inkjet technology based on pneumatic diaphragm actuator. *Science China Technological Sciences*, 53(6), 1605-1611.

- Xu, J., Xi, N., Zhang, C., Shi, Q., & Gregory, J. (2011). Real-time 3D shape inspection system of automotive parts based on structured light pattern. *Optics & Laser Technology*, 43(1), 1-8.
- Yan, X., & Gu, P. E. N. G. (1996). A review of rapid prototyping technologies and systems. *Computer-Aided Design*, 28(4), 307-318.
- Yang, Y., Loh, H. T., Fuh, J. Y. H., & Wang, Y. G. (2002). Equidistant path generation for improving scanning efficiency in layered manufacturing. *Rapid Prototyping Journal*, 8(1), 30-37.
- Yap, Y. L., & Yeong, W. Y. (2014). Additive manufacture of fashion and jewellery products: a mini review: This paper provides an insight into the future of 3D printing industries for fashion and jewellery products. *Virtual and Physical Prototyping*, 9(3), 195-201.
- Yap, Y. L., & Yeong, W. Y. (2015). Shape recovery effect of 3D printed polymeric honeycomb: This paper studies the elastic behaviour of different honeycomb structures produced by PolyJet technology. *Virtual and Physical Prototyping*, 10(2), 91-99.
- Yau, H. T., Chen, C. Y., & Wilhelm, R. G. (2000). Registration and integration of multiple laser scanned data for reverse engineering of complex 3D models. *International Journal of Production Research*, 38(2), 269-285.
- Yin, Z. (2004). Reverse engineering of a NURBS surface from digitized points subject to boundary conditions. *Computers & Graphics*, 28(2), 207-212.
- Yin, S., Ren, Y., Guo, Y., Zhu, J., Yang, S., & Ye, S. (2014). Development and calibration of an integrated 3D scanning system for high-accuracy large-scale metrology. *Measurement*, 54, 65-76.
- Yoo, J., Cima, M. J., Khanuja, S., & Sachs, E. M. (1993). Structural ceramic components by 3D printing. In *Solid Freeform Fabrication Symposium* (pp. 40-50).
- Yoon, H. S., Lee, J. Y., Kim, H. S., Kim, M. S., Kim, E. S., Shin, Y. J., ... & Ahn, S. H. (2014). A comparison of energy consumption in bulk forming, subtractive, and additive processes: Review and case study. *International Journal of Precision Engineering and Manufacturing-Green Technology*, 1(3), 261-279.
- Yu, Y. (1999, January). Surface reconstruction from unorganized points using self-organizing neural networks. In *IEEE Visualization* (Vol. 99, pp. 61-64).
- Zaimovic-Uzunovic, N., & Lemes, S. (2010). Influence of surface parameters on laser 3D scanning. In *IMEKO Conference Proceedings: International Symposium on Measurement and Quality Control: Osaka, Japan* (pp. D024-026).

- Zhang, K. (2008). Minimum Zone Evolution of Circularity Error Based on an Improved Genetic Algorithm. In *Advanced Computer Theory and Engineering, 2008. ICACTE'08. International Conference on* (pp. 523-527). IEEE.
- Zhang, Y., & Chou, K. (2008). A parametric study of part distortions in fused deposition modelling using three-dimensional finite element analysis. *Proceedings of the Institution of Mechanical Engineers, Part B: Journal of Engineering Manufacture*, 222(8), 959-968.
- Zhang, J. W., & Peng, A. H. (2012). Process-parameter optimization for fused deposition modeling based on Taguchi method. In *Advanced Materials Research* (Vol. 538, pp. 444-447). Trans Tech Publications.
- Zhao, H. K., Osher, S., & Fedkiw, R. (2001). Fast surface reconstruction using the level set method. In *Variational and Level Set Methods in Computer Vision, 2001. Proceedings. IEEE Workshop on* (pp. 194-201). IEEE.
- Zhongwei, Y. (2004). Direct integration of reverse engineering and rapid prototyping based on the properties of NURBS or B-spline. *Precision Engineering*, 28(3), 293-301.
- Zhou, J. G., Herscovici, D., & Chen, C. C. (2000). Parametric process optimization to improve the accuracy of rapid prototyped stereolithography parts. *International Journal of Machine Tools and Manufacture*, 40(3), 363-379.

Appendix A. Measured data set of straightness error

No.	Example 1		Example 2		Example 3		Example 4	
	X	Y	X	Y	X	Y	X	Y
1	0.6981	-1.9966	0.0674	0.0009	2.3481	2.2383	2.3786	-1.6979
2	1.0762	-1.9901	0.2251	-0.0002	2.5964	2.2382	2.5497	-1.6972
3	1.4104	-1.9827	0.3761	-0.0004	2.9185	2.2371	2.6900	-1.6963
4	1.8294	-1.9732	0.5463	-0.0002	3.2000	2.2354	2.8297	-1.6956
5	2.2831	-1.9632	0.7011	-0.0002	3.4936	2.2330	2.9489	-1.6946
6	2.7328	-1.9531	0.8730	-0.0002	3.8226	2.2326	3.0709	-1.6937
7	3.1660	-1.9441	0.9773	-0.0001	4.0315	2.2316	3.2127	-1.6929
8	3.5183	-1.9362	1.0734	0.0000	4.1963	2.2313	3.3633	-1.6922
9	3.8147	-1.9294	1.1821	-0.0001	4.4125	2.2308	3.4880	-1.6913
10	4.1650	-1.9223	1.2896	0.0003	4.6058	2.2299	3.6903	-1.6896
11			1.4353	0.0002	4.8005	2.2300	3.8789	-1.6897
12			1.5221	0.0003	5.0218	2.2301	4.0420	-1.6892
13			1.6652	0.0002	5.2660	2.2310	4.2596	-1.6855
14			1.7786	0.0003	5.4763	2.2305	4.3979	-1.6861
15			1.8625	0.0006	5.6524	2.2302	4.5625	-1.6856
16			2.0028	0.0006	5.8317	2.2300		
17			2.0884	0.0005	6.0326	2.2302		
18			2.1836	0.0006	6.2811	2.2303		
19			2.2842	0.0008	6.4739	2.2305		
20			2.3745	0.0009	6.7640	2.2307		
21			2.4790	0.0010				
22			2.6024	0.0011				
23			2.6805	0.0012				
24			2.7522	0.0012				

25	2.8591	0.0011
26	2.9650	0.0014
27	3.0973	0.0012
28	3.2302	0.0015
29	3.3711	0.0021
30	3.4836	0.0017
32	3.6605	0.0012
32	3.8265	0.0015
33	3.9174	0.0011
34	4.0053	0.0014
35	4.1246	0.0012

Appendix B. Measurement data set of flatness error

No.	Example 1			Example 2		
	X	Y	Z	X	Y	Z
1	9.9995	5.0000	4.0103	14.9992	5.0006	4.0095
2	10.0002	29.9981	4.0138	14.9995	30.0002	4.0145
3	10.0015	55.0007	4.0009	15.0010	55.0014	4.0010
4	9.9996	79.9988	4.0095	15.0002	79.9992	4.0087
5	9.9997	104.9981	4.0161	14.9992	105.001	4.0157
6	35.0003	4.9986	4.0029	40.0019	4.9996	4.0032
7	35.0003	30.0012	4.0044	40.0001	30.0012	4.0039
8	34.9974	54.9996	3.9987	39.9998	54.9993	3.9983
9	35.0013	80.0012	4.0025	40.0005	80.0011	4.0022
10	34.9993	104.9982	4.0201	40.0002	105.0005	4.0207
11	59.9989	4.9982	4.0050	65.0001	5.0000	4.0042
12	60.0003	29.9987	4.0100	65.0010	29.9992	4.0110

13	60.0013	54.9986	4.0025	65.0011	55.0004	4.0022
14	60.0010	80.0019	4.0048	65.0002	80.001	4.0044
15	59.9978	105.0005	4.0024	64.9990	105.0002	4.0033
16	84.9988	5.0010	4.0126	90.0002	5.0003	4.0134
17	84.9981	30.0000	4.0114	90.0002	29.9990	4.0119
18	85.0007	55.0008	4.0021	90.0004	55.0012	4.0021
19	85.0000	80.0003	4.0054	90.0004	80.0003	4.0050
20	84.9988	105.0020	4.0056	89.9990	105.0003	4.0060
21	109.9984	4.9981	4.0161	115.0003	4.9999	4.0168
22	110.0000	29.9992	4.0119	115.0003	29.9992	4.0124
23	109.9986	55.0004	4.0122	115.0002	55.0003	4.0126
24	109.998	79.9988	4.0115	115.0001	79.999	4.0119
25	110.0003	104.9984	4.0056	115.0010	105.0003	4.0053

Appendix C. Measurement data set of Circularity Error

No.	Example 1		Example 2	
	X	Y	X	Y
1	38.31	11.366	107.5811	114.2119
2	34.513	20.123	102.2909	119.9906
3	23.592	32.254	95.6848	124.2034
4	15.369	36.868	88.2128	126.5634
5	5.528	39.564	80.3826	126.9159
6	-7.719	39.201	72.7251	125.2311
7	-22.854	32.773	65.7612	121.6196
8	-25.527	30.736	59.9721	116.3233
9	-36.656	15.84	55.7576	109.7039
10	-38.982	8.735	53.4073	102.218

11	-38.526	-10.518	53.0774	94.3816
12	-25.315	-30.885	54.7849	86.7302
13	-6.078	-39.444	58.4107	79.7824
14	12.757	-37.82	63.7075	74.0083
15	29.873	-26.504	70.3176	69.8019
16	37.178	-14.592	77.7899	67.4519
17			85.6152	67.1081
18			93.2669	68.7926
19			100.2245	72.4009
20			106.0093	77.6929
21			110.2199	84.3073
22			112.5676	91.7864
23			112.8977	99.6156
24			111.2129	107.2695

Appendix D. Measurement data set of cylindricity error

No.	Example 1			Example 2		
	X	Y	Z	X	Y	Z
1	60.05112	0.002953	3.946134	11.0943	0.4522	65.2328
2	-57.932	15.39931	15.98302	5.094	10.845	65.0765
3	57.43213	17.48871	20.36594	-6.9063	10.8439	65.0089
4	55.02276	-23.9366	11.50506	-12.9065	0.4498	65.0897
5	29.1801	-52.4231	1.037163	-6.9063	-9.9429	65.054
6	-58.8616	-11.1136	20.13448	5.0940	-9.9418	65.2216
7	-44.5972	40.11373	2.005267	10.9546	0.522	75.2316
8	-23.2474	-55.4067	17.6693	4.9544	10.9148	75.0752
9	34.04157	-49.3091	15.80786	-7.0459	10.9137	75.077

10	-34.0841	-49.4277	12.47998	-13.0461	0.5196	74.8964
11	50.68422	-32.022	22.86594	-7.0459	-9.8731	75.0528
12	57.31868	17.61954	22.08246	4.95447	-9.8720	75.2204
13	-40.4081	-44.4857	22.69232	10.8150	0.5918	85.2304
14	-39.8384	44.99439	7.411167	4.8148	10.9846	85.074
15	-10.2614	-59.1468	22.60068	-7.1855	10.9835	85.0641
16	53.91984	26.49319	18.94904	-13.1858	0.5894	84.8952
17	-8.54001	59.44297	13.09234	-7.1855	-9.8033	85.0516
18	-59.3691	8.361285	7.133233	4.8149	-9.8022	85.2171
19	-38.0298	46.40484	4.995216	10.6754	0.6616	95.2291
20	47.9461	-35.9254	27.27624	4.6752	11.0544	95.0728
21				-7.3253	11.0533	94.9077
22				-13.3254	0.6592	95.094
23				-7.3252	-9.7335	95.0504
24				4.6752	-9.7323	95.2179

PAPER PUBLISHED BASED ON THIS WORK

Peer-reviewed Journal Publications

1. **Vimal Kumar Pathak** and Amit Kumar Singh. "Optimization of morphological process parameters in contactless laser scanning system using modified particle swarm algorithm." *Measurement*, Vol. 109, 2017, pp. 27-35. (SCI)
2. **Vimal Kumar Pathak** and Amit Kumar Singh, Ramanpreet Singh and Himanshu Chaudhary. "A modified algorithm of Particle Swarm Optimization for form error evaluation." *tm - technisches messen*, Vol. 84 (4), 2017, 272-292. (SCI)
3. **Vimal Kumar Pathak**, Amit Kumar Singh, "Accuracy control of contactless laser sensor system using MFO algorithm" *tm - technisches messen*, Vol. 84 (11), 2017, 734-746. (SCI)
4. **Vimal Kumar Pathak**, Chitresh Nayak, Amit Kumar Singh and Himanshu Chaudhary. "A virtual reverse engineering methodology for accuracy control of transtibial prosthetic socket." *Biomedical engineering: Applications, Basis and Communications*, Vol. 28 (5), 2016 pp. 1-9.
5. **Vimal Kumar Pathak**, Amit Kumar Singh, M Sivadasan and N. K. Singh. "Framework for automated GD&T inspection using 3D scanner." *Journal of the Institution of Engineers (India): Series C* (2016): 1-9.
6. **Vimal Kumar Pathak** and Amit Kumar Singh. "Assessing the challenges and issues in entry-level additive manufacturing machine." *International Journal of Rapid Manufacturing*, Vol. 6 (1), 2016 pp. 53-74.
7. **Vimal Kumar Pathak**, Chitresh Nayak, Amit Kumar Singh and Himanshu Chaudhary. "An Integrated reverse engineering approach for accuracy control of free-form objects." *Archive of Mechanical Engineering*, Vol. 63 (4), 2016 pp. 635-651.
8. **Vimal Kumar Pathak** and Amit Kumar Singh. "Form error evaluation of non-contact scan data using constriction factor Particle Swarm Optimization." *Journal of Advanced Manufacturing Systems*, Vol. 16 (4), 2017

9. **Vimal Kumar Pathak** and Amit Kumar Singh. "Investigating alignment effect on inspection accuracy of AM part using 3D scanner." *Journal of Advanced Manufacturing Systems (JAMS)*, Vol. 16 (2), 2017 pp. 157-169
10. **Vimal Kumar Pathak** and Amit Kumar Singh. "A particle swarm optimization approach for minimizing GD&T error in Additive manufactured parts." *International Journal of Manufacturing, Materials, and Mechanical Engineering (IJMMME)*, Vol 7(3), 2017.

International/ National Conferences

1. **Vimal Kumar Pathak** and Amit Kumar Singh. "Sustainable fused deposition modeling (FDM) parts with minimized GD&T error using PSO algorithm." *International Conference on sustainable smart manufacturing*. Oct. 2016. Lisbon, Portugal.
2. **Vimal Kumar Pathak** and Amit Kumar Singh. "Alignment Based Inspection Framework for Additive Manufactured Parts." *CAD/CAM, Robotics and Factories of the Future*. Springer India, 2016 pp. 335-344.
3. **Vimal Kumar Pathak** and Amit Kumar Singh. "Framework for automated inspection using reverse engineering." *International conference on AM, 3D printing and 3D scanning (ICAM-3D)*. Feb 2015, Chennai India.
4. **Vimal Kumar Pathak** and Amit Kumar Singh. "A comparative study of tolerance stack up analysis technique." *International Colloquium on Materials, Manufacturing and Metrology*. 2014, IIT Chennai, India.
5. **Vimal Kumar Pathak**, Angelus Khoh and Amit Kumar Singh. "Useful tool for sustainable product design." *National Conference on Sustainable manufacturing (NCSM-2015)* MNIT Jaipur, January 2015.

BRIEF BIO-DATA OF THE AUTHOR

Name : **Vimal Kumar Pathak**
Date of birth : August 25, 1986
Address for correspondence : SF-4, 267/3, Sector-1, Vaishali, Ghaziabad
(Uttar Pradesh-201010) India

Education:

Degree	Discipline	Institute	Board/ University	Percentage	Year
High School	Science	Sarvodaya Bal Vidyalaya, Delhi	C.B.S.E.	69.67	2002
Senior Secondary	PCM	Sarvodaya Bal Vidyalaya, Delhi	C.B.S.E.	70.2	2004
B. Tech	Mechanical Engineering	Krishna Engineering College Ghaziabad	U.P.T.U.	65.14	2008
M.Tech	Production Technology	I.S.M. Dhanbad	I.S.M.U. Dhanbad	8.63	2013
Ph.D.	Mechanical Engineering	Malaviya National Institute of Technology Jaipur	Autonomous	---	Thesis submitted in June 2017

Teaching/Industrial Experience:

University / Institute	Duration	Post
MNIT, Jaipur, (Rajasthan)	July 2013-June 2017	Ph.D. Research Scholar
Indiana Gratings Pvt Ltd	August 2008-May 2010	Marketing Engineer